Programa de Doctorado en Tecnologías Industriales y Materiales

Escuela de Doctorado de la Universitat Jaume I

Subcooling systems in transcritical CO_2 refrigeration cycles. Experimental evaluation of energy improvement.

A dissertation presented by Laura Nebot Andrés **for the Degree of Doctor of Philosophy from the Universitat Jaume I**

Laura Nebot Andrés

LAURA\|NEBOT\|ANDRES

Firmado digitalmente por LAURA\|NEBOT\|ANDRES
Nombre de reconocimiento (DN): cn=LAURA\|NEBOT\|ANDRES, serialNumber=20902447R, givenName=LAURA, sn=NEBOT ANDRES, ou=CIUDADANOS, o=ACCV, c=ES
Fecha: 2022.02.02 15:38:44 +01'00'

Rodrigo Llopis Doménech

RODRIGO\|LLOPIS\|DOMENECH

Firmado digitalmente por RODRIGO\|LLOPIS\|DOMENECH
Nombre de reconocimiento (DN): cn=RODRIGO\|LLOPIS\|DOMENECH, serialNumber=73391682Q, givenName=RODRIGO, sn=LLOPIS DOMENECH, ou=CIUDADANOS, o=ACCV, c=ES
Fecha: 2022.02.02 17:08:18 +01'00'

Castelló de la Plana, February 2022

Programa de Doctorat en / Programa de Doctorado en Tecnologías Industriales y Materiales

Escola de Doctorat de la Universitat Jaume I / Escuela de Doctorado de la Universitat Jaume I

Sistemas de subenfriamiento en ciclos de refrigeración con CO_2 transcrítico. Evaluación experimental de mejora energética.

Memòria presentada per **Laura Nebot Andrés** per a optar al grau de doctor/a per la Universitat Jaume I
Memoria presentada por **Laura Nebot Andrés** para optar al grado de doctor/a por la Universitat Jaume I

Laura Nebot Andrés

Rodrigo Llopis Doménech

Castelló de la Plana, febrer 2022

Castelló de la Plana, febrero 2022

Funding

Predoctoral contract:

- Ayudas para la formación de profesorado universitario (FPU) del Ministerio de Educación, Cultura y Deporte de España, 2016 (Ref. FPU16/00151).
  1st August 2018 – 14th May 2022

- Subvenciones para la contratación de personal investigador de carácter predoctoral (ACIF) del Programa para la Promoción de la Investigación Científica, el Desarrollo tecnológico y la Innovación en la Comunitat de Generalitat Valenciana, 2017 (Ref. ACIF/2017/194).
  15th December 2017 – 31st July 2018

Research stays:

- Refrigeration lab (LTF) at Dipartimento di Ingegneria Industriale (DIIN), Università degli Studi di Salerno, Fisciano, Italy.
  30th September 2021 – 29th December 2021
  Financed by Ayudas complementarias de movilidad destinadas a beneficiarios del programa de Formación del Profesorado Universitario (FPU) del Subprograma Estatal de Formación en I+D+i del Ministerio de Universidades de España, 2021 (Ref. EST21/00293).

- Refrigeration lab (LTF) at Dipartimento di Ingegneria Industriale (DIIN), Università degli Studi di Salerno, Fisciano, Italy.
  1st July 2020 – 30th September 2020
  Not financed.

Compendium of publications

- Nebot-Andrés, L., Llopis, R., Sánchez, D., Catalán-Gil, J., Cabello, R.;CO2 with mechanical subcooling vs. CO_2 cascade cycles for medium temperature commercial refrigeration applications thermodynamic analysis (2017) Applied Sciences (Switzerland), 7 (9), art. no. 955.
  Cited 24 times.
  DOCUMENT TYPE: Article DOI: 10.3390/app7090955
  **Award : Best Congess Paper Award 10º Congreso Nacional de Ingeniería Termodinámica, Lleida, 2017*

- Llopis, R., Nebot-Andrés, L., Sánchez, D., Catalán-Gil, J., Cabello, R.; Subcooling methods for CO_2 refrigeration cycles: A review (2018) International Journal of Refrigeration, 93, pp. 85-107.
  Cited 86 times.
  DOCUMENT TYPE: Article DOI: 10.1016/j.ijrefrig.2018.06.010
  **Award: 2018 Best Paper International Journal of Refrigeration (Institute International du Froid)*

- Nebot-Andrés, L., Calleja-Anta, D., Sánchez, D., Cabello, R., Llopis, R.; Thermodynamic analysis of a CO_2 refrigeration cycle with integrated mechanical subcooling (2019) Energies, 13 (1), art. no. 4.
  Cited 6 times.
  DOCUMENT TYPE: Article DOI: 10.3390/en13010012

- Nebot-Andrés, L., Catalán-Gil, J., Sánchez, D., Calleja-Anta, D., Cabello, R., Llopis, R.; Experimental determination of the optimum working conditions of a transcritical CO_2 refrigeration plant with integrated mechanical subcooling (2020) International Journal of Refrigeration, 113, pp. 266-275.
  Cited 18 times.
  DOCUMENT TYPE: Article DOI: 10.1016/j.ijrefrig.2020.02.012

- Nebot-Andrés, L., Sánchez, D., Calleja-Anta, D., Cabello, R., Llopis, R.;Experimental determination of the optimum working conditions of a commercial transcritical CO_2 refrigeration plant with a R-152a dedicated mechanical subcooling (2021) International Journal of Refrigeration, 121, pp. 258-268.
  Cited 8 times.
  DOCUMENT TYPE: Article DOI: 10.1016/j.ijrefrig.2020.10.002

- Nebot-Andrés, L., Sánchez, D., Calleja-Anta, D., Cabello, R., Llopis, R.; Experimental determination of the optimum intermediate and gas-cooler pressures of a commercial transcritical CO_2 refrigeration plant with parallel compression (2021) Applied Thermal Engineering, 189, art. no. 116671.
  Cited 4 times.
  DOCUMENT TYPE: Article DOI: 10.1016/j.applthermaleng.2021.116671

- Llopis, R., Toffoletti, G., Nebot-Andrés, L., Cortella, G.; Experimental evaluation of zeotropic refrigerants in a dedicated mechanical subcooling system in a CO_2 cycle (2021) International Journal of Refrigeration, 128, pp. 287-298.
  Cited 2 times.
  DOCUMENT TYPE: Article DOI: 10.1016/j.ijrefrig.2021.05.028

- Nebot-Andrés, L., Calleja-Anta, D., Fossi, C., Sánchez, D., Cabello, R., Llopis, R.; Experimental assessment of different extraction points for the integrated mechanical subcooling system of CO_2 transcritical plant (2022) International Journal of Refrigeration, online 6 January 2022
  DOCUMENT TYPE: Article DOI: 10.1016/j.ijrefrig.2022.01.006

- Nebot-Andrés, L., Calleja-Anta, D., Sánchez, D., Cabello, R., Llopis, R.; Experimental assessment of dedicated and integrated mechanical subcooling systems vs parallel compression in transcritical CO_2 refrigeration plants (2022) Energy Conversion and Managment, online 2 December 2021, 115051.
  DOCUMENT TYPE: Article DOI: 10.1016/j.enconman.2021.115051

"This thesis has been accepted by the co-authors of the publications listed above that have waved the right to present them as a part of another PhD thesis"

To my family.

Abstract

This thesis aims to offer a competitive and free technology solution to the current problems related to refrigeration systems and their efficiency. The main objective of the work is to study and evaluate different mechanical subcooling systems that imply an improvement in the energy performance of transcritical CO_2 refrigeration facilities.

Global warming is one of the main problems in today's society and in order to reduce the CO_2 emissions responsible for global warming, different regulations and directives have been established both at the global and the European level. Specifically, regulations that directly affect refrigeration, responsible for almost 8% of these emissions, regulate or prohibit the use of certain refrigerants in these facilities. This leaves CO_2 as the best solution that can be implemented in centralized commercial refrigeration.

The problem arises especially in hot climates, where simple CO_2 cycles are not very efficient and therefore, although we face the problems derived from direct emissions, indirect emissions are greater than those of the systems used to date.

In this thesis, therefore, the focus is on improving the efficiency of these systems thanks to the use of subcooling systems. Specifically, it focuses on two systems, called the dedicated mechanical subcooling (DMS) and the integrated mechanical subcooling (IMS). The first, the dedicated mechanical subcooling, has great potential for improvement although it uses a refrigerant other than CO_2 in the auxiliary cycle. On the other hand, the much less studied integrated mechanical subcooling only works with CO_2, which can be an important advantage.

The thermodynamic study of these systems is fundamental to establish which are the applications to which they can give service and to determine their limits of operation. For this reason, different thermodynamic simulations of both systems and also of the reference system have been developed to be able to know the behavior of these new systems and also their behavior against the different operating parameters. From these studies it has been deduced that they are systems that must be optimized both in terms of gas-cooler pressure and of subcooling degree.

As a continuation of this first analysis, an experimental laboratory plant has been designed and set up, which integrates all the aforementioned technologies and in which all the systems have been studied.

As a result, the optimal pressures and the subcooling degree of each one of the systems have been experimentally determined and the main energy parameters of the systems have been obtained under different operation conditions: evaporation levels

close to -5ºC, -10ºC and -15ºC and temperatures of the hot sink of 25ºC, 30ºC and 35ºC. In turn, the use of zeotropic mixtures in the dedicated mechanical subcooling system has also been studied and different configurations of the integrated system have been analyzed.

Finally, the two systems have been compared experimentally against the reference system, the parallel compressor, corroborating the positive effects of both systems and quantifying the improvements achieved.

The main results show experimentally that the IMS provides increments in COP of 4.1% at 25.0ºC, 7.2% at 30.4ºC and 9.5% at 35.1ºC and the DMS of 7.8%, 13.7% and 17.5% respectively when comparing them to the use of the parallel compressor for an evaporating level near -10ºC. From these results it can be concluded that the best system, from an energy point of view, is the DMS since it achieves more significant increases.

Resumen

La presente tesis pretende ofrecer una solución, competitiva y de tecnología libre, a la problemática actual relacionada con los sistemas de refrigeración y su eficiencia. El objetivo principal del trabajo es estudiar y evaluar diferentes sistemas de subenfriamiento mecánico que supongan una mejora del comportamiento energético de las instalaciones de refrigeración de CO_2 transcrítico.

El calentamiento global es uno de los principales problemas de la sociedad actual y con el fin de reducir las emisiones de CO_2 responsables del calentamiento global, se han establecido diferentes regulaciones y directivas tanto a nivel mundial como europeo. En concreto, las reglamentaciones que afectan directamente a la refrigeración, responsable de casi el 8% de esas emisiones, regulan o prohíben el uso de ciertos refrigerantes en las instalaciones. Esto deja al CO_2 como la mejor solución que se puede implementar en refrigeración comercial centralizada.

La problemática surge sobretodo en climas cálidos, donde los ciclos simples de CO_2 no son muy eficientes y por lo tanto, si bien hacemos frente a los problemas derivados de las emisiones directas, las emisiones indirectas son mayores que las de los sistemas utilizados hasta la actualidad.

En esta tesis por tanto, el foco está puesto en la mejora de la eficiencia de dichos sistemas gracias al uso de sistemas de subenfriamiento. En concreto se centra en dos sistemas, llamados subenfriamiento mecánico dedicado (DMS) y el subenfriamiento mecánico integrado (IMS). El primero, el subenfriamiento mecánico dedicado, tiene un gran potencial de mejora aunque utiliza un refrigerante diferente al CO_2 en el ciclo auxiliar. Por su parte, el subenfriamiento mecánico integrado, mucho menos estudiado, únicamente trabaja con CO_2, lo que puede resultar una ventaja importante.

El estudio termodinámico de estos sistemas es fundamental para establecer cuáles son las aplicaciones a las cuales pueden dar servicio y determinar sus límites de funcionamiento. Por ello se han desarrollado diferentes simulaciones termodinámicas de ambos sistemas y también del sistema de referencia para poder conocer el comportamiento de estos nuevos sistemas y también su comportamiento frente a los diferentes parámetros de operación. De estos estudios se ha deducido que son sistemas que deben ser optimizados tanto en términos de presión de gas-cooler como de grado de subenfriamiento.

Como continuación a este primer análisis, se ha diseñado y montado una planta experimental de laboratorio, que integra todas las tecnologías mencionadas y en la cual se han estudiado todos los sistemas.

Como resultado, se han determinado experimentalmente las presiones y grados de subenfriamiento óptimos de cada uno de los sistemas y se han obtenido los principales parámetros energéticos de los sistemas bajo diferentes condiciones: niveles de evaporación cercanos a los -5ºC, -10ºC y -15ºC y temperaturas de foco caliente de 25ºC, 30ºC y 35ºC. A su vez, también se ha estudiado el uso de mezclas zeotrópicas en el sistema de subenfriamiento mecánico dedicado y se han analizado diferentes configuraciones del sistema integrado.

Finalmente, se han comparado los dos sistemas experimentalmente frente al sistema de referencia, el compresor paralelo, comprobando los efectos positivos de ambos sistemas y cuantificando las mejoras conseguidas.

Los principales resultados experimentales muestran que el IMS proporciona incrementos en COP de 4.1% a 25.0ºC, 7.2% a 30.4ºC y 9.5% a 35.1ºC y el DMS de 7.8%, 13.7% y 17.5% respectivamente al compararlos con el uso de el compresor paralelo para un nivel de evaporación cercano a los -10ºC. De estos resultados se puede concluir que el mejor sistema, desde el punto de vista energético, es el DMS ya que logra incrementos más significativos.

Resum

Aquesta tesi pretén oferir una solució, competitiva i de tecnologia lliure, a la problemàtica actual relacionada amb els sistemes de refrigeració i la seva eficiència. L'objectiu principal del treball és estudiar i avaluar diferents sistemes de subrefredament mecànic que suposin una millora del comportament energètic de les instal·lacions de refrigeració de CO_2 transcrític.

L'escalfament global és un dels principals problemes de la societat actual i per reduir les emissions de CO_2 responsables de l'escalfament global, s'han establert diferents regulacions i directives tant a nivell mundial com europeu. En concret, les reglamentacions que afecten directament la refrigeració, responsable de gairebé el 8% d'aquestes emissions, regulen o prohibeixen l'ús de certs refrigerants a les instal·lacions. Això deixa el CO_2 com a la millor solució que es pot implementar en refrigeració comercial centralitzada.

La problemàtica sorgeix sobretot en climes càlids, on els cicles simples de CO_2 no són gaire eficients i per tant, si bé fem front als problemes derivats de les emissions directes, les emissions indirectes són més grans que les dels sistemes utilitzats fins a l'actualitat.

En aquesta tesi, per tant, el focus està posat en la millora de l'eficiència dels sistemes esmentats gràcies a l'ús de sistemes de subrefredament. En concret se centra en dos sistemes, anomenats cicle de subrefredament mecànic dedicat (DMS) i subrefredament mecànic integrat (IMS). El primer, el subfredament mecànic dedicat, té un gran potencial de millora encara que utilitza un refrigerant diferent del CO_2 al cicle auxiliar. Per la seva banda, el subfredament mecànic integrat, molt menys estudiat, únicament treballa amb CO_2, cosa que pot resultar un avantatge important.

L'estudi termodinàmic d'aquests sistemes és fonamental per establir quines són les aplicacions a les quals poden donar servei i determinar-ne els límits de funcionament. Per això s'han desenvolupat diferents anàlisis termodinàmiques dels dos sistemes i també del sistema de referència per poder conèixer el comportament d'aquests nous sistemes i també el comportament davant dels diferents paràmetres d'operació. D'aquests estudis s'ha deduït que són sistemes que s'han d'optimitzar tant en termes de pressió de gas-cooler com de grau de subfredament.

Com a continuació a aquesta primera anàlisi, s'ha dissenyat i muntat una planta experimental de laboratori, que integra totes les tecnologies esmentades i on s'han estudiat tots els sistemes.

Com a resultat, s'han determinat experimentalment les pressions i els graus de subrefredament òptims de cadascun dels sistemes i s'han obtingut els principals paràmetres energètics dels sistemes sota diferents condicions: nivells d'evaporació propers als -5ºC, -10ºC i -15ºC i temperatures de focus calent de 25ºC, 30ºC i 35ºC. Alhora, també s'ha estudiat l'ús de barreges zeotròpiques al sistema de subrefredament mecànic dedicat i s'han analitzat diferents configuracions del sistema integrat.

Finalment, s'han comparat els dos sistemes experimentalment davant del sistema de referència, el compressor paral·lel, comprovant els efectes positius dels dos sistemes i quantificant-ne les millores aconseguides.

Els principals resultats experimentals mostren que l'IMS proporciona increments en COP de 4.1% a 25.0ºC, 7.2% a 30.4ºC i 9.5% a 35.1ºC i el DMS de 7.8%, 13.7% i 17.5% respectivament en comparar-los amb l'ús del compressor paral·lel per a un nivell d'evaporació proper als -10ºC. D'aquests resultats es pot concloure que el millor sistema, des del punt de vista energètic, és el DMS, ja que aconsegueix increments més significatius.

Acknowledgements

I would like to thank Rodri who, a lot of years ago, gave me the opportunity to start on this beautiful path that we did not know where it would lead us. Thank you for having taught me everything you know and what we have discovered together, be it related to research, teaching or even climbing. The goal has been always to get as far as possible. And thank you for becoming a good friend. I would also like to thank the rest of the Thermal Engineering Group, for their collaboration over these years.

I want to thank the entities that have participated into the funding of this thesis too: the Ministerio de Educación, Cultura y Deporte de España for the pre-doctoral grant FPU16/00151 in the program Ayudas para la formación de profesorado universitario (FPU) 2016, the Generalitat Valenciana for the pre-doctoral grant ACIF/2017/194 in the program Promoción de la Investigación Científica, el Desarrollo tecnológico y la Innovación en la Comunitat de Generalitat Valenciana, 2017 and the mobility grant EST21/00293, of the program Subprograma Estatal de Formación en I+D+i del Ministerio de Universidades de España, 2021, that funded part of the research carried in this work.

I would also like to express my gratitude to Prof. Angelo Maiorino from Università degli Studi di Salerno for taking me into his group on both my research stays, one virtual due to the current situation and fortunately the last one face-to-face.

I would also thank Prof. Samer Sawalha from KTH Royal Institute of Technology in Stockholm for giving me the opportunity to do a research stay with them even though it ultimately could not take place.

I would also like to express my gratitude to the people at Universitat Jaume I who have accompanied me on this path and have let me be part of this family, including academic and extra-academic events. Especially to Daniel and Nuria, who have been a fundamental pillar of my live during these years and I am sure that many more will be, even if our paths diverge. Thanks for being my social bubble. And I am not forgetting Gabriele, thank you for helping me in the development of this thesis and for always being there for whatever I need. Thanks to my friends who have followed me over these years and greatly appreciate what I do.

Thanks to my family and Ángel for having made me the person I am today, for having given me strength to continue through difficult times and for having included the word "subcooling" into your dictionary.

Contents

List of figures

List of tables

List of tables

Chapter 1 Introduction

1. Introduction

1.1. Motivation

One of the challenges of current refrigeration is the development of cold production technologies that are respectful with the environment, both in the efficiency of the equipment and in the use of refrigerants with low environmental impact. The exponential growth of the world population, industrialization and globalization have made global warming of the planet one of the biggest problems that humanity must face today.

The refrigeration sector is totally linked to the current lifestyle, it being necessary in many applications. From the most necessary, such as the preservation of food or medical materials, to those most related to comfort and quality of life, such as air conditioning. In turn, it is also necessary for many industrial processes and other applications. Population growth and the universal use of cooling technologies make refrigeration one of the sectors with a significant environmental impact. The International Institute of Refrigeration (IIR) estimates that the global amount of refrigeration and air-conditioning systems is near 5 billion and it consumes about 20% of the overall electricity used worldwide in 2014 [1]. According to the IIR, the refrigeration sector is responsible of around 7.8% of global GHG emissions, 37% of this global-warming impact is due to direct emissions (leakage) of fluorinated refrigerants (HFCs) and 63% are due to indirect emissions.

Two lines of action can be followed to drive centralized commercial refrigeration towards a more sustainable technology.

The first of these resides in the reduction of direct emissions into the atmosphere. This is totally related to the refrigerant used. For this, various regulations and directives have already established limits that regulate the use of refrigerants based on their global warming potential. The Kigali Amendment [2] to the Montral Protocol intend to phase down progressively the use of HFCs and and the F-gas [3] establishes the limit for centralized commercial refrigeration plants with a power greater than 40kW in a GWP lower than 150. This is intended to reduce the direct impact of refrigeration caused by gas emissions from leaks. Within the availability of refrigerant gases with a GWP below 150, not all of them can ensure the necessary safety conditions for implementation in premises with large influx of people as would be its use in supermarkets. Some of these refrigerants can be toxic or flammable, not being suitable for use in these facilities. This makes CO_2 one of the only alternatives as a refrigerant in centralized commercial refrigeration. CO_2, a natural refrigerant and with almost no environmental impact, has good thermophysical properties although its characteristic critical point, at relatively low

temperature (30.9ºC) and high pressure (73.9bar), make it a refrigerant with certain peculiarities to consider when it is implemented.

The second line of action focuses on equipment and installations, trying to make them as efficient as possible in order to reduce their indirect effect, i.e. the environmental impact associated with electricity consumption. In reference to this action, the use of CO_2 makes this even more important, since the efficiency of classic CO_2 systems is drastically reduced when ambient temperatures exceed 15ºC [4]. For the improvement of the equipment, there are currently various trends that seek to improve the efficiency of CO_2 systems: the use of the parallel compressor, the use of ejectors and the combination with other systems or subcooling systems.

All these aspects have meant that the centralized commercial refrigeration sector has undergone a very pronounced evolution in the last decade. CO_2 appeared in supermarkets as a fluid in subcritical cascades in the early 1990s. It was not until the beginning of the 2000s that the first transcritical system was implemented in a supermarket. It took 10 years to start implementing solutions that would improve the efficiency of these systems. The rapid evolution of CO_2 systems can be seen in the growth of the number of supermarkets that work with these systems nowadays.

It is estimated that there are more than 35500 transcritical CO_2 installations globally today, of which 29000 are located in Europe, where the 90% of the installations are concentrated in supermarkets [5]. The global distribution of CO_2 facilities can be seen in Figure 1.1. From the image it can be deduced that this growth is clearly motivated by the directives and regulations applied in each continent.

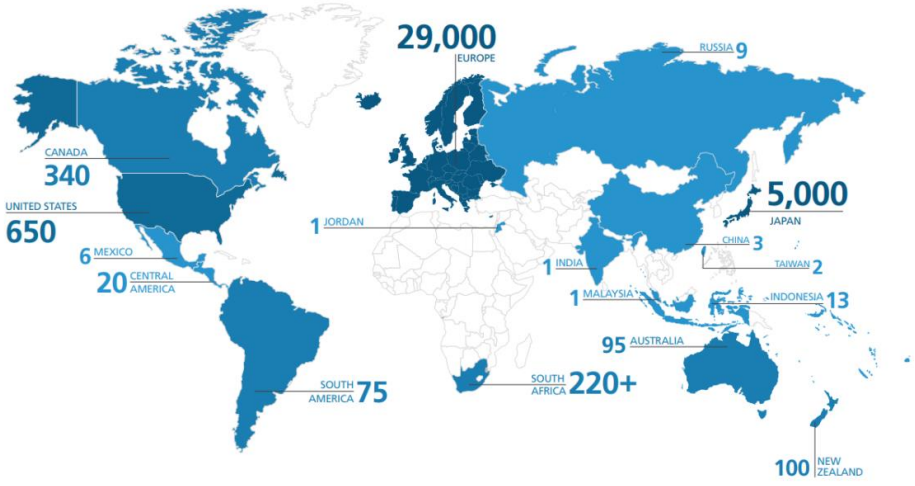

Figure 1.1. CO_2 transcritical installations around the world in 2020 [5].

Table 1.1 shows the number of CO_2 transcritical plants installed in supermarkets from 2008 to 2018. It can be seen how the number of facilities was really small in 2008 and that it grew significantly in the following 10 years. However, the most notable growth is that carried out between 2018 and 2020, that is, in a 2-year period where the number of installations in Europe grew by 81%, 76% in the United States and 375% in Australia.

Table 1.1. Number of transcritical CO_2 installations [5].

	2008	2018	2020	Growth (from 2018 to 2020)
Europe	140	16000	29000	81%
U.S.		370	650	76%
Canada		245	340	39%
Japan		3530	5000	42%
Australia		20	95	375%
New Zealand		40	100	150%
South Africa		110	220	100%

Transcritical CO_2 systems used nowadays are not only applied to centralized commercial refrigeration but can also be found in other applications [6], such as:

- Small store applications: convenience stores.
- Commercial applications: supermarkets, retail.
- Industrial applications: refrigerated warehousing, cold storage, wineries and breweries, bakeries.
- Food and drinks processing.
- Niche applications or others: ice rinks, ski slopes, cruise ships, fast food, pharmaceutical processes and laboratories, product testing…

Even so, the main objective of this thesis is the commercial application, for which the European directive is more restrictive and therefore solutions for high-capacity plants will be sought.

1.2. Research context and background

As mentioned above, CO_2 systems are less efficient than those that work with HFCs, especially in hot climates [7] and they were not widely implemented until the present decade. However, research on these systems started many years before and presents a large number of scientific productions.

Figure 1.2 outlines chronologically the evolution of the implementation of CO_2 systems as well as the main improvements that are the subject of this research. CO_2 was first

implemented in subcritical cascades and it was at the beginning of the 21st century when the first transcritical plants appeared in supermarkets. As one of the main improvements of CO_2 plants, the parallel compressor began to be implemented around 2008 and following this, many other improvements emerged such as the different types of ejector (2012), the dedicated mechanical subcooling (2015) and the integrated mechanical subcooling (2019). These last two, together with the parallel compressor, are object of study in this thesis.

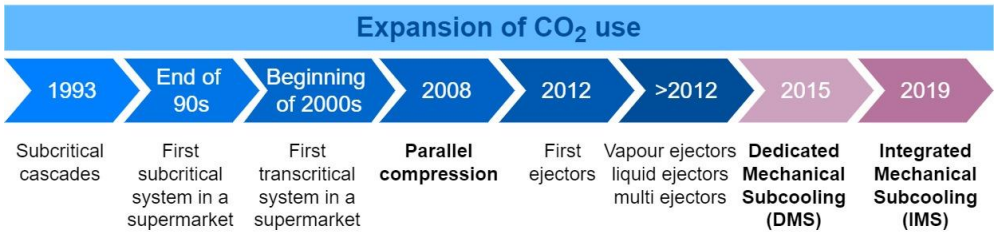

Figure 1.2. Expansion of the use of CO_2 and the evolution of the systems over the years (adapted from [6]).

Girotto's work [7] confirmed the low efficiency of CO_2 systems but concluded there was room for improvement, believing that these differences could be cut [8] thermodynamically analyzed different CO_2 systems including the basic single-stage cycle and the single-throttling with two-stage compression cycle. In this study the operation parameters were optimized and results showed that the most elaborate cycles present the greatest improvement, especially for the heaviest operating conditions.

The parallel compression (PC) applied to transcritical refrigerating CO_2 cycle, first appeared in theoretical studies that showed its improvements when compared with the traditional cycle [9]. These reported benefits were increments in COP and cooling capacity and also reductions on the optimal operation pressure. The optimization of this system also showed the necessity of optimizing both, the upper and the intermediate pressure [8].

The optimization of the cycle with parallel compression economization showed that this system is more effective at lower evaporator temperature and offers maximum COP improvements up to 47.3% compared to the basis CO_2 cycle at evaporation temperature of -55ºC and 60ºC of gas-cooler exit temperature [10]. The increments obtained at 30ºC were near 40%.

The experimental evaluation of a reciprocating prototype working with CO_2 with parallel compression was presented in 2011 [11]. The study focused on the parallel compressor behavior showing a high influence of the intermediate pressure on the efficiency of the

compressor and the system. It was also found that the increase of the intermediate pressure leads to a degradation in performance.

Experimental analysis of a CO_2 parallel compressor in flash tank configuration was performed without optimizing the intermediate pressure [12]. First theoretical studies were performed to define the limitations of the system and later the experimental tests were made with a fixed parallel compressor speed, so the maximum improvements were not reached.

The application of parallel compressor to supermarket facilities was investigated based on field measurements and showed that booster systems with PC were the best performant at that moment [13]. Combining parallel compression with heating and air conditioning allowed obtaining a COP increment of 8% in a Swedish supermarket. [14, 15].

Among several supermarket configurations in warm climates, the CO_2 parallel compression turned out to be a configuration that achieved energy savings comparable to that of cascade systems [16].

From a numerical model with good correlation to experimental data obtained from a fully instrumented test rig machine, the increase in the COP reached by using a PC is up to 10% in usual operating conditions, without optimizing the intermediate pressure [17].

Studies of the parallel compression for different weather conditions showed that it was the most energy efficient system for moderate and warm climates. Energy efficiency improvement was of 5.0% for the warm climate and 3.6% for the moderate climate when comparing to the conventional CO_2 booster [18]. PC has become the state-of-the-art system in Europe [19].

There are several studies that focus on this system. However, few analyze it in depth in a simple cycle. In addition, the optimization of the intermediate pressure is lacking since in supermarkets this pressure normally remains fixed [20].

The easiest way to improve the performance is through a subcooling performed using an internal heat exchanger (IHX). However, the improvements achieved with this system are limited; even so, its installation is very frequent since it acts as a security element.

Its performance was analyzed experimentally and a maximum increment on cooling capacity of 12% and also 12% in COP were measured for a gas-cooler outlet temperature of 34ºC and -15ºC in the evaporator [21]. The negative aspect of the use of this heat exchanger is the increase in the compressor discharge temperature.

Specifically, in this study, an increase of 10K was measured for the evaporation level of -15ºC.

The inclusion of the IHX significantly increases the COP when the heat exchanger has a reasonable size, which has been proved by an experimental validation of a numerical simulation [22]. The benefits are higher when higher the ambient temperature is.

It was experimentally proved that different positions of the IHX can be considered, obtaining the best improvements when using two IHX, one at the exit of the gas-cooler and the other at the exit of the liquid receiver [23].

An alternative solution for the improvement of CO_2 systems is the use of gas ejectors in booster systems. It is an element that improves the operation of the plants at high dissipation temperatures, acting on two fundamental aspects: reduces the flow transferred by the medium temperature compressors and increases the pressure of the refrigerant in the medium temperature service without using additional electrical energy consumption. The ejector has a very specific operation curve so it only works in optimal conditions for a given condition. That is why ejector systems capable of working in a wider range of operation have been developed, among them the multi-ejector [24] or the variable geometry ejector [25].

The multi-ejector, consisting of several fixed ejectors working in parallel, showed improvements in supermarket CO_2 facilities with heat recovery [26].

Evaluating the ejector experimentally, increments in COP of 7% were measured [27]. Another positive aspect of the use of this element is the exergy efficiency of the plant, which reached an improvement up to 13.7%.

Numerical results showed that the use of one group or two groups of ejectors, combined with PC allow the power consumption to be further diminished compared to the system onfly with PC. Reductions are around 5% and 8% at 30°C, respectively [28].

What is clear about the ejector and its peculiar operation is the imperative need to optimize its control and regulation strategies. Upwards of 4% in COP can be lost due to not properly controlling high-side pressure [29]. Vortex control on the adjustable motive nozzle inlet of the ejector can also be used to improve the COP of the system by adjusting the high-side pressure by 8.1% [30].

The complexity of the ejector makes its simulation in numerical models very difficult. In order to better characterize these systems, a performance map was designed that

allowed predicting their behavior with 89.3% of the data within 20% accuracy [31]. This may be a first step to improving system model fidelity.

However, it is a technology totally linked to the companies that manufacture it, and furthermore its effectiveness is not interesting outside of a narrow range of application. This casts doubt on whether it is the best solution to improve CO_2 installations. Also, this technology still needs a more remarkable development.

A totally different technology to the ejector is found in the dedicated mechanical subcooling (DMS), being one of the options proposed to improve CO_2 performance through subcooling [32]. It is a simple vapor compression cycle thermally connected to the transcritical CO_2 cycle through a subcooler placed after the gas-cooler. The aim of the cycle is to subcool the CO_2 thanks to an auxiliary cycle working with a higher COP than the CO_2 cycle. This technology was put into value from a theoretical study that showed the possible improvements introduced by this system [33]. Improvements are up to a 20% in COP optimizing gas-cooler pressure but not yet the degree of subcooling. In this study, the interest of this system was seen for temperatures above 25ºC. Experimentally, the potential of this system was verified with R-1234yf as DMS refrigerant [34], where maximum COP improvements of 30.3% were measured, again without optimizing the degree of subcooling.

The applicability of this system for hot climates and for evaporation temperatures above -15ºC was proven against the use of cascade systems [35]. This strongly promoted the study of this system as an improvement of transcritical CO_2.

The full theoretical optimization of this system leads to significant improvements in COP up to 43.8% [36]. The use of zeotropic mixtures whose temperature glide fits well with the CO_2 temperature profile in the subcooler can also be beneficial based on the studies found [37]. This hypothesis was experimentally proven, achieving additional COP increases of up to 1.4% [38]. After that, the experimental optimization of the system was performed and maximum achievable COP was obtained with R-152a [39].

DMS has also been implemented in booster systems with significant improvement in both capacity and efficiency at all operating conditions with the DMS [40].

The design of the DMS has to be optimized depending on the application and there is an important factor to be controlled: the gas-cooler pressure. Compared the the PC or the subcooling performed through a water chiller dedicated to HVAC it turns to be the most effective solution [41]. The importance of optimizing the operation parameters considering a thermoeconomic analysis is more crucial at hot climates, where the highest benefits are found [42].

The DMS has also been implemented in heat pump applications where a reduction of annual energy consumption of 8.65% can be reached in comparison with simple CO_2 system [43]. Combined with cascade systems, improvements can be increased up to 19.4% in the whole heating season [44]. When using the DMS for space heating applications, it is the medium-temperature as well as the high pressure the operation parameters that must be optimized [45, 46].

From the review of subcooling methods [32], a new mechanical subcooling system took interest: the integrated mechanical subcooling (IMS), which performed the subcooling only using CO_2. Presented first as a patent [47] for enhancing the COP, theoretical studies have shown a possible increment of COP up to 17.3% at -10ºC of evaporation temperature and 30ºC at the gas-cooler exit [8], which showed its potential interest but was not studied in greater depth. The system was optimized thermodynamically [48] and then the operating parameters were optimized experimentally [49].

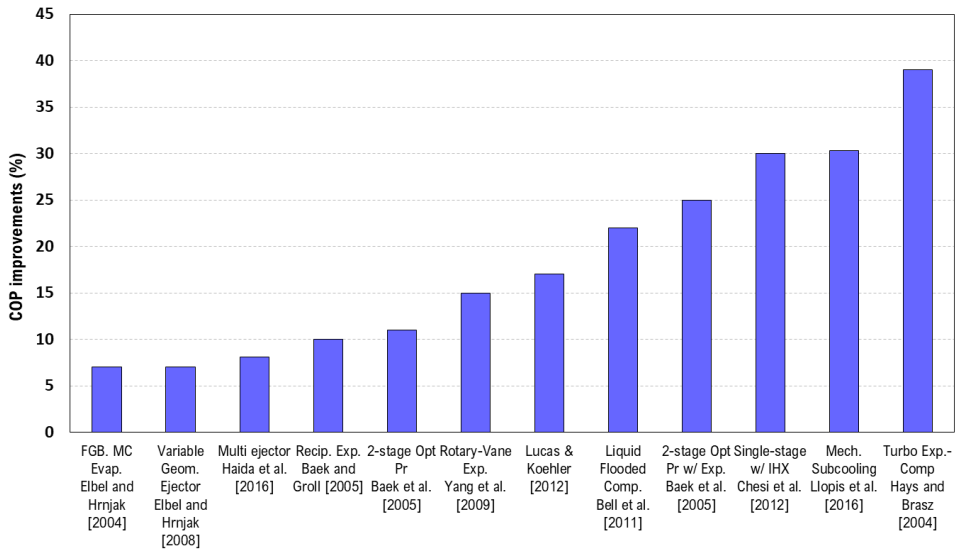

Figure 1.3. Summary of potential COP improvements of modifications to transcritical CO_2 cycles [51].

Thermodynamic models of the IMS and the DMS in CO_2 booster systems for supermarket applications achieved annual energy consumption reductions in relation to the configuration with parallel compressor. The DMS offers annual energy reductions for tempered places up to 2.9%, for warm up to 3.4% and for hot until 5.1%. The IMS obtains reductions of 4.0% for cold regions, up to 2.9% for tempered, up to 3.4% for warm and to 2.4% for hot regions [50]. These figures show the interest of these systems, which achieve improvements even when comparing them with the PC

reference system, which already achieves notable increases in COP. Therefore, the need to quantify these improvements experimentally is evident.

As presented in Figure 1.3, mechanical subcooling is one of the best COP improvements achived experimentally up to the moment [51] so it deserves future research.

Figure 1.4 summarizes the main contributions to the field of CO_2 carried out by the research group in which this thesis is developed and more specifically the contributions of this thesis. All the referenced papers are experimental works. Those represented by a blue circle are CO_2-only systems and those with a green circle use an additional fluid other than CO_2.

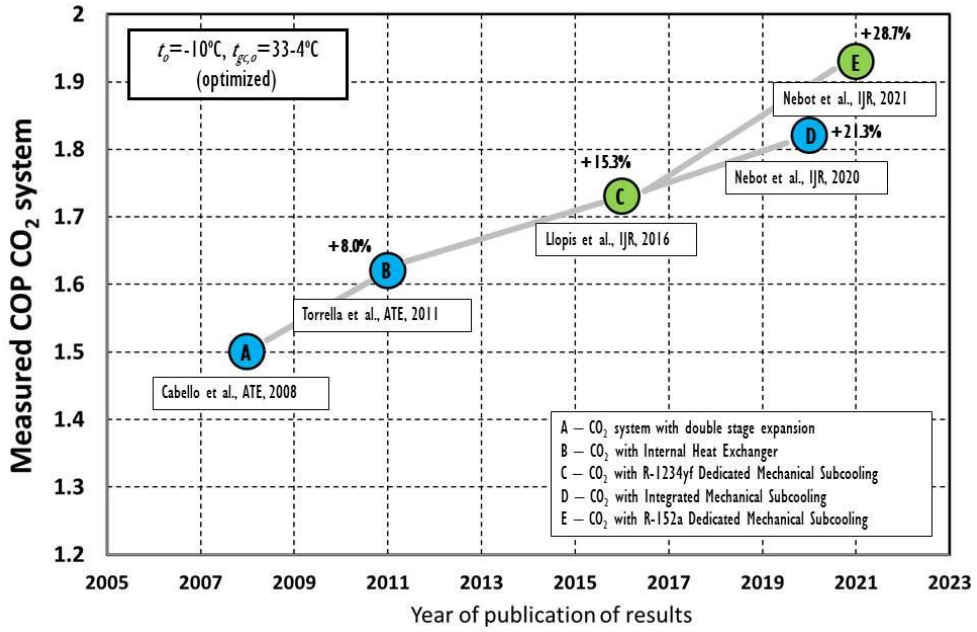

Figure 1.4. Evolution of the experimental results of COP CO_2 systems over the years obtained by the research group G.I.T.

The use of the internal heat exchanger (point B) represented a significant improvement in terms of COP compared to the simple CO_2 cycle [21]. Subsequently, with the appearance of dedicated mechanical subcooling (point C), which was tested without optimizing the subcooling values, an increase of 15.3% in COP was achieved [34]. It is at this point where the present thesis begun to be developed, following the line of study of subcooling systems, specifically those of mechanical subcooling. Two systems are studied in parallel: the dedicated mechanical subcooling (DMS) and the integrated mechanical subcooling (IMS). This second has the advantage of working only with CO_2

and the results of its experimental test (point D) show increases of up to 21.3% working under optimal conditions of subcooling degree and pressure [49]. Subsequently, the DMS system was experimentally analyzed [39], working with R-152a, this time under optimal operating conditions (point E), reaching increases of 28.7%.

From this graphic summary it can be concluded that there is a clear line of research followed by the present work and that it contributes very important results to the scientific field.

1.3. Identified gaps and research questions

From this research background, different gaps and research questions that had to be resolved are identified.

The main solution that was being proposed at that time to improve the efficiency of CO_2 systems was the use of the ejector, a complicated technology totally linked to companies. The different manufacturers that worked with this solution proposed this element as a black box, of which its exact operation is unknown. To this had to be added its high market price. So, an existing problem is that there are no free technologies available in the market to enhance CO_2 cycles.

Parallel compressor can be considered the baseline or the state-of-the-art system [19]. However, its study has not been deepened to the point of optimization. Since its use in booster systems is common, the intermediate pressure is not optimized since it is marked by the value of the pressure in the liquid receiver. Even so, all operating pressures of the system with PC should be optimized, since it is considered the reference system and therefore, must work at its best operating point. Numerical optimizations of this type of system are found, but all the experimental tests have some limitation in this regard. Therefore, another of the gaps found is that the base line not really optimized.

In the literature there are studies about mechanical subcooling systems, but these are not complete or are not experimentally optimized. The question that arises is whether once these systems are optimized and experimentally tested, they will continue to achieve improvements with respect to the base cycle as shown in the theoretical studies. And how important these differences are.

1.4. Objectives of the thesis

In order to solve the questions arising from the current state-of-the-art, the main objectives of this thesis are:

- To perform a theoretical comparison of the mechanical subcooling systems and compare them with the current reference system: the parallel compressor.
- To propose an organized summary of the possible subcooling methods existing nowadays.
- To propose an experimental test methodology to determine the maximum COP of transcritical CO_2 plants with mechanical subcooling systems both integrated and dedicated.
- To determine the optimal operating parameters that maximize the COP of the transcritical CO_2 plants with parallel compression and dedicated and integrated mechanical subcooling systems.
- To compare mechanical subcooling systems versus parallel compressor solution and determine the energy efficiency improvements achieved.

Figure 1.5. Objectives of the thesis.

1.5. Structure of the thesis

This thesis is organized in twelve chapters. The first of them is the introductory chapter where the objectives and structure of the thesis are stated. The second chapter summarizes the methodology used in the development of this thesis, both for theoretical studies and experimental tests where a laboratory plant has been built up. The main body of the document, between chapters 3 and 11, presents the results of the

work carried out, organized based on the objectives of the thesis and adapted from articles published in high-impact journals. Next, in chapter 12, the conclusions of the work, future research and the contributions that this thesis has made to the state of the art are presented.

It is important to notice that the structure of each chapter corresponds to the structure of the published article, although they have been adapted to the format of the present document. At the beginning of each chapter, the journal in which it is published is specified as well as the co-authors who have contributed to this work.

Chapter 3 presents the comparison of the mechanical subcooling systems, specifically the DMS, against the use of cascade cycles. Both cycles have in common the use of two compressors, an additional heat exchanger and a refrigerant different from CO_2. The theoretical simulation is based on compressors' curves obtained from experimental data and is analyzed for an environment temperature range between 15ºC and 40ºC and evaporation temperatures between -20ºC and 5ºC. Given the range of work, both transcritical and subcritical behavior are studied, defining the transition zone between both modes.

For the first time, the influence of the subcooling degree on the COP of the system with dedicated mechanical subcooling is analyzed. The analysis of the operating conditions shows the existence of an optimal subcooling degree for which the COP is maximum.

As main results, the working limit between subcritical and transcritical has been defined for systems with DMS. The ambient temperature at which the system begins to work in transcritical conditions is 25.3ºC. It was also concluded that the cascade configuration using CO_2 as low temperature refrigerant will have highest performance than the DMS cycle when the temperature lift between the cold and heat sources is higher than 28.5 K.

Finally, the analysis is extended to different climatic conditions, studying its operation throughout a whole year. Under this assumption, it is concluded that the system with DMS offers better energy efficiency for evaporation levels above -15ºC for the whole-year operation. However, for evaporation levels of -20ºC, the cascade will be the most suitable system for its implementation.

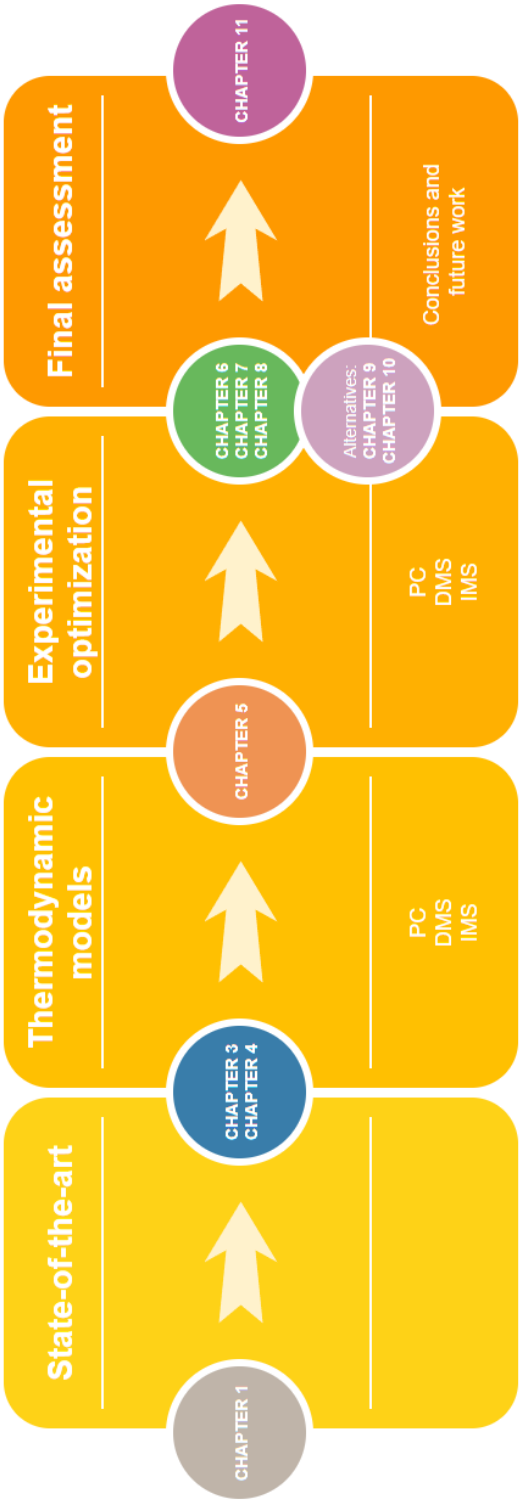

Figure 1.6. Structure of the thesis.

Chapter 4 presents a deep review of the state-of-the-art of subcooling methods for refrigeration with CO_2. First, it describes the effects of subcooling on CO_2 both for transcritical and subcritical conditions, analyzing the benefits of the subcooling but also its cost. Subcooling methods are divided into two types: internal methods or dedicated methods. Among the internal methods we can found the internal heat exchanger, in different positions, the economizer or subcooler, the integrated mechanical subcooling and heat storage systems. Regarding the dedicated methods, the dedicated mechanical subcooling, the thermoelectric subcooling systems and other hybrid systems are found.

From this review, it was concluded that the dedicated mechanical subcooling had a lot of potential and needed to be studied deeper since the results found in literature showed the evaluation of this system without optimization. This second chapter gives an idea of the possibilities of enhancing CO_2 systems through subcooling and of what was done until the moment.

In addition, it brings to light, another system with a long potential for improvement, the integrated mechanical subcooling system, which until that moment was not practically analyzed for its use with CO_2. This gives rise to its study, both theoretical and experimental; in order to better understand its operation and its limits of improvement.

Chapter 5 studies from a thermodynamic point of view the CO_2 cycle with integrated mechanical subcooling. For this study an IMS cycle with extraction from the gas-cooler outlet is considered and a simple thermodynamic model based on the operation of real components is performed.

This chapter studies the main energy parameters of the cycle, cooling capacity and COP, taking into account the need to optimize the degree of subcooling and the gas-cooler pressure in order to maximize the COP. The optimum gas-cooler pressure and subcooling degree are optimized, after demonstrating the existence of an optimum COP, and the energy parameters of the cycle are evaluated for different evaporation temperatures, between -15ºC and 5ºC and environment temperatures from 0 to 40ºC.

The cycle is also analyzed from a second law approach, concluding that the gas-cooler and the compressor are the components where more irreversibilities are found and the subcooling reduces the exergy destruction of the expansion process. The performance of the cycle is also compared to that of a base cycle with IHX, obtaining increments in COP of 11.7% for an evaporating level of 5ºC, 12.9% at 0ºC, 14.8% at -5ºC and 15.9% at -10ºC for environment temperatures of 35ºC. The IMS also allows reductions of the optimum pressure up to 12 bar for the highest ambient temperatures.

Chapter 6 presents the experimental evaluation of a single CO_2 cycle with two-stage expansion and liquid receiver with an integrated mechanical subcooling cycle where the extraction is performed at the subcooler outlet. The experimental plant is presented as well as the measuring system, which will be the same for the evaluation of the other systems presented in the following chapters. Test methodology, used to find the optimum working conditions of the cycle, is described.

The process followed to identify the degree of subcooling and the gas-cooler pressure that make the COP maximum is detailed as well as the execution and conditions of each test.

Then the optimum points for the three evaluated heat rejection levels and cold sink temperatures are presented, including COP, cooling capacity and optimum subcooling degree and gas-cooler pressure. In addition, two correlations made to find the optimum parameters that maximize the COP are stated based on these experimental results.

Chapter 7 is the experimental determination of the optimum parameters of the CO_2 transcritical refrigeration plant working with an R-152a dedicated mechanical subcooling. The laboratory plant used in this study is the same as the one used in the previous chapter, with some differences as the heat exchanger of the subcooler since in this system, the heat exchange is performed between CO_2 and the DMS fluid, it being R-152a. The description of the plant is presented as well as the test procedure. Energy parameters as COP and cooling capacity corresponding to the maximum COP for each condition are presented as main results.

Optimum gas-cooler pressure and subcooling degree are determined and two correlations are obtained to kwon these optimum conditions as a function of the evaporation and gas-cooler outlet temperatures.

Chapter 8 presents the experimental evaluation of a commercial transcritical CO_2 refrigeration plant with parallel compression. The CO_2 refrigeration system with parallel compressor is considered today as the state-of-the-art in commercial refrigeration applications. Contrary to the two previous chapters, the experimentation of this system aims to define an operating parameter that is different from that of subcooling systems: it is the intermediate pressure. In this chapter, therefore, the optimization of the COP of the system is presented through the search of the optimal gas-cooler pressure and the intermediate pressure.

In addition to the main energetic results presented in this chapter due to the optimization of the system, there are also certain limits of operation that have been

found as a result of the experimentation and that cause that the operation of said system deviated from the theoretical optimal working point.

Chapter 9 presents the experimental evaluation of the CO_2 transcritical refrigeration plant with dedicated mechanical subcooling working with different zeotropic mixtures as refrigerant. The evaluated fluids on the DMS are the mixtures composed of R-600, of R-32, CO_2 and R-152a and their performances are compared to the pure fluid R-152a. First, in this chapter, a theoretical study is carried out with the aim of identifying the most profitable mixtures. Once the mixtures are identified they were tested on the experimental plant under the same test conditions and the energy performance was compared. The three refrigerant blends tested on the laboratory facility are R-152a/R32 [60/40%], R-600/R-152a [60/40%] and R-152a/CO_2 [90/10%].

Results show that the best mixture is R-600/R-152a [60/40%], incrementing COP up to 1.4% with respect to the pure fluid, corroborating Baomin's theory but also demonstrating that the energetic behavior of the global installation will not vary excessively depending on the fluid used in the DMS.

Chapter 10 presents three different configurations of the integrated mechanical subcooling. These configurations depend on the extraction point of the CO_2. It can be extracted from the exit of the gas-cooler, the exit of the subcooler and the liquid vessel. The aim of this chapter is to compare the differences in the behavior of the three different configurations. For doing that, all configurations have been evaluated under the same test conditions.

The results do not show significant differences regarding the maximum COP of each of the systems, concluding that the three configurations have practically identical energy performance.

The results referring to the cooling capacity and the optimal working pressure do not show significant differences either. However, different optimal subcooling degrees are obtained for each of the configurations. This results in a different cooling capacity in the subcooler for each system, this being less for the configuration with extraction from the gas-cooler outlet. This can have consequences on the design of the exchanger and therefore on the cost of the system.

The operating points of the auxiliary compressor are also analyzed, seeing that for all the conditions tested, the compressor is outside the application limits established by the manufacturer. This can lead to a drop in overall performance and also forces the need to design CO_2 compressors adapted to this application.

Chapter 11 sumps up all the evaluated systems and establishes a comparison between the mechanical subcooling methods versus the parallel compressor. Despite the benefits of the integrated mechanical subcooling system (IMS), which only uses CO_2 as the refrigerant, it is seen in this chapter that the dedicated mechanical subcooling system (DMS) has greater benefits in terms of performance. This chapter presents both the energetic results of the three main systems analyzed in this thesis as well as the increments in COP obtained by the subcooling systems with respect to the parallel compressor. The increments are 4.1%, 7.2% and 9.5% with the IMS for 25.0ºC, 30.4ºC and 35.1ºC of heat dissipation temperature and 7.8%, 13.7% and 17.5% with the DMS respectively.

The main conclusions and contributions to the scientific field derived from this thesis the as well as possible future research to be carried out are presented in **Chapter 12**.

1.6. References

[1] Dupont J. L. DP, Lebrun P., Ziegler F. The Role of Refrigeration in the Global Economy (2019), 38th Note on Refrigeration Technologies. 2019. p. 12.
[2] Nations U. Amendment to the Montreal Protocol on Substances that Deplete the Ozone Layer. Kigali 2016.
[3] European Commission. Regulation (EU) No 517/2014 of the European Parliament and of the Council of 16 April 2014 on fluorinated greenhouse gases and repealing Regulation (EC) No 842/2006. 2014.
[4] Hafner A, Hemmingsen AK. R744 refrigeration technologies for supermarkets in warm climates. Conference R744 refrigeration technologies for supermarkets in warm climates. p. 2313-20.
[5] Publications S. World Guide to Transcritical CO_2 Refrigeration - Part II. 2020.
[6] Publications S. World Guide to Transcritical CO_2 Refrigeration - Part I. 2020:182.
[7] Girotto S, Minetto S, Neksa P. Commercial refrigeration system using CO_2 as the refrigerant. International Journal of Refrigeration. 2004;27(7):717-23.
[8] Cecchinato L, Chiarello M, Corradi M, Fornasieri E, Minetto S, Stringari P, et al. Thermodynamic analysis of different two-stage transcritical carbon dioxide cycles. International Journal of Refrigeration. 2009;32(5):1058-67.
[9] Minetto S, Cecchinato L, Corradi M, Fornasieri E, Zilio C, Schiavon A. Theoretical and experimental analysis of a CO_2 refrigerating cycle with two-stage throttling and suction of the flash vapour by an auxiliary compressor. IIR International conference on thermophysical properties and transfer processes of refrigerants. Vicenza (Italy)2005.
[10] Sarkar J, Agrawal N. Performance optimization of transcritical CO_2 cycle with parallel compression economization. International Journal of Thermal Sciences. 2010;49(5):838-43.
[11] Bella B, Kaemmer N. Experimental Performance of Carbon Dioxide Compressor with Parallel Compression. DKV-Tagung. Aachen (Germany)2011.

[12] Chesi A, Esposito F, Ferrara G, Ferrari L. Experimental analysis of R744 parallel compression cycle. Applied Energy. 2014;135:274-85.
[13] Sawalha S, Karampour M, Rogstam J. Field measurements of supermarket refrigeration systems. Part I: Analysis of CO_2 trans-critical refrigeration systems. Applied Thermal Engineering. 2015;87:633-47.
[14] Karampour M, Sawalha S. Integration of heating and air conditioning into a CO_2 trans-critical booster system with parallel compression Part I: Evaluation of key operating parameters using field measurements. Conference Integration of heating and air conditioning into a CO_2 trans-critical booster system with parallel compression Part I: Evaluation of key operating parameters using field measurements. p. 323-31.
[15] Karampour M, Sawalha S. Integration of heating and air conditioning into a CO_2 trans-critical booster system with parallel compression part II: Performance analysis based on field measurements. Conference Integration of heating and air conditioning into a CO_2 trans-critical booster system with parallel compression part II: Performance analysis based on field measurements. p. 332-40.
[16] Gullo P, Elmegaard B, Cortella G. Advanced exergy analysis of a R744 booster refrigeration system with parallel compression. Energy. 2016;107:562-71.
[17] Fritschi H, Tillenkamp F, Löhrer R, Brügger M. Efficiency increase in carbon dioxide refrigeration technology with parallel compression. International Journal of Low-Carbon Technologies. 2017;12(2):171-80.
[18] Tsamos KM, Ge YT, Santosa I, Tassou SA, Bianchi G, Mylona Z. Energy analysis of alternative CO_2 refrigeration system configurations for retail food applications in moderate and warm climates. Energy Conversion and Management. 2017;150:822-9.
[19] Karampour M, Sawalha S. State-of-the-art integrated CO_2 refrigeration system for supermarkets: A comparative analysis. International Journal of Refrigeration. 2018;86:239-57.
[20] Catalán-Gil J, Sánchez D, Llopis R, Nebot-Andrés L, Cabello R. Energy evaluation of multiple stage commercial refrigeration architectures adapted to F-gas regulation. Energies. 2018;11(7).
[21] Torrella E, Sánchez D, Llopis R, Cabello R. Energetic evaluation of an internal heat exchanger in a CO_2 transcritical refrigeration plant using experimental data. International Journal of Refrigeration. 2011;34(1):40-9.
[22] Rigola J, Ablanque N, Pérez-Segarra CD, Oliva A. Numerical simulation and experimental validation of internal heat exchanger influence on CO_2 trans-critical cycle performance. International Journal of Refrigeration. 2010;33(4):664-74.
[23] Sánchez D, Patiño J, Llopis R, Cabello R, Torrella E, Fuentes FV. New positions for an internal heat exchanger in a CO_2 supercritical refrigeration plant. Experimental analysis and energetic evaluation. Applied Thermal Engineering. 2014;63(1):129-39.
[24] Danfoss. Multi Ejector Solution for R744 (CO_2). https://assets.danfoss.com/documents
[25] Carel. Electronic Modulating Ejector. https://www.carel.com/documents.

[26] Hafner A, Försterling S, Banasiak K. Multi-ejector concept for R-744 supermarket refrigeration. International Journal of Refrigeration. 2014;43:1-13.
[27] Haida M, Banasiak K, Smolka J, Hafner A, Eikevik TM. Experimental analysis of the R744 vapour compression rack equipped with the multi-ejector expansion work recovery module. International Journal of Refrigeration. 2016;64:93-107.
[28] Pardiñas ÁÁ, Hafner A, Banasiak K. Novel integrated CO_2 vapour compression racks for supermarkets. Thermodynamic analysis of possible system configurations and influence of operational conditions. Applied Thermal Engineering. 2018;131:1008-25.
[29] Lawrence N, Elbel S. Experimental investigation on control methods and strategies for off-design operation of the transcritical R744 two-phase ejector cycle. International Journal of Refrigeration. 2019.
[30] Zhu J, Elbel S. Experimental investigation into the influence of vortex control on transcritical R744 ejector and cycle performance. Applied Thermal Engineering. 2020;164.
[31] Haider M, Elbel S. Development of ejector performance map for predicting fixed-geometry two-phase ejector performance for wide range of operating conditions. International Journal of Refrigeration. 2021;128:232-41.
[32] Llopis R, Nebot-Andrés L, Sánchez D, Catalán-Gil J, Cabello R. Subcooling methods for CO_2 refrigeration cycles: A review. International Journal of Refrigeration. 2018;93:85-107.
[33] Llopis R, Cabello R, Sánchez D, Torrella E. Energy improvements of CO_2 transcritical refrigeration cycles using dedicated mechanical subcooling. International Journal of Refrigeration. 2015;55(0):129-41.
[34] Llopis R, Nebot-Andrés L, Cabello R, Sánchez D, Catalán-Gil J. Experimental evaluation of a CO_2 transcritical refrigeration plant with dedicated mechanical subcooling. International Journal of Refrigeration. 2016;69:361-8.
[35] Nebot-Andrés L, Llopis R, Sánchez D, Catalán-Gil J, Cabello R. CO_2 with mechanical subcooling vs. CO_2 cascade cycles for medium temperature commercial refrigeration applications thermodynamic analysis. Applied Sciences (Switzerland). 2017;7(9).
[36] Dai B, Liu S, Sun Z, Ma Y. Thermodynamic Performance Analysis of CO_2 Transcritical Refrigeration Cycle Assisted with Mechanical Subcooling. Conference Thermodynamic Performance Analysis of CO_2 Transcritical Refrigeration Cycle Assisted with Mechanical Subcooling, vol. 105. p. 2033-8.
[37] Dai B, Liu S, Li H, Sun Z, Song M, Yang Q, et al. Energetic performance of transcritical CO_2 refrigeration cycles with mechanical subcooling using zeotropic mixture as refrigerant. Energy. 2018;150:205-21.
[38] Llopis R, Toffoletti G, Nebot-Andrés L, Cortella G. Experimental evaluation of zeotropic refrigerants in a dedicated mechanical subcooling system in a CO_2 cycle. International Journal of Refrigeration. 2021;128:287-98.
[39] Nebot-Andrés L, Sánchez D, Calleja-Anta D, Cabello R, Llopis R. Experimental determination of the optimum working conditions of a commercial transcritical CO_2

refrigeration plant with a R-152a dedicated mechanical subcooling. International Journal of Refrigeration. 2021;121:258-68.
[40] Bush J, Beshr M, Aute V, Radermacher R. Experimental evaluation of transcritical CO_2 refrigeration with mechanical subcooling. Science and Technology for the Built Environment. 2017;23(6):1013-25.
[41] D'Agaro P, Coppola MA, Cortella G. Effect of dedicated mechanical subcooler size and gas cooler pressure control on transcritical CO_2 booster systems. Applied Thermal Engineering. 2021;182.
[42] Cortella G, Coppola MA, D'Agaro P. Sizing and control rules of dedicated mechanical subcooler in transcritical CO_2 booster systems for commercial refrigeration. Applied Thermal Engineering. 2021;193.
[43] Dai B, Zhao X, Liu S, Yang Q, Zhong D, Cao Y, et al. Heating and cooling of residential annual application using DMS transcritical CO_2 reversible system and traditional solutions: An environment and economic feasibility analysis. Energy Conversion and Management. 2020;210.
[44] Cheng JH, He YJ, Zhang CL. New scenario of CO_2 heat pump for space heating: Automatic mode switch between modified transcritical and cascade cycle in one system. Applied Thermal Engineering. 2021;191.
[45] Song Y, Ye Z, Wang Y, Cao F. The experimental verification on the optimal discharge pressure in a subcooler-based transcritical CO_2 system for space heating. Energy and Buildings. 2018;158:1442-9.
[46] Song Y, Cao F. The evaluation of the optimal medium temperature in a space heating used transcritical air-source CO_2 heat pump with an R134a subcooling device. Energy Conversion and Management. 2018;166:409-23.
[47] Lesage G, Kantchev J. Mechanical subcooling of transcritical R-744 refrigeration systems with heat pump heat reclaim and floating head pressure. Google Patents; 2013.
[48] Nebot-Andrés L, Calleja-Anta D, Sánchez D, Cabello R, Llopis R. Thermodynamic analysis of a CO_2 refrigeration cycle with integrated mechanical subcooling. Energies. 2019;13(1).
[49] Nebot-Andrés L, Catalán-Gil J, Sánchez D, Calleja-Anta D, Cabello R, Llopis R. Experimental determination of the optimum working conditions of a transcritical CO_2 refrigeration plant with integrated mechanical subcooling. International Journal of Refrigeration. 2020;113:266-75.
[50] Catalán-Gil J, Llopis R, Sánchez D, Nebot-Andrés L, Cabello R. Energy analysis of dedicated and integrated mechanical subcooled CO_2 boosters for supermarket applications. International Journal of Refrigeration. 2019.
[51] Barta RB, Groll EA, Ziviani D. Review of stationary and transport CO_2 refrigeration and air conditioning technologies. Applied Thermal Engineering. 2021;185.

Chapter 2 Methodology

2. Methodology

This chapter describes the methodologies used for the development of this thesis. First, the calculation models and the main assumptions of the theoretical approach are described. Then, the optimization process used to calculate the analyzed systems is detailed. Finally, the experimental methodology is presented, which includes the assembly of the installation and its components, configuration of the data logger and signal processing, and the procedure for conducting tests as well as the experimental optimization process.

2.1. Simulation and model calculations

The first step of this thesis was the numerical simulation of the studied cycles to understand their operation, to define the operating ranges and also to select the necessary components for the assembly of the installation.

The main assumptions that have been taken into account and the optimization process carried out to find the maximum COP of each system are detailed below. Later, in each chapter, each specific case is explained in more detail.

2.1.1. Main assumptions

The initial calculations of the systems were carried out establishing some operating parameters, which were maintained for the simulation of all the arquitectures, which are:

For all systems, the gas-cooler outlet temperature was calculated considering a temperature approach with respect to environment temperature, as described by Eq. (2.1).

$$t_{gc,o} = t_{env} + app \tag{2.1}$$

The temperature approach between gas-cooler outlet temperature and environment temperature was set to 5K when working in subcritical conditions and 2K in transcritical.

$$SUB = t_{gc,o} - t_{sub,o} \tag{2.2}$$

Firstly, the heat transfer in the subcooler was simulated considering a temperature difference between the evaporation temperature and the temperature at subcooler exit temperature. This temperature difference was of 2K for transcritical conditions where heat exchange was favourable and 5K for subcritical conditions [1].

$$t_{0,sub} = t_{sub,o} - \Delta t \tag{2.3}$$

Once first experimental results were performed, the efficiency of the subcooler was analyzed and corroborated that the temperature difference considered was consistent, even conservative [1].

The three auxiliary cycles, the DMS, the IMS and also the PC were driven by a variable speed compressor. Volumetric and global efficiencies of the compressors were calculated with Eq. (2.4) with the coefficients presented in Table 2.1 and Table 2.2. These curves correspond to the operation at nominal speed, obtained from manufacturer's data.

$$\eta_V = \eta_G = a_0 + a_1 \cdot p_{suc} + a_2 \cdot p_{dis} + a_3 \cdot \left(\frac{p_{dis}}{p_{suc}}\right) + a_4 \cdot v_{suc} \quad (2.4)$$

Table 2.1. Coefficients of the CO_2 compressor curves for the main compressor with a $\dot{V}_G$ of 3.48 $m^3 \cdot h^{-1}$ and the IMS/PC compressor of 1.12 $m^3 \cdot h^{-1}$.

Transcritical operation				**Subcritical operation**			
η_V **Eq. (2.4)**		η_G **Eq. (2.4)**		η_V **Eq. (2.4)**		η_G **Eq. (2.4)**	
a_0	1.0473	a_0	0.7634	a_0	1.0350	a_0	0.4868
a_1	0.0031	a_1	-0.0021	a_1	0.0019	a_1	-0.0086
a_2	-0.0030	a_2	0.0013	a_2	-0.0017	a_2	0.0115
a_3	0.0012	a_3	-0.0571	a_3	-0.0588	a_3	-0.2687
a_4	-11.1282	a_4	0.5425	a_4	-3.6174	a_4	20.8432

Table 2.2. Coefficients of the curves of the DMS compressor with a $\dot{V}_G$ of 4.06 $m^3 \cdot h^{-1}$.

Subcritical operation			
η_V	**Eq. (2.4)**	η_G	**Eq. (2.4)**
a_0	0.9926	a_0	0.9692
a_1	-0.099	a_1	-0.1178
a_2	0.0248	a_2	0.0263
a_3	-0.0786	a_3	-0.0495
a_4	0.7683	a_4	-0.6042

The main compressor was considered to be operated at its nominal speed but the auxiliary compressors can modify the velocity in order to adapt the cooling power to the subcooling requirements. To consider the difference rotational speeds, nominal refrigerant mass flow was obtained from Eq. (2.4) and (2.5).

$$\dot{m}_{nom} = \eta_v \cdot \frac{\dot{V}_G}{v_{suc}} \quad (2.5)$$

The mass flow rate required to perform the desired subcooling was obtained from an energy balance in the subcooler for the subcooling systems and the energy balance in the vessel for the PC system. The mass flows were obtained as follows:

- Parallel compression:

$$\dot{m}_{PC} = \dot{m}_0 \cdot \frac{(h_{gc,o} - h_{0,in})}{(h_{suc,PC} - h_{gc,o})} \quad (2.6)$$

- Dedicated mechanical subcooling:

$$\dot{m}_{DMS} = \dot{m}_0 \cdot \frac{(h_{gc,o} - h_{sub,o})}{(h_{suc,DMS} - h_{exp,DMS})} \quad (2.7)$$

- Integrated mechanical subcooling (extracting from gas-cooler exit):

$$\dot{m}_{IMS} = \dot{m}_0 \cdot \frac{(h_{gc,o} - h_{sub,o})}{(h_{suc,IMS} - h_{gc,o})} \quad (2.8)$$

A linear relationship between the mass flow transferred by the compressor and its rotational speed was considered. Therefore, the desired rotational speed can be estimated thanks to the Eq. (2.9). In the same way, a linear relationship between the power consumption and the rotation speed was considered, calculated as Eq. (2.10).

$$N = 1450 \cdot \frac{\dot{m}_{aux}}{\dot{m}_{nom}} \quad (2.9)$$

$$P_{c,aux} = P_{c,nom} \cdot \frac{N}{1450} \quad (2.10)$$

Where the nominal power consumption was:

$$P_{c,nom} = \frac{\dot{m}_{nom} \cdot (h_{dis,aux,s} - h_{suc,aux})}{\eta_{G,aux}} \quad (2.11)$$

The power consumption of the main compressor was calculated by Eq. (2.12).

$$P_{c,main} = \frac{\dot{m}_0 \cdot (h_{dis,s} - h_{suc})}{\eta_G} \quad (2.12)$$

The cooling capacity of the overall system was calculated as shown in Eq. (2.13).

$$\dot{Q}_0 = \dot{m}_0 \cdot (h_{suc} - h_{0,in}) \quad (2.13)$$

The enthalpy at the inlet of the evaporator ($h_{0,in}$) depends on the analyzed system:

- Parallel compression:

$$h_{0,in} = h_{vess,l,o} = f(p_{vess}, x = 0) \quad (2.14)$$

- Dedicated mechanical subcooling:

$$h_{0,in} = h_{sub,o} = f(p_{gc}, t_{sub,o}) \quad (2.15)$$

- Integrated mechanical subcooling:

$$h_{0,in} = h_{sub,o} = f(p_{gc}, t_{sub,o}) \tag{2.16}$$

Finally, the COP of the overall systems was analyzed as the division of the cooling capacity and the sum of the powers consumptions of the compressors:

$$COP = \frac{\dot{Q}_0}{P_{c,main} + P_{c,aux}} \tag{2.17}$$

2.1.2. Optimization

All the equations described above have been computed in Matlab 2016 and Refrop's complement [2], for their optimized study. The numerical model works with 4 variables as input to give as a result the main energy parameters as well as the intermediate calculations of the cycle. The inputs were the external working conditions: evaporation temperature (t_0) and environment temperature (t_{env}); and the operating conditions: gas-cooler pressure (p_{gc}) and subcooling degree (SUB).

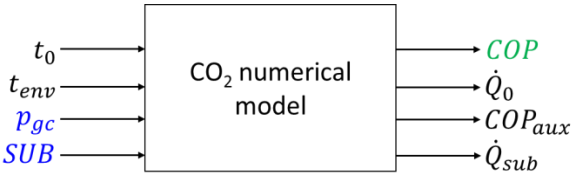

Figure 2.1. Scheme of computational model.

Figure 2.1 shows the scheme of the computational model. Inputs are placed at left side and the main outputs at the right side. Two inputs are marked in blue, gas-cooler pressure and subcooling degree. These are the variables that were modified in the optimization procedure, to find the highest value of COP (green).

The optimization procedure is described in Figure 2.2. For given conditions of evaporation and environment temperature, the COP of the overall system was calculated with an initial value of p_{gc} and SUB. Then, gas-cooler pressure was increased by steps of 0.01 bar until the new value of COP was lower than the previous one. Once the optimum pressure was found, the procedure was repeated with the subcooling degree, increasing it by steps of 0.01 K. When the optimum subcooling degree was found, gas-cooler pressure was optimized again, since for each degree of subcooling the optimum pressure is different. This process was repeated in a loop until the COP value no longer increases.

The maximum point COP corresponds to the optimum working point and the pressure and subcooling degree for which this maximum value is achieved will be the optimum gas-cooler pressure and the optimum subcooling degree.

All systems were studied and compared among them in optimum conditions.

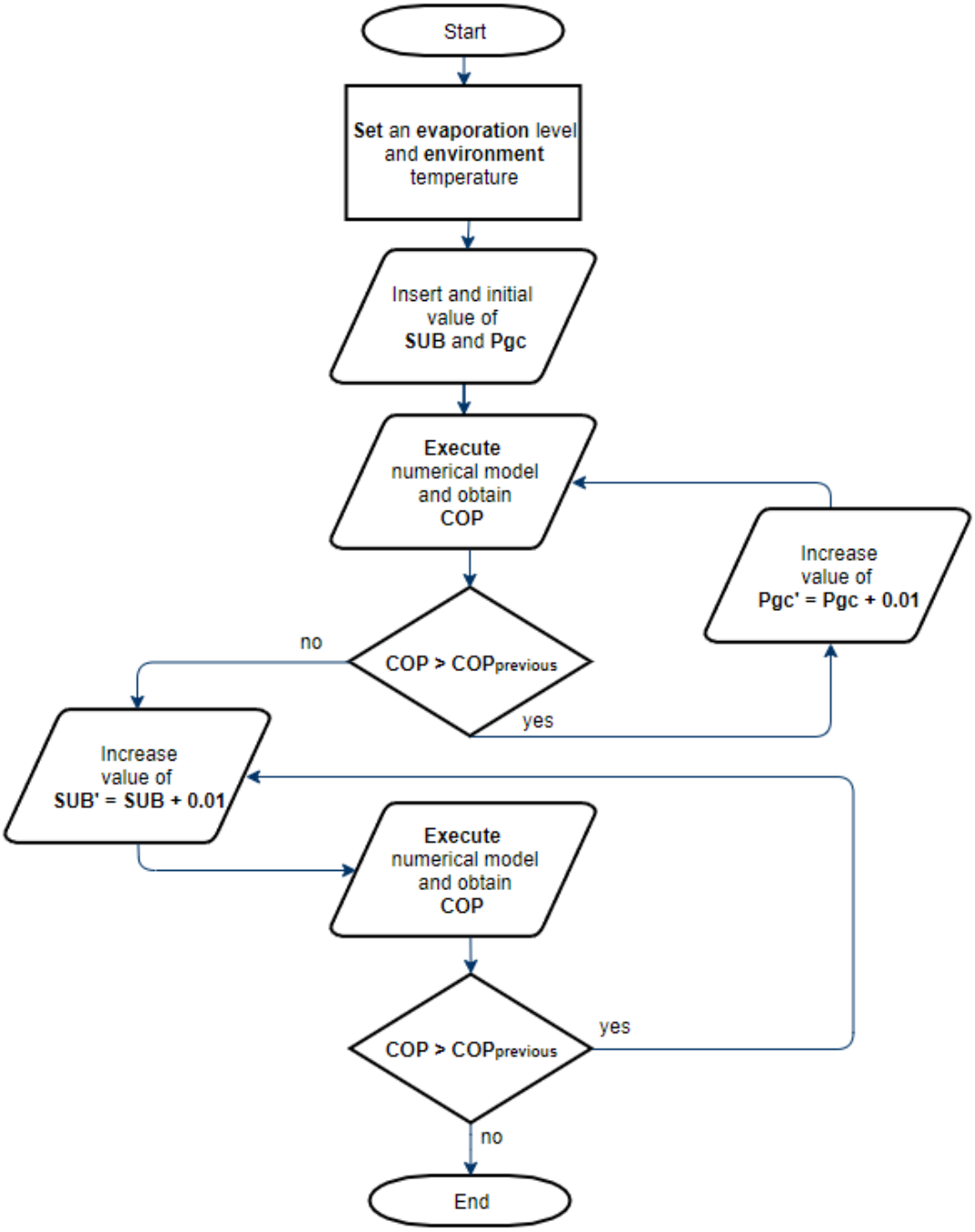

Figure 2.2. Optimization process of the numerical model.

2.2. Experimental plant

In this section, the entire process that has been carried out for the construction and start-up of the transcritical CO_2 plant is exposed, with the possibility of testing a multitude of solutions to achieve energy improvements. It covers from the design of the cycles to be tested, deduced from the theoretical simulations presented in the previous section, selection of components, elements of measurement and data acquisition, assembly and handling of the installation.

When sizing the installation, it has been taken into account which configurations need to be integrated into the experimental plant. The main configurations of the installation are:

- Base cycle
- Cycle with internal heat exchanger (IHX)
- Cycle with parallel compression (PC)
- Cycle with dedicated mechanical subcooling (DMS)
- Cycle with integrated mechanical subcooling (IMS)
    - Extracting from gas-cooler exit
    - Extracting from subcooler exit
    - Extracting the liquid tank

Therefore, the installation consists of the base cycle, which can be tested with or without an internal heat exchanger and it can also be tested with a parallel compressor or the two different mechanical subcooling systems. In turn, the IMS cycle was designed with three different configurations, in order to determine which was the most beneficial. The different configurations can be enabled or disabled thanks to the use of by-passes and several valves.

2.2.1. Main components common to all the cycles

All the cycles mentioned in the previous section are evaluated in the same test bench and with the aim of comparing them; they are built with the same components. Only the specific components of each cycle are different. Therefore, the main components are common to all cycles. These are: the main compressor, the expansion system, the evaporator, the gas-cooler and the liquid accumulation tank and they are detailed below.

Main compressor

The main compressor is a semi-hermetic compressor able to work in supercritical conditions at high pressures. It is a single stage compressor from the Italian manufacturer DORIN, model DORIN TCS340/4-D (Figure 2.3), with a compression displacement of 3.48 m^3/h at 1450 rpm with nominal power of 4 kW. The recommended working range is shown in Figure 2.4.

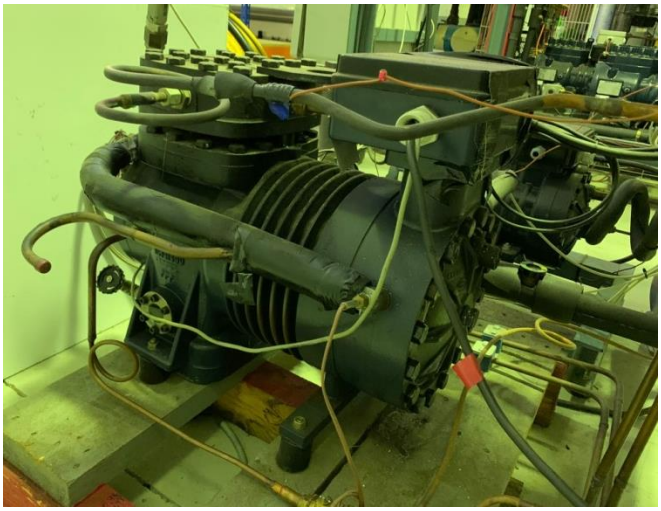

Figure 2.3. TCS340/4-D CO_2 main compressor.

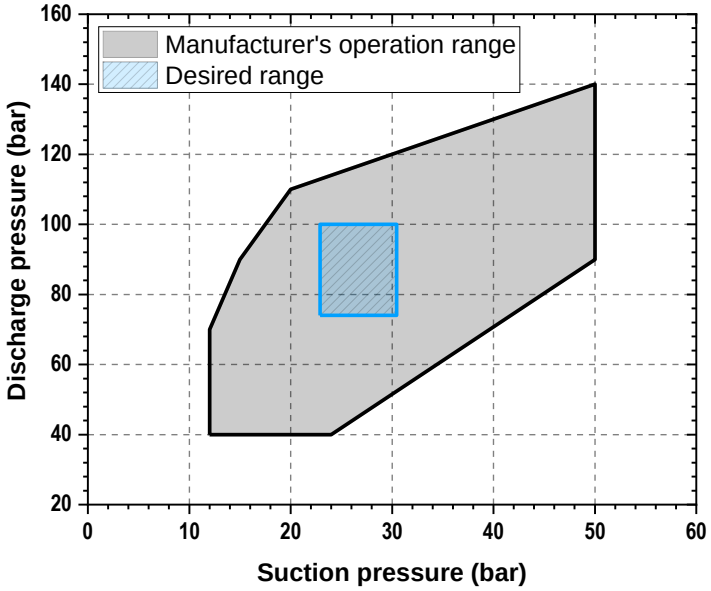

Figure 2.4. Working range of the TCS340/4-D compressor.

The objective of this thesis is to evaluate mechanical subcooling systems for CO_2 in applications where this system is the most appropriate solution. In other words, the aim is to study the evaporation temperature range between -15ºC and -5ºC, always under transcritical conditions (pressures higher than the critical pressure) as it will be justified in Chapter 3. The desired work area to be evaluated is drawn in Figure 2.4 in blue. As it

can be observed, it is inside the manufacturer's operation range so the compressor fits well the necessities for this thesis.

Back-pressure valve

The back-pressure valve is one of the most important components of the plant since for ensuring the correct operation of the systems it is necessary to precisely control the pressure in the high line. The expansion device is composed of three components (back-pressure valve, liquid tank and expansion valve) in order to regulate simultaneously the superheat in the evaporator and the pressure in the gas-cooler. The back-pressure valve is responsible of regulating this pressure.

In the initial plant there was a manually regulated back-pressure valve, the blue valve observed in Figure 2.5. In order to improve the control and the performance of the tests, said valve was replaced by an electronic expansion valve, controlled through an own PID controller to achieve the desired upstream pressure. The selected valve is an electronic expansion valve E2V18, shown in Figure 2.6 [3].

Figure 2.5. Previous back-pressure valve (blue) and new electronic back-pressure valve (red).

Figure 2.6. E2V18 Back-pressure valve.

Liquid vessel

The liquid tank is located after the back-pressure valve and it has a volume of 13.4 liters. This element is essential in this type of installation to be able to make the control of the heat rejection pressure independent from the evaporation level. In turn, this vessel allows the accumulation of the refrigerant mass so that the behavior of the plant is independent of its charge.

The tank has an inlet through the upper part where the CO_2 from the back-pressure valve enters and three possible outlets:

- a main outlet through the lower part where the liquid that will reach the evaporator is extracted.
- an outlet in the upper part from which CO_2 is extracted in saturated steam for its use in the PC system.
- another outlet from the bottom where liquid is extracted for one of the IMS configurations.

The liquid vessel with the different injection and suction points can be seen Figure 2.7 and the scheme of the tank in Figure 2.8.

Figure 2.7. Liquid vessel.

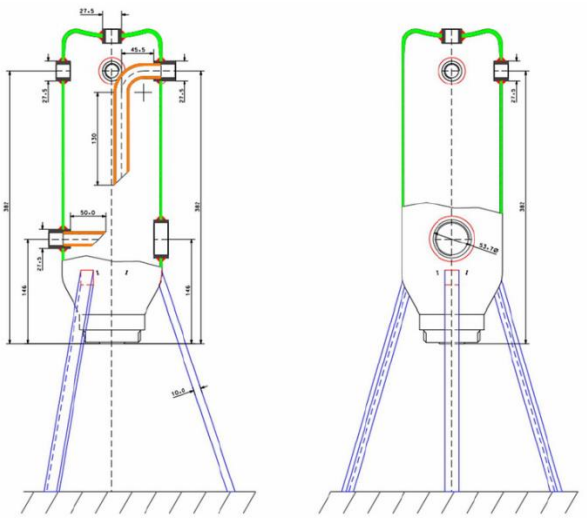

Figure 2.8. Scheme of the liquid vessel [4].

The tank also has a sight glass through which the liquid level can be observed. To ensure the correct operation of the installation, it is necessary that the liquid level is at the level of the sight glass or above, to ensure that the flow that is extracted from the lower part is liquid. In Figure 2.9 a photo of the tank can be seen, in which the liquid level can be observed in the sight glass.

Figure 2.9. Liquid vessel sight glass with liquid level.

Expansion valves

These valves should act as thermostatic valves, comtrolling the evaporation process. They are electronic expansion valves specific for CO_2 from the company Egelhof [5] and they are connected in parallel. They have a controller and two Pt1000 temperature gauges used to maintain a certain temperature difference in the evaporator.

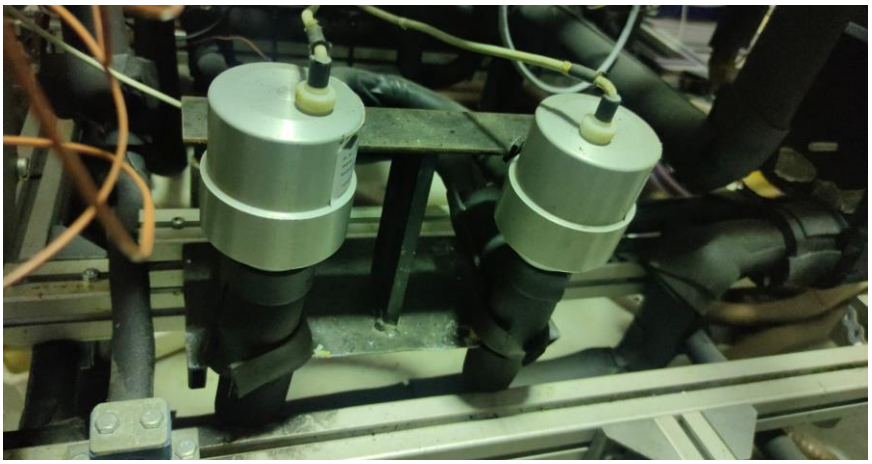

Figure 2.10. Expansion valves.

Evaporator

This heat exchanger that must work between the temperature ranges of -15ºC and -5ºC. The selected evaporator is a brazed plate heat exchanger with a heat transfer area of 4.794 m^2. The maximum cooling capacity it must exchange is 15 kW and the maximum pressure it must withstand is 45 bar. The heat exchanger is the CBXP52-96H-F of Alfa Laval [6], presented in Figure 2.11.

Figure 2.11. Evaporator brazed plate heat exchanger of 4.794 m^2 of exchange surface area.

The evaporator is connected countercurrent, for carbon dioxide in the primary side and a mixture of propylene glycol-water in the secondary side.

2.2.1.6. Gas-cooler

The gas-cooler is a countercurrent connected brazed plate heat exchanger with a heat transfer area of 1.224 m^2. The heat exchange is performed between CO_2 (hot side) and water (cold side). The selected heat exchanger is the AXP52-26M-F of Alfa Laval [7] which exchanges up to 19.35 kW and supports pressures up to 130 bar. The gas-cooler can be seen in Figure 2.12 and its scheme in Figure 2.13.

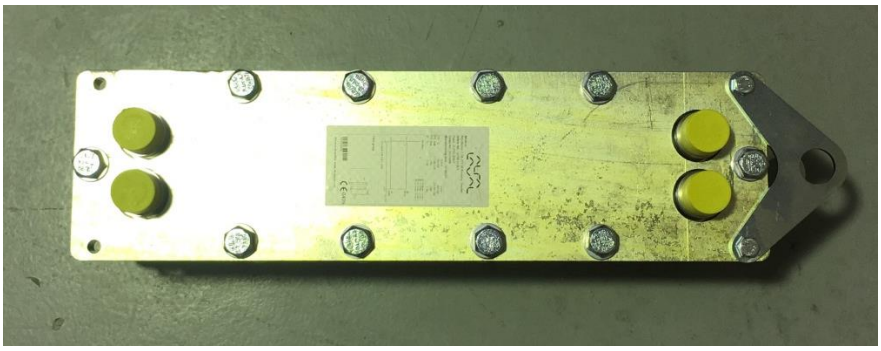

Figure 2.12. Gas-cooler brazed plate heat exchanger of 1.224 m^2 of exchange surface area.

All the heat exchangers are isolated with foam to reduce heat losses to the environment and ensure the correct exchange between both fluids. Figure 2.14 shows the isolated gas-cooler.

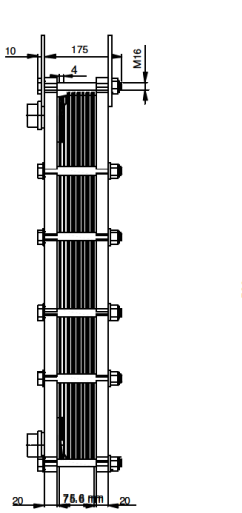

Figure 2.13. Gas-cooler AXP52-26M-F scheme.

Figure 2.14. Isolated gas-cooler.

2.2.2. Components of the IMS cycle

The IMS cycle is fully integrated within the CO_2 plant. There is a bifurcation installed in the main CO_2 pipeline from which a part of the flow is extracted to circulate through the IMS cycle and later be reintroduced in the main cycle. It is a simple compression cycle, the components of which are explained below. The IMS cycle is schematized in Figure 2.15 and marked in blue. In the configuration marked with A, the CO_2 is extracted from the gas-cooler outlet, in configuration B the extraction is performed from the subcooler exit and in C from the liquid tank. For all the three configurations, the CO_2 is injected in point 7.

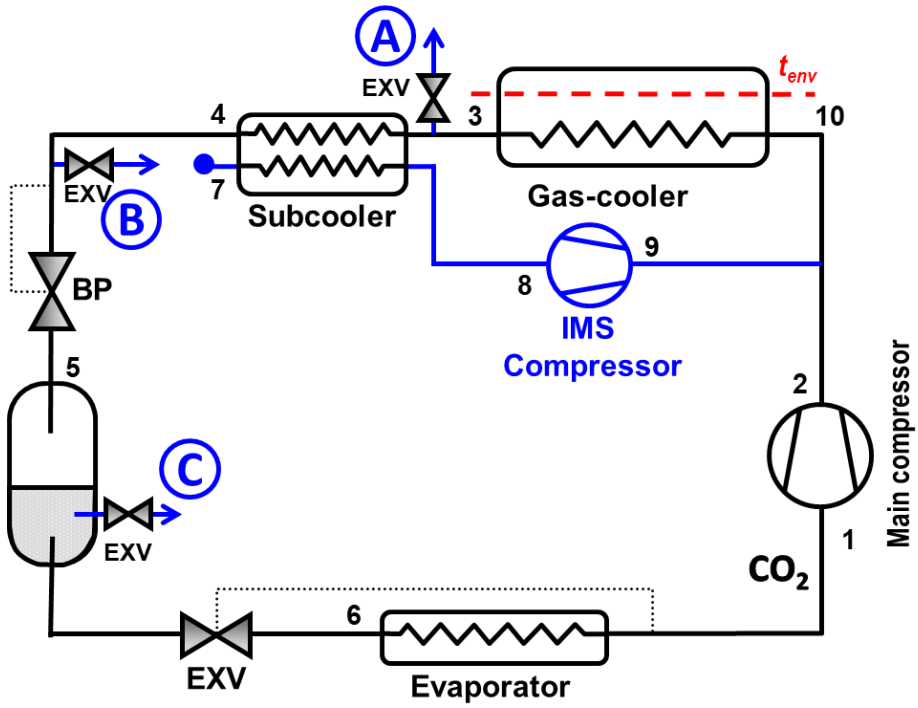

Figure 2.15. Scheme of all IMS configurations.

Compressor

The compressor selected for the IMS cycle is a DORIN [8] semi-hermetic compressor specific for transcritical CO_2. The selected model is the CD 150M (Figure 2.16) since it is the smallest in the range and for this specific application relatively low capacity is needed, around 2 kW. The compressor has been equipped with an inverter (Figure 2.17), which can be controlled remotely, to test different rotation speeds in order to find the optimum subcooling degree of the cycle.

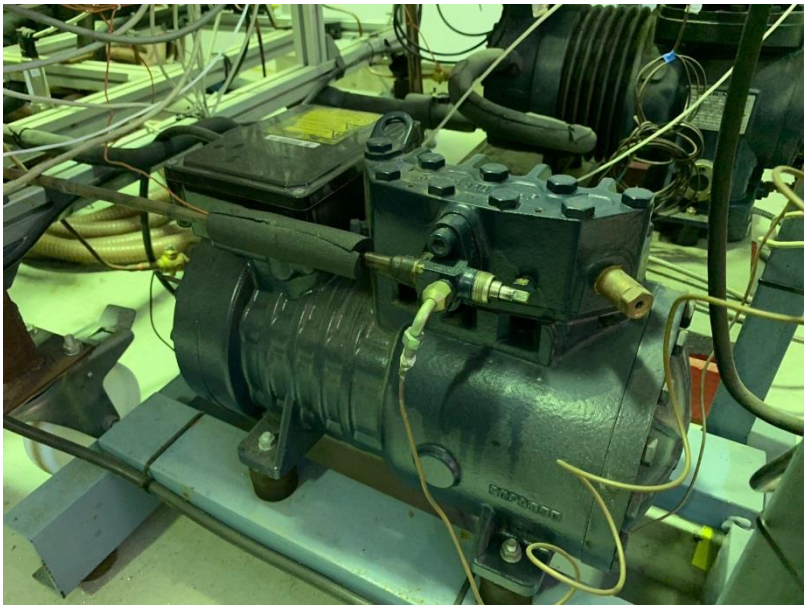

Figure 2.16. IMS compressor Dorin CD 150M.

Figure 2.17. Inverter of the IMS compressor.

The operation limits of the compressor are shown in Figure 2.18. As it can be seen, the range in which the tests need to be carried out is outside the limits established by the manufacturer. It should be mentioned that no commercial compressor of these characteristics has been found that allows working at such high evaporation temperatures.

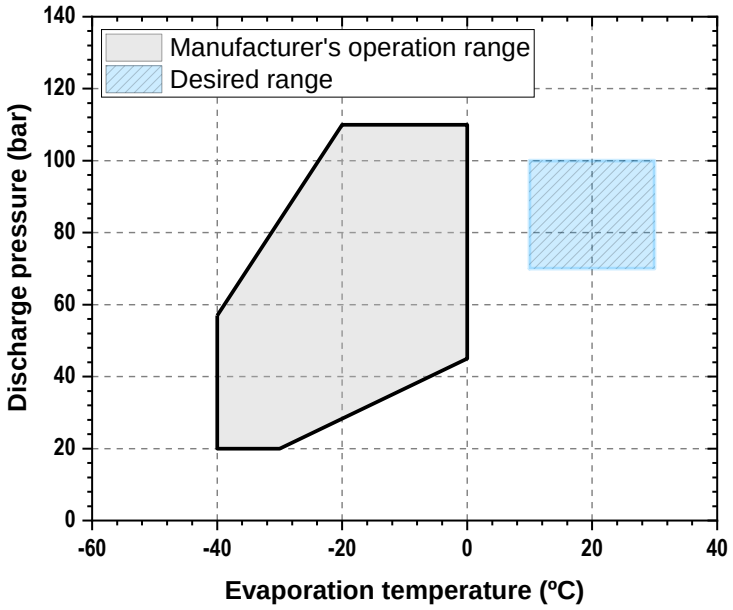

Figure 2.18. Working range of the CD 150M compressor.

Subcooler

The subcooler is a countercurrent brazed plate heat exchanger with a heat transfer area of 0.85 m^2. The heat exchange is performed between CO_2 in both sides. One of the CO_2 streams is subcooled after the gas-cooler exit and the other stream is evaporated. The selected heat exchanger is the AXP27-36H-F of Alfa Laval [7] which exchanges up to 9.91 kW, supports pressures up to 130 bar and is capable to work with temperatures between -20ºC and 150ºC. The scheme of the subcooler can be seen in Figure 2.19 and it is placed next to the gas-cooler (Figure 2.20).

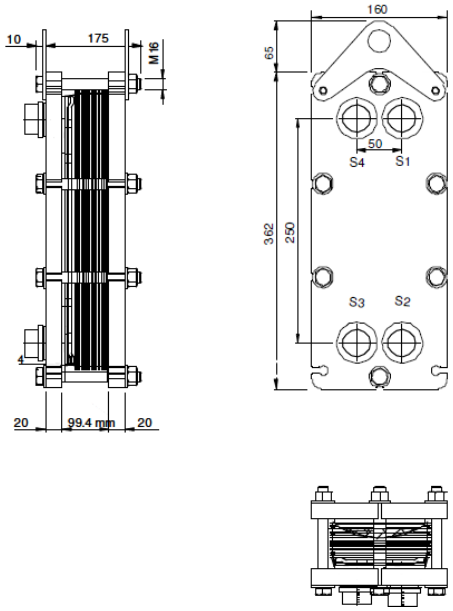

Figure 2.19. IMS subcooler AXP27-36H-F scheme.

Figure 2.20. Subcooler (left) and gas-cooler (right) on the test bench.

Expansion valve

The expansion valve, placed before the subcooler in the IMS stream is configurated to act as a thermostatic valve, maintaining a constant superheat at the evaporator outlet, which is set at 5 K. It is an electronic expansion valve for CO_2 from the company Carel, model E2V11 [3].

2.2.3. Components of the DMS cycle

The DMS cycle is mounted on a separate bench and can be connected and disconnected from the main cycle (Figure 2.21). It is a simple compression cycle, the components of which are explained below. The scheme of the plant with DMS is detailed in Figure 2.22 and where the DMS configuration is marked in blue.

Compressor

The compressor selected for the DMS is the Bitzer 2KES-05Y 230/400V(40S) [9] semi-hermetic, being the smaller of the range, since by varying its frequency between 30 and 45 Hz it is be possible to satisfy the cooling capacity needs in the subcooler.

Figure 2.21. DMS system.

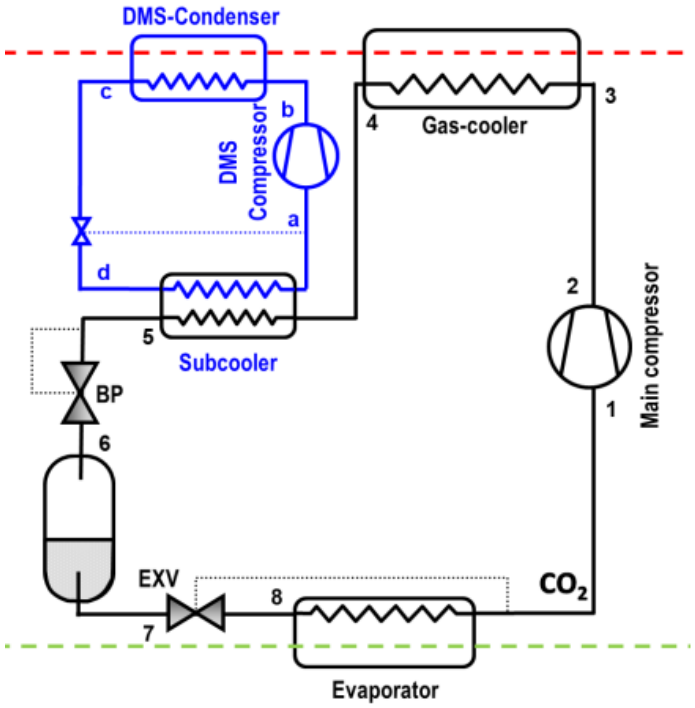

Figure 2.22. Scheme of the plant with DMS system.

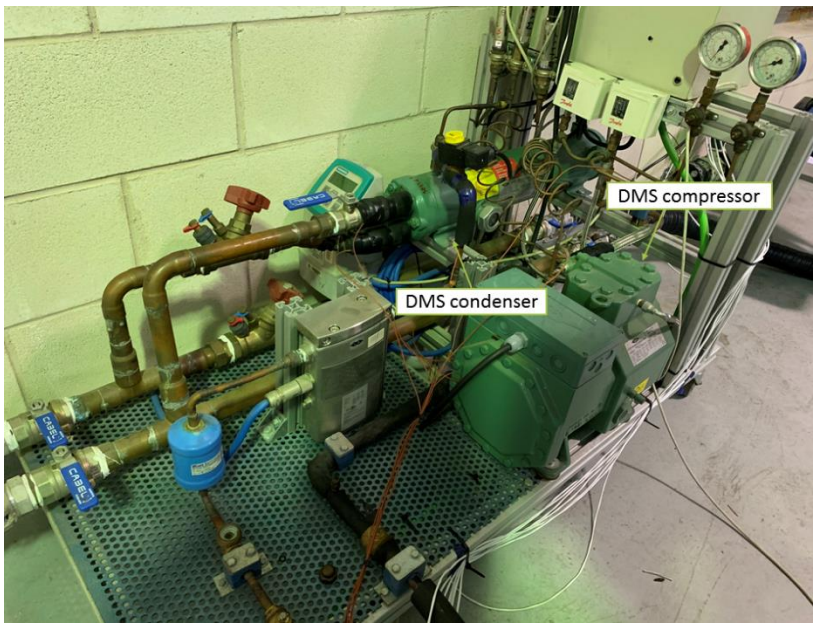

Figure 2.23. DMS system.

It is a semi-hermetic piston compressor (Figure 2.23), prepared to work with R-134a. The displacement is 4.06 m³/h and its nominal power at -10ºC is 1.01 kW.

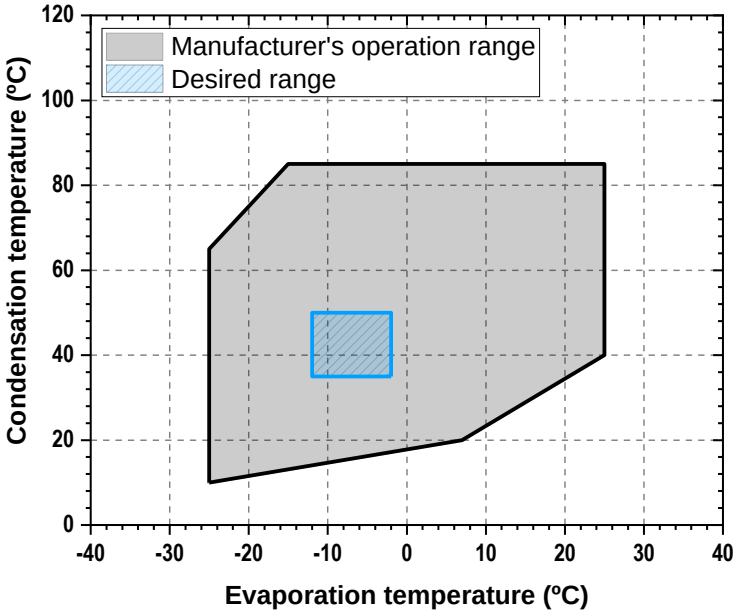

Figure 2.24. Aplication limits of the 2KES-05Y DMS compressor.

Figure 2.25. Scheme of the plant with DMS system.

The compressor is equipped with a variable frequency driver, seen in Figure 2.25, to adapt the rotation speed to the requirements of the experiment.

Subcooler

The evaporator of the dedicated mechanical subcooling circuit is one of the most important elements, as it is the link between the two cycles. Since this heat exchanger will also work with CO_2, it must be resistant to high pressures.

The selected heat exchanger is the Alfa Laval AXP14-40H-F [7] with 40-plates and a exchange surface area of 0.576 m^2 (Figure 2.26), made of stainless steel and designed to work with CO_2.

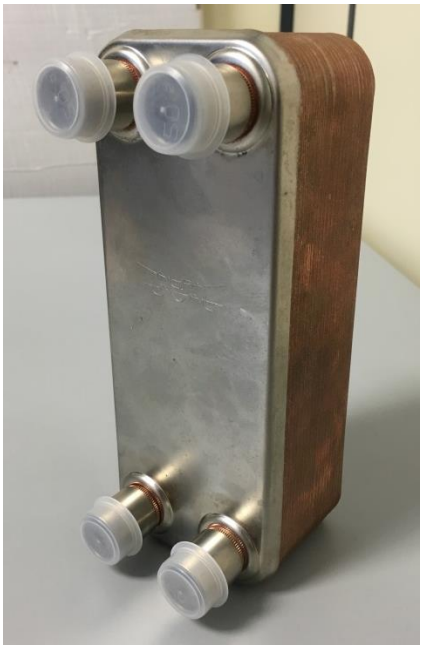

Figure 2.26. DMS subcooler AXP14-40H-F.

Expansion valve

The expansion valve of the DMS is an electronic one, with proportional modulation to ensure efficient control in the installation. The system has two Carel valves installed in parallel: E2V14 and E2V05 [3], in order to cover all the desired range of experimentation. However, it is the E2V05 the valve that has been used for all the work presented in this research.

A radiometric pressure probe and an NTC temperature probe are installed at the outlet of the evaporator, to control the operation. The expansion valves are driven by a driver and the refrigerant information that can be customized depending on which refrigerant is being used on the DMS.

Condenser

The condenser must work with water (heat dissipation medium) and the refrigerant R-152a or some mixtures. Any heat exchanger designed for Water/R-134a will be suitable for this application. In order to simplify the machine, a carcase-tube exchanger has beeninstalled, which will do in the vault of condenser and liquid tank.

The selected condenser is a 4-step Bitzer K033N [10], presented in Figure 2.23, with a receiver volume refrigerant of 3.8 liters.

2.2.4. Components of the PC cycle

The CO_2 cycle with parallel compressor is described in Figure 2.27. As it can be seen, to implement the PC (blue line in the scheme) only one additional compressor is needed. Said compressor is the main element of this upgrade cycle. In order to compare the systems with each other and at the same time to ensure that the selected compressor is correctly dimensioned for the analyzed installation, the selected compressor is the same as the one implemented in the IMS cycle.

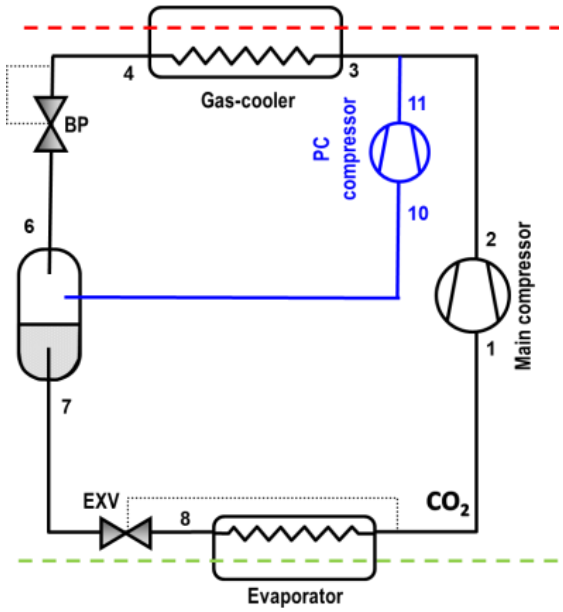

Figure 2.27. Scheme of the plant with PC system.

Compressor

The compressor selected for the PC cycle is the DORIN semi-hermetic compressor, model CD 150M [8], installed next to the main compressor and provided of a by-pass in the suction line to both suck both from the IMS circuit and from the tank's steam intake when using the PC.

2.2.5. Heat supply and dissipation system

The unit that is responsible for dissipating the heat generated in the refrigeration plant and also responsible for simulating the cooling demand is presented in Figure 2.28. It consists of two circuits, one dedicated to dissipating heat from the refrigeration circuit and the other dedicated to thermal input. The system has an accumulation tank with three variable electrical resistances of 3kW each and two systems to reduce the temperature of the secondary fluid used (water in this case). One of them is an aero-thermo, which dissipates heat to the environment by means of a fan and a battery of finned tubes, and the other system is a vapor compression system with a cooling capacity of up to 8 kW. Both the dry-cooler and the compressor are driven with frequency variators, in order to adjust to the thermal dissipation power necessary for each of the tests. The water is pumped through a recirculation pump, equipped with a frequency drive, to adjust the required water flow. This flow is measured by a magnetic flow meter.

Figure 2.28. Heat supply system.

The thermal supply circuit consists of an accumulation tank with three fixed 1.5 kW electric resistances and 3 other 3 kW variable resistances, governed by a PID controller to regulate the thermal power supplied to the fluid, depending on the temperature of the desired setpoint. In addition, it has a recirculation pump with a frequency drive and a Coriolis mass flow meter. The fluid used in this loop is a mixture of propylene glycol-water at 60% by volume.

2.2.6. Measurement and data acquisition elements

Data acquisition is crucial for measuring the performance of the experimental tests. To obtain the data, measurement elements have to be installed all long the installation. These elements are thermocouples, pressure gauges, flow meters and wattmeters.

Pressure gauges

Pressure gauges are installed in different points of the plant in order to measure the pressure in each of the important points of the circuit. The main part of these preassure gauges are current sensors, producing a 4-20 mA signal. Three other sensors are voltage gauges with a signal between 0-10 V. There are three different pressure range sensors in the plant: 0-60 bar, 0-100 bar and 0-160 bar, depending on where they are installed. All the pressure gauges were calibrated by using a calibrated digital manometer (Figure 2.29) and the calibration curves were obtained for all the measurement range.

Figure 2.29. Pressure gauge calibration.

Thermocpuples

In order to measure the temperature in different parts of the circuit, 34 T-type thermocouples have been installed, both immersion and surface. There are also additional thermocouples installed on the DMS circuit and on the secondary fluid loops.

The immersion thermocouples are used in the most important points of the circuit as the exit of each heat exchanger (Figure 2.30). The surface thermocouples are placed in

the rest of the points, in contact with the external part of the copper pipe. The uncertainty of the used thermocouples is presented in Table 2.3.

Figure 2.30. Immersion thermocouple at the exit of the IMS subcooler.

Mass and volumetric flow meters

For the measurement of the CO_2 flows it is necessary to have up to two Coriolis mass flow meters: one in the main branch and another that will measure the circulating flow by the auxiliary branch, either the IMS or the PC. The other mass flow will be obtained by the difference of the two previous ones. The DMS mass flow is also measured with another Coriolis mass flow meter.

The secondary fluids loops are measured by three mass flow meters. In the propylene glycol line, a Coriolis mass flow meter is installed while two magnetic volumetric flow meters are installed in the water supply and in the condenser water side of the DMS.

Wattimeters

Digital wattmeters are used to measure the electrical consumption of the compressors. There is a wattmeter installed in each compressor, with a measurement error of 0.5%.

Accurancy

The accurancies of all the measurement devices used in this thesis are shown Table 2.3 in as well as their range of operation.

Table 2.3. Accuracies and calibration range of the measurement devices.

Measured variable	Measurement device	Range	Calibrated accuracy
Temperature (ºC)	T-type thermocouple	-40.0 to 145.0	±0.5K
CO_2 pressure (bar)	Pressure gauge	0.0 to 160.0	±0.96 bar
CO_2 pressure (bar)	Pressure gauge	0.0 to 100.0	±0.6 bar
CO_2 pressure (bar)	Pressure gauge	0.0 to 60.0	±0.36 bar
DMS pressure (bar)	Pressure gauge	0.0 to 16.0	±0.096 bar
DMS pressure (bar)	Pressure gauge	0.0 to 40.0	±0.24 bar
CO_2 main mass flow rate ($kg \cdot s^{-1}$)	Coriolis mass flow meter	0.00 to 1.38	±0.1% of reading
CO_2 IMS/PC mass flow rate ($kg \cdot s^{-1}$)	Coriolis mass flow meter	0.00 to 0.083	±0.1% of reading
DMS mass flow rate ($kg \cdot s^{-1}$)	Coriolis mass flow meter	0.00 to 0.05	±0.1% of reading
Water volume flow rate ($m^3 \cdot h^{-1}$)	Magnetic flow meter	0.0 to 5.0	±0.3% of rate
Glycol volume flow rate ($kg \cdot s^{-1}$)	Coriolis mass flow meter	0.0 to 13.88	±0.1% of reading
Power consumption (kW)	Digital wattemeter	0.0 to 6.0	±0.5% of reading

Processing and representation of measurements

The plant is provided with measurement and control elements, managed through an interface developed with the software LabView. By means of this software, different operating parameters of the system can be controlled and modified, such as the rotational speed of the compressors and the gas-cooler pressure thanks to the regulation of the opening of the back-pressure valve.

For this, a PID-type regulator has been implemented in the program to control the gas-cooler pressure. The rotational speeds are adapted directly according to the needs, to avoid that the two controllers are coupled.

The sampling and conditioning of the electrical signals of the measurement elements is carried out by a National Instruments® acquisition system, model cRIO-9074 [11], which consists of different modules in charge of receiving the signal from the measurement elements. For this, it has:

- 2 Power Input Modules (NI 9208).

- 2 Thermocouple Input Modules (NI 9213).
- 1 Analog Output Module (NI 9263).
- 1 Analog Input Module (NI 9201).

The signals of these modules are visualized in real time through the graphical interface created with the Labview software. The data is stored to later analyze it and make the necessary calculations thanks to the Microsoft Excel and Refprop tools.

2.2.8. Plant assembly

All the plant has been assembled in different steps, starting by dismantling the previously existing plant and changing the gas-cooler and evaporator. At first it was installed in DMS and later the necessary modifications were made in the circuit to be able to evaluate the IMS and the PC. Figure 2.31 shows the plant during the assembly and Figure 2.32 shows the final plant during a CO_2 charge.

Figure 2.31. Experimental plant during the assembly.

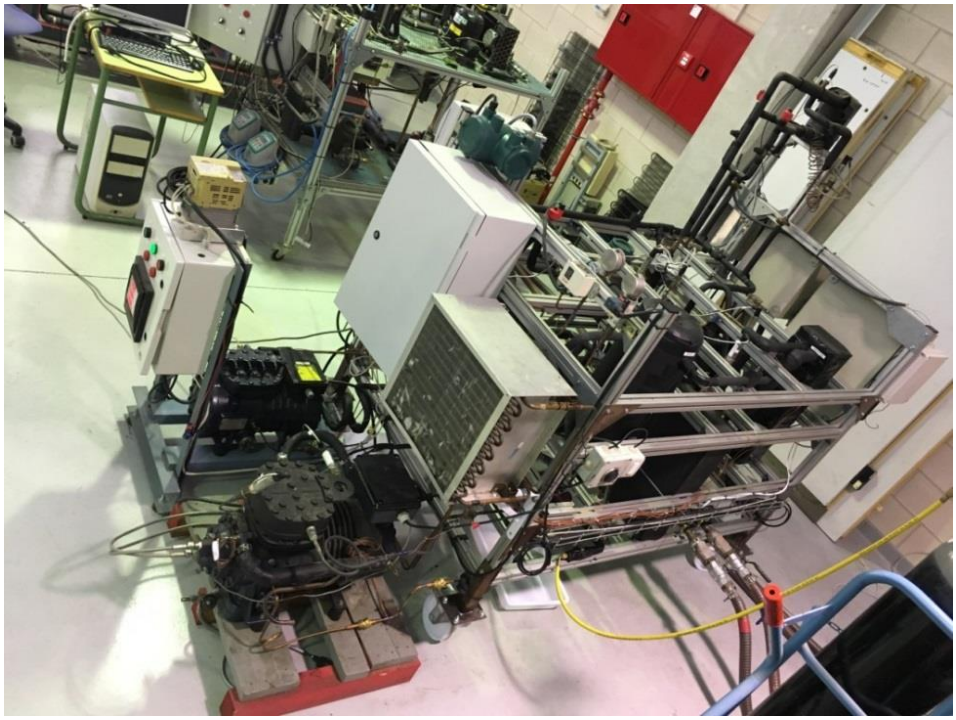

Figure 2.32. Experimental plant during CO_2 charging.

2.2.9. Test procedure

To evaluate the refrigeration plant using the improvement systems mentioned before, the system has been tested at different working conditions, always operating in the transcritical region. The evaluated conditions were:

- Several heat rejection levels: the inlet temperature of the water at the entrance of the gas-cooler and the DMS condenser can be fixed to a desired temperature. The water flow rate can also be fixed to simulate external test conditions.
- Several evaporation levels: The inlet temperature of the secondary fluid in the evaporator and its flow rate can be fixed to the desired values. The secondary fluid is a mixture propylene glycol-water (60% by volume).
- During the test, the gas-cooler pressure must be optimized so it is necessary to test different values. For that, it is regulated with an electronic BP fixed during each test thanks to a PID controller. The pressure is modified in order to reach the optimum COP conditions.
- Compressors: The main compressor always operated at nominal speed of 1450 rpm. The speed of the IMS compressor, DMS compressor and PC compressor is varied in order to modify and test different subcooling degrees, in the case of

the subcooling systems, or intermediate pressures in the case of the PC system.

- The electronic expansion valves were set to obtain a superheating degree in the evaporator of 10K and of 5K on the subcoolers.
- All the tests are carried out in steady state conditions for periods longer than 10 minutes, taking data each 5 seconds, for at least 10 minutes (120 data minimum). The test point is obtained as the average value of the whole test.
- The measured data is used to calculate the thermodynamic properties of the points using Refprop v.9.1. [2]
- Once all the properties of the fluid are obtained, the main energy parameters are calculated.

The test procedure is outlined in Figure 2.33.

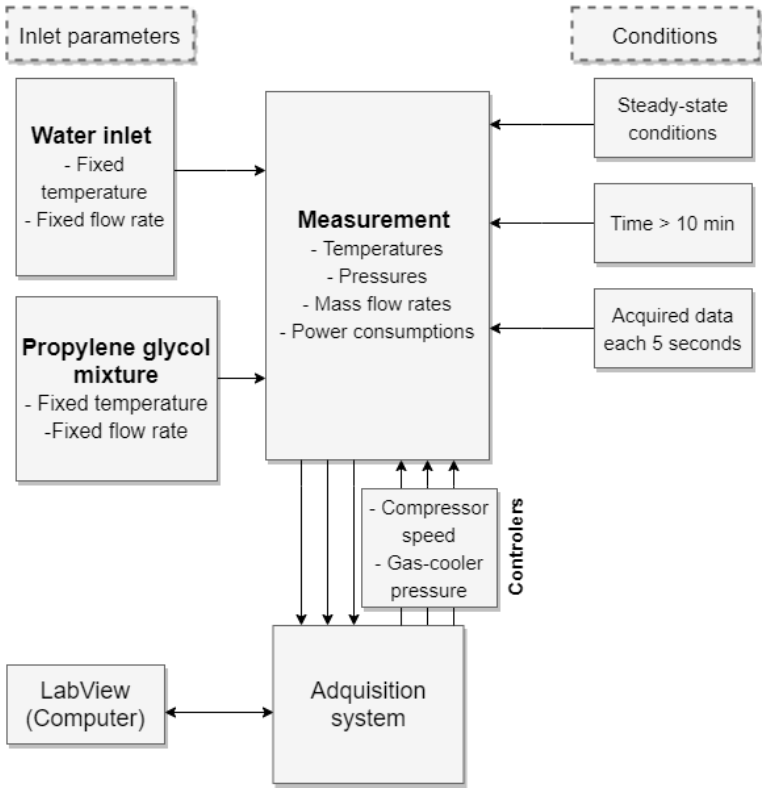

Figure 2.33. Scheme of the test procedure.

2.2.10. Optimization procedure

The optimization procedure of the experimental test is carried out at the same time as the execution of the tests. When one of the tests is finished and the measured values lasting 10 minutes are saved, the cooling capacity of the plant is calculated. Then the

COP of the system is the ratio between the cooling capacity and the sum of the power consumption of the compressors. This value of COP is ploted in a contour map as a function of the gas-cooler pressure and the subcooling degree (or intermediate pressure in the case of the PC). After ploting this point, a parameter is varied, either the compressor speed (varying subcooling or intermediate pressure) or the gas-cooler pressure and a new point is obtained.

Once three points are ploted, a COP trend can be observed. To obtain the maximum COP, the gas-cooler pressure and compressor speed are modified following a method similar to a Simplex algorithm. These parameters are increased or decreased following the trend of the previous points, in order to get closer and closer to the point of maximum COP. The process ended when the increments achieved between the new value and the previous one are less than 1%, as outlined in Figure 2.34. When the maximum COP is already found, the external conditions (temperature and flow rate of the water and propylene glycol) are changed to carry out another batch of tests.

An example of the steps followed for the optimization of the system with PC is shown in Figure 2.35.

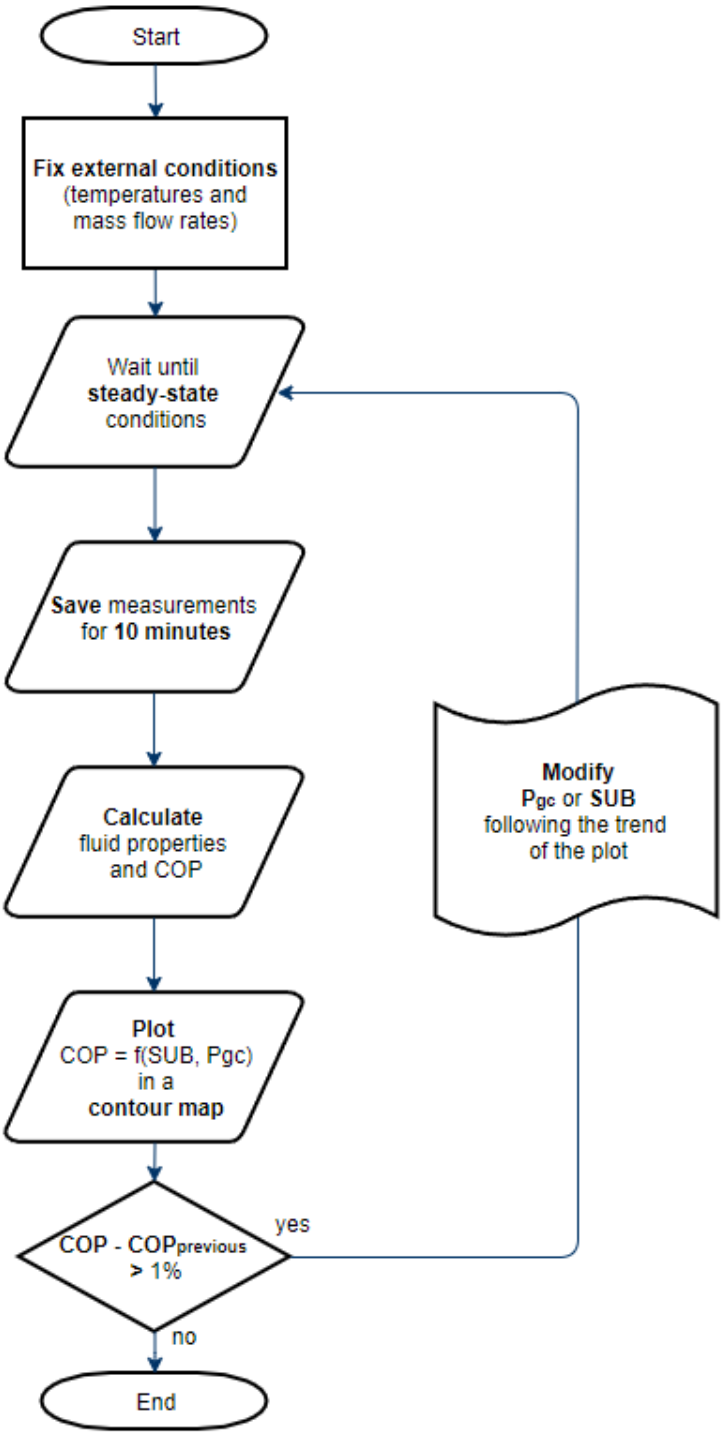

Figure 2.34. Scheme of the experimental optimization.

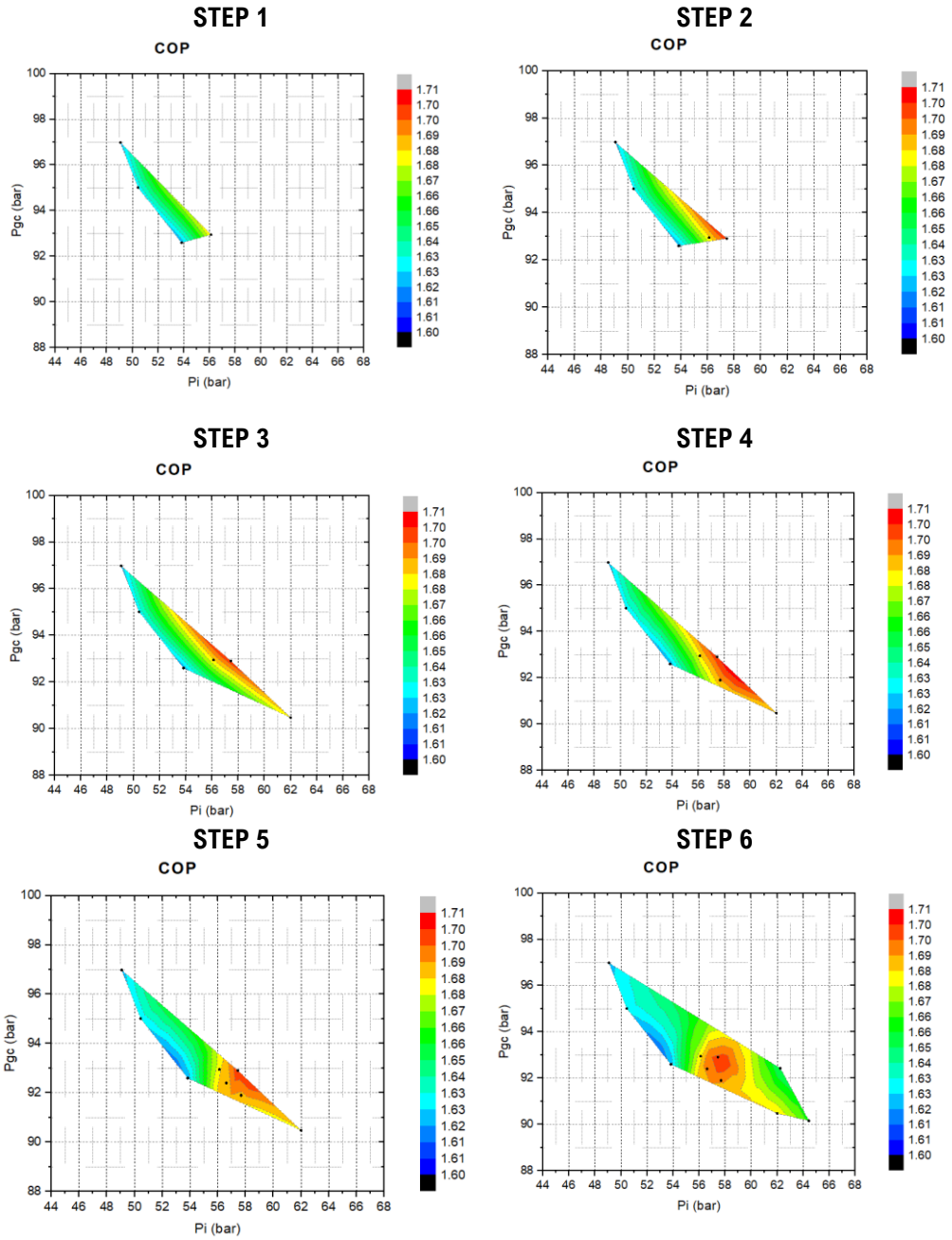

Figure 2.35. Steps of the experimental optimization of the PC system.

2.2.11. Uncertainty analysis

The uncertainty analysis has been carried out on all the results obtained during the experimental tests.

For the calculation of the uncertainty of the enthalpy values, the Moffat method [12] has been followed, as detailed by Aprea et al. [13]. This variable is obtained from two measured values, for example pressure and temperature as stated in Eq. (2.18). The uncertainty of this variable depends on the measured variables and the uncertainty of the measurement devices of both properties. The uncertainty of the measurement devices used to calculate the uncertainties are presented in Table 2.3.

$$h_1 = f(P_1, T_1) \tag{2.18}$$

$${h_1}^{p+} = f(P_1 + u(P_1), T_1) \tag{2.19}$$

$${h_1}^{p-} = f(P_1 - u(P_1), T_1) \tag{2.20}$$

$${h_1}^{t+} = f(P_1, T_1 + u(T_1)) \tag{2.21}$$

$${h_1}^{t-} = f(P_1, T_1 - u(T_1)) \tag{2.22}$$

$$I^p = \frac{\left|{h_1}^{p+} - h_1\right| + \left|{h_1}^{p-} - h_1\right|}{2} \tag{2.23}$$

$$I^t = \frac{\left|{h_1}^{t+} - h_1\right| + \left|{h_1}^{t-} - h_1\right|}{2} \tag{2.24}$$

$$u_{h_1} = \sqrt{{I^p}^2 + {I^t}^2} \tag{2.25}$$

The cooling capacity is calculated as shown in Eq. (2.26).

$$\dot{Q}_0 = \dot{m}_0 \cdot (h_{0,o} - h_{0,in}) \tag{2.26}$$

Considering this, the uncertainty of the cooling capacity is obtained as follows:

$$u_{\dot{Q}_0} = \sqrt{\left(\frac{\partial \dot{Q}_0}{\partial \dot{m}_0} \cdot u_{\dot{m}_0}\right)^2 + \left(\frac{\partial \dot{Q}_0}{\partial h_{0,o}} \cdot u_{h_{0,out}}\right)^2 + \left(\frac{\partial \dot{Q}_0}{\partial h_{0,in}} \cdot u_{h_{0,in}}\right)^2} \tag{2.27}$$

$$\frac{\partial \dot{Q}_0}{\partial \dot{m}_{co2}} = (h_{0,o} - h_{0,in}) \tag{2.28}$$

$$\frac{\partial \dot{Q}_0}{\partial h_{0,o}} = \dot{m}_0 \tag{2.29}$$

$$\frac{\partial \dot{Q}_0}{\partial h_{0,in}} = -\dot{m}_0 \tag{2.30}$$

The COP is obtained as:

$$COP = \frac{\dot{Q}_0}{P_{C,main} + P_{C,aux}} \tag{2.31}$$

The uncertainty of the measured COP is also calculated as previously described:

$$u_{COP} = \sqrt{\left(\frac{\partial COP}{\partial \dot{Q}_0} \cdot u_{\dot{Q}_0}\right)^2 + \left(\frac{\partial COP}{\partial P_{C,CO2}} \cdot u_{P_{C,main}}\right)^2 + \left(\frac{\partial COP}{\partial P_{C,aux}} \cdot u_{P_{C,aux}}\right)^2} \tag{2.32}$$

$$\frac{\partial COP}{\partial \dot{Q}_0} = \frac{1}{P_{C,main} + P_{C,aux}} \tag{2.33}$$

$$\frac{\partial COP}{\partial P_{C,main}} = -\frac{\dot{Q}_0}{\left(P_{C,main} + P_{C,aux}\right)^2} \tag{2.34}$$

$$\frac{\partial COP}{\partial P_{C,aux}} = -\frac{\dot{Q}_0}{\left(P_{C,main} + P_{C,aux}\right)^2} \tag{2.35}$$

2.3. Nomenclature

app	Temperature approach, K
COP	coefficient of performance
DMS	Dedicated mechanical subcooling
h	specific enthalpy, kJ·kg^{-1}
I	contribution to the accuracy
IMS	Integrated mechanical subcooling
N	Rotational speed, rpm
$\dot{m}$	mass flow rate, kg·s^{-1}
p	pressure, bar
P_C	compressor power consumption, kW
$\dot{Q}_O$	cooling capacity, kW
SUB	degree of subcooling at the subcooler, K

t	temperature, ºC
$\dot{V}_G$	compressor displacement, $m^3 \cdot h^{-1}$

Greek symbols

η_v	volumetric compressor efficiency
η_G	overall compressor efficiency
Δ	increment
u	uncertainity
v	Specific volumen, $m^3 \cdot kg^{-1}$

Subscripts

aux	referring to the auxiliary cycle
CO_2	referring to CO_2
main	referring to CO_2 main cycle
dis	discharge
DMS	referring to the dedicated mechanical subcooling cycle
env	environment
exp	expansion
gc	gas-cooler
IMS	referring to the integrated mechanical subcooling cycle
in	inlet
l	saturated liquid
nom	nominal
O	evaporating level
o	outlet
PC	referring to the parallel compression cycle

s	isentropic
sub	referring to the subcooler
suc	suction
vess	referring to the vessel

Superscript

p	corresponding to the measured pressure value
p+	corresponding to the measured pressure value plus the measurement uncertainty
p+	corresponding to the measured pressure value minus the measurement uncertainty
t	corresponding to the measured temperature value
t+	corresponding to the measured temperature value plus the measurement uncertainty
t-	corresponding to the measured temperature value minus the measurement uncertainty

2.4. References

[1] L. Nebot-Andrés, J. Catalán-Gil, D. Sánchez, D. Calleja-Anta, R. Cabello, R. Llopis, Experimental determination of the optimum working conditions of a transcritical CO2 refrigeration plant with integrated mechanical subcooling, International Journal of Refrigeration, 113 (2020) 266-275

[2] Lemmon EW, Huber ML, McLinden MO. REFPROP, NIST Standard Reference Database 23, v.9.1. National Institute of Standards, Gaithersburg, MD, U.S.A. 2013.

[3] Carel. E2V smart. Electronic expansion valves. Padova (Italy): Carel Industries HQs.

[4] D. Sánchez, Desarrollo de una planta frigorífica de compresión de vapor empleando el fluido natural CO2 como refrigerante en condiciones supercríticas. Análisis experimental y evaluación energética de diferentes configuraciones., in: Dpto. Ingeniería Mecánica y Construcción, Universitat Jaume I, Castellón de la Plana, 2010.

[5] Egelhof. https://www.egelhof.com/.

[6] Alfa Laval CBXP52. https://productguide.alfalaval.com/en-es/brazed-plate-heat-exchangers-replacement-units--ru_bhe/cbxp52-70l-f--1317817-.

[7] Alfa Laval. Brazed plate heat exchangers. https://www.alfalaval.com/globalassets/documents/

[8] DORIN. CO2 semi-hermetic compressors. CD series CO2 transcritical application. Italy: OFFICINE MARIO DORIN S.p.A.; 2018.

[9] GmbH B. Operating Instructions Bitzer Ecoline Varispeed. https://www.bitzer.de/shared_media/documentation/kb-104-7.pdf.

[10] GmbH B. Products and solutions. 2018;A-201-7 EN.
[11] Instruments N. User manual and specifications NI cRIO-9074XT. In: CompactRIO RECwIIRCf, editor. https://www.ni.com/pdf/manuals
[12] R.J. Moffat, Using Uncertainty Analysis in the Planning of an Experiment, Journal of Fluids Engineering, 107 (1985) 173-178.
[13] C. Aprea, F. de Rossi, R. Mastrullo, The uncertainties in measuring vapour compression plant performances, Measurement, 21 (1997) 65-70.

Chapter 3 CO_2 with mechanical subcooling vs. CO_2 cascade cycles for medium temperature commercial refrigeration applications. Thermodynamic analysis.

Chapter 3. CO_2 with mechanical subcooling vs. CO_2 cascade cycles for medium temperature commercial refrigeration applications. Thermodynamic analysis.

3. CO_2 with mechanical subcooling vs. CO_2 cascade cycles for medium temperature commercial refrigeration applications. Thermodynamic analysis.

Chapter adapted from the paper: Nebot-Andrés, L., Llopis, R., Sánchez, D., Catalán-Gil, J., Cabello, R. CO_2 with mechanical subcooling vs. CO_2 cascade cycles for medium temperature commercial refrigeration applications thermodynamic analysis (2017) Applied Sciences, 7 (9), art. no.955. DOI: 10.3390/app7090955

Abstract

A recent trend to spread the use of CO_2 refrigeration cycles in warm regions of the world is to combine a CO_2 cycle with another one using a high performance refrigerant. Two alternatives are being considered: cascade and mechanical subcooling systems. Both respond to a similar configuration of the refrigeration cycle, they being based on the use of two compressors and same number of heat exchangers. However, the compressor, heat exchanger sizes and energy performance differ a lot between them. This work, using experimental relations for CO_2 and R1234yf semi-hermetic compressors analyses in depth both alternatives under the warm climate of Spain. In general, it has been concluded that the CO_2 refrigeration solution with mechanical subcooling will cover all the conditions with high overall energy efficiency, thus it being recommended for further extension of the CO_2 refrigeration applications.

Keywords

CO2; transcritical; cascade; mechanical subcooling; energy efficiency

Chapter 3. CO_2 with mechanical subcooling vs. CO_2 cascade cycles for medium temperature commercial refrigeration applications. Thermodynamic analysis.

Chapter 3. CO_2 with mechanical subcooling vs. CO_2 cascade cycles for medium temperature commercial refrigeration applications. Thermodynamic analysis.

3.1. Introduction

Carbon dioxide has been spread out all over the world as refrigerant because it combines excellent environmental (GWP=1) and safety properties (A1), despite its differences regards traditional refrigerants, such as high working pressures, low critical temperature and high densities. After the approval of the F-Gas Regulation [1] in Europe in 2014, the implication of the industry with this refrigerant has been taken a step forward, especially in commercial refrigeration, whose systems are extremely energy consumers and commonly characterized by large leakages rates of refrigerant. Regarding the environmental impact, the use of CO_2 practically eliminates the direct effect of the refrigeration system, thanks to its low GWP. However, the indirect impact associated to the energy consumption of the plant is an issue still under analysis and contrast among the scientific community and the industry sector. In cold regions of the planet, with low average annual temperatures below 14-15 ºC, the standard CO_2 cycles perform with energy efficiency levels higher than the conventional HFC-based plants [2]. However, when the environment temperature rises, the standard CO_2 systems [3] are not able to reach the performance of the formers, and thus, advanced and more complex systems must be considered to be able to mitigate indirect impact of the system.

The search for improvements in CO_2 standard refrigeration cycles follow two main directions: new components and the combination of CO_2 cycles with other systems. Regarding new components, the CO_2 expander concept is still under maturation, few experimental works have been found in the literature, such as the experimental tests with a rotary vane expander of Jia et al. [4] and with a two-rolling piston expander of Hu et al. [5]. However, great progress has been achieved in the last decade regarding the ejector technology; it has been already implemented in lots of plants all over the world, where the energy improvements have been experimentally demonstrated [6]. Now, research on ejector technology is focused on achieving adaptable ejectors to all the operation range of the plants, such as the multi-ejector concept of Hafner et al. [7] or the adjustable ejector concept of Lawrence & Elbel [8], among others. On the other side, scientists and industry are working on the thermal integration of CO_2 refrigeration cycles with other energy systems to obtain higher overall energy efficiency to make CO_2 more competitive. The attempts correspond to the integration of the CO_2 refrigeration plants with water heating systems and air conditioning systems [9], desiccant wheels [10], absorption plants [11], etc…; where in all the cases important overall increases of the energy efficiency have been achieved.

Another type of CO_2 combined refrigeration system, widely implemented in the last decade in the commercial sector, is the cascade system using CO_2 as low temperature

refrigerant [12]. This combination corresponds to the thermal coupling of two single stage cycles working with different refrigerants, where the high temperature cycle keeps the CO_2 low temperature cycle always in subcritical conditions, thus avoiding the high operating pressures of CO_2 and the need for regulation of the high pressure in transcritical conditions [13]. As analysed by Llopis et al. [14], this cycle overcomes the energy efficiency levels of standard CO_2 refrigeration cycles and it reaches comparable COP values than the current systems in commercial refrigeration at low evaporation levels and high environment temperatures. In addition, from the point of view of environmental impact, this system presents low values of TEWI among the solutions adapted to the new F-Gas Regulation. Similar to the cascade solution, since the operating cycle is equivalent, another CO_2 combined cycle is attracting attention in the last years, the thermal joining of a CO_2 cycle with a dedicated mechanical subcooling system. This option has been studied from a theoretical point of view by Hafner et al. [15], Gullo el. at. [16] and Llopis et al. [17], and from an experimental point of view by Nebot-Andrés et al. [18] and Eikevik et al. [19]. This cycle is characterized by a main refrigeration cycle working with CO_2 that can be operated in subcritical or transcritical modes which is helped by another vapour compression system, the dedicated mechanical subcooling cycle, providing CO_2 a large subcooling at the exit of the gas-cooler/condenser. The benefits of this combination are a big increment of the cooling capacity, reductions of the optimum CO_2 high working pressure and an important increment of the overall energy efficiency. Nebot-Andrés et al. [18], for an evaporation level of 0 ºC, measured increments on cooling capacity of 34.9% and 40.7% and on COP of 22.8% and 17.3% at 30.2 and 40ºC of heat rejection temperature, respectively, considering as base line a single-stage CO_2 transcritical plant without internal heat exchanger.

These last approaches, the cascaded CO_2 and the subcooled CO_2 solutions, are being considered to spread the use of CO_2 in centralized refrigeration systems at a medium temperature level in medium to warm regions of the planet such Spain or Italy. As mentioned, both refrigeration schemes have similar configuration of the refrigeration cycle: one rack of compressors for the CO_2 and another for the high temperature / subcooling cycle and same number of heat exchangers. But, they have differences in the operation of the components that compose the cycle. One of the main differences, which is discussed in Section 4.2, is that the high-pressure CO_2 heat exchangers can operate as single-phase/two-phase or two-phase/two-phase (cascade) heat exchangers, being the heat transfer rate different in each operating mode. This work aims to analyse which cycle configuration (cascade or mechanical subcooling) is recommended for different operating conditions. The analysis is based on simplified models close to reality, since they use real performances of the compressors. The comparison provides

clear conclusions about the application range, advantages and disadvantages of each cycle. In the paper, first, the optimum operating conditions of each cycle are established; then for the optimum conditions, the reached COP values and the ratio of electrical consumption of the compressors are presented. Next, energy efficiency results of both solutions are merged to determine at which operating conditions each solution is the best performing system. Finally, both systems are evaluated under the different climate conditions of Spain to obtain clear conclusions about their possible implementation.

3.2. Refrigeration cycles, models and assumptions

The cascade refrigeration cycle and the MS cycle can be represented by the refrigeration scheme detailed in Figure 3.1. Essentially, both systems include these main components with the following operating characteristics:

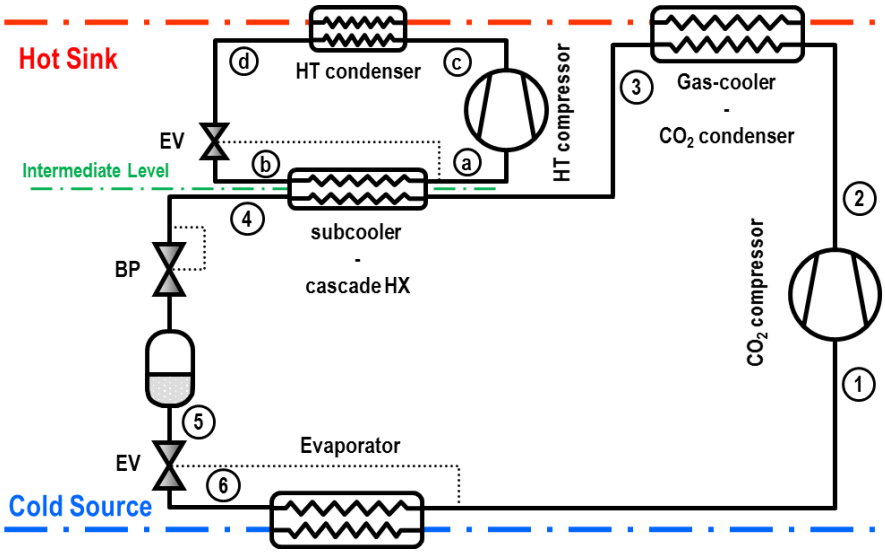

Figure 3.1. Schematic representation of cascade and CO_2 with mechanical subcooling.

- A main cycle, working with CO_2 as refrigerant, which absorbs energy from the cold source.
- A CO_2 compressor, subcritical-rated for the cascade configuration and transcritical-rated for the MS configuration.
- A CO_2 gas-cooler, which performs heat rejection to the hot sink.
- A second CO_2 heat exchanger acting as CO_2 condenser for the cascade system and as CO_2 subcooler for the MS configuration.
- An expansion system: composed of the 'vessel + expansion valve' for the cascade configuration and of a 'back-pressure + vessel + expansion valve' for the MS cycle.

- An auxiliary single-stage refrigeration cycle: working with another refrigerant (HCs, HFOs, NH_3, HFCs) as high temperature cycle in the cascade configuration and as dedicated mechanical subcooling cycle for the MS configuration. The auxiliary system, whose refrigerant is not distributed to the cooling appliances, absorbs heat from the intermediate temperature level and performs heat rejection to the same hot sink as the main cycle. In the cascade configuration, the auxiliary cycle performs CO_2 condensation and in the MS it only subcools the CO_2 at the exit of the gas-cooler.

The operation of the cycle of Figure 3.1 as cascade or as MS cycle will depend on the hot sink temperature (T_H) and on the high-pressure fixed by the back-pressure valve (P_{high}), as detailed in the following subsections.

3.2.1. CO2 refrigeration cycle with mechanical subcooling (MS cycle)

Essentially, the CO_2 refrigeration cycle with mechanical subcooling corresponds to a main CO_2 single-stage cycle that uses an auxiliary cycle, with small capacity, to provide subcooling at the exit of the gas-cooler/condenser [17]. This cycle operates in subcritical or transcritical conditions depending on the heat rejection temperature (T_H) and on the high-pressure established by the back-pressure valve (P_{high}).

The transition from subcritical to transcritical conditions was investigated by Ge et al. [20], Shao et al. [21], Tsamos el at. [22] and Sanchez et al. [23] for standard CO_2 refrigeration cycles, however, no reference for the transition has been found when the CO_2 cycle uses a mechanical subcooling system. For the analysis of the MS cycle, the transition from transcritical to subcritical has been established in terms of the maximum COP value reached by each operating mode although this transition in real plants would be difficult. The considerations are the following:

If saturation pressure of CO_2 at T_H is lower than the pressure fixed by the back-pressure (P_{high}) and this last is lower than the critical pressure of CO_2 (73.773 bar) , the optimum operation conditions will be in subcritical-mode with liquid subcooling. These boundary conditions are detailed by Eq.(3.1), and the corresponding pressure-enthalpy diagram of CO_2 represented in Figure 3.2. In this type of operation, the first CO_2 heat exchanger acts as condenser (point 2 to 3) and the subcooler subcools liquid CO_2 (points 3 to 4). The case of partial condensation in the CO_2 heat exchanger (point 2 to 3*) is possible, but the best energy results are obtained for complete condensation.

$$P_{sat,CO2}(T_H) < P_{high} \leq P_{crit,CO2} \quad (3.1)$$

$$P_{high} > P_{crit,CO2} \quad (3.2)$$

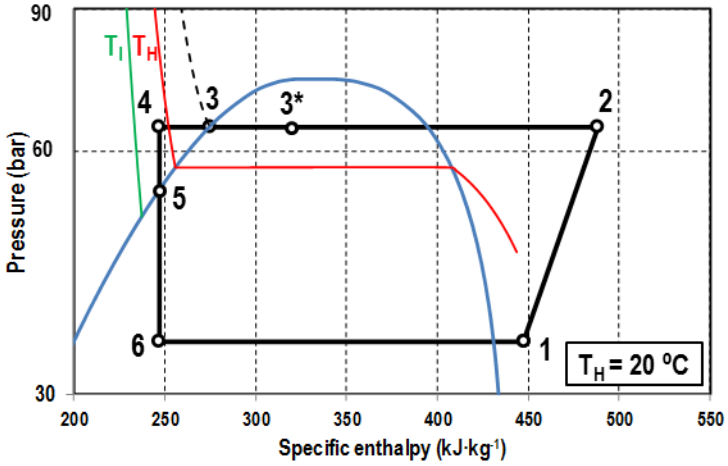

Figure 3.2. Pressure-enthalpy diagram of MS cycle in subcritical conditions.

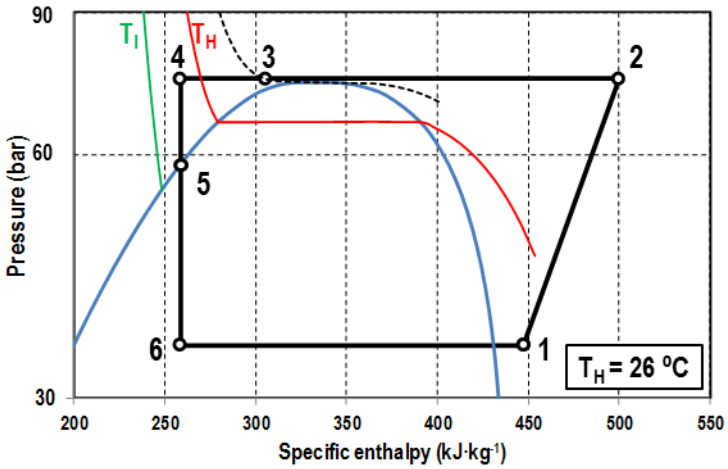

Figure 3.3. Pressure-enthalpy diagram of MS cycle in transcritical conditions.

For pressures fixed by the back-pressure (P_{high}) higher than the critical pressure, Eq.(3.2), the optimum operating conditions are in transcritical mode, as represented by Figure 3.3. For this mode of operation, the first CO_2 heat exchanger acts as gas-cooler (point 2 to 3) and the subcooler subcools gas or liquid depending on the high-pressure and T_H temperature.

3.2.2. Cascade refrigeration cycle

Cascade refrigeration cycle corresponds to the combination of two main refrigeration cycles, one cycle working with CO_2 in the low temperature level, which is condensed

and maintained in subcritical, by another cycle that uses a refrigerant with good performance at high evaporation temperatures. In this case, both cycles are necessary, since the operation of the low temperature cycle depends on the operation of the high temperature cycle. In addition in this case, the high temperature cycle has similar or higher cooling capacity than the low temperature cycle.

Figure 3.4 represents the operation of the CO_2 cycle in a cascade system. This is the mode of operation if the condition established by Eq.(3.3)or Eq.(3.4) is satisfied. That is, when the pressure established by the back-pressure (if present) or by the thermal equilibrium of condensation (P_{high}) is lower than the CO_2 saturation pressure at T_H, Eq. (3.3). As established in Eq.(3.4), if T_H is higher than the critical temperature of CO_2, the high-pressure (P_{high}) must be lower than the critical one to satisfy the condition.

$$P_{high} < P_{sat,CO2}(T_H) \; if \; T_H \leq T_{crit,CO2} \tag{3.3}$$

$$OR$$

$$P_{high} < P_{crit,CO2} \; if \; T_H > T_{crit,CO2} \tag{3.4}$$

In the subcritical mode, the gas-cooler performs a small heat rejection to T_H and then the high-temperature cycle condenses CO_2 until saturated liquid. Subcooling is possible, but it offers worse results than the exit in saturation conditions because the intermediate temperature will need to descend.

This cycle has been experimentally investigated by Dopazo et al. [24] using NH_3/CO_2 and Sanz et al. [12] using HFC134a/CO_2.

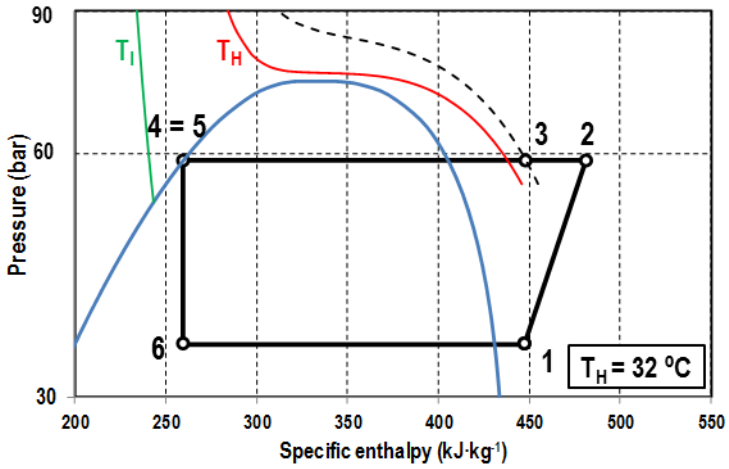

Figure 3.4. Pressure-enthalpy diagram of the low temperature cycle (CO_2) of the cascade.

3.2.3. Calculation models and assumptions

We performed the analysis of the MS and the cascade cycles using simplified but realistic models, which assumptions are detailed then.

CO_2 compressor for both configurations is modelled using the overall efficiency as a linear relation with the compression ratio, as detailed by Eq.(3.5). We fitted this relation using experimental data of a semi-hermetic single-stage CO_2 compressor able to operate in subcritical or transcritical [23].

$$\eta_{G,CO2} = 0.7359 - 0.0517 \cdot t_{CO2} \quad (3.5)$$

For either the MS and cascade configurations, an approach temperature in gas-cooler of 5 K regards the environment temperature and 10 K of superheating degree in evaporator are chosen. For the MS configuration, when working in transcritical conditions, the high-pressure is established by the back-pressure. The tunable parameters are the high-pressure and the subcooling degree in subcooler (SUB = T_3 - T_4). Both parameters are optimized to obtain the best performing conditions. When working in subcritical, high pressure is computed as saturation temperature of CO_2 at the environment temperature plus a temperature difference in condenser of 5 K, to maintain the same reference level as in transcritical. The exit of the condenser is considered in saturation. Only the subcooling degree in the subcooler is free, being it optimized in the calculations. For the cascade configuration, the tunable variable is the temperature of the intermediate level, being the CO_2 condensing temperature taken as reference and optimized in the calculations. In this case, the exit condition of CO_2 of the cascade heat exchanger is considered in saturation. For both cycles, the lamination processes are assumed isenthalpic and pressure losses and heat transfer to the environment in the lines are neglected.

Regarding the secondary refrigerant, R1234yf is selected for the MS cycle and for the high-temperature cycle. This HFO is one of the new generation of refrigerants introduced to the market with the aim of substitute the R134, being an alternative with low GWP but light inflammable (A2L), that can perform as drop-in replacement. Aprea et al. [25] find out that this drop-in allows increasing the cooling capacity, being a refrigerant suitable for new plants and plants that are already working.

The overall efficiency of the compressor is also adjusted as a linear relation with the compression ratio, as detailed by Eq.(3.6), in this case fitted from experimental data of a semi-hermetic compressor [26].

$$\eta_{G,R1234yf} = 0.9721 - 0.0533 \cdot t_{R1234yf} \quad (3.6)$$

The high-temperature cycle or dedicated mechanical subcooling cycle, is thermally linked to the CO_2 cycle using two different approaches: when working as condenser in the cascade configuration, the evaporation temperature of R1234yf is considered to be 5 K below the CO_2 condensing temperature [12], thus being optimized during the calculation. On the other hand, when this cycle operates as mechanical subcooler, its evaporation temperature is computed considering a thermal effectiveness of the subcooler of 60 %, Eq.(3.7), being this effectiveness the average value measured in [27]. This temperature is indirectly optimized by tuning of the optimum subcooling degree in the CO_2 cycle.

$$T_{O,R1234yf,MS} = T_3 - \frac{SUB}{\varepsilon} = T_3 - \frac{T_3 - T_4}{\varepsilon} \tag{3.7}$$

For this cycle, a degree of superheat in the evaporator of 5 K is chosen. The exit of the condenser is in saturation and the expansion process is isenthalpic. Also, pressures losses and heat transfer to the environment in pipes are neglected.

The relation between the refrigerant mass flow rates of both cycles is obtained through the energy balance in the subcooler/cascade HX as established by Eq. (3.8) according to nomenclature of Figure 3.1.

$$\frac{\dot{m}_{R1234yf}}{\dot{m}_{CO2}} = \frac{h_3 - h_4}{h_a - h_b} \tag{3.8}$$

Using relation (3.8), the main energy parameters can be expressed as a function of the refrigerant enthalpies and the overall efficiencies of the compressors. Eq. (3.9) expresses the overall COP of the cycle combination as quotient between the cooling capacity of the CO_2 cycle and the sum of power consumptions of both compressors. Eq. (3.10) establishes the relation between the power consumption of the MS/cascade compressor regards the power consumption of the CO_2 compressor, it being an indicative of the size of the auxiliary cycle.

$$COP = \frac{\dot{Q}_O}{P_{C,CO2} + P_{C,R1234yf}} = \frac{h_1 - h_4}{\frac{h_{2,s} - h_1}{\eta_{G,CO2}} + \frac{h_3 - h_4}{h_a - h_b} \cdot \frac{h_{c,s} - h_a}{\eta_{G,R1234yf}}} \tag{3.9}$$

$$\frac{P_{C,R1234yf}}{P_{C,CO2}} = \frac{(h_3 - h_4) \cdot (h_{c,s} - h_a)}{(h_a - h_b) \cdot (h_{2,s} - h_1)} \cdot \frac{\eta_{G,CO2}}{\eta_{G,R1234yf}} \tag{3.10}$$

All the thermophysical properties of the refrigerants have been calculated using Refprop database [28].

3.3. Results

This section establishes the optimum operating conditions of the CO_2 refrigeration cycle with mechanical subcooling (subsection 2.3.1) and of the cascade cycle using CO_2 as low temperature fluid (subsection 2.3.2) using the model detailed in Section 2. The evaluation has been made considering environment temperatures from 15 to 40 ºC and evaporating levels from 5 to -20 ºC. No lower evaporating levels have been analysed because -20 ºC corresponds to the lowest evaporating temperature at which the CO_2 compressor used to build the correlations can be operated. For lower evaporating levels, two stage solutions should be considered.

3.3.1. Operating conditions of the CO_2 cycle with mechanical subcooling

As mentioned, the operating parameters to be tuned to obtain the best performing conditions of the CO_2 cycle with mechanical subcooling are the pressure at the gas-cooler (P_{high}) and the degree of subcooling provided by the auxiliary system (SUB). To illustrate the behaviour of this cycle, the dependence of the overall COP, Eq.(3.9), versus the environment temperature and the subcooling degree for an evaporating level of 0 ºC is presented in Figure 3.5. Data of Figure 3.5 are evaluated for the optimum gas-cooler pressures. For environment temperatures below 25 ºC the best results are in subcritical operation and for warmer temperatures in transcritical. As it can be observed, for any environment temperature, an optimum degree of subcooling exists, maximizing the overall COP. Furthermore, it is observed that the subcooling degree increases when going to warmer temperatures.

Maximum COP for the considered range and the corresponding optimum subcooling degrees are detailed in Figure 3.6 and in Figure 3.7, respectively, for all the considered range. As it can be observed in Figure 3.6, the transition between subcritical to transcritical operation occurs, from a theoretical energy point of view, at an environment temperature of 25.3 ± 0.2 ºC. Since this temperature is commonly reached in any location, the plant must be designed to be able to operate in subcritical conditions when possible, since forcing it to operate in transcritical would result in reductions of COP. That means that the first CO_2 heat exchanger must be sized as condenser, but it must be ready to operate also as gas-cooler. The trend is the same as in pure CO_2 transcritical systems, as it can be observed in the work presented by Sanchez D. et al. [23]. Another important aspect is that the presence of the optimum subcooling degree disappears when temperature difference between T_C and T_H is high. It can be observed for the operation at -5ºC and below. It will be mentioned later, but the reason is that at a high temperature lift the MS cycle is overcome by the cascade solution.

Finally, the ratio between the power consumption of the auxiliary cycle (R1234yf) and the main compressor (CO_2), Eq.(3.10), are represented in percentage for the optimum

operating conditions in Figure 3.8. For the considered range, the needed power consumption of the auxiliary compressor ranges from 4 % at an evaporation of 5ºC and environment temperature of 15ºC to 21 % approximately for 5 ºC at 40 ºC. The most important observation is that sizing the auxiliary compressor for high environment temperatures will cover the operation in transcritical and subcritical without problems.

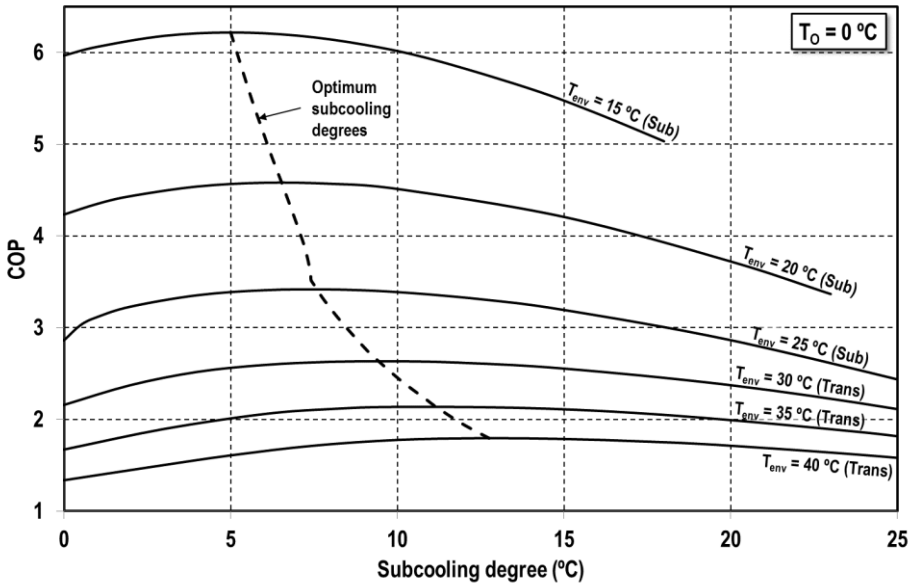

Figure 3.5. COP dependence on the subcooling degree of MS cycle. (T_O=0ºC).

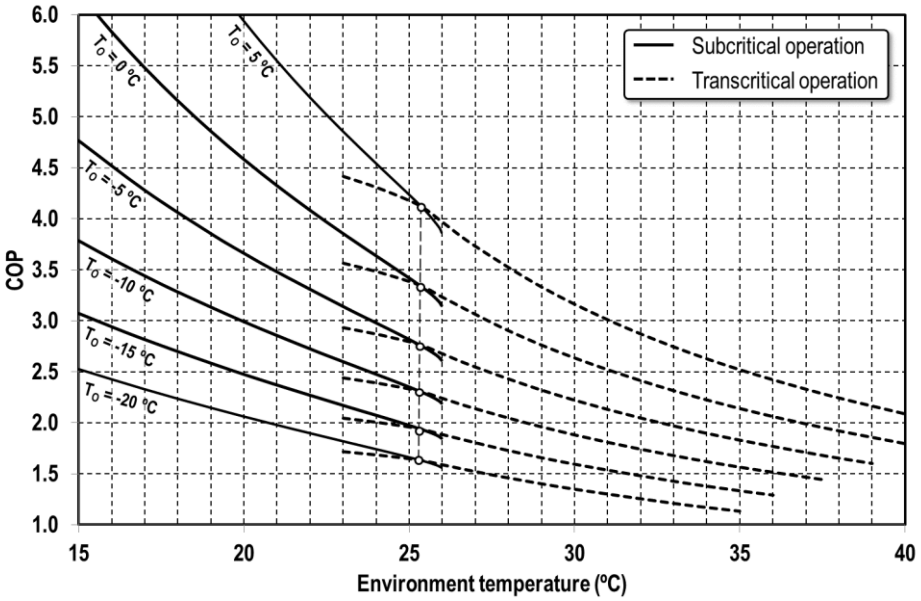

Figure 3.6. COP of the MS cycle at optimum conditions.

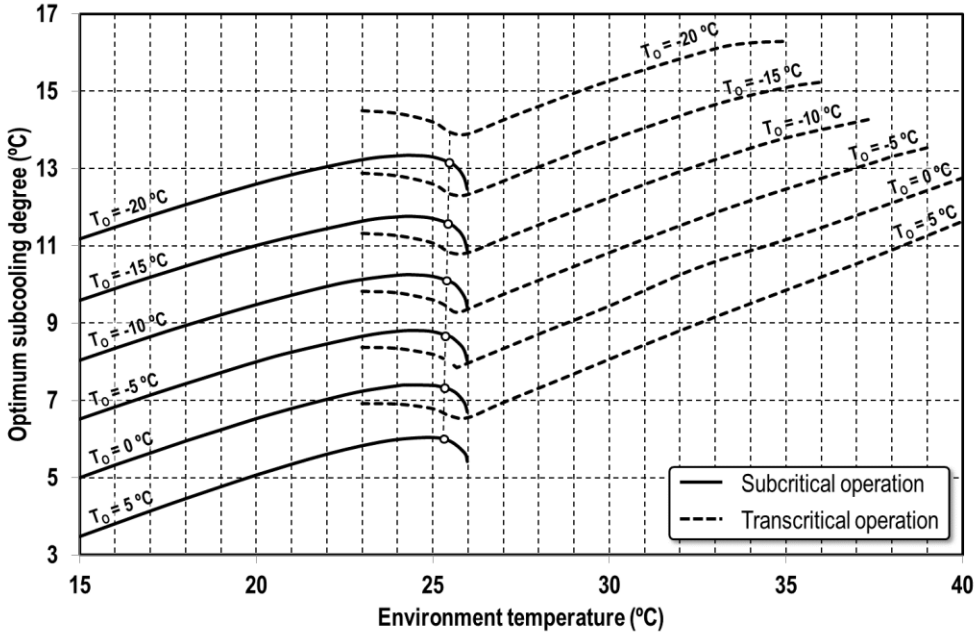

Figure 3.7. Optimum subcooling degrees of the MS cycle.

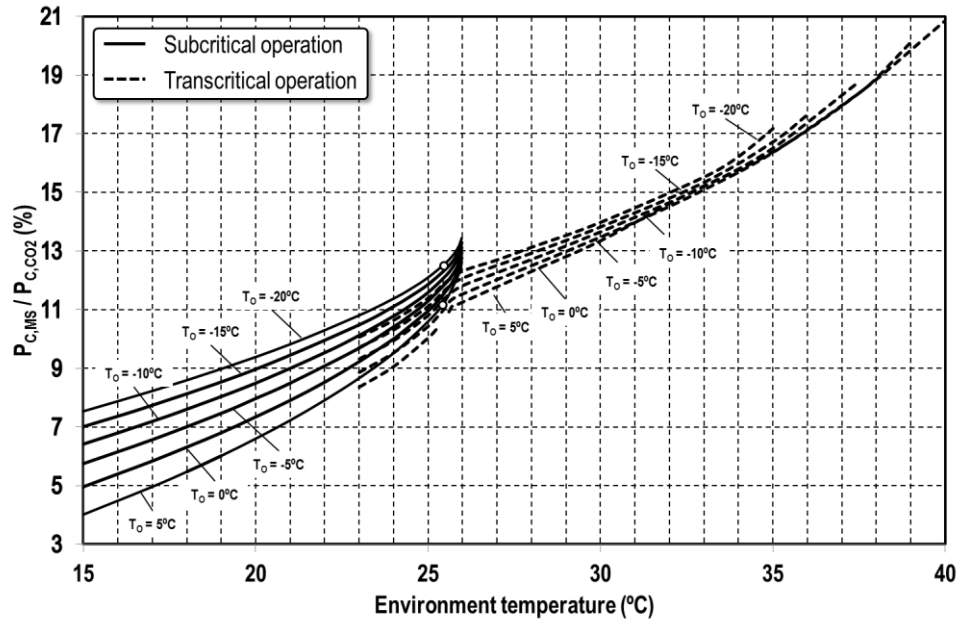

Figure 3.8. Ratio of compressor's power consumptions of the MS cycle.

3.3.2. Operating conditions of the cascade cycle

For the cascade cycle, the parameter that must be optimized is the intermediate temperature level (T_I), the condensing temperature of CO_2 ($T_{K,L}$) being considered in this case for its representation. As mentioned, exit of CO_2 cascade condenser is in saturation, no subcooling is considered, because it provides lower efficiency results. Figure 3.9 presents the evolution of the overall COP of the cascade solution for an evaporation level of 0 ºC for all the considered environment temperatures. Limits of variation of $T_{K,L}$ are any temperature over the evaporating pressure up to a condensing temperature 5 K below the environment temperature (if T_{env} < 25.978 ºC) or the critical temperature. In Figure 3.9 it becomes clear that an optimum $T_{K,L}$ temperature exists. No more emphasis is done because different authors have studied it in detail [29, 30]. COP values at the optimum $T_{K,L}$ are presented in Figure 3.10. In contrast to the COP evolutions of the MS cycle, it needs to be highlighted that the reduction of COP of cascade systems due to variations of the environment temperature is smoother, being these systems less sensitive to variations of environmental conditions, as previously mentioned by Llopis et al. [14]. Also, to compare the design of the cascade system, the ratio of the high-temperature and low-temperature power consumption are presented in Figure 3.11. In this case, the power consumption of the high-temperature compressor inside the evaluated range is of the same order of magnitude as that of the CO_2 cycle. With a design of the plant as cascade, it could operate with the MS cycle but not the other way round.

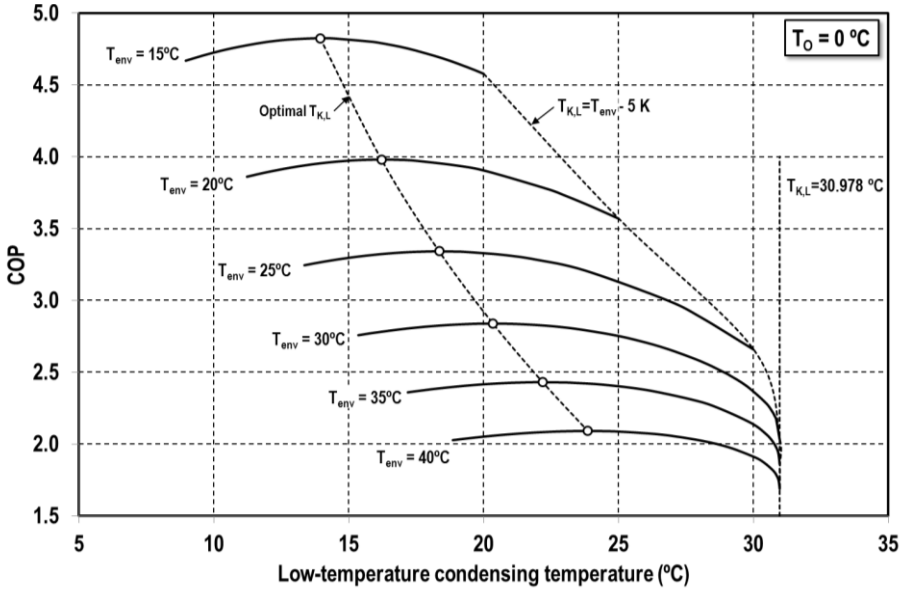

Figure 3.9. COP dependence on the low-temperature condensing temperature of cascade system. (T_O=0ºC).

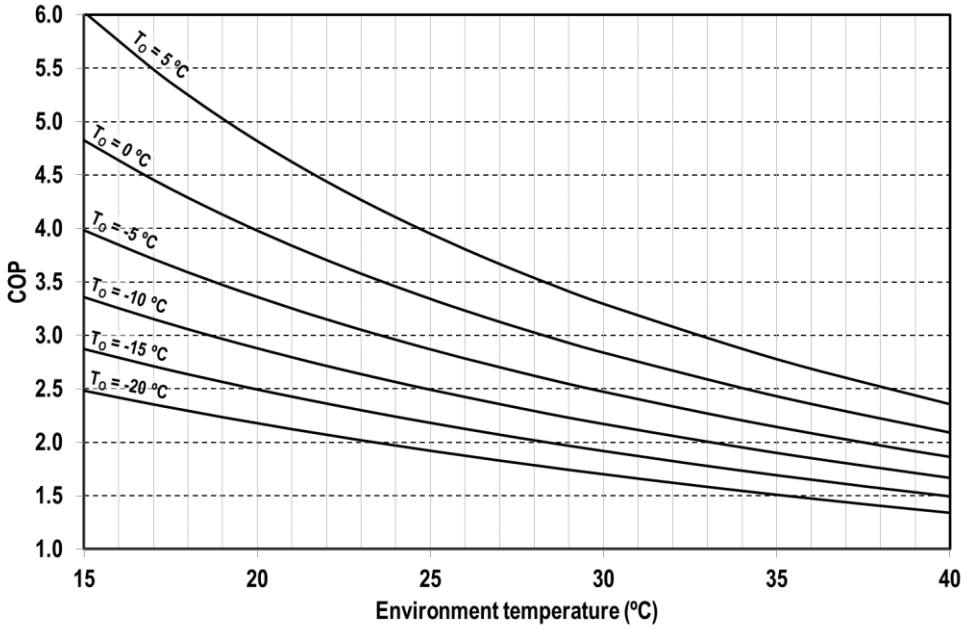

Figure 3.10. COP of the cascade cycle at optimum conditions.

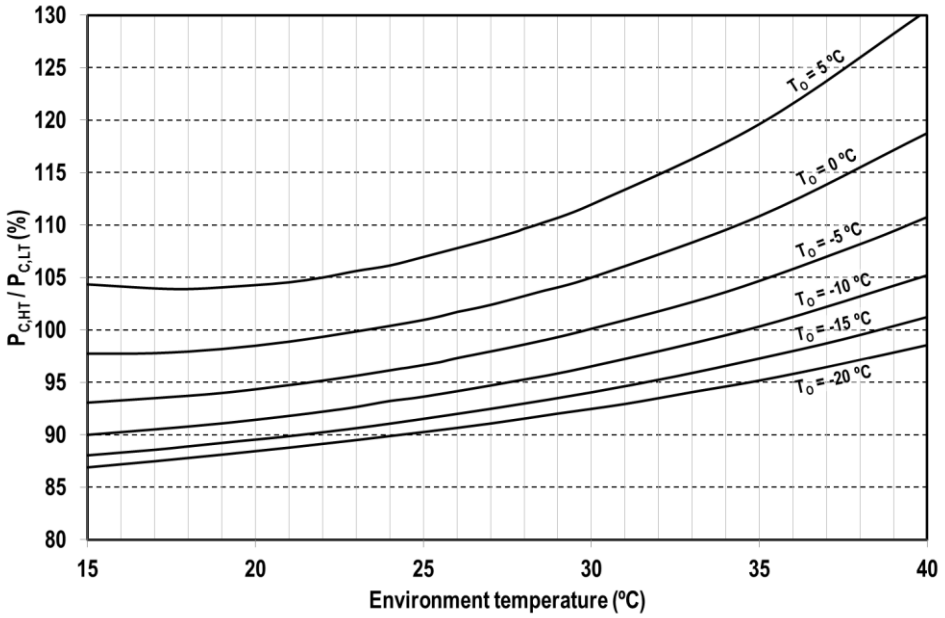

Figure 3.11. Ratio of compressor's power consumptions of the cascade cycle.

3.4. Discussion of results

The optimum operating conditions of both cycles have been analysed in Section 2.3. As mentioned, both refrigeration cycles respond to the same scheme of operation (Figure 3.1) and may be able to operate with one scheme or the other if some components of the plant are over-sized. However, in practice, only one design of the plant is implemented due to economic reasons, for example: if the plant is designed to be operated in both modes the cascade / subcooler heat exchanger must be sized as cascade heat exchanger, while if it were designed to be operated as MS cycle the subcooler would be size reduced. The same happens for the gas-cooler, a gas-cooler of a cascade system is smaller than that of the MS cycle. Furthermore, if optimum COP results of both solutions are compared (Figure 3.6 and Figure 3.10) it can be seen that the MS cycle offers the best results at low environment temperatures and the cascade at high temperatures. Thus, this section is devoted to compare the COP values offered by both solutions. First, the recommended operating range of each cycle is analysed in terms of COP, and then the results are translated to the different climatic regions of Spain through the computation of the average annual COP. The objective is to obtain conclusions about which system would be more recommended for a given evaporating level in a given climatic region.

3.4.1. Recommended operating conditions

COP values offered by both cycle configurations are merged in Figure 3.12, where the COP value at each evaporating and environment level corresponds to the best performing system. As it can be observed, the cascade system gets over the MS solution at high environment temperatures and low evaporating levels. In fact, the environment temperature for a given evaporating level that defines the border of both systems is expressed by Eq. (3.11), which has been fitted from the results of the models. At environment temperatures above the value given by Eq. (3.11), the cascade solution operates with highest COP. Also, the optimum modes of operation of the MS cycle are depicted in Figure 3.12. The operating conditions between an environment temperature of 25.3 ºC and that defined by Eq. (3.11) will be in transcritical conditions, whereas all lower environment levels the best performing cycle will be in subcritical. As it is observed in Figure 3.12, the environmental conditions at which the plant would be operated in transcritical are very narrow, what means that the correct design of the first CO_2 heat exchanger would be as condenser. In an attempt to summarize all the results of Figure 3.12, the COP dependence of both cycles versus the temperature difference between the cold and hot sources, Eq.(3.12), is presented in Figure 3.13. Data used in Figure 3.13 correspond to all the calculated points to represent. It can be observed that the MS cycle offers highest COP values at reduced temperature lifts and the cascade the other way round. The limit is at a temperature lift of 28.5 K approximately. But, it is

important to note that the difference between the COP values of the MS cycle regards the cascade are higher at low temperature lifts that the difference between them at high temperature lifts. Those COP differences will condition the operation of the system along different environment temperatures, therefore a climatic evaluation would be needed to compare both cycles. That is discussed in subsection 2.4.2.

$$T_{env} = 25.95 + 0.4 \cdot T_O \quad (3.11)$$

$$\Delta T = T_{env} - T_O \quad (3.12)$$

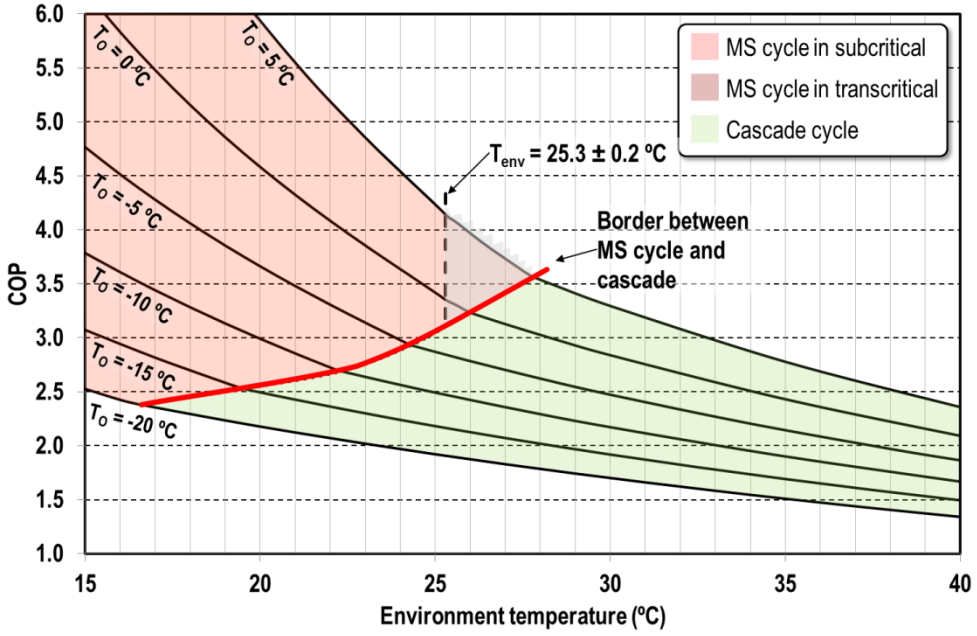

Figure 3.12. Best performing cycle for the different operating conditions.

Although in Figure 3.12 it seems that a smooth transition between the MS and the cascade cycle would be possible, it will only happen when the cycle is sized to operate in both configurations. To illustrate this reasoning, the compressor's displacements for the low and high temperature cycles for both configurations are presented in Figure 3.14. Those data correspond to the displacements for a refrigeration plant with 50 kW of cooling capacity designed for an environment temperature of 30ºC. It can be observed that the differences of the CO_2 compressor are not much significant between both cycles solutions, but the compressor of the cascade cycle would be up to 300% higher than that needed for the MS cycle. If the plant is sized to be operated as MS cycle, its operation as cascade would not be possible because of the compressors, and, although not evaluated, because of the size of the subcooler and the gas-cooler.

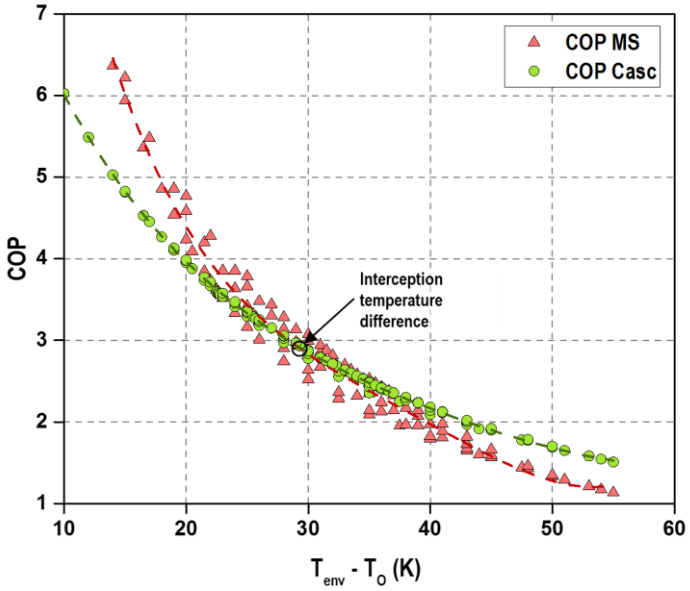

Figure 3.13. COP dependence on cold and hot sink temperature lift. MS and cascade cycles.

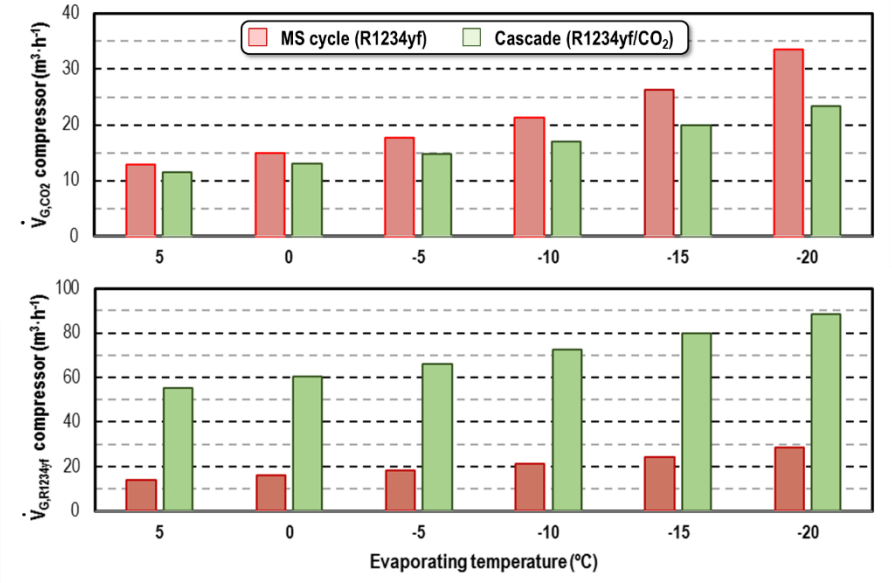

Figure 3.14. Compressor's displacements of a plant with 50 kW capacity at an environment at 30 °C.

3.4.2. Operation in different climate conditions

As mentioned by Minetto et al. [31], the superiority of one refrigeration system regards another in terms of energy efficiency must be discussed with reference to the climatic

conditions of the installation site and the characteristics of cooling profile. In agreement with them, and in order to obtain conclusions about the performance of the MS cycle configuration regards the cascade design, in this subsection an evaluation of the systems at different climate conditions is reported. In this case, a climatic evaluation has been made using the BIN temperature methodology [32] with the Energy Plus meteorological data (https://energyplus.net/weather) for different locations of Spain. In fact, the energy performance of the systems has been evaluated for the twelve climatic regions of Spain [33], Table 3.1, covering cold, mild and warm climates, using 20 temperature BINs from -3 to 33 ºC of dry bulb temperature. For the evaluation, two simplified cooling load profiles have been considered. Representing air-conditioning (AC) applications, no cooling load has been considered below 21ºC, a linear dependence on the cooling load from temperatures above 21 up to 29ºC and 100% from 29ºC on. For commercial applications a constant value of 50% of cooling load up to 23ºC, linear dependence from 23 to 31ºC and 100% from 31 on. Cooling load profiles are detailed in Table 3.1.

Using the meteorological data of dry-bulb temperature, an averaged COP value for both cycle configurations has been evaluated using Eq. (3.13). Where $COP(T_{env,i})$ is the COP of each system evaluated at the average temperature of the 'i' temperature BIN, NH_i is the number of hours of operation inside the 'i' temperature BIN and FQ_i the cooling load fraction inside the 'i' temperature BIN.

$$\overline{COP} = \frac{\sum_{i=1}^{nbin}\left[COP\left(T_{env,i}\right)\cdot NH_i \cdot FQ_i\right]}{\sum_{i=1}^{nbin}\left(NH_i \cdot FQ_i\right)} \quad (3.13)$$

Averaged COP values for both refrigeration systems, for the different climatic regions using the cooling load profiles detailed in Table 3.1, are summarized in Table 3.2. Regarding AC application (T_0=5ºC), it can be seen that the MS cycle over performs the cascade configuration for all the climatic regions except for the D3, C3, C4 and B4, that are regions with high environment temperatures during summer, where both configuration perform similar. Regarding the general application, for evaporating temperatures from 0 to -20 ºC, the MS cycle also presents highest performance for all the climatic regions up to an evaporating level of -10ºC. At -15ºC both solutions perform similar and for -20ºC the cascade solution is the best performing. The differences between both refrigeration systems for the different climate conditions and the different evaporating levels and cooling load profiles have been represented in Figure 3.15 as percentage variation from the MS cycle COP values, according to Eq. (3.14). Values of Eq. (3.14) represent the averaged annual COP advantage of the MS cycle regard the cascade cycle. It can be observed that the MS cycle is recommended from an energy point of view for any evaporating level higher or equal to -10ºC, both systems similar

perform at -15ºC and the cascade should be recommended for the temperature level of -20ºC.

$$\Delta COP\ (\%) = \frac{COP_{MS} - COP_{casc}}{COP_{casc}} \cdot 100 \tag{3.14}$$

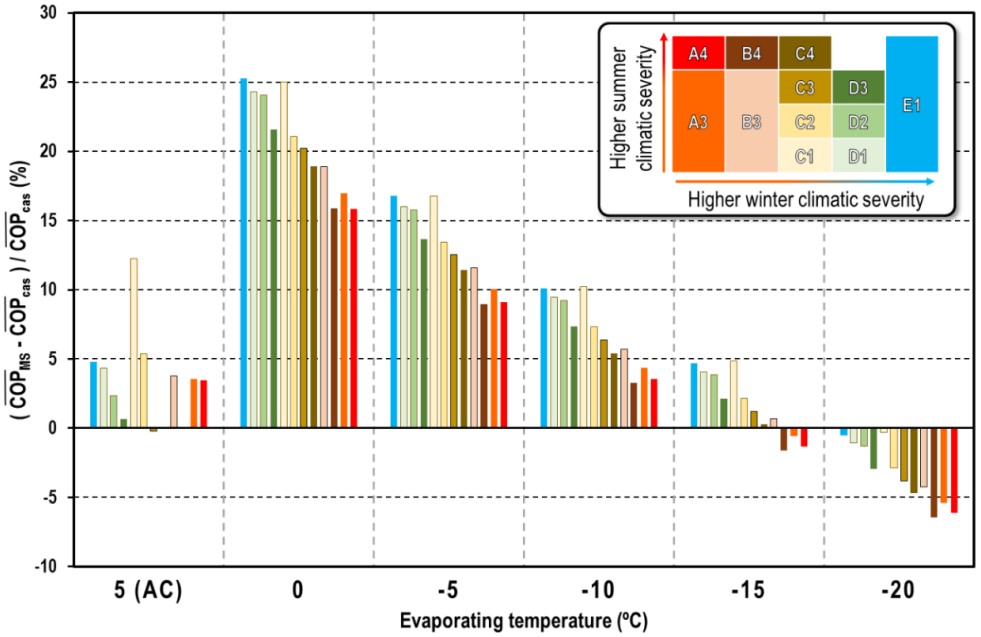

Figure 3.15. COP percentage variation of MS cycle vs. the cascade system at different climatic conditions.

As previously mentioned, both refrigeration cycle designs could be implemented in a system if some of the components are oversized, mainly the high temperature compressor, subcooler and gas-cooler/condenser, although it is not commonly done. Nonetheless, if only one cycle of operation is selected, it is important to quantify what would be its overall performance regards a plant with possibility to operate as cascade or as MS cycle, that would be the plant that will offer the best average annual COP values. To quantify the differences of the individual systems, their average annual COP values according to Eq. (3.13) have been compared to the ones obtained by an ideal refrigeration system with COP values equal to the maximum COP values of the MS or the cascade system. Percentage annual COP deviations regards the ideal system are specified in Table 3.3 for the different Spanish climate regions, and represented for two representative cases in Figure 3.16, which correspond to the operation at -5ºC and -20ºC of evaporating temperature. As it can be observed, any individual system has reductions of annual COP values regards the optimum or best system, since in some

hours of the year the other solution would be more performing. That occurs for all the climatic regions and evaporating levels except for the climatic region C1 with evaporating levels from 5 to -5ºC. In general, for all the climatic regions, the system that better performs is the MS cycle configuration, with annual deviations from the best system up to 5% at evaporating levels higher or equal than -15 ºC. On the other side, if the considered evaporating level is -20ºC, the solution with less deviation from the ideal system is the cascade, however, it is important to note that the MS cycle will have deviations lower than 5% regards the ideal system for all the climatic regions except for the C4, B4, A3 and A4. That indicates that although the MS cycle does not reach the performance of the cascade solution at -20ºC, its average annual performance would be good enough for all the climatic conditions without large reductions of efficiency. This solution will avoid the over sizing of the plant, and thus, allow to operate with a lower cost plant.

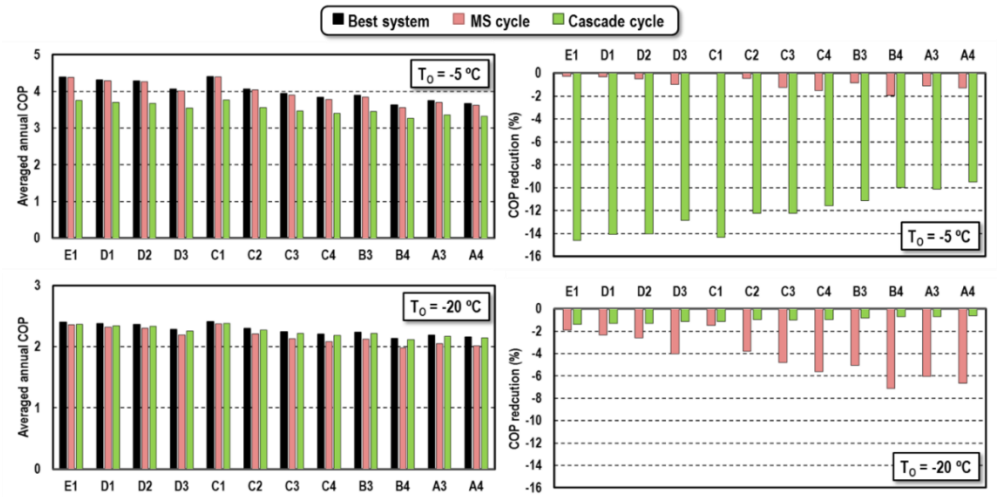

Figure 3.16. Percentage average annual COP deviations of MS and cascade cycles regards the best system.

3.5. Conclusions

This communication analyses two modes of operation of a CO_2-based two-stage refrigeration cycle with equivalent design that can be operated as cascade refrigeration system or as a CO_2 refrigeration plant with dedicated mechanical subcooling system. Both schemes are being considered now to spread the use of CO_2 in medium and warm regions of the planet for medium temperature applications.

Using relations of the overall efficiency of compressors, adjusted from experimental data of a semi-hermetic CO_2 and a semi-hermetic R1234yf compressors, a simplified model of both cycles has been developed. With the thermodynamic models, the optimum operating conditions of each refrigeration cycle, covering evaporating temperatures from -20 to 5ºC and environment temperatures from 15 to 40 ºC, have been determined. Then, by merging the COP values of each refrigeration solution, the external conditions at which each refrigeration solution is the best performing have been established. Furthermore, the analysis has been translated the different climatic regions of Spain to compare the systems.

Regarding the CO_2 refrigeration cycle with mechanical subcooling, it has been concluded that the environment temperature that will limit the operation in subcritical or transcritical is 25.3 ºC, thus the design of the gas-cooler would be always as condenser, since the region at which this system will operate in transcritical is very narrow. Furthermore, the optimum subcooling degree results higher at lowest evaporating levels and high environment levels. Nonetheless, the maximum ratio of power consumption of the mechanical subcooling compressor will not exceed from 21% of the power consumption of the CO_2 compressor.

It has been concluded that the cascade configuration using CO_2 as low temperature refrigerant will have highest performance than the MS cycle when the temperature lift between the cold and heat sources is higher than 28.5 K. However, in this case the power consumption of the high-temperature cycle will be even higher than the power consumption of the CO_2 rack.

The analysis has been extended to the different climatic regions of Spain using a based temperature-BIN methodology. It has been calculated that the MS cycle would offer highest energy efficiencies in overall-year operation than the cascade solution for evaporating levels below -15ºC, including the air-conditioning application. However, at the evaporating level of -20ºC the cascade solution will over perform the MS cycle. Also, the individual systems have been compared to an ideal refrigeration cycle that could be operated as CO_2 with mechanical subcooling or as cascade at any climatic condition, which is called the best system. The averaged annual COP of each individual system has been compared with the best system. It has been observed that the MS cycle will have annual reductions of efficiency up to 5% at evaporating levels higher or equal than -15ºC, and also reductions below 5% at the evaporating level of -20ºC except for 4 climatic regions of Spain.

As general conclusion of this work, it can be affirmed that if this cycle configuration is sized as cascade or as a single-stage cycle with mechanical subcooling, the

configuration that will offer the best performing levels at the analysed conditions would be the CO_2 refrigeration cycle with mechanical subcooling.

3.6. Acknowledgements

The authors gratefully acknowledge the Spanish Ministry of Economy and Competitiveness (project ENE2014-53760-R.7) for financing this research work.

3.7. Nomenclature

Casc	cascade cycle with CO_2 as low temperature refrigerant
COP	coefficient of performance
FQ	cooling load fraction inside a temperature BIN
HX	heat exchanger
h	specific enthalpy, $kJ \cdot kg^{-1}$
NH	number of hours inside a temperature BIN
nbin	number of temperature bins
MS	CO_2 cycle with mechanical subcooling
$\dot{m}$	mass flow rate, $kg \cdot s^{-1}$
P	pressure, bar
P_C	compressor power consumption, kW
$\dot{Q}_O$	cooling capacity, kW
SUB	degree of subcooling at the subcooler, K
T	temperature, ºC
t	compression ratio
$\dot{V}_G$	compressor displacement, $m^3 \cdot h^{-1}$

Greek symbols

η_G	overall compressor efficiency
Δ	Increment

Subscripts

CO_2	referring to CO_2 cycle
crit	critical point
env	environment
gc	gas-cooler
H	hot sink
high	refers to pressure at gas-cooler and subcooler or cascade heat exchanger
I	intermediate temperature level
K	condensing level
L	cold source, low temperature cycle
MS	referring to the dedicated mechanical subcooling cycle
O	evaporating level
R1234yf	referring to the R1234yf cycle
sat	saturation

3.8. References

1. European Commission. Regulation (EU) No 517/2014 of the European Parliament and of the Council of 16 April 2014 on Fluorinated Greenhouse Gases and Repealing Regulation (EC) No 842/2006; 2014.
2. Hafner, A.; Hemmingsen, A.K. R744 refrigeration technologies for supermarkets in warm climates. In Proceedings of the 24th IIR International Congress of Refrigeration, Yokohama, Japan, 16–22 August 2015.
3. Kim, M.H.; Pettersen, J.; Bullard, C.W. Fundamental process and system design issues in CO2 vapor compression systems. Prog. Energy Combust. Sci. 2004, 30, 119–174.
4. Jia, X.; Zhang, B.; Pu, L.; Guo, B.; Peng, X. Improved rotary vane expander for trans-critical CO2 cycle by introducing high-pressure gas into the vane slots. Int. J. Refrig. 2011, 34, 732–741.
5. Hu, J.; Li, M.; Zhao, L.; Xia, B.; Ma, L. Improvement and experimental research of CO2 two-rolling piston expander. Energy 2015, 93, 2199–2207.
6. Elbel, S.; Lawrence, N. Review of recent developments in advanced ejector technology. Int. J. Refrig. 2016, 62, 1–18.

7. Hafner, A.; Banasiak, K.; Herdlitschka, T.; Fredslund, K.; Girotto, S.; Haida, M.; Smolka, J. 'R744 Ejector System Case: Italian Supermarket, Spiazzo', in Refrigeration Science and Technology. 2016, pp. 471–478.
8. Lawrence, N.; Elbel, S. 'Experimental Study on Control Methods for Transcritical CO2 Two-Phase Ejector Systems at Off-Design Conditions', in Refrigeration Science and Technology. 2016, pp. 511–518.
9. Karampour, M.; Sawalha, S. 'Integration of Heating and Air Conditioning into a Co2 Trans-Critical Booster System with Parallel Compression Part I: Evaluation of Key Operating Parameters Using Field Measurements', in Refrigeration Science and Technology. 2016, pp. 323–331.
10. Aprea, C.; Greco, A.; Maiorino, A. The application of a desiccant wheel to increase the energetic performances of a transcritical cycle. Energy Convers. Manag. 2015, 89, 222–230.
11. Arora, A.; Singh, N.K.; Monga, S.; Kumar, O. Energy and exergy analysis of a combined transcritical CO2 compression refrigeration and single effect H2O-LiBr vapour absorption system. Int. J. Exergy 2011, 9, 453–471.
12. Sanz-Kock, C.; Llopis, R.; Sánchez, D.; Cabello, R.; Torrella, E. Experimental evaluation of a R134a/CO2 cascade refrigeration plant. Appl. Therm. Eng. 2014, 73, 39–48.
13. Peñarrocha, I.; Llopis, R.; Tárrega, L.; Sánchez, D.; Cabello, R. A new approach to optimize the energy efficiency of CO2 transcritical refrigeration plants. Appl. Therm. Eng. 2014, 67, 137–146.
14. Llopis, R.; Sánchez, D.; Sanz-Kock, C.; Cabello, R.; Torrella, E. Energy and environmental comparison of two-stage solutions for commercial refrigeration at low temperature: Fluids and systems. Appl. Energy 2015, 138, 133–142.
15. Hafner, A.; Hemmingsen, A.K.; Van De Ven, A. 'R744 Refrigeration System Configurations for Supermarkets in Warm Climates', in Refrigeration Science and Technology. 2014, pp. 125–133.
16. Gullo, P.; Elmegaard, B.; Cortella, G. Energy and environmental performance assessment of R744 booster supermarket refrigeration systems operating in warm climates. Int. J. Refrig. 2016, 64, 61–79.
17. Llopis, R.; Cabello, R.; Sánchez, D.; Torrella, E. Energy improvements of CO2 transcritical refrigeration cycles using dedicated mechanical subcooling. Int. J. Refrig. 2015, 55, 129–141.
18. Nebot-Andrés, L.; Llopis, R.; Sánchez, D.; Cabello, R. Experimental evaluation of a dedicated mechanical subcooling system in a CO2 transcritical refrigeration cycle, Refrigeration Science and Technology. 2016, pp. 965–972.
19. Eikevik, T.M.; Bertelsen, S.; Haugsdal, S.; Tolstorebrov, I.; Jensen, S. 'Co2 Refrigeration System with Integrated Propan Subcooler for Supermarkets in Warm Climate', in Refrigeration Science and Technology. 2016, pp. 211–218.
20. Ge, Y.T.; Tassou, S.A.; Santosa, I.D.; Tsamos, K. Design optimisation of CO2 gas cooler/condenser in a refrigeration system. Appl. Energy 2015, 160, 973–981.
21. Shao, L.L.; Zhang, C.L. Thermodynamic transition from subcritical to transcritical CO2 cycle. Int. J. Refrig. 2016, 64, 123–129.

22. Tsamos, K.M.; Ge, Y.T.; Santosa, I.D.M.C.; Tassou, S.A. Experimental investigation of gas cooler/condenser designs and effects on a CO2 booster system. Appl. Energy. 2017, 186, 470–479.
23. Sánchez, D.; Patiño, J.; Sanz-Kock, C.; Llopis, R.; Cabello, R.; Torrella, E. Energetic evaluation of a CO2 refrigeration plant working in supercritical and subcritical conditions. Appl. Therm. Eng. 2014, 66, 227–238.
24. Dopazo, J.A.; Fernández-Seara, J. Experimental evaluation of a cascade refrigeration system prototype with CO2 and NH3 for freezing process applications. Int. J. Refrig. 2011, 34, 257–267.
25. Aprea, C.; Greco, A.; Maiorino, A. An experimental investigation on the substitution of HFC134a with HFO1234YF in a domestic refrigerator. Appl. Therm. Eng. 2016, 106, 959–967.
26. Sánchez, D.; Torrella, E.; Cabello, R.; Llopis, R. Influence of the superheat associated to a semihermetic compressor of a transcritical CO2 refrigeration plant. Appl. Therm. Eng. 2010, 30, 302–309.
27. Llopis, R.; Nebot-Andrés, L.; Cabello, R.; Sánchez, D.; Catalán-Gil, J. Experimental evaluation of a CO2 transcritical refrigeration plant with dedicated mechanical subcooling. Int. J. Refrig. 2016, 69, 361–368.
28. Lemmon, E.W.; Huber, M.L.; McLinden, M.O. REFPROP, NIST Standard Reference Database 23, v.9.1; National Institute of Standards: Gaithersburg, MD, USA, 2013.
29. Torrella, E.; Llopis, R.; Cabello, R. Experimental evaluation of the inter-stage conditions of a two-stage refrigeration cycle using a compound compressor. Int. J. Refrig. 2009, 32, 307–315.
30. Lee, T.S.; Liu, C.H.; Chen, T.W. Thermodynamic analysis of optimal condensing temperature of cascade-condenser in CO2/NH3 cascade refrigeration systems. Int. J. Refrig. 2006, 29, 1100–1108.
31. Minetto, S.; Rossetti, A.; Girotto, S.; Marinetti, S. 'Seasonal Performance of Supermarket Refrigeration Systems', in Refrigeration Science and Technology. 2016, pp. 455–462.
32. The Australian Institute of Refrigeration, Air Conditioning and Heating (AIRAH), Methods of calculating Total EquivalentWarming Impact (TEWI) 2012. Available online: http://www.airah.org.au/imis15_prod/Content_Files/BestPracticeGuides/Best_Practice_Tewi_June2012.pdf (accessed on 21 April 2017).
33. Ministry of Housing, Royal Decree 314/2006, Spanish Technical Building Code. HE Enegy Saving Document. Available online: http://www.codigotecnico.org/ (accessed on 17 March 2017)

Table 3.1. Reference Spanish cities for the evaluation of the systems. Climatic regions, temperature BINs, hours of operation and cooling load profiles

City			León	Pamplona	Teruel	Albacete	La Coruña	Barcelona	Granada	Toledo	Castellón de la Plana	Sevilla	Málaga	Almería
Spanish climatic region			E1	D1	D2	D3	C1	C2	C3	C4	B3	B4	A3	A4
Average annual temperature (ºC)			10.79	12.22	11.55	13.51	14.14	15.37	14.88	15.57	16.74	18.25	17.99	18.54
Temperature BIN	**AC cooling load (%)**	**Commercial cooling load (%)**	**Annual hours inside the temperature BIN**											
<-3	0	0.5	0	0	0	0	0	0	0	0	0	0	0	0
-3 to -1	0	0.5	0	0	0	0	0	0	0	0	0	0	0	0
-1 to 1	0	0.5	248	0	391	0	0	0	0	0	0	0	0	0
1 to 3	0	0.5	990	341	878	633	0	0	248	155	0	0	0	0
3 to 5	0	0.5	936	962	875	847	0	0	692	602	0	0	0	0
5 to 7	0	0.5	847	1114	633	817	0	540	843	663	124	62	0	0
7 to 9	0	0.5	915	819	887	571	537	909	571	876	903	754	62	0
9 to 11	0	0.5	818	884	734	981	1697	1057	827	663	968	846	996	810
11 to 13	0	0.5	943	846	751	604	1364	819	668	949	813	785	1055	943
13 to 15	0	0.5	826	944	855	756	1553	1063	851	572	854	789	941	933
15 to 17	0	0.5	552	765	733	669	1556	824	814	638	943	858	884	975
17 to 19	0	0.5	492	615	522	705	950	817	795	578	909	841	1061	1094
19 to 21	0	0.5	244	430	430	583	673	1046	612	764	976	1008	1002	851
21 to 23	0.2	0.5	304	274	213	339	430	613	307	615	800	581	919	1068
23 to 25	0.4	0.6	304	304	244	306	0	518	461	431	552	581	738	800
25 to 27	0.6	0.7	155	276	273	273	0	337	214	275	394	523	397	488
27 to 29	0.8	0.8	186	186	217	304	0	217	243	183	338	275	426	458
29 to 31	1	0.9	0	0	124	124	0	0	273	393	186	243	279	340
31 to 33	1	1	0	0	0	217	0	0	124	155	0	304	0	0
>33	1	1	0	0	0	31	0	0	217	248	0	310	0	0

Table 3.2. Averaged annual COP of cascade and MS cycles for Spanish Climate Regions.

Climatic region	E1	D1	D2	D3	C1	C2	C3	C4	B3	B4	A3	A4
Cascade cycle annual averaged COP												
T_0=5ºC (AC)	3.74	3.72	3.57	3.41	4.30	3.79	3.33	3.33	3.66	3.34	3.63	3.63
T_0=0ºC	4.51	4.45	4.42	4.23	4.53	4.26	4.13	4.04	4.11	3.87	4.00	3.94
T_0=-5ºC	3.75	3.70	3.68	3.54	3.77	3.56	3.46	3.39	3.45	3.26	3.37	3.32
T_0=-10ºC	3.18	3.14	3.12	3.01	3.19	3.03	2.95	2.90	2.95	2.80	2.88	2.84
T_0=-15ºC	2.73	2.70	2.69	2.60	2.74	2.61	2.55	2.51	2.54	2.42	2.49	2.46
T_0=-20ºC	2.37	2.35	2.33	2.26	2.38	2.27	2.22	2.18	2.22	2.12	2.17	2.15
MS cycle annual averaged COP												
T_0=5ºC (AC)	3.92	3.88	3.65	3.43	4.82	4.00	3.32	3.33	3.80	3.34	3.76	3.76
T_0=0ºC	5.65	5.52	5.48	5.14	5.67	5.16	4.97	4.81	4.89	4.49	4.68	4.56
T_0=-5ºC	4.38	4.29	4.26	4.02	4.40	4.04	3.89	3.78	3.85	3.55	3.70	3.62
T_0=-10ºC	3.50	3.44	3.41	3.23	3.52	3.25	3.14	3.06	3.11	2.89	3.00	2.94
T_0=-15ºC	2.86	2.81	2.79	2.65	2.87	2.67	2.58	2.51	2.56	2.38	2.48	2.43
T_0=-20ºC	2.36	2.32	2.30	2.19	2.37	2.21	2.13	2.08	2.12	1.98	2.06	2.02

Table 3.3. Percentage deviation of annual COP values of MS and cascade cycles regards the best system

Climatic region	E1	D1	D2	D3	C1	C2	C3	C4	B3	B4	A3	A4
Cascade cycle												
T_0=5ºC (AC)	-4.7	-4.3	-3.1	-2.6	-10.9	-5.2	-2.5	-2.8	-4.3	-2.7	-4.2	-4.1
T_0=0ºC	-20.2	-19.6	-19.6	-18.2	-20.0	-17.5	-17.4	-16.6	-16.2	-14.6	-14.9	-14.2
T_0=-5ºC	-14.6	-14.1	-14.1	-12.9	-14.3	-12.3	-12.3	-11.6	-11.2	-10.0	-10.1	-9.5
T_0=-10ºC	-9.7	-9.3	-9.3	-8.4	-9.3	-7.8	-7.9	-7.4	-6.9	-6.1	-6.2	-5.7
T_0=-15ºC	-5.5	-5.2	-5.2	-4.6	-5.0	-4.1	-4.2	-4.0	-3.6	-3.1	-3.1	-2.8
T_0=-20ºC	-1.4	-1.3	-1.3	-1.1	-1.1	-1.0	-1.0	-1.0	-0.8	-0.7	-0.7	-0.6
MS cycle												
T_0=5ºC (AC)	-0.2	-0.2	-0.8	-2.0	0.0	-0.1	-2.7	-2.8	-0.7	-2.7	-0.8	-0.8
T_0=0ºC	-0.1	-0.1	-0.2	-0.5	0.0	-0.1	-0.7	-0.9	-0.4	-1.1	-0.5	-0.6
T_0=-5ºC	-0.3	-0.3	-0.5	-1.0	0.0	-0.5	-1.3	-1.5	-0.8	-1.9	-1.1	-1.3
T_0=-10ºC	-0.6	-0.7	-0.9	-1.6	-0.1	-1.0	-2.0	-2.4	-1.6	-3.1	-2.1	-2.4
T_0=-15ºC	-1.1	-1.3	-1.5	-2.5	-0.4	-2.0	-3.1	-3.7	-2.9	-4.7	-3.6	-4.1
T_0=-20ºC	-1.9	-2.4	-2.6	-4.0	-1.5	-3.8	-4.8	-5.6	-5.0	-7.1	-6.1	-6.7

Chapter 4 Subcooling methods for CO_2 refrigeration cycles: A review.

4. Subcooling methods for CO_2 refrigeration cycles. A review.

Chapter adapted from the paper: Llopis, R., Nebot-Andrés, L., Sánchez, D., Catalán-Gil, J., Cabello, R. Subcooling methods for CO_2 refrigeration cycles: A review (2018) International Journal of Refrigeration, 93, pp. 85-107. DOI: 10.1016/j.ijrefrig.2018.06.010

Abstract

CO_2 subcooling has resulted a method to upgrade the performance of CO_2 refrigeration plants in the recent years, with overall improvements up to 12% with internal heat exchangers, 22% with economizers, 25.6% with thermoelectric systems and 30.3% with dedicated subcooling methods. This paper comprehensively reviews the recent studies that consider subcooling as a way to upgrade the performance of CO_2 refrigeration cycles. The review is limited to CO_2 refrigeration cycles with accumulation receiver for commercial purposes and does not consider air conditioning or MAC systems. It is organized as follows: first, the thermodynamic aspects of subcooling in CO_2 refrigeration cycles are described and discussed; second, the main results and conclusions of the recent investigations are analysed inside two big groups: subcooling internal methods and subcooling external methods. Finally, the review synthesizes the current state of the art and points out the lines of research that deserve future developments.

Keywords

CO_2, subcooling, dedicated mechanical subcooling, integrated mechanical subcooling, thermoelectric subcooling

Chapter 4: Subcooling methods for CO_2 refrigeration cycles. A review.

4.1. Introduction

CO_2 refrigeration systems were rescued by Prof. Lorentzen (1994) in the nineties as a reasonable and technical possible solution to replace artificial refrigerants in air conditioning and refrigeration applications. As Lorentzen and Pettersen stated, implementation of CO_2 cycles would avoid 'continued emissions of several hundred thousand tonnes of alien chemicals to the atmosphere each year, involving the potential risk of unforeseen environmental effects' (Lorentzen and Pettersen, 1993).

Renaissance of CO_2 as working fluid for refrigerant applications was slow, because the initial CO_2 refrigeration systems, especially those working or analysed in transcritical conditions, reached an energy efficiency level not comparable to that of artificial refrigerants. To solve the problem, the scientific community did great effort on the last decades. First, research was focused on defining alternative refrigeration schemes and on improving the performance of individual components (Groll and Kim, 2007; Kim et al., 2004). This initial stage of research clearly showed that the working schemes of competitive plants would be very different from the traditional schemes used with artificial refrigerants. Second, CO_2 refrigeration was taken a step forward due to the development of expanders (Singh and Dasgupta, 2016) and ejector systems (Elbel, 2011; Elbel and Lawrence, 2016), which allowed to recover energy in the expansion processes. Finally, CO_2 refrigeration systems have been combined with other systems (hybrid systems) to provide air-conditioning, to perform heat recovery, etc,.., i. e., to supply all thermal demands of an application using a very efficient combined system (Pardiñas et al., 2018).

In the last years, in parallel with the approval of the F-Gas Regulation in Europe (European Commission, 2014) and the adoption and ratification of the Kigali amendment to the Montreal Protocol (UNEP, 2016), CO_2 refrigeration is in a massive expansion stage, especially in supermarket refrigeration. One of the main reasons is that CO_2 is the unique existing refrigerant combining favourable environmental properties (GWP=1) and high security properties (A1 Ashrae classification), and probably the unique in the future, as analysed by McLinden et al. (2017). The second reason is that the advance of the technique has allowed to implement CO_2 refrigeration systems competitive or even better than with traditional systems, which increased complexity of course.

Although some upgrades of CO_2 refrigeration systems have been extensively covered in the last decade, the improvements associated with subcooling of CO_2 at the exit of the gas-cooler/condenser have not been analysed globally. Accordingly, the purpose of this review is to join the most recent research in relation to cycles, mechanisms and possibilities to improve the energetic performance of CO_2 refrigeration plants using subcooling at the exit of the gas-cooler/condenser. Revision of the state of the art

shows that considering as base line system the CO_2 cycle without improvements, the possibilities to enhance the overall performance reach 12% using internal heat exchangers, 22% using economizers, 25.6% using thermoelectric systems, 21.3% using integrated mechanical subcooling systems and 30.3% using dedicated mechanical subcooling systems. Most of the review research is at an initial stage and there is room for improvement in some of the methods.

This review is limited to subcooling systems devoted to CO_2 refrigeration systems and concretely to cycles with subcooling at the exit of the gas-cooler/condenser with the use of heat exchanger. Other subcooler options, such as parallel compression technologies (Chesi et al., 2014) are not covered. Heat pump application is also out of this review. Here, we make emphasis on refrigeration systems including an accumulation vessel, thus its design is the most appropriate for supermarket or medium to large systems.

The review is organized as follows: First, in Section 3.2 the thermodynamic aspects of subcooling in CO_2 refrigeration systems are analysed: cycle modification in subcritical and transcritical conditions, benefits and cost of subcooling and optimization of the systems are addressed. Second, Section 3.3 is devoted to subcooling mechanisms based on internal methods, i. e., using the CO_2 cycle to provide subcooling: internal heat exchangers, economizers, integrated mechanical subcooling systems and heat storage systems are covered. Third, Section 3.4 is focused on dedicated subcooling methods, consisting on hybrid systems: dedicated mechanical subcooling, thermoelectric systems and others are reviewed. Finally, Section 3.5 extracts the main conclusions of the current state-of-the-art and highlights the points and options that require further developments, since as it is concluded there is room for improvement using this approach.

4.2.Thermodynamic aspects of CO_2 subcooling

This section is dedicated to discuss the main thermodynamic aspects of CO_2 refrigeration cycles with subcooling. Subsection 3.2.1 details the basic subcooled cycle and describes the cycle operation principles. Subsection 3.2.2 establishes the benefits of subcooling, in terms of capacity and COP improvements. Subsection 3.2.3 discusses about the cost or additional energy input needed to provide the subcooling. And finally, subsection 3.2.4 details the operating parameters that must be optimized in a subcooled cycle.

4.2.1. Cycle with subcooling and operation

CO_2 reference cycle configuration considered for the analysis of subcooling corresponds to the most basic classical layout used for commercial purposes, it being detailed in Figure 4.1. It consists of a compression system, a gas-cooler/condenser performing

heat rejection to the hot sink (T_H), a generic subcooling system which function is to subcool the CO_2 absorbing energy along the subcooler at an intermediate temperature (T_I<T_H), a back-pressure valve to control the heat rejection pressure and a receiver where the non-in-service refrigerant is stocked. Then, liquid refrigerant is extracted from the vessel and sent to the evaporators where the cycle absorbs the heat load from the cold source (T_C). Evaporators are usually controlled by expansion valves maintaining a constant degree of superheat.

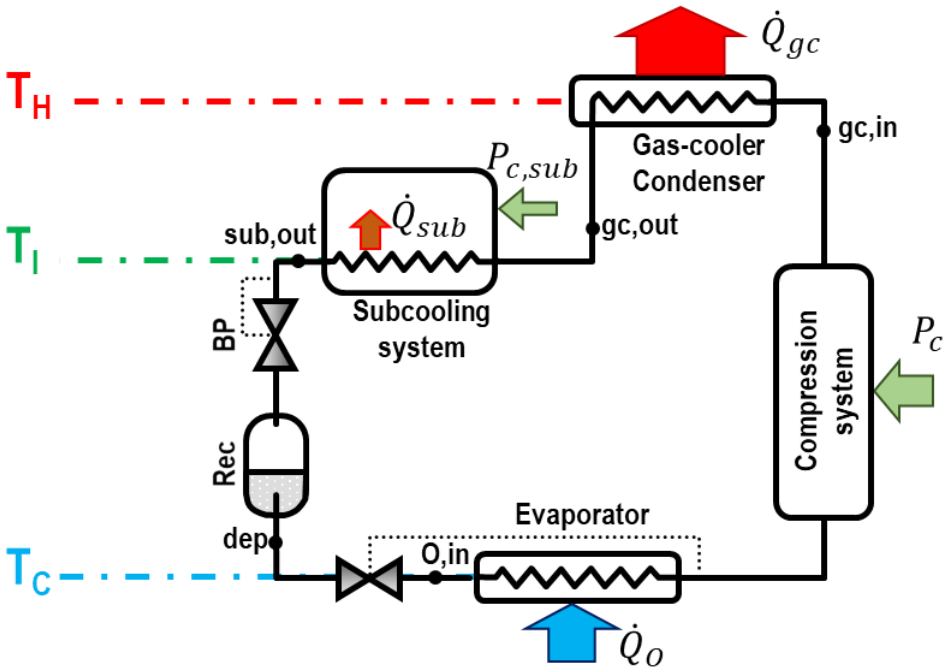

Figure 4.1. Schematic layout of a CO_2 refrigeration system with double-stage expansion with subcooling system.

The low critical temperature of CO_2 (T_{crit}=30.978ºC) implies that these refrigeration systems run according to two principal modes of operation: at low heat rejection temperatures the cycle works in subcritical conditions, where the heat exchanger performs heat rejection through condensation at constant temperature. At high heat rejection temperatures, theoretically for heat rejection temperatures above the critical value but in practice for temperatures also below the critical (Sánchez et al., 2014b), the cycle works in supercritical conditions. In this case, the heat exchanger acts as gas-cooler with a decreasing temperature profile through heat rejection. (Kim et al., 2004). Throughout a year, the refrigeration cycle alternate its operation in subcritical and supercritical conditions, being the analysis needed for both modes of operation.

4.2.1.1. Subcooling in subcritical conditions

CO_2 subcooling in subcritical conditions can be performed using two types of strategies, extensively analysed by Koeln and Alleyne (2014).

The first one consists of condensing at a forced pressure higher than the minimal that the condenser allows. This situation is represented in Figure 4.1 with dashed line, with condensing temperature T_K* higher than T_K. In this case, the condenser performs heat rejection at a high temperature and is able to provide a small degree of subcooling by itself (a subcooler device can be used before). This strategy is used in practice for small capacity refrigeration systems for commercial use working with capillary tubes, where the refrigerant mass charge is optimized to obtain a desired subcooling degree in the condenser, as described by Pisano et al. (2015), and thus maximize the energy performance of the system. According to Pottker and Hrnjak (2015), liquid subcooling below saturation increases the refrigerant effect and the COP of the system, because liquid subcooling reduces the throttling losses in the expansion device. Their simulations for air conditioning systems indicated COP improvements of 8.4% with R-1234yf, 7.0% with R-410A, 5.9% with R-134a and 2.7% with R-717. The application of this strategy in CO_2 refrigeration plants for commercial purposes (Figure 4.1) would be possible in practice due to the presence of the back-pressure, which would rise the heat rejection pressure and increase the subcooling degree. However, no research studies have been found about.

The second strategy corresponds to the usual in commercial systems, which is represented in continuous line in Figure 4.2. It consist of performing heat rejection at the minimal temperature that the condenser allows (T_K) until saturation and then incorporate a subcooling system to reduce CO_2 liquid temperature. Again, due to availability of the back-pressure, the condensing pressure could be forced to be higher, but the theoretical results of Nebot-Andrés et al. (2017) indicate that the best performing situation is when CO_2 at the exit of the condenser is in saturation. In this case, as presented in Figure 4.2, the subcooling brings about three positive effects in relation to the cycle without subcooling: a pressure reduction in the vessel (ΔP_{rec}), an increase of the specific refrigerating effect (Δq_o) and a reduction of the vapour title at the inlet of the evaporator (Δx_v), which can result in a slight increment of the evaporating level (Qureshi et al., 2013). No negative effects are introduced except of the cost of subcooling, which is discussed in subsection 3.2.3.

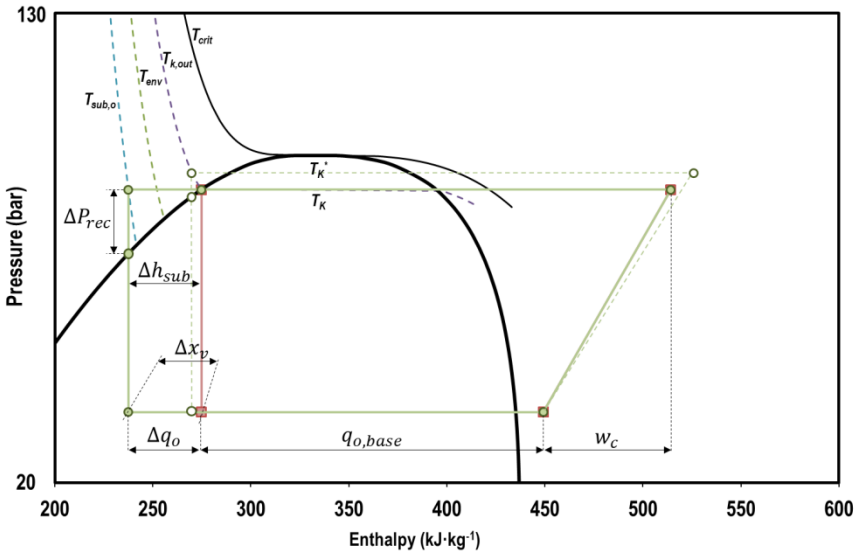

Figure 4.2. CO_2 cycle (red) and CO_2 with dedicated mechanical subcooling (green) in subcritical conditions. T_{env}=20ºC, T_O=-10ºC, ΔT_{gc}=5K. Adapted from Nebot-Andrés et al. (2017).

4.2.1.2. Subcooling in transcritical conditions

At high heat rejection temperatures, the refrigeration system operates in transcritical conditions and there is only one possible strategy to subcool the CO_2, which is represented in Figure 4.3. It is based on the use of a subcooling system at the exit of the gas-cooler and prior to the back-pressure to provide the desired degree of subcooling. Research discussed in Sections 4 and 5 indicates that subcooling reduces the optimum heat rejection pressure in relation to non-subcooled layouts. Accordingly, the beneficial effects of subcooling are enhanced in transcritical conditions, since it allows: a reduction of the optimum heat rejection pressure (ΔP_{gc}), a reduction of the specific compression work in the compressor (Δw_{comp}), a pressure reduction in the receiver (ΔP_{rec}), an increment of the specific refrigerating effect (Δq_o) and a reduction of the vapour title at the inlet of the evaporators (Δx_v), which can result also in an increment of the evaporating level (Qureshi et al., 2013). Again, the unique drawback is the cost of subcooling, which is discussed in 3.2.3. The subcooling device in transcritical conditions will operate near the critical point, generally crossing the critical isotherm and sometimes the pseudocritical temperature line where the isobaric specific heat of CO_2 reaches maximum values (Liao and Zhao, 2002). At high heat rejection temperatures this cross will occur inside the subcooling system and at low temperatures inside the gas-cooler. It indicates that the design principles of the subcooling heat exchanger should follow the same guidelines as gas-coolers.

4.2.2. Benefits of subcooling

Subcooling in CO_2 refrigeration systems presents the different advantages or improvements detailed in Section 3.2.1, nevertheless, a common approach to quantify the practical effects of subcooling is attending to the energy parameters of the refrigeration cycle: capacity and COP.

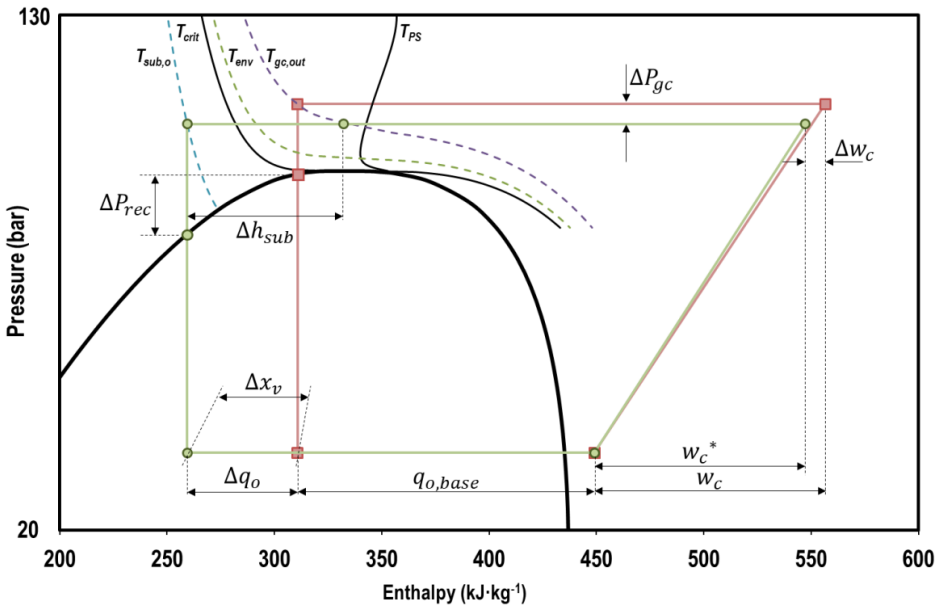

Figure 4.3. CO_2 cycle (red) and CO_2 with dedicated mechanical subcooling (green) in transcritical conditions. T_{env}=33ºC, T_O=-10ºC, ΔT_{gc}=5K. Adapted from Nebot-Andrés et al. (2017).

4.2.2.1. Capacity

Eq. (4.1) expresses the cooling capacity of the CO_2 refrigeration system with subcooling (Figure 4.1), which corresponds to the product of refrigerant mass flow rate and the specific refrigerating effect in the evaporator. This term can be expressed as the addition of the capacity of the CO_2 cycle without considering the subcooling ($\dot{m}_r \cdot q_{o,base}$) and the heat extracted by the subcooling device ($\dot{Q}_{sub}$), as expressed by Eq. (4.2) and (4.3). The specific refrigerating effect of the cycle without subcooling ($q_{o,base}$), Eq. (4.4), is the difference between the enthalpy at the exit of the evaporator and at the exit of the gas-cooler/condenser, where '*' represents enthalpy value at the exit of the gas-cooler/condenser in the new optimum conditions considering the subcooling system, which could be different than of the optimized cycle without subcooling.

$$\dot{Q}_O = \dot{m}_r \cdot q_o = \dot{m}_r \cdot \left(h_{O,out} - {h_{gc,out}}^* + \Delta h_{sub}\right) \quad (4.1)$$

$$\dot{Q}_O = \dot{m}_r \cdot q_{o,base} + \dot{Q}_{sub} \quad (4.2)$$

$$\dot{Q}_{sub} = \dot{m}_r \cdot \Delta h_{sub} = \dot{m}_r \cdot \left({h_{gc,out}}^* - h_{sub,out}\right) \quad (4.3)$$

$$q_{o,base} = h_{o,out} - {h_{gc,out}}^* \quad (4.4)$$

Table 4.1 relates the capacity increments achieved by some general subcooling systems, which are expressed in percentage in relation to the reference system used for the evaluation. Torrella et al. (2011) measured up to 12% capacity enhancement by the use of an internal heat exchanger in a single-stage refrigeration plant in relation to the basic layout at high heat rejection temperatures and Llopis et al. (2016a) measured up to 55.7% increase in capacity for a single-stage plant operating with an R-1234yf dedicated mechanical subcooling system at optimum COP conditions. However, the rest of studies where evaluated from a theoretical approach and did not reported the possible capacity increments.

Li et al. (2017) proposed the parameter *RICOSP*, Eq.(4.5), to quantify the relationship between the increase in capacity of a subcooled vapor compression system ($\dot{Q}_O - \dot{Q}_{O,no-sub}$) to the power or heat extracted by the subcooling device ($\dot{Q}_{sub}$). From a theoretical approach in subcritical cycles, they concluded that the subcooling power cannot be fully transformed into an increase of the cooling output and established the thermodynamic limit of RICOSP to 1. In Li et al. (2017) simulations, they calculated a RICOSP value of 0.805. However, and also stated by the same authors, if the subcooling modifies the operating conditions of the cycle, as in the case of transcritical conditions (Figure 4.3), the RICOSP can exceed the unit. For example, Llopis et al. (2016a) measured a RICOSP value of 1.19 using an R-1234yf dedicated mechanical subcooling in a single-stage CO_2 refrigerating plant at -10ºC of evaporating and 40ºC of gas-cooler outlet temperatures at the optimum heat rejection pressure. The use of the subcooling system offered a reduction of the optimum gas-cooler pressure of 5.2 bar, which resulted in an increment of the refrigerant mass flow rate in the CO_2 cycle of 0.5%.

$$RICOSP = \frac{\dot{Q}_O - \dot{Q}_{O,no-sub}}{\dot{Q}_{sub}} \quad (4.5)$$

Accordingly, it can be deduced that the use of subcooling systems in CO_2 cycles offers highest possibilities than in subcritical conditions, since the subcooling system modifies the operating conditions of the CO_2 cycle towards lower pressures. However, the thermodynamic limits of subcooling in transcritical conditions have not been extensively analyzed. Also, expression of RICOSP for CO_2 cycles must be evaluated at the optimum heat rejection pressures.

Table 4.1. Improvements of CO_2 refrigeration systems with different subcooling systems. Simple effects.

Subcooling system	Reference system	T_O (ºC)	$T_{gc,out}$ (ºC)	Capacity increment (%)	COP increment (%)	Type	Reference
Internal heat exchanger	basic cycle	-15 to -5 ºC	31 and 34ºC	12% max	12% max.	E, O	(Torrella et al., 2011)
Economizer	double-stage cycle with intercooling	2.7ºC	22, 33ºC	-	21.1, 22.1 %	T, O	(Cavallini et al., 2005)
Thermoelectric	basic cycle	-15 to 5ºC	30 to 50ºC	-	7.0 to 25.6%	T, O	(Sarkar, 2013)
Integrated mechanical subcooler	basic cycle	-10ºC	30 to 42ºC		20.5 to 21.3%	T, O	(Gullo and Cortella, 2016)
Dedicated mechanical subcooler	basic cycle	0, -10ºC	24, 30, 40ºC	55.7% max.	30.3% max.	E	(Llopis et al., 2016a)

T=Theoretical, E= Experimental, O= optimized cycle, Basic cycle: single-stage cycle without IHX.

4.2.2.2. COP

Eq. (4.6) expresses the COP of a CO_2 refrigeration cycle with subcooling, where: $\dot{Q}_O$ is the cooling capacity offered by the cycle, Eq.(4.1); P_C is the power consumption of the CO_2 compressor; and $P_{C,sub}$ is the energy input to the subcooling system.

$$COP = \frac{\dot{Q}_O}{P_{C,CO2} + P_{C,sub}} \tag{4.6}$$

Defining the COP of the subcooling system as the quotient between the heat extracted by the subcooling device and the energy input to activate the subcooling system, Eq.(4.7), the overall COP of the subcooled CO_2 refrigeration system can be expressed through an energy balance in the subcooler system as detailed by Eq.(4.8). In Eq. (4.8) it is observed that the overall COP depends on the CO_2 enthalpy difference caused by the subcooling system (Δh_{sub}) and on the COP of the subcooler system (COP_{sub}). The subcooling will have positive effect on the COP only if $\frac{\partial COP}{\partial \Delta h_{sub}}$ results positive. It can be easily demonstrated that the subcooling system will enhance the overall *COP* if the *COP* of the subcooling system satisfies Eq.(4.9) at the operating conditions of the cycle. That is to say that a subcooling system would enhance the performance of a CO_2 cycle as

long as $COP_{sub} = f(T_H, T_I)$ is higher than the $COP_{sub} = f(T_H, T_C)$ of the CO_2 cycle. In the case of mechanical subcooling systems (subsections 3.3.3 and 3.4.1), condition of Eq. (4.9) is generally satisfied if the subcooling system performs heat rejection to the same hot sink as the CO_2 cycle (T_H), because the cold source of the subcooling system (T_I) is higher than the cold source of the CO_2 cycle (T_C). However, when the subcooling system presents low COP values, such as with the use of thermoelectric devices (subsection 3.4.2) the improvements are restricted to fulfil Eq.(4.9) and obtain lower improvements due to the low values of COP_{sub}. These effects can be observed in the results presented in Table 4.1. Vapour compression systems used as subcooling systems obtain large improvements in the overall COP because they operate with low temperature difference between the cold source and the heat sink (Llopis et al., 2016a), however, improvements achieved by thermoelectric systems are shorter due to their low COP values (Sarkar, 2013).

$$COP_{sub} = \frac{\dot{Q}_{sub}}{P_{C,sub}} \tag{4.7}$$

$$COP = \frac{q_{o,base} + \Delta h_{sub}}{w_c{}^* + \frac{\Delta h_{sub}}{COP_{sub}}} \tag{4.8}$$

$$COP_{sub} > COP_{CO2} \tag{4.9}$$

Accordingly, it can be affirmed that the subcooling systems would offer higher COP increments when higher the COP of the subcooling system is, however, the thermodynamic limits of this improvement have not been extensively analyzed.

4.2.3. Cost of subcooling

The cost of subcooling or the additional energy input that the system requires to obtain the subcooling depends on the amount of subcooling to be provided and on the thermodynamic behavior of the subcooling system. Eq.(4.10) expresses the total energy input to the system, which considers the energy consumption of the CO_2 cycle and of the subcooling system. Eq. (4.11) expresses the increment on energy consumption of a subcooled system ('*') in relation to a non-subcooled one.

$$P_C{}^* = P_{C,CO2} + P_{C,sub} = \dot{m}_r \cdot w_c + P_{C,sub} \tag{4.10}$$

$$\Delta P_C = P_C{}^* - P_C = (\dot{m}_r{}^* \cdot w_c{}^* - \dot{m}_r \cdot w_c) + \frac{\dot{Q}_{sub}}{COP_{sub}} \tag{4.11}$$

Taking as reference the ideal system of Figure 4.1, if the subcooling is performed in subcritical conditions (Figure 4.2), the subcooling does not modify the optimum heat rejection pressure and thus the behavior of condenser and compressor. Correspondingly, the increment on energy input of the subcooled system is the quotient

between the heat extracted by the subcooling device and the COP of the subcooling system, Eq.(4.12). This situation occurs in CO_2 subcritical systems and it is also applicable to conventional refrigerants working in subcritical conditions (Qureshi et al., 2013; Zubair, 1994).

$$\Delta P_C = \frac{\dot{Q}_{sub}}{COP_{sub}} = \dot{m}_r \cdot \frac{\Delta h_{sub}}{COP_{sub}} \tag{4.12}$$

However, the use of subcooling in transcritical conditions is able to reduce the heat rejection pressure (Figure 4.3) and thus modify the operating conditions of the compressor. If the heat rejection pressure is lower, the CO_2 refrigerant mass flow rate of the subcooled cycle is higher than the non-subcooled ($\dot{m}_r{}^* > \dot{m}_r$), but the specific compression work of the subcooled cycle is lower than the non-subcooled ($w_{comp}{}^* < w_{comp}$), whose trends are opposite. Nonetheless, the experimental results of Llopis et al. (2016a) with a dedicated mechanical subcooling system (DMS) single-stage plant showed that the CO_2 compressor power consumption was reduced when subcooling the cycle, and the results of Bush et al. (2017) with a DMS two-stage plant even resulted in decrements of the total system power consumption. Subsequently, it can be affirmed that the increment on energy consumption due to the subcooling system in transcritical conditions will be lower than the one established in subcritical condition, as expressed by Eq.(4.13).

$$\Delta P_C < \frac{\dot{Q}_{sub}}{COP_{sub}} = \dot{m}_r \cdot \frac{\Delta h_{sub}}{COP_{sub}} \tag{4.13}$$

4.2.4. Optimization of subcooling

As mentioned before, subcooling in a CO_2 refrigeration system modifies its optimum operating conditions, especially in transcritical conditions, where the subcooling is able to reduce the optimum high rejection pressure and thus modify the behaviour of the CO_2 compressor. Obviously, it is required for such systems to determine the operating parameters that maximize the COP of the overall system.

COP of the subcooled cycle, Eq.(4.6), depends on the cooling capacity and on the energy input to the compressor and to the subcooling system. For a fixed operating condition, with defined evaporating level and gas-cooler outlet temperature, the power consumption of the CO_2 compressor only depends on the high rejection pressure, Eq. (4.14)(Cabello et al., 2008), and the cooling capacity depends on the high rejection pressure as well as on the subcooling, Eq.(4.15). Referring to the subcooling system, its cold source at T_I only depends on the subcooling degree, subsequently the energy input to the subcooling system is a function of the subcooling, Eq. (4.16). Therefore, it can be affirmed that the COP of the whole system is function of the heat rejection pressure and

of the subcooling degree, as expressed by Eq.(4.17). In subcritical conditions the optimum heat rejection pressure is equal to the condensing pressure, as discussed in subsection 3.2.1, and only the subcooling degree needs to be optimized. However, in transcritical conditions the COP of the plant is bounded to two parameters (Nebot-Andrés et al., 2017) that must be optimized together.

$$P_C = f(P_{gc}) \tag{4.14}$$

$$\dot{Q}_O = f(P_{gc}, SUB) \tag{4.15}$$

$$T_I = f(SUB) \rightarrow P_{C,sub} = f(SUB) \tag{4.16}$$

$$COP = f(P_{gc}, SUB) \tag{4.17}$$

It is important to highlight that the classical relations to define the optimum heat rejection pressure in CO_2 transcritical cycles (Chen and Gu, 2005; Kauf, 1999; Liao et al., 2000) are not suitable for subcooled cycles, since the optimum condition also depends on the used subcooling system. This is another subject to be investigated concretely for each type of subcooling system.

4.3. Internal methods

This section reviews the methods evaluated to provide the subcooling at the exit of the gas-cooler/condenser internally, i. e. using the cycle itself to cool down CO_2 at the exit of the heat exchanger. Suction-line to liquid-line or internal heat exchangers and their use in different cycle layouts are included in subsection 3.3.1; the economizer or subcoolers used in two-stage cycles in subsection 3.3.2; integrated mechanical subcooling systems based on the use of additional compressors in subsection 3.3.3.; and other internal methods in subsection 3.3.4.

4.3.1. Internal Heat Exchanger (IHX)

The use of the IHX was the first subcooling device implemented in the renewed use of CO_2 as refrigerant. In fact, the first researchers who revived the use of CO_2, Lorentzen and Pettersen (1993), stated that its use in CO_2 refrigeration systems is completely convenient, since it improves COP due to the reduction of the throttling loss from cooling the refrigerant before entering the throttling device, however, they also stated that its use causes strong increments on the compressor discharge temperature.

4.3.1.1 Classical positions

The IHX or liquid-line-to-suction-line heat exchanger, placed at the exit of the gas-cooler/condenser and at the exit of the evaporator (Figure 4.5, Layout A), subcools the CO_2 through reheating of the vapours at the exit of the evaporator. In an overall vision, this device increments the specific refrigerating effect in the evaporator due to the subcooling and increments the compressor suction temperature, as with conventional artificial refrigerants. However, when it is used in transcritical conditions, its use is able

to reduce the optimum heat rejection pressure, enhancing the performance of the plant through an increment of the refrigerant mass flow rate and a reduction of the specific compression work in the compressor (section 3.2.1). Table 4.2 and Figure 4.4 collect the experimental COP increments achieved with the use of the IHX in CO_2 refrigeration plants with different typologies. Only specific investigations devoted to the IHX analysis are collected.

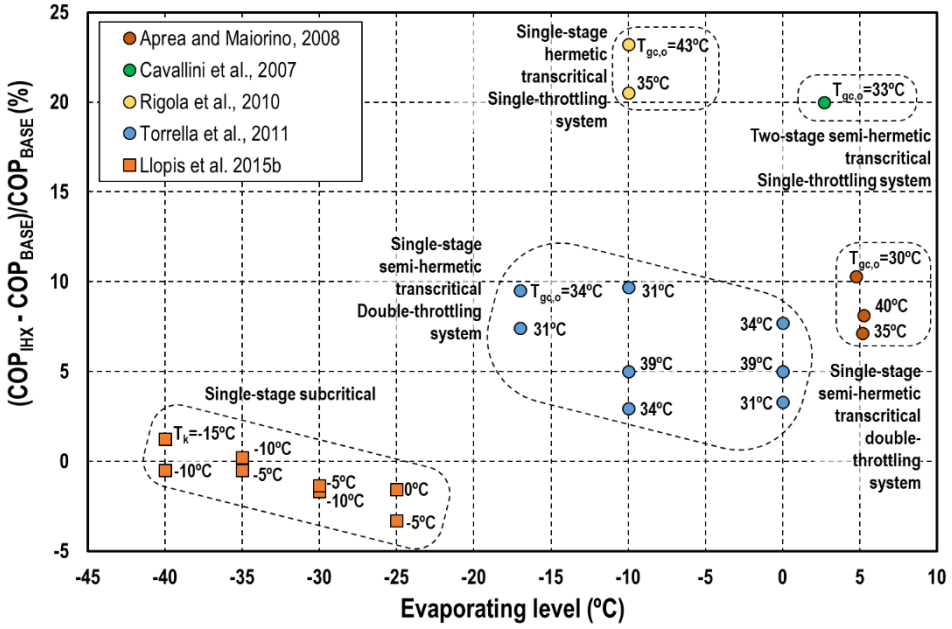

Figure 4.4. Reported experimental COP improvements in CO_2 refrigeration plants.

On the one hand, considering transcritical operation, for environment temperatures higher than 30ºC, Cavallini et al. (2005) first simulated an air-to-air double compression with intercooling single-stage throttling cycle with and without IHX quantifying a 7.6% COP improvement due to the IHX, however, in its later experimental verification (Cavallini et al., 2007) they measured 20% COP increment. They argued that the deviation from the theoretical approach was the increased temperature at compressor suction that led to higher heat rejection at the intercooler. Aprea and Maiorino (2008) measured experimentally the IHX effect in an air-to-air single-stage compression two-stage throttling plant for air-conditioning purposes. They measured COP increments from 8.1 to 10.5%. Rigola et al. (2010) evaluated a water-to-water single-throttling plant with an hermetic compressor at -10ºC of evaporation, measuring COP increments due to the IHX between 20.5 to 23.2%. This is the largest reported increment, and could be related to the use of a single-stage expansion device or to the use of a hermetic

compressor, however, no additional data was reported. Sánchez et al. (2016) tested another water-to-water plant working with a hermetic compressor measuring a maximum COP increment of 6.7% when using the IHX. Finally, Torrella et al. (2011) presented an extensive experimentation of the IHX using a water-to-water double-stage throttling with single-stage semihermetic compressor at evaporating temperatures from -17 to 0ºC. They verified the COP increment, however, the improvements were the lowest among the transcritical tested plants, varying between 3.3 to a 9.7%. All these experimental improvements are summarized in Figure 4.4.

Table 4.2. Conducted research to quantify the COP improvement due to IHX in CO_2 refrigeration plants.

Authors	**Character**	**Analysed system**	**Base system**	**T_0 (ºC)**	**$T_{gc,o}$ / [T_{env}] / (T_K) (ºC)**	**COP**	**ΔCOP (%)**
(Cavallini et al., 2005)	T	Air-to-air double compression with intercooling single-stage throttling with IHX, air-cooled	Same without IHX	2.7	33 [30]	2.82	7.6
(Cavallini et al., 2007)	E	Air-to-air double compression with intercooling single-stage throttling with IHX, air-cooled	Same without IHX	2.7	33 [30]	2.20	20
(Aprea and Maiorino, 2008)	E	Air-to-air single-stage compression two-stage throttling with IHX	Same without IHX	4.5 / 5.25	25 / 40	2.11 / 1.2	8.1 / 10.5
(Cecchinato et al., 2009)	T	Single-throttling single-compression with IHX	Same without IHX	-30 / 4	[30]	1.05 / 3.25	4.8 / 16.5
(Rigola et al., 2010)	E	Water-to-water single-throttling single-compression with IHX	Same without IHX	-10	[35 / 43]	0.875 / 1.175	20.5 / 23.2
(Torrella et al., 2011)	E	Water-to-water double-stage throttling single-compression with IHX	Same without IHX	-17 / 0	31 / 39	1.3 / 2.5	3.3 / 9.7
(Llopis et al., 2015b)	E	Refrigerant-to-water single-stage throttling single-compression with IHX and desuperheater	Same without IHX	-40 / -25	(-15 / -5)	2.1 / 4.7	-1.7 / 1.22

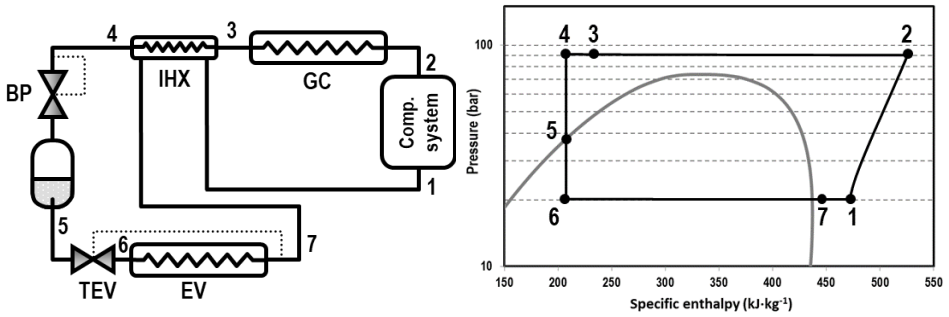

IHX at the exit of the gas-cooler/condenser (Layout A)

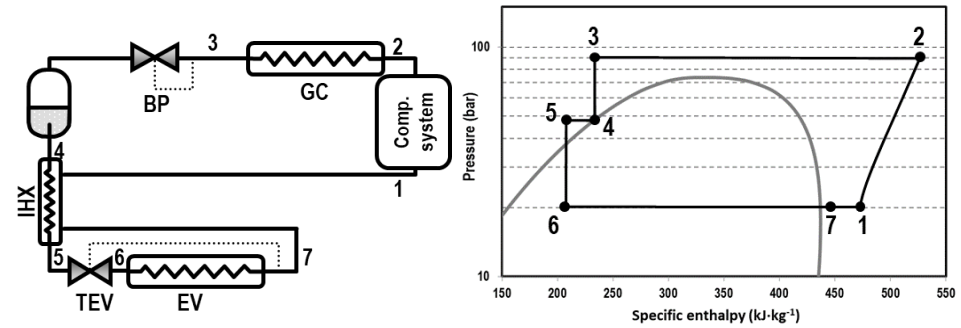

IHX at the exit of the receiver (Layout B)

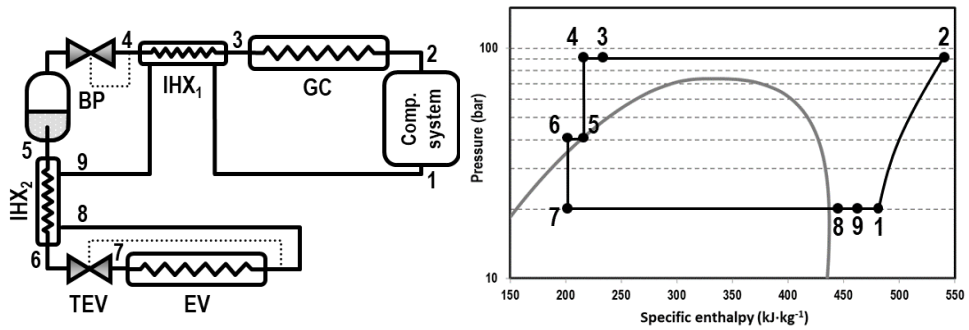

Double IHX at the exit of the gas-cooler and at the exit of the receiver (Layout C)

Figure 4.5. Different IHX layouts.

On the other hand, considering the effect of the IHX in subcritical conditions, Zhang et al. (2011) theoretically predicted a slight COP reduction due to the use of the IHX and advised not to use it in subcritical plants. This COP trend was experimentally verified by

Llopis et al. (2015b) in the CO_2 subcritical cycle of a cascade plant with a semihermetic compressor, however, they highlighted that its use at low evaporating levels is needed to guarantee the proper operation of the lubricant oil. Furthermore, in a subsequent investigation (Llopis et al., 2016b) they evaluated the IHX effect in the overall COP of a cascade cycle, concluding that the use of the IHX in the low temperature cycle is also recommended because the overall COP of the cascade was improved up to 3.7%.

Accordingly, from the reported experimental results it is evident that the use of the IHX in the classical layout (exit gas-cooler/exit evaporator) is recommendable for transcritical systems, not for stand-alone subcritical cycles and yes for low-temperature cycles of cascade systems.

Moreover additional research was also conducted to evaluate the IHX in different layouts in the refrigeration cycle. Karampour and Sawalha (2014) theoretically evaluated nine positions of the IHX in a two-stage booster system with heat recovery. After modelling the booster supplying 150kW cooling demand at medium temperature and 50kW at low temperature, they concluded that the IHX provided no significant improvement in terms of refrigeration COP. However, considering simultaneous refrigeration and heat recovery they calculated up to 12% efficiency improvement with IHX at gas-cooler outlet, double IHX at gas-cooler outlet and at the exit of the accumulation tank and double IHX at gas-cooler outlet and at the liquid line to low temperature cabinets, for the booster system with flash gas by-pass; and up to 11% improvement with double IHX at the exit of gas-cooler and at the exit of the accumulation tank, double IHX at gas-cooler outlet and liquid line to low temperature cabinets, double IHX at exit of the accumulation tank and double IHX at exit of accumulation tank and liquid line to low temperature cabinets. Sánchez et al. (2014a) conducted experimental research with the IHX at three positions in the classical cycle for commercial refrigeration at medium temperature. They evaluated the IHX at the exit of the gas-cooler (Layout A, Figure 4.5), at the exit of the accumulation receiver (Layout B, Figure 4.5) and double IHX at the exit of gas-cooler and at the exit of the accumulation receiver (Layout C, Figure 4.5). They concluded that in any position the IHX resulted positive in terms of COP. However, improvement with Layout B was lower than in the classical position (Layout A) and the Layout C with double IHX provided the largest COP increment up to 13%, however, authors advised that the use of two IHX caused increments on the compressor's discharge temperature up to 20K.

4.3.1.2. Combination of the IHX with ejectors

Use of IHX has also been considered in CO_2 refrigeration systems using ejectors, whose representative cycle layout is detailed in Figure 4.6.

First of all, Elbel and Hrnjak (2004) trough simulation analysed four different CO_2 air conditioning systems for mobile appliances including a gas ejector and analysed the effect of the IHX on this cycle at 35ºC of gas-cooler outlet temperature. They observed that for matching cooling capacities the system with ejector and IHX obtained highest COP and reduced optimum heat rejection pressure, however, when the system was analysed under constant rotational speed of the compressor, they observed that the use of the IHX in combination with the ejector reduced the capacity of the system. After further analysis, they concluded that the use of the IHX in combination with ejectors with variable displacement compressors was not recommended. Previous theoretical hypothesis were experimentally corroborated by Xu et al. (2011) although in a CO_2 cycle with a two-phase fixed ejector for water heating purposes. They corroborated that the use of the IHX in combination with the ejector weakened the ejector contribution to the system.

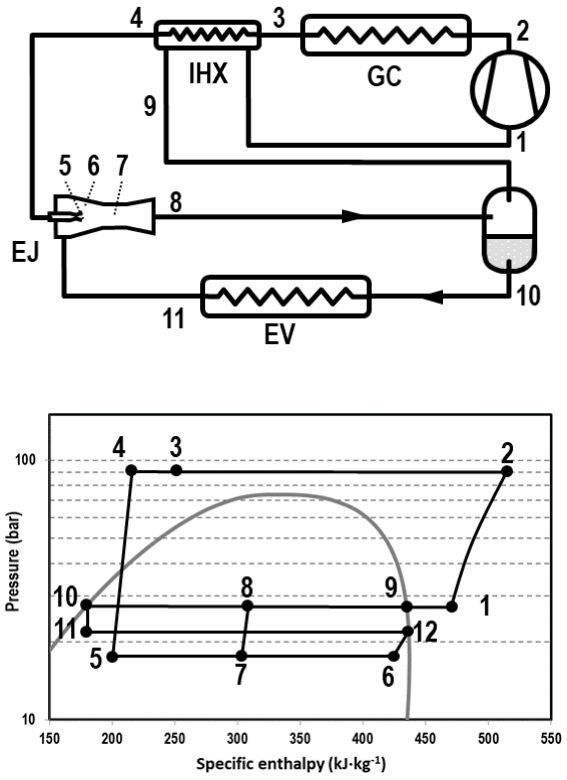

Figure 4.6. Position of the IHX in CO_2 refrigeration systems with ejector.

However, experimental results of Nakagawa et al. (2011) with a 2 to 4kW capacity CO_2 refrigeration system with two-phase ejector showed that the IHX was beneficial in combination with the ejector. This different trend can be associated, as stated by the authors, that the improvement achieved by the IHX was larger when higher the heat rejection temperature was and this improvement lowered and even worsened at low temperatures, due to the reduction of pressure recovery in the ejector. In this case, experimental results of Nakagawa et al. (2011) were obtained for gas-cooler outlet temperatures from 42 to 47ºC, far away from Xu et al.'s evaluation range.

Finally, Zhang et al. (2013), using a theoretical approach, extended the analysis of the use of IHX in ejector refrigeration systems. They included in the analysis the ejector isentropic efficiency and extended the simulations to a wide range of evaporating and gas-cooler exit temperatures. They discovered that the use of the IHX is only beneficial in terms of COP for high gas-cooler and evaporating temperatures and for ejector systems with low isentropic efficiency. For systems with ejectors with low isentropic efficiency, the use of the IHX provided highest improvements than the ejector itself, thus its use was not recommendable.

4.3.1.3. Combination of the IHX with expanders

Use of IHX has scarcely been evaluated in combination with CO_2 refrigeration cycles using expanders to recover energy during the expansion process of the refrigerant, which schematic cycle layout is presented in Figure 4.7.

Zhang et al. (2014) and J.Shariatzadeh et al. (2016) using theoretical approaches based on first and second Law of Thermodynamics evaluated the effect of the IHX in the cycle. They concluded that the IHX increases the specific cooling capacity and the compression work, as well as reduced the optimum working pressure. This last effect affected the energy recovered in the expander, making the IHX only beneficial for expanders with low isentropic efficiency at high gas-cooler exit temperatures. They calculated that an ideal expander cycle with IHX presented 12.3 to 16.1% COP reduction in relation to the same cycle without IHX (Zhang et al., 2013).

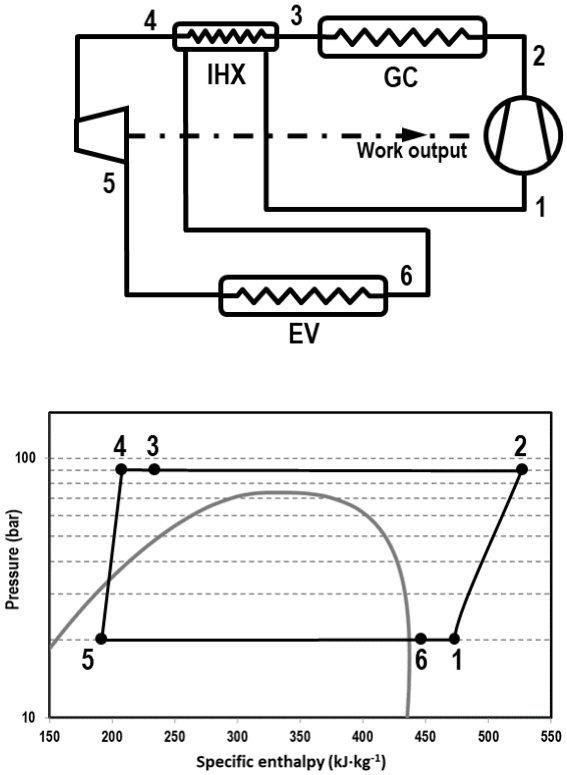

Figure 4.7. Position of the IHX in CO_2 refrigeration systems with expander.

4.1.4. IHX with vapour extraction from the intermediate vessel

Finally, the use of the IHX has also been evaluated in combination with vapour extraction from the accumulation vessel. Vapour extraction is performed to increase the specific refrigerating effect in the evaporator through recompression of the extracted vapours. Temperature of extracted vapour is colder than that at the exit of the gas-cooler, thus, it can be used to subcool the main refrigerant steam, as presented in Figure 4.8 (injection point 'a') in combination with an IHX. Cabello et al. (2012) experimentally evaluated the effect of vapour extraction with expansion from the intermediate vessel and their injection in three positions of the cycle: a) before the IHX, b) after the IHX and c) at the suction port of the compressor. They concluded that any of the three configurations reached similar increments in capacity and COP reaching maximum values of 9.8 and 7% respectively. However, the position providing subcooling (point 'a') allowed the minimum reduction of compressor's discharge temperature among the evaluated configurations. Similar conclusions were obtained theoretically by Karampour and Sawalha (2014) for a booster system.

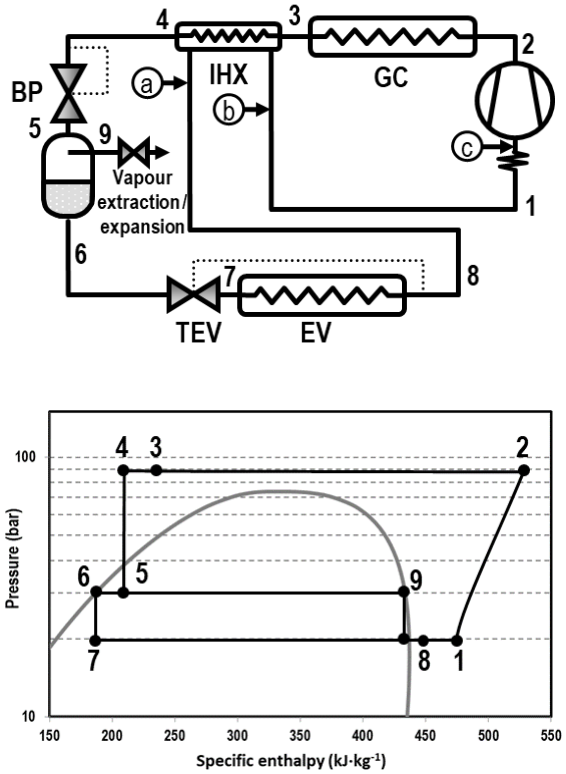

Figure 4.8. Position of the IHX in CO_2 refrigeration systems with ejector.

4.3.2. Economizer or subcooler

Use of two-stage cycles brings about the possibility to use specific and more controllable subcooling systems, such as the economized cycle or two-stage cycle with subcooler, which principle scheme is detailed in Figure 4.9. In this configuration the refrigerant leaving the gas-cooler/condenser is split into two streams. The auxiliary stream is throttled to the intermediate pressure and evaporated inside the economizer or subcooler, allowing to subcool the main steam of refrigerant. As analysed by Torrella et al. (2009), the COP increment that economization allows is dependent on the thermal effectiveness of the subcooler or the closed flash tank separator and the improvement for 100% effectiveness reaches the open flash separator performance at the intermediate pressure.

The first reference found about system was the theoretical study of Cavallini et al. (2005), who denoted it as split cycle and was evaluated for air-conditioning purposes. At an evaporating temperature of 2.7ºC and gas-cooler outlet temperature of 33ºC they predicted a COP of 3.17 without IHX at the low temperature suction and 3.25 using the

IHX. Taking as reference the two-stage cycle with IHX and intercooler, the economized cycle reached a COP improvement of 12.4% and 15.2%, respectively. It must be said that in this study the intermediate pressure considered for the calculation was the geometric mean value of gas-cooler and evaporator temperature, thus not subjected to optimization. Then, Cecchinato et al. (2009) theoretically optimized the two-stage split cycle in transcritical conditions and contrasted it to other CO_2 two stage cycles for evaporating levels of 4, -10 and -30ºC and external environment temperatures from 25 to 35ºC. They concluded that both the open flash tank and split cycle presented the greatest improvement, especially for the heaviest operating conditions (-30 / 35ºC).

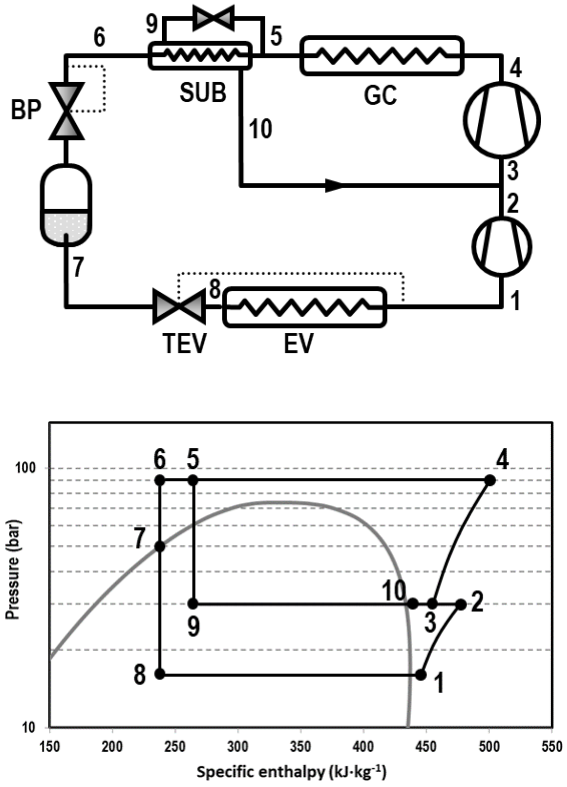

Figure 4.9. CO_2 two-stage cycle with subcooler or economizer.

Later, Wang et al. (2011) theoretically and experimentally analysed a two-stage cycle with closed flash tank separator at the intermediate pressure in contrast to a two-stage cycle with additional gas-cooler at the low-pressure compressor discharge. Through optimization of the intermediate pressure, they verified the higher performance of the closed flash-tank system (10.87% COP increment), but the experimental improvements were lower than those predicted theoretically. Finally, Zhang et al. (2016) theoretically

analysed the two-stage cycle with closed flash tank without gas-cooler at the low compression discharge analysing the effect of the use of an expander instead of an expansion valve in the throttling at the gas-cooler exit. They concluded that the two-stage cycle with closed flash tank was best option, it offering higher COP values at low evaporating levels and high gas-cooler outlet temperatures than even the two-stage cycle with intercooler and expander. Despite being a high-performance cycle no more references, especially experimental, have been found by the authors.

In a similar way, Fazelpour and Morosuk (2014) theoretically considered the use of the economizer in a single-stage compression system, where vapours at the exit of subcooler were driven directly to compressor suction. The economizer did not affect neither the optimum gas-cooling pressure neither the energy performance of the plant. However, from a second law approach they calculated that the use of the economizer improved by 7% the exergetic efficiency of the cycle, and from an exergoeconomic point of view that the economizer increased the cost of the plant by 4% at an evaporating level of 25ºC.

4.3.3. Integrated Mechanical subcooler

Another mechanism to provide large subcooling degrees in the CO_2 at the exit of the gas-cooler/condenser is the integrated mechanical subcooler, whose principle scheme is detailed in Figure 4.10. This system splits the stream at the exit of the gas-cooler/condenser and uses the auxiliary one, through throttling in an expansion valve, to subcool CO_2 at the exit of the subcooler. The auxiliary steam is evaporated and compressed by an auxiliary compressor to the high pressure gas-cooler. The advantage of this cycle in contrast to the economized cycle is that the evaporating level in the subcooler could be higher than the intermediate pressure in economized cycles, therefore, the auxiliary compressor could operate with lower compression ratios with higher efficiency. Also, it needs to be mentioned that the extraction of refrigerant for subcooling can be performed at the exit of the gas-cooler (point 4, Figure 4.10), at the exit of the subcooler (point 5, Figure 4.10) or at the exit of the vessel (point 5, Figure 4.10), however no references have been found regarding the two last positions. This cycle can be used as one-level evaporator or as high pressure cycle in booster configurations.

The main advantage of this cycle, in contrast to the split cycle (Figure 4.9) is that the auxiliary compressor operates with reduced compression ratios and thus with large efficiencies, and in relation to parallel compression systems (Karampour and Sawalha, 2016) is that the displacement of the auxiliary compressor is reduced because it only compresses the evaporated refrigerant instead of vapours from the intermediate vessel. However, at the moment, the operation of the auxiliary compressor and thus the

performance of the cycle is limited by the operating restrictions of the compressor, which are a maximum suction pressure (around 55 bar) and minimum compression ratio (around 1.5). This cycle provides an important increase in cooling capacity and large increments in energy efficiency in relation to basic CO_2 refrigeration cycles.

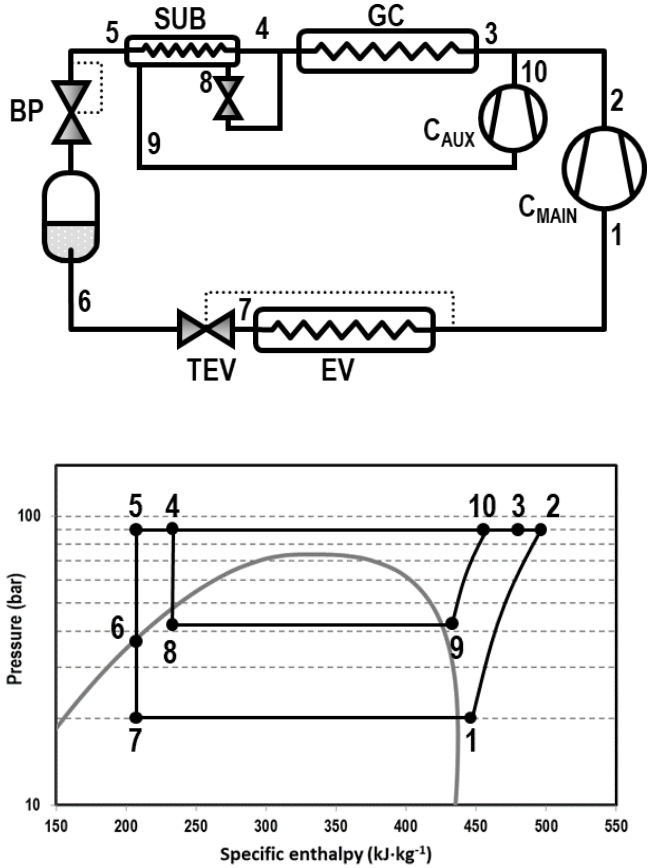

Figure 4.10. CO_2 cycle with integrated mechanical subcooling.

The first reference found to the integrated mechanical subcooling system is the patent of Shapiro (2007). This patent did not referred directly to any refrigerant, therefore it could cover the application in CO_2 systems. Shapiro (2007) reported that the COP of the system was bonded to the evaporating temperature at the subcooler and that the optimum subcooling degree raised at high heat rejection temperature. The first patent covering the integrated mechanical subcooling systems in CO_2 refrigeration cycles is of Kantchev and Lesage (2013), who specifically considered this system as a way to reduce power consumption in compressors and thus enhancing the COP and to increase the cooling capacity of this systems.

Using a theoretical approach, Cecchinato et al. (2009) evaluated 17.5% increase in energy efficiency in relation to a basic single-stage CO_2 cycle at -10ºC of evaporating temperature. They concluded that this cycle also overcame the standard double compression cycle, reaching COP increments up to 12%. They recommendation is to use this system for high evaporating temperature applications. Then Qureshi and Zubair (2012, 2013) theoretically studied and review the use of the integrated mechanical subcooling system in single-stage refrigeration cycles with artificial refrigerants. They concluded that this auxiliary system enhances the performance of the cycle, however they did not considered CO_2 in their analysis. An finally, Gullo and Cortella (2016) performed an exergoeconomic analysis of the integrated mechanical subcooling system in relation to a standard parallel compressor and a system using a gas ejector for medium temperature applications. They concluded that the integrated system allowed a COP increase 2.5 to 5.5% in relation to the parallel compression system but did not reached the ejector system one. One of the main reasons is that they considered 3K increase in the evaporating level due to the possibility of flooded evaporators. They also highlighted that the integrated solution presented a total investment cost much larger than solutions based on ejector.

Although the possibilities of this subcooling system, no references have been found by the authors in relation to the optimum working conditions (optimum pressures and optimum subcooling degrees) neither validation in experimental systems.

4.3.4. Heat storage systems

Polzot et al. (2016) evaluated the performance of a CO_2 booster system (with and without parallel compressor) when using a water storage system to provide subcooling at the exit of the gas-cooler/condenser for mild climate applications, using the scheme of Figure 4.11. For the simulations they considered as heat reservoir the fire prevention water tank of a supermarket. During night-time, when the COP of the plant is higher and the cooling demand of the system is low, the water tank is cooled by evaporating liquid CO_2 from the intermediate vessel then it being returned to the vessel. During day-time, the cooled water of the tank is used to subcool the refrigerant at the exit of the gas-cooler/condenser to increase the capacity of the system. Their simulation, for a standard European supermarket of 140kW capacity at MT and 22kW at LT placed in Northern Italy with a 950m^3 water reservoir, resulted in a 2.4% reduction in annual energy consumption of the installation. They also evaluated the possibility to increase the capacity of the reservoir, for double volume the reduction reached 3.5% and for larger volumes the ratio of energy reduction did not increase. Similar conclusions were obtained from a theoretical point of view by Fidorra et al. (2016).

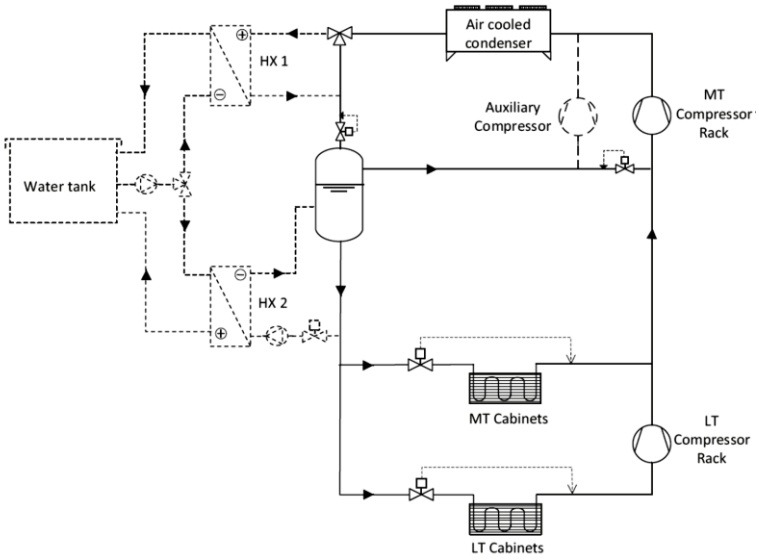

Figure 4.11. CO_2 booster system with water storage tank (Polzot et al., 2016).

4.4. Dedicated subcooling methods

This section revises the methods evaluated to provide the subcooling at the exit of the gas-cooler/condenser using external or dedicated systems. Dedicated mechanical subcooling systems based on vapor compression technology are analyzed in subsection 3.4.1, thermoelectric subcooling devices in subsection 3.4.2 and subsection 3.4.3 collects other scattered external methods.

4.4.1. Dedicated mechanical subcooling (DMS)

Dedicated mechanical subcooling (DMS) or dedicated mechanical desuperheating in CO_2 refrigeration cycles, understood as the use of an additional vapor compression cycle to provide subcooling at the exit of gas-cooler/condenser is one of the recent improvements being investigated by different authors. The DMS, as detailed in Figure 4.12, consists of an auxiliary vapor compression system especially devoted to subcool the refrigerant at the exit of gas-cooler/condenser. This function can also be performed by air conditioning chillers. Auxiliary and CO_2 cycles perform heat rejection to the same hot source, the CO_2 cycle evaporates at its cool production temperature and the auxiliary one at an intermediate level corresponding to the average temperature in the subcooler minus the temperature difference in the subcooler (ΔT_{sub}), thus this last operates with a reduced temperature lift between the cold source and hot sink, reaching high COP values. The auxiliary cycle generally works with a different refrigerant and is sized to obtain the optimum subcooling degrees, which are dependent on the heat rejection temperature and evaporating level. As analyzed theoretically by Llopis et al. (2015a), this

system is able to increase the overall COP and the cooling capacity provided by the CO_2 cycle, and its performance is not much dependent on the refrigerant used in the auxiliary cycle. Furthermore, theoretical results of Nebot-Andrés et al. (2017) indicate that this system overcomes the performance of cascade plants for temperature lifts below 28.5K, but considering annual operation its yearly-performance is higher than that of cascades for evaporating levels higher than -15ºC, thus covering the medium temperature application range and even the high-pressure cycle of two-stage CO_2 cycles.

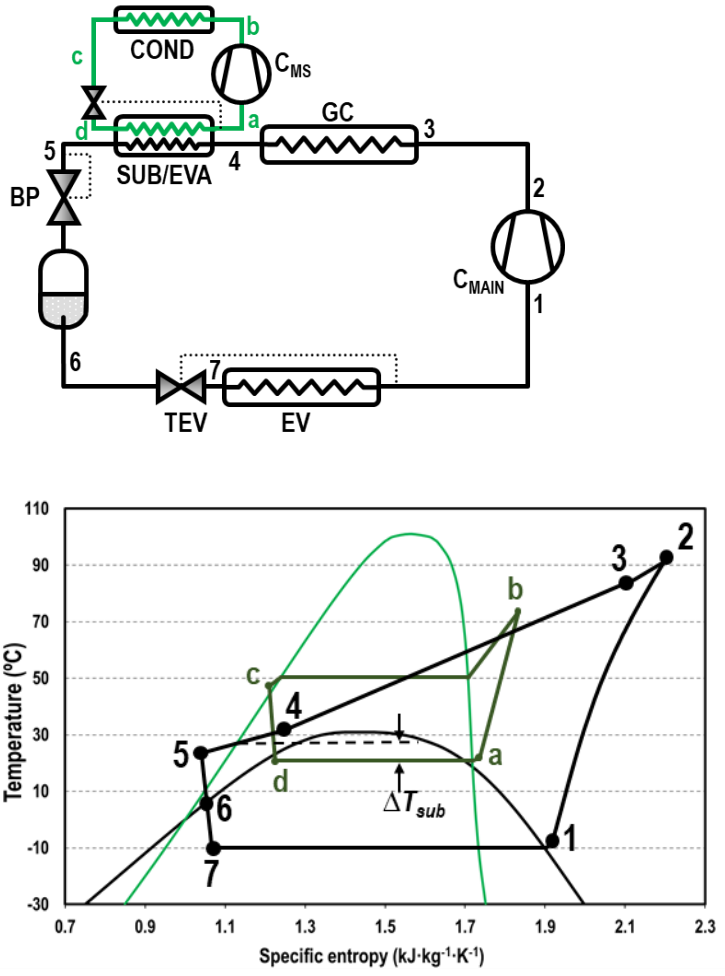

Figure 4.12. CO_2 refrigeration system with R-134a dedicated mechanical subcooling.

The first theoretical studies of DMS systems for CO_2 cycles were performed by Hafner A. and Hemmingsen A. K. (2015), who rated the performance of a R-290 DMS system in a single-stage compression system with flash-tank and IHX at the evaporator exit. In

their simulation, they fixed the pressure at the receiver tank at 40bar and considered a DMS with maximum capacity of 30% in relation to the main cycle. They compared the performance of this system with an R-404A direct expansion plant (base line), with the same system without DMS and with a system working with an ejector and parallel compressor. The simulation was extended to different cities and it was observed that the DMS system required between 77 to 97% of the energy input of the base system, and stated that the DMS obtained the highest improvements at high heat rejection temperatures. However, it needs to be mentioned that subcooling optimization was not considered in this study.

Then, Llopis et al. (2015a) using experimental overall efficiencies of compressors evaluated theoretically the energy improvement of the DMS in single- and double-stage with intercooling compression cycles at 5, -5 and -30ºC of evaporating temperature over a wide range of environment temperatures. Considering as reference system the same cycles without DMS, they predicted maximum COP increments of 20% and maximum capacity enhancement of 28.8%, being the improvement of the system higher at higher heat rejection levels and high evaporating temperatures. The largest improvement was achieved for environment temperatures from 25ºC on. However, this last work also did not considered optimization of subcooling, it being limited to 10K maximum.

In the same line, Gullo et al. (2016) simulated the operation of a booster refrigeration system with R-290 DMS for a typical European supermarket (97kW / -10ºC MT, 18kW / -35ºC LT) placed in Valencia (Spain) and Athens (Greece). A minimum condensing temperature in the systems was set to avoid low compression ratios in the high pressure compressor. They also simulated two designs of the DMS, one that allowed achieving 7ºC at the exit of the subcooler and another smaller rated to provide a minimum temperature at the exit of the subcooler of 15ºC. In contrast to a booster system with flash gas, they quantified an average COP improvement of 23.2% for the DMS at 15ºC and 23.3% for the DMS at 7ºC. They emphasized that the DMS at 7ºC would operate most of the year at low partial load, and both designs will equally operate at high environment temperature, where the needed capacity in the subcooler decreases. They also evaluated the use of the DMS in booster systems with parallel compressors using R-290 and R-1270 as refrigerants, however those systems did not achieved enough improvement to be recommended.

Dai et al. (2017a) evaluated the impact of the DMS in a single-stage cycle using simplifying assumptions, mainly constant isentropic efficiencies of compressors, for three evaporating levels (5, -5, -15ºC) in a wide range of environment temperatures (20-40ºC). They focused the study on the evaluation of the COP improvement and high-pressure reduction using different pure refrigerants in the DMS, results were

established through optimization of the subcooling degree. They concluded that the optimum subcooling degree is higher as higher the heat rejection and lower the evaporating levels are. Also, they obtained the best improvement with R-717 and the lowest with R-41 as DMS refrigerants, however, it needs to be mentioned that the differences among the different fluids were small.

Next, Purohit et al. (2017) compared different two temperature supermarket refrigeration systems among which there was an R-744 booster solution with a R-290 DMS. Using compressor efficiencies relations obtained from the manufacturer's data, they examined the systems considering temperature and heat load variation along a year for four locations. In relation to the DMS, they concluded that the DMS configuration could be more energetically beneficial than the parallel compression at high outdoor temperature operation. And recently, Dai et al. (*In-Press*) from a theoretical point of view evaluated the possibility to use zeotropic refrigerant mixtures as working fluid in the DMS through optimization of high-pressure and subcooling. For an operation of the cycle at -5ºC of evaporation and 35ºC of environment temperatures, they concluded that COP and optimum high pressure of mixtures with low temperature glide in evaporation are directly correlated with the glide, and that optimized refrigerant mixtures in terms of glide offer a COP improvement and optimum pressure reduction in relation to pure refrigerants. They evaluated different refrigerant mixtures and concluded that mixture R-32/R-1234ze(Z) (55/45 by mass) increased COP by 4.91% and reduced optimum pressure by 11 bar in relation to the use of R-32 as pure refrigerant in the DMS. However, no experimental validation was presented.

A similar approach, was used by She et al. (2014), who studied the classical DMS scheme (Figure 4.12) but it being activated by the energy recovered by an expander in the CO_2 expansion process. They predicted theoretical COP increments up to 67.76% and recommended R-12 and R-717 as the most beneficial fluids for the auxiliary system.

Using an experimental approach, Nebot-Andrés et al. (2016) presented a preliminary experimental study of the use of an R-1234yf DMS in a single-stage double-throttling refrigeration plant with a 4kW CO_2 and 0.7kW R-1234yf semihermetic compressors. They evaluated the performance of the plant at nominal speed of compressors at 0ºC of evaporation temperature for two gas-cooler exit temperatures (30.2 and 40ºC). At the optimum gas-cooler pressures, they measured increments on capacity of 34.9% and 40.7% at 30.2 and 40.0ºC respectively and COP increments of 22.8% at 30.2 and 17.3% at 40.0ºC. Llopis et al. (2016a) using the same plant extended the experimentation to two evaporating levels (0 and -10ºC) and three water inlet temperatures to condenser and gas-cooler (24.0, 30.2 and 40.0ºC). The evaluation was also made at constant compressor speeds and only optimization of CO_2 heat rejection pressure was

considered. They verified that the optimum heat rejection pressures are reduced by the use of the DMS (up to 8 bar), measured cooling capacity increments at optimum pressure from 23.1 to 55.7% and COP increments from 6.9 to 30.3%. However, this study did not considered optimization of the subcooling degree neither was extended to subcritical conditions. Eikevik et al. (2016) simulated, using as reference an experimental prototype, a single-stage compression double-stage throttling refrigeration cycle using a R-290 DMS with scroll compressor. The DMS was activated when the CO_2 high pressure reached 67 bar, thus it did not operated in subcritical conditions. The heat rejection of this prototype was performed by an integrated air cooled CO_2/R-290 condenser. Their simulations indicated that the best environment temperature to start the DMS was 23.5ºC. And they observed high increments on COP and refrigerating capacity over all the tested range, however, they not provided quantification of the improvements. Using data obtained from DMS CO_2 refrigeration systems placed in different warm and hot countries (maximum external temperatures up to 48ºC), Mazzola et al. (2016) analyzed real effects of the DMS. The systems activated the DMS when the temperature at the exit of the gas-cooler reached 30ºC, its operation was restricted to transcritical operation. They compared measurements of energy consumption and maximum discharge temperature as a function of the environment temperature in relation to the same system without DMS. They observed that the DMS allowed 10bar reduction in the discharge pressure and quantified an electric peak reduction between 16 to 40%. After further analysis they concluded that the use of the DMS in those locations reached 25% reduction of energy consumption. And finally, Beshr et al. (2016) and Bush et al. (2017) first simulated and then experimentally validated a prototype of a booster system for supermarket applications with flash tank using an indirect DMS working with R-134a and water-glycol mixture as heat transfer fluid. They evaluated the system under variable speed of the MT compressor and fixed speed of LT and auxiliary compressors for three heat rejection levels, 29, 35 and 39ºC. In the experimental verification they observed the theoretical predicted effects, a reduction of the optimum heat rejection pressure (1.9 bar at 29ºC, 0.9 bar at 35ºC), a large increment of the cooling capacity (+23.7% at 29ºC and +37.9% at 35ºC) and a big improvement in the overall COP of the system (+33.5% at 29ºC and +36.7% at 35ºC). Nonetheless, authors did not mentioned if the system was optimized in terms of subcooling.

As it can be seen from the state-of-the-art, the DMS is a system with predicted and evaluated large possibilities of improving the performance of CO_2 refrigeration systems. However, the experimentation phase is not complete, since the experimental evaluation has been only focused on transcritical conditions, in most of the cases the optimum subcooling degree has not been quantified and the use of zeotropic refrigerant mixtures in the DMS system should be explored.

4.4.2. Thermoelectric subcooling systems (TSS)

Subcooling at the exit of the gas-cooler, at least with low subcooling degrees, can be also provided using thermoelectric systems, using the simplified scheme of Figure 4.13. Thermoelectric elements, due to the Peltier effect, generate a temperature difference between both semiconductors that make the element when a DC current is applied to them, therefore they can remove heat from the refrigerant (subcool) and drive it to the environment. One of the advantages of the thermoelectric elements for subcooling is that they operate at a low temperature difference between the cold and hot surfaces (environment temperature and average temperature of CO_2 in the subcooler), where these elements show high COP values. However, the maximum temperature difference at which it can be of profit is when $COP_{CO2}<COP_{TSS}$ as discussed in subsection 3.2.2. The other advantage of the TSS is that it can be activated by the electricity generated by an expander associated with a DC electric generator (Figure 4.14), thus it being an easy mechanism to take profit of the energy recovered in the expansion process.

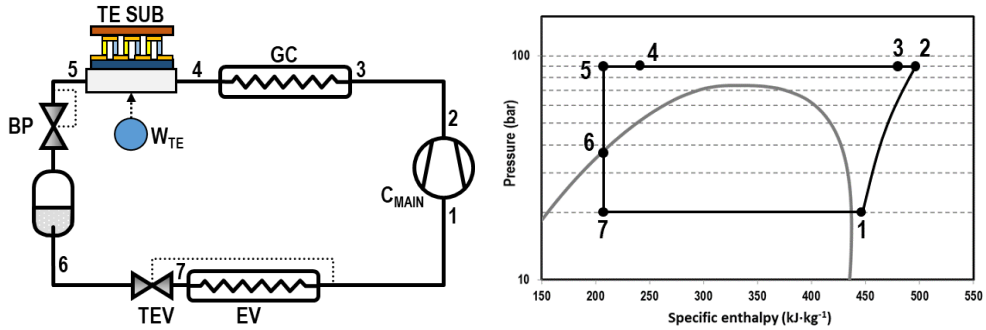

Figure 4.13. CO_2 refrigeration system with thermoelectric subcooling system.

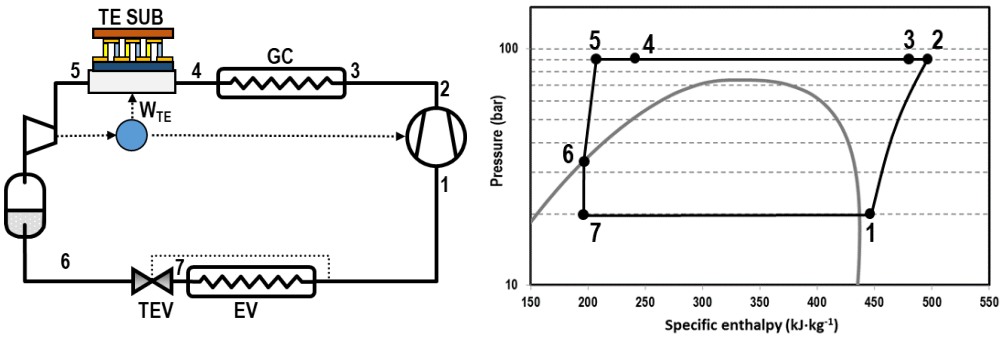

Figure 4.14. CO_2 refrigeration system with thermoelectric subcooling system and expander.

Schoenfield et al. (2008) and Schoenfield et al. (2012) were the first found references testing a TSS in a CO_2 single-stage transcritical refrigeration plant. They used Bismuth-

Telluride thermoelectric modules between a microchannel heat exchanger at the cold-side and a single-stage closed thermosyphon working with R22 as heat transfer refrigerant to the environment. They tested the TSS under variable current applied to the thermoelectric elements. In terms of COP, they observed that the highest improvement was achieved for low input current, condition at which the COP_{TSS} is highest, however, the COP increment was reduced for higher input currents. Nonetheless, they observed that the capacity of the system also increased with increased input currents. They established two scenarios for comparison with the base line system. When the overall COP value was maximized, they measured 3.3% COP increase jointly with 7.9% increment in capacity, and when the objective function was the capacity, they measured 18.7% increment in capacity jointly with 2.1% reduction in the overall COP. They also theoretically evaluated the possibility to activate the TSS using the energy generated by an expander-electrical generator (Figure 4.14), reaching the conclusion that it could provide 13% COP enhancement and 11% capacity increment, values higher than those obtained experimentally.

Sarkar (2013) theoretically evaluated a single-stage CO_2 compression system using a TSS to provide subcooling at the exit of the gas-cooler. Using a constant value of the isentropic efficiency of the compressor of 75% and a TSS based on 100 couples bismuth-telluride, he optimized the set performance for gas-cooler exit temperatures from 30 to 50ºC and evaporating levels from -15 to 5ºC. He highlighted that such a system is bonded to three optimization parameters: high-pressure, subcooling degree and current input to the TSS. He quantified as maximum improvement for an input current of 11A, 25.6% increase in COP and 15.4% discharge pressure reduction. Next, Yazawa et al. (2015) and Yazawa et al. (2016) theoretically evaluated the thermodynamic profit of using an hypothetical TSS to air conditioning systems for data centers. Using thermoelectric elements with a figure-of-merit of 1.5 and 70% isentropic efficiency for the compressor, they predicted 20% COP improvement at a subcooler exit temperature of 12ºC for a gas-cooler exit temperature of 40ºC. They also presented a cost analysis of the TSS, evaluating a minimum cost of the TSS of 1.5 to 3 $\$\cdot W^{-1}$ of cooling capacity, a cost comparable to the cost of a heat exchanger according to the authors. Dai et al. (2017b) theoretically studied the use of a TSS to a double-compression single-stage CO_2 refrigeration cycle, obtaining similar conclusions to the other authors. In addition, they analysed the possibility of integrating an expander in the system (Figure 4.14) and the corresponding electric generator to supply the needed DC current to the TSS. They evaluated two possible allocations of the expander, one between the subcooler and the accumulation vessel and the second between the vessel and the evaporator. Their analysis confirmed that the best position was after the subcooler, and for that location the system with TSS and expander predicted a 37.8% COP improvement. And finally,

Jamali et al. (2017) gave a step forward and also considered a TSS composed of a two-stage thermoelectric generator recovering energy at the gas-cooler to supply the energy input to another two-stage thermoelectric cooler providing subcooling to the CO_2 at the exit of the gas-cooler. Their simulations at gas-cooler outlet temperatures form 35 to 50ºC and evaporating temperatures from -10 to 10ºC indicated that, the thermoelectric generator provided only a part of the power needed by the thermoelectric cooler, and for the mentioned cycle the COP improvement reached 18.9% at 5ºC of evaporation. However, no experimental validation was presented.

From the literature review about thermoelectric subcooling systems, it is observed that from a theoretical point of view the possibilities of enhancing the performance of the CO_2 refrigeration systems is large, from 3.3 to 37.8%, however the main challenge of this technology is the integration of the thermoelectric elements with the corresponding heat exchangers, where minimization of the thermal resistance is needed to avoid reductions in the operating COP of the thermoelectric elements. Further research, especially with experimental approach is needed.

4.4.3. Other hybrid systems

Literature reveals some other scattered methods to improve the performance of CO_2 refrigeration systems. Although some of them are not directly focused on achieving subcooling at the exit of the gas-cooler, their principle scheme reveals that it would be possible, and in most of the cases it should be recommended. Arora et al. (2011) combined theoretically a single-stage CO_2 refrigeration plant with a single-stage BrLi-H_2O absorption plant, activated by heat recovery at gas-cooler, and used to provide additional capacity in the evaporator, at the same temperature level that the refrigeration system. They estimated an increase in capacity from 3.5 to 49.8% and an enhancement of the overall COP between 3.7 to 48.9%. Nonetheless, authors did not investigated the use of the cooling capacity of the absorption system to provide subcooling at the exit of the gas-cooler, method that will also reduce the optimum working pressure and benefit the operation of the compressor. Salajeghe and Ameri (2016) used a similar system but the capacity of the absorption system was used to provide subcooling at the exit of the gas-cooler. They concluded that the combination reduces the optimum high working pressure, improves the energy utilization factor and reduces the energy consumption in relation to conventional vapor compression systems.

Also, Mazzola et al. (2016) analyzed experimental data from a CO_2 supermarket installation using groundwater subcooling. The subcooling system was activated at environment temperatures from 25ºC, reaching reductions of the optimum high pressure of 15bar at 35ºC and 30% energy savings during a year.

Finally, Chen et al. (2017) theoretically analyzed and optimized an hybrid CO_2 refrigeration cycle assisted by an ejector cooling system driven by heat rejected by the CO_2 cycle. At evaporation temperatures from 0 to 10ºC, the hybrid system allowed 25-30% increase of the overall COP.

4.5. Concluding remarks

In recent years, the use of subcooling methods has been researched and different developments have shown that subcooling of CO_2 at the exit of the gas-cooler/condenser presents numerous advantages in relation to artificial refrigerant cycles, which makes it an improvement to be considered to enhance the performance of such cycles.

This paper comprehensively reviews the work done so far, and the following conclusions have been obtained from the reviewing process:

- CO_2 subcooling, with internal or external methods, enhances the performance of the cycle if the COP of the subcooling system is higher than that reached by the isolated CO_2 cycle. At that situation, benefits of subcooling are a large increase in capacity and an improvement of the overall COP. However, expected improvement in subcritical conditions is lower than in transcritical conditions (high heat rejection temperatures), because in transcritical conditions subcooling reduces the optimum working pressure and maximizes the improvement. Optimization of a CO_2 plant with a subcooling system is bonded to at least two variables, the optimum heat rejection pressure and the degree of subcooling, both bonded to the type of subcooling system.
- About internal methods to provide subcooling: it results obvious that the use of the internal heat exchanger (IHX) is mandatory when CO_2 operates in transcritical conditions, with reported COP increments up to 20% or even more, but this component presents the drawback of increased discharge temperature. The combination of the IHX with expansion energy recovery elements (ejectors and expanders) results negative, since the IHX penalizes those elements. Economization of CO_2 cycles, generally used with double-stage compression systems, showed COP improvements up to 15.2%, the use of integrated mechanical subcooling systems up to 17.5%, and the combination with heat storage systems up to 3.5%.
- Considering external subcooling systems: dedicated mechanical subcooling systems, generally based on the use of an additional vapour compression system with another refrigerant, have been widely investigated, with predicted COP improvements up to 28.8% and up to 67.7% using the dedicated subcooling system jointly with an expander. However, the theoretical approach

seems to be based on conservative assumptions, since the reviewed experimental work reported COP increments nearly up to 40%. It is mentioned that subcooling reduces the size of the CO_2 refrigeration system, however, existing research did not cover it. Thermoelectric subcooling systems are said to enhance the COP of the cycle between 20 to 25.6%, but, its combination with energy recovery systems (expanders or thermoelectric generators) increases this figure up to 37.8%. However, the main drawback of thermoelectric subcooling still relies on the design of the heat exchanger that joins the thermoelectric elements with the subcooler, where thermal resistances have an important role.

Conclusions from actual research reveal that subcooling is a worth method to increase the performance of CO_2 refrigeration systems, however, due to its recent approach the following subjects require further attention:

- Optimum conditions (theoretical or experimental) of integrated and external mechanical methods (subcooling degree and optimum high pressure) have extensively investigated. It should be needed to include in the analysis the CO_2 system size reduction and also a thermoeconomic approach would be needed to reach definite conclusions.
- Due to the complexity of the systems, experimental research is needed with integrated mechanical subcooling systems and economized cycles, since the actual research has not reached the improvement limits. Also, the dedicated subcooling systems must be explored from an experimental approach, where the use of refrigerant mixtures in the auxiliary refrigeration cycle could even enhance more the performance. Heat recovery systems integrated with the refrigeration cycle and those based on phase-change materials should be addressed.
- Finally, combination of CO_2 refrigeration cycles with heat recovery systems for subcooling such as absorption systems or adsorption systems is nearly inexistent.

4.6. Acknowledgment

Authors gratefully acknowledge Ministerio de Economía y Competitividad of Spain (project ENE2014-53760-R.7, grant FPI BES- 2015-073612), Jaume I University of Spain (project UJI-B2017-06) and Generalitat Valenciana of Spain (grant ACIF/2017/194) for financing this research work.

4.7. Nomenclature

BP	back-pressure
COND	condenser
COP	coefficient of performance
EJ	ejector
EV	evaporator
GC	gas-cooler/condenser
h	specific enthalpy, J·kg^{-1}
IHX	internal heat exchanger
MAC	mobile air conditioning system
$\dot{m}_r$	refrigerant mass flow rate, kg·s^{-1}
P	pressure, bar
P_C	electric power consumption, W
$\dot{Q}$	heat transfer rate, W
q	specific enthalpy difference, J·kg^{-1}
Rec	receiver
RISCOP	ratio of increase in capacity related to subcooling capacity
SUB	subcooling degree, K
T	temperature, ºC
TEV	thermostatic expansion valve
TSS	thermoelectric subcooling system
w_C	specific compression work, J·kg-1
x_v	vapour title

Greek symbols

Δ	Increment

Subscripts

AUX	auxiliary compressor
base	base line system
C	cold source level
crit	critical point conditions
dep	accumulation vessel
env	environment
gc	gas-cooler/condenser
H	hot sink level
I	intermediate temperature level
K	condenser
MAIN	main compressor
O	evaporator
out	outlet
PS	pseudocritical temperature
sub	subcooler, subcooling device, subcooling

4.8. References

Aprea, C., Maiorino, A., 2008. An experimental evaluation of the transcritical CO2 refrigerator performances using an internal heat exchanger. International Journal of Refrigeration 31, 1006-1011.

Arora, A., Singh, N.K., Monga, S., Kumar, O., 2011. Energy and exergy analysis of a combined transcritical CO2 compression refrigeration and single effect H2O-LiBr vapour absorption system. International Journal of Exergy 9, 453-471.

Beshr, M., Bush, J., Aute, V., Radermacher, R., 2016. Steady state testing and modeling of a CO2 two-stage refrigeration system with mechanical subcooler, Refrigeration Science and Technology, pp. 893-900.

Bush, J., Beshr, M., Aute, V., Radermacher, R., 2017. Experimental evaluation of transcritical CO2 refrigeration with mechanical subcooling. Science and Technology for the Built Environment, 1-13.

Cabello, R., Sánchez, D., Llopis, R., Torrella, E., 2008. Experimental evaluation of the energy efficiency of a CO2 refrigerating plant working in transcritical conditions. Applied Thermal Engineering 28, 1596-1604.

Cabello, R., Sánchez, D., Patiño, J., Llopis, R., Torrella, E., 2012. Experimental analysis of energy performance of modified single-stage CO 2 transcritical vapour compression cycles based on vapour injection in the suction line. Applied Thermal Engineering 47, 86-94.

Cavallini, A., Cecchinato, L., Corradi, M., Fornasieri, E., Zilio, C., 2005. Two-stage transcritical carbon dioxide cycle optimisation: A theoretical and experimental analysis. International Journal of Refrigeration 28, 1274-1283.

Cavallini, A., Corradi, M., Fornasieri, E., 2007. Experimental investigation on the effect of the Internal Heat Exchanger and Intercooler effectiveness of the energy performance of a two-stage transcritical carbondioxde cycle., in: IIR (Ed.), 22nd International Congress of Refrigeration, Beijin, China.

Cecchinato, L., Chiarello, M., Corradi, M., Fornasieri, E., Minetto, S., Stringari, P., Zilio, C., 2009. Thermodynamic analysis of different two-stage transcritical carbon dioxide cycles. International Journal of Refrigeration 32, 1058-1067.

Chen, G., Volovyk, O., Zhu, D., Ierin, V., Shestopalov, K., 2017. Theoretical analysis and optimization of a hybrid CO2 transcritical mechanical compression – ejector cooling cycle. International Journal of Refrigeration 74, 86-94.

Chen, Y., Gu, J., 2005. The optimum high pressure for CO2 transcritical refrigeration systems with internal heat exchangers. International Journal of Refrigeration 28, 1238-1249.

Chesi, A., Esposito, F., Ferrara, G., Ferrari, L., 2014. Experimental analysis of R744 parallel compression cycle. Applied Energy 135, 274-285.

Dai, B., Liu, S., Li, H., Sun, Z., Song, M., Yang, Q., Ma, Y., In-Press. Energetic performance of transcritical CO2 refrigeration cycles with mechanical subcooling using zeotropic mixture as refrigerant. Energy.

Dai, B., Liu, S., Sun, Z., Ma, Y., 2017a. Thermodynamic Performance Analysis of CO2 Transcritical Refrigeration Cycle Assisted with Mechanical Subcooling. Energy Procedia 105, 2033-2038.

Dai, B., Liu, S., Zhu, K., Sun, Z., Ma, Y., 2017b. Thermodynamic performance evaluation of transcritical carbon dioxide refrigeration cycle integrated with thermoelectric subcooler and expander. Energy 122, 787-800.

Eikevik, T.M., Bertelsen, S., Haugsdal, S., Tolstorebrov, I., Jensen, S., 2016. CO2 refrigeration system with integrated propan subcooler for supermarkets in warm climate., in: IIR (Ed.), 12th IIR Gustav Lorentzen Natural Working Fluids Conference,, Edinburgh, United Kingdom.

Elbel, S., 2011. Historical and present developments of ejector refrigeration systems with emphasis on transcritical carbon dioxide air-conditioning applications. International Journal of Refrigeration 34, 1545-1561.

Elbel, S., Hrnjak, P., 2004. Effect of Internal Heat Exchanger on Performance of Transcritical CO2 Systems with Ejector, International Refrigeration and Air Conditioning Conference. Paper 708., Purdue University, EEUU.

Elbel, S., Lawrence, N., 2016. Review of recent developments in advanced ejector technology. International Journal of Refrigeration 62, 1-18.

European Commission, 2014. Regulation (EU) No 517/2014 of the European Parliament and of the Council of 16 April 2014 on fluorinated greenhouse gases and repealing Regulation (EC) No 842/2006.

Fazelpour, F., Morosuk, T., 2014. Exergoeconomic analysis of carbon dioxide transcritical refrigeration machines. International Journal of Refrigeration 38, 128-139.

Fidorra, N., Minetto, S., Hafner, A., Banasiak, K., Köhler, J., 2016. Analysis of cold thermal energy storage concepts in CO2 refrigeration systems, Refrigeration Science and Technology, pp. 495-502.

Groll, E.A., Kim, J.-H., 2007. Review Article: Review of Recent Advances toward Transcritical CO2 Cycle Technology. HVAC&R Res. 13, 499-520.

Gullo, P., Cortella, G., 2016. Comparative Exergoeconomic Analysis of Various Transcritical R744 Commercial Refrigeration Systems, in: Ljubljana, U.o. (Ed.), ECOS 2016 - The 29th International conference on efficiency, cost, optimization, simulation and environmental impact of energy systems., Portoroz, Slovenia.

Gullo, P., Elmegaard, B., Cortella, G., 2016. Energy and environmental performance assessment of R744 booster supermarket refrigeration systems operating in warm climates. International Journal of Refrigeration 64, 61-79.

Hafner A., Hemmingsen A. K., 2015. R744 refrigeration technologies for supermarkets in warm climates., in: IIR (Ed.), 24th International Congress of Refrigeration, Yokohama, Japan.

J.Shariatzadeh, O., Abolhassani, S.S., Rahmani, M., Ziaee Nejad, M., 2016. Comparison of transcritical CO2 refrigeration cycle with expander and throttling valve including/excluding internal heat exchanger: Exergy and energy points of view. Applied Thermal Engineering 93, 779-787.

Jamali, S., Yari, M., Mohammadkhani, F., 2017. Performance improvement of a transcritical CO2 refrigeration cycle using two-stage thermoelectric modules in sub-cooler and gas cooler. International Journal of Refrigeration 74, 105-115.

Kantchev, J., Lesage, G., 2013. Mechanical subcooling of transcritical r-744 refrigeration systems with heat pump heat reclaim and floating head pressure. Google Patents.

Karampour, M., Sawalha, S., 2014. Investigation of using Internal Heat Exchangers in CO2 Trans-critical Booster System, in: IIF, I.-. (Ed.), 11th IIR Gustav Lorentzen Conference on Natural Refrigerants, Hanzhou, China.

Karampour, M., Sawalha, S., 2016. Integration of heating and air conditioning into a CO2 trans-critical booster system with parallel compression. Part I: Evaluation of key operating parameters using field measurements, in: IIR (Ed.), 12th IIR Gustav Lorentzen Natural Working Fluids Conference,, Edinburgh, United Kingdom.

Kauf, F., 1999. Determination of the optimum high pressure for transcritical CO2-refrigeration cycles. International Journal of Thermal Sciences 38, 325-330.

Kim, M.H., Pettersen, J., Bullard, C.W., 2004. Fundamental process and system design issues in CO2 vapor compression systems. Progress in Energy and Combustion Science 30, 119-174.

Koeln, J.P., Alleyne, A.G., 2014. Optimal subcooling in vapor compression systems via extremum seeking control: Theory and experiments. International Journal of Refrigeration 43, 14-25.

Li, Z., Chen, E., Jing, Y., Lv, S., 2017. Thermodynamic relationship of subcooling power and increase of cooling output in vapour compression chiller. Energy Conversion and Management 149, 254-262.

Liao, S.M., Zhao, T.S., 2002. Measurements of heat transfer coefficients from supercritical carbon dioxide flowing in horizontal mini/micro channels. Journal of Heat Transfer 124, 413-420.

Liao, S.M., Zhao, T.S., Jakobsen, A., 2000. A correlation of optimal heat rejection pressures in transcritical carbon dioxide cycles. Applied Thermal Engineering 20, 831-841.

Llopis, R., Cabello, R., Sánchez, D., Torrella, E., 2015a. Energy improvements of CO2 transcritical refrigeration cycles using dedicated mechanical subcooling. International Journal of Refrigeration 55, 129-141.

Llopis, R., Nebot-Andrés, L., Cabello, R., Sánchez, D., Catalán-Gil, J., 2016a. Experimental evaluation of a CO2 transcritical refrigeration plant with dedicated mechanical subcooling. International Journal of Refrigeration 69, 361-368.

Llopis, R., Sanz-Kock, C., Cabello, R., Sánchez, D., Nebot-Andrés, L., Catalán-Gil, J., 2016b. Effects caused by the internal heat exchanger at the low temperature cycle in a cascade refrigeration plant. Applied Thermal Engineering 103, 1077-1086.

Llopis, R., Sanz-Kock, C., Cabello, R., Sánchez, D., Torrella, E., 2015b. Experimental evaluation of an internal heat exchanger in a CO2 subcritical refrigeration cycle with gas-cooler. Applied Thermal Engineering 80, 31-41.

Lorentzen, G., 1994. Revival of carbon dioxide as a refrigerant. International Journal of Refrigeration 17, 292-301.

Lorentzen, G., Pettersen, J., 1993. A new, efficient and environmentally benign system for car air-conditioning. International Journal of Refrigeration 16, 4-12.

Mazzola, D., Sheehan, J., Bortoluzzi, D., Smitt, G., Orlandi, M., 2016. Supermarket application. Effects of sub-cooling on real R744 based trans-critical plants in warm and hot climate. Data analysis, Refrigeration Science and Technology, pp. 551-558.

McLinden, M.O., Brown, J.S., Brignoli, R., Kazakov, A.F., Domanski, P.A., 2017. Limited options for low-global-warming-potential refrigerants. Nature Communications 8, 14476.

Nakagawa, M., Marasigan, A.R., Matsukawa, T., 2011. Experimental analysis on the effect of internal heat exchanger in transcritical CO2 refrigeration cycle with two-phase ejector. International Journal of Refrigeration 34, 1577-1586.

Nebot-Andrés, L., Llopis, R., Sánchez, D., Cabello, R., 2016. Experimental evaluation of a dedicated mechanical subcooling system in a CO2 transcritical refrigeration cycle, Refrigeration Science and Technology, pp. 965-972.

Nebot-Andrés, L., Llopis, R., Sánchez, D., Catalán-Gil, J., Cabello, R., 2017. CO2 with Mechanical Subcooling vs. CO2 Cascade Cycles for Medium Temperature Commercial Refrigeration Applications Thermodynamic Analysis. Applied Sciences 7, 955.

Pardiñas, Á.Á., Hafner, A., Banasiak, K., 2018. Novel integrated CO2 vapour compression racks for supermarkets. Thermodynamic analysis of possible system configurations and influence of operational conditions. Applied Thermal Engineering 131, 1008-1025.

Pisano, A., Martínez-Ballester, S., Corberán, J.M., Mauro, A.W., 2015. Optimal design of a light commercial freezer through the analysis of the combined effects of capillary tube diameter and refrigerant charge on the performance. International Journal of Refrigeration 52, 1-10.

Polzot, A., D'Agaro, P., Gullo, P., Cortella, G., 2016. Modelling commercial refrigeration systems coupled with water storage to improve energy efficiency and perform heat recovery. International Journal of Refrigeration 69, 313-323.

Pottker, G., Hrnjak, P., 2015. Effect of the condenser subcooling on the performance of vapor compression systems. International Journal of Refrigeration 50, 156-164.

Purohit, N., Gullo, P., Dasgupta, M.S., 2017. Comparative Assessment of Low-GWP Based Refrigerating Plants Operating in Hot Climates. Energy Procedia 109, 138-145.

Qureshi, B.A., Inam, M., Antar, M.A., Zubair, S.M., 2013. Experimental energetic analysis of a vapor compression refrigeration system with dedicated mechanical sub-cooling. Applied Energy 102, 1035-1041.

Qureshi, B.A., Zubair, S.M., 2012. The impact of fouling on performance of a vapor compression refrigeration system with integrated mechanical sub-cooling system. Applied Energy 92, 750-762.

Qureshi, B.A., Zubair, S.M., 2013. Mechanical sub-cooling vapor compression systems: Current status and future directions. International Journal of Refrigeration 36, 2097-2110.

Rigola, J., Ablanque, N., Pérez-Segarra, C.D., Oliva, A., 2010. Numerical simulation and experimental validation of internal heat exchanger influence on CO2 trans-critical cycle performance. International Journal of Refrigeration 33, 664-674.

Salajeghe, M., Ameri, M., 2016. Effects of further cooling the gas cooler outlet refrigerant by an absorption chiller, on a transcritical CO2-compression refrigeration system. International Journal of Exergy 21, 110-125.

Sánchez, D., Catalán-Gil, J., Llopis, R., Nebot-Andrés, L., Cabello, R., Torrella, E., 2016. Improvements in a CO2 transcritical plant working with two different subcooling systems, Refrigeration Science and Technology, pp. 1014-1022.

Sánchez, D., Patiño, J., Llopis, R., Cabello, R., Torrella, E., Fuentes, F.V., 2014a. New positions for an internal heat exchanger in a CO2 supercritical refrigeration plant. Experimental analysis and energetic evaluation. Applied Thermal Engineering 63, 129-139.

Sánchez, D., Patiño, J., Sanz-Kock, C., Llopis, R., Cabello, R., Torrella, E., 2014b. Energetic evaluation of a CO2 refrigeration plant working in supercritical and subcritical conditions. Applied Thermal Engineering 66, 227-238.

Sarkar, J., 2013. Performance optimization of transcritical CO2 refrigeration cycle with thermoelectric subcooler. Int. J. Energy Res. 37, 121-128.

Schoenfield, J., Hwang, Y., Radermacher, R., 2012. CO 2 transcritical vapor compression cycle withthermoelectric subcooler. HVAC and R Research 18, 297-311.

Schoenfield, J., Muehlbauer, J., Hwang, Y., Radermacher R., 2008. Integration of a thermoelectric subcooler into a carbon dioxide transcritical vapor compression cycle refrigeration system, International Refrigeration and Air Conditioning Conference. Paper 903. http://docs.lib.purdue.edu/iracc/903.

Shapiro, D., 2007. Refrigeration system with mechanical subcooling. Google Patents.

She, X., Yin, Y., Zhang, X., 2014. A proposed subcooling method for vapor compression refrigeration cycle based on expansion power recovery. International Journal of Refrigeration 43, 50-61.

Singh, S., Dasgupta, M.S., 2016. Evaluation of research on CO2 trans-critical work recovery expander using multi attribute decision making methods. Renewable and Sustainable Energy Reviews 59, 119-129.

Torrella, E., Llopis, R., Cabello, R., Sánchez, D., 2009. Experimental energetic analysis of the subcooler system in a two-stage refrigeration facility driven by a compound compressor. HVAC and R Research 15, 583-596.

Torrella, E., Sánchez, D., Llopis, R., Cabello, R., 2011. Energetic evaluation of an internal heat exchanger in a CO2 transcritical refrigeration plant using experimental data. International Journal of Refrigeration 34, 40-49.

UNEP, 2016. Report of the Twenty-Eighth Meeting of the Parties to the Montreal Protocol on Substances that Deplete the Ozone Layer, Kigali, Rwanda.

Wang, H., Ma, Y., Tian, J., Li, M., 2011. Theoretical analysis and experimental research on transcritical CO2 two stage compression cycle with two gas coolers (TSCC+TG) and the cycle with intercooler (TSCC+IC). Energy Conversion and Management 52, 2819-2828.

Xu, X.-x., Chen, G.-m., Tang, L.-m., Zhu, Z.-j., Liu, S., 2011. Experimental evaluation of the effect of an internal heat exchanger on a transcritical CO2 ejector system. Journal of Zhejiang University-SCIENCE A 12, 146-153.

Yazawa, K., Dharkar, S., Kurtulus, O., Groll, E.A., 2015. Optimum design for thermoelectric in a sub-cooled trans-critical CO2 heat pump for data center cooling, Annual IEEE Semiconductor Thermal Measurement and Management Symposium, pp. 19-24.

Yazawa, K., Liu, Y., Kurtulus, O., Groll, E.A., 2016. Cost optimization of thermoelectric sub-Cooling in air-cooled CO2 air conditioners, International Refrigeration and Air Conditioning Conference. Paper 1626. http://docs.lib.purdue.edu/iracc/1626.

Zhang, F.Z., Jiang, P.X., Lin, Y.S., Zhang, Y.W., 2011. Efficiencies of subcritical and transcritical CO2 inverse cycles with and without an internal heat exchanger. Applied Thermal Engineering 31, 432-438.

Zhang, Z.-y., Ma, Y.-t., Wang, H.-l., Li, M.-x., 2013. Theoretical evaluation on effect of internal heat exchanger in ejector expansion transcritical CO2 refrigeration cycle. Applied Thermal Engineering 50, 932-938.

Zhang, Z., Tian, L., Chen, Y., Tong, L., 2014. Effect of an Internal Heat Exchanger on Performance of the Transcritical Carbon Dioxide Refrigeration Cycle with an Expander. Entropy 16, 5919.

Zhang, Z., Wang, H., Tian, L., Huang, C., 2016. Thermodynamic analysis of double-compression flash intercooling transcritical CO2 refrigeration cycle. The Journal of Supercritical Fluids 109, 100-108.

Zubair, S.M., 1994. Thermodynamics of a vapor-compression refrigeration cycle with mechanical subcooling. Energy 19, 707-715.

Chapter 5 Thermodynamic analysis of a CO_2 refrigeration cycle with integrated mechanical subcooling

5. Thermodynamic analysis of a CO_2 refrigeration cycle with integrated mechanical subcooling

energies

MDPI

Chapter adapted from the paper: Nebot-Andrés, L., Calleja-Anta, D., Sánchez, D., Cabello, R., Llopis, R. Thermodynamic analysis of a CO2 refrigeration cycle with integrated mechanical subcooling (2020) Energies, 13 (4), art. no.1. DOI: 10.3390/en13010004

Abstract

Different alternatives are being studied nowadays in order to enhance the behaviour of transcritical CO_2 refrigeration plants. Among the most studied options, subcooling is one of the most analysed methods in the last years, it increasing cooling capacity and COP, especially at high hot sink temperatures. A new cycle, called Integrated Mechanical Subcooling cycle, has been developed, as a total-CO_2 solution, to provide the subcooling in CO_2 transcritical refrigeration cycles. It corresponds to a promising solution from the point of view of energy efficiency.

The purpose of this work is to present, for the first time, thermodynamic analysis of a CO_2 refrigeration cycle with integrated mechanical subcooling cycle from first and second law approach. Using simplified models of the components, the optimum operating conditions, optimum gas-cooler pressure and subcooling degree, are determined in order to obtain the maximum COP. The main energy parameters of the system were analysed for different evaporation levels and heat rejection temperatures.

The exergy destruction was analysed for each component, identifying the elements of the system that introduce more irreversibilities. It has been concluded that the new cycle could offer COP improvements from 11.7 to 15.9% in relation to single-stage cycles with IHX at 35ºC ambient temperature.

Keywords

CO2; COP; energy efficiency; Integrated Mechanical Subcooling

5.1. Introduction

The refrigeration sector has been highly altered in recent years due to the latest European directive [1] and other restrictions and protocols [2,3], which leave carbon dioxide as the only alternative for centralised commercial refrigeration because of his low GWP and its security characteristics (non-flammable nor toxic, A1 ASHRAE classification). However, CO_2 working in classical refrigeration cycles has some inconvenients as its low performance comparing it to systems working with other HFC refrigerants. This is the reason why the greatest technological advances in last years have been developed specifically in line with the search for solutions to improve the performance of this refrigerant in hot climates, where classical configurations are not enough performant.

Some research lines have proposed the use of a parallel compressor in the system to improve the energy behaviour. By simulation, Sarkar and Agrawal [4] have optimized three cycles with different architectures including (parallel compression economization alone, parallel compression economization with subcooler and multistage compression with flash gas bypass). The cycle with parallel compression economization reached improvements in COP of 47,3% in relation to the basis CO_2 transcritical refrigeration cycle. Chesi, et al. [5] showed experimentally the limits that present the parallel compressor in a real plant, which lead to increments in COP not as promising as the theoretical results. Also the use of ejectors is widely studied as a way to improve CO_2 installations either using multi-ejectors [6] or adjustable ejectors [7]. Even the promising results of this solution, the operation and control remain complex.

The other great research line is focused on subcooling methods [8]. The purpose of subcooling methods is to subcool the CO_2 at the exit of the gas-cooler, which increases the COP of the plant due to the increment on the specific cooling capacity, the reduction of the optimum working pressure and the reduction of the specific compression work [9]. Firsts studies show that when higher is the subcooling higher are the increments. However, not all the subcooling systems have the same performance neither the same range of application. The improvements they can produce depend on the cost of the subcooling and on the working conditions. To obtain the greatest benefits of this type of systems, they must be optimized in terms of pressure and subcooling degree to achieve maximum COP. In addition to the benefits that contribute to the energy efficiency of the plant, these systems also have benefits from an exergy analysis. The reduction of the optimum pressure and the subcooling allow reducing the exergy destruction that take place in the expansion process, leading to configurations with greater exergy performance.

The main subcooling methods are classified as internal methods and dedicated subcooling methods. The first studied method and widely applied in nowadays applications is the use of an internal heat exchanger (IHX). This heat exchanger produces a light subcooling of the CO_2 which improves slightly its performance but also has some negative effects which decrease that improvement as it is the superheat produced at the suction line of the compressor [10].

Among the dedicated systems, the dedicated mechanical subcooling is a solution which involves and addition vapour compressor cycle that is combined with the CO_2 cycle through a subcooler. This cycle, is independent and can operate with other fluids different from CO_2. First theoretical studies, presented by Llopis et al. [9], show important improvements in COP by the use of the DMS when comparing it to a basic CO_2 cycle. This study showed the existence of an optimum pressure, and evaluating different subcooling degrees it was observed that the improvement was greater for the highest subcooling degree (10K). Later, this results have been corroborated experimentally, where increments up to 26.1% in COP and 39.4% in cooling capacity are obtained for 40ºC of heat rejection temperature and an evaporating level of 0ºC [11]. These experiments where optimized in terms of discharge pressure but the subcooling degree was not optimized. Sanchez et al. [12] also carried out test in a smaller plant and compared them with the same system with IHX.

Dai et al. [13] studied a R152a DMS single-stage cycle optimizing gas-cooler pressure and subcooling degree, obtaining the best results at low evaporation levels and high heat rejection temperatures. The advantages of using zeotropic mixtures in the DMS cycle have also been analysed [14] obtaining higher increments in COP due to the small heat transfer irreversibility that its generated directly related the glide of the mixture.

The implementation of this cycle has also been experimentally studied for booster systems [15-17]. Nebot-Andrés et al. [18] compared the dedicated mechanical subcooling versus the cascade system concluding that the DMS is more energy efficient for warm climates considering annual operating times for applications whose evaporation level is greater than -15ºC. That is why subcooling systems are interesting for medium temperature applications in hot climates where the temperature lift between the cold and heat sources is lower than 28.5 K.

Classified as an internal cycle we found the integrated mechanical subcooling (IMS, Figure 1) that has some similarities with the DMS in its main characteristics. The subcooling is also reached thanks to a subcooler placed after the gas-cooler and performed by a vapour compressor cycle. The main difference is that the working fluid of the IMS is also CO_2, extracted from the main cycle. Another benefit of this cycle is

that it has less components than the DMS because it doesn't need a condenser because the CO_2 is injected in the gas-cooler after the compression stage. This cycle therefore presents the same potential benefits of the DMS cycles, such as the improvement of the COP and the reduction of the entropy generation, but it only works with CO_2 and its precise configuration requires a smaller number of components. This cycle is also similar to the parallel compression with economizer presented by Sarkar and Agrawal [4], with the advantage of controlling gas-cooler pressure and useful superheat at the evaporator at the same time, allowing to optimize the cycle.

The first time this cycle has been presented was in the patent of Shapiro [19]. Then, Cecchinato et al. [20] evaluated theoretically this system obtaining promising increments in relation to the basic single-stage cycle. The cycle has also been studied by Qureshi and Zubair [21] but not for CO_2 applications.

Catalán-Gil et al. [17] have compared both the integrated and the dedicated mechanical subcooling cycles in booster systems for supermarket applications, where the most favourable regions for the implementation of each of the systems are identified. They presented annual energy consumption reductions between 2.9% and 3.4% for warm countries and between 1.3% to 2.4% for hot regions by using the IMS. Nebot-Andrés et al. [22] also presented a theoretical comparison of both mechanical subcooling cycles, obtaining similar increments for both cycles in relation to the cycle with IHX but, at medium environment temperatures; the IMS cycle was more beneficial.

This work has been developed in order to analyse the benefits of energetic and exergetic performance of the integrated mechanical subcooling and also to study the behaviour of this cycle for applications of medium temperature (evaporating levels between -15ºC and 5ºC) both in transcritical and subcritical conditions. It has been demonstrated the COP depends on the environment and application conditions, on the components but also on the subcooling degree and gas-cooler pressure. The existence of optimal pressure and subcooling for which the COP is maximum has been demonstrated and these optimal conditions have been determined. In the same way, two correlations that allow the identification of these optimal parameters for this type of cycle are presented.

The results presented on the paper correspond to the evaluation a single-stage CO_2 refrigeration cycle with integrated mechanical subcooling cycle, based on manufacturers data. The cooling capacity and COP of the cycle have been evaluated at five different evaporation levels (-15ºC, -10ºC, -5ºC, 0ºC and 5ºC) and ambient temperatures between 15ºC and 40ºC, always for the optimum conditions of gas-cooler pressure and subcooling degree.

5.2. Integrated mechanical subcooling cycle. Model description.

The integrated mechanical subcooling cycle is one of the subcooling methods that can be applied in CO_2 systems and aims to subcool the CO_2 at the exit of the gas-cooler to improve its energy behaviour.

5.2.1. Description of the cycle

The schema of this cycle is shown in Figure 5.1 as well as the Ph diagram of the cycle. The subcooling is performed at the subcooler, placed next to the gas-cooler, thanks to the extraction of a current of CO_2 that is expanded and evaporated in the subcooler. Then, this CO_2 is re-compressed by an auxiliary compressor and re-injected into the main circuit. This system can be configured in three different architectures, the extraction of the CO_2 can be done from the exit of the gas-cooler, the exit of the subcooler or from the liquid tank. In this work, the studied configuration is the one extracting from the gas-cooler exit.

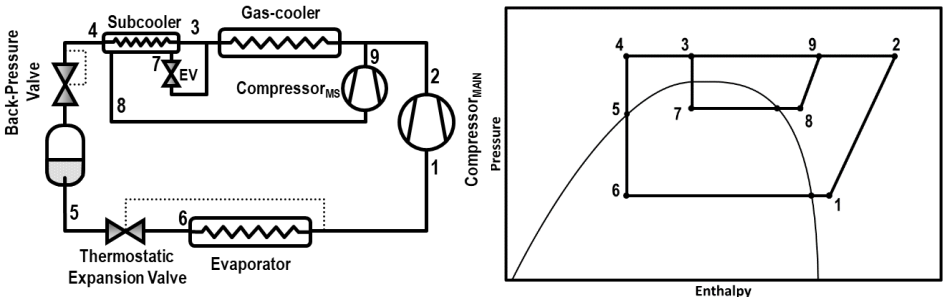

Figure 5.1. Schematic diagram and Ph diagram of the cycle.

5.2.2. First law approach. Thermodynamic analysis

This section describes the thermodynamic model and assumptions used to simulate this cycle and to assess the critical parameters that influence the performance of the cycle for both operational modes, transcritical and subcritical. The thermodynamic model is based on REFPROP v.9.1. [23] for the thermo-physical properties of the fluid and it is calculated by assuming the following hypothesis:

- Environment temperatures from 15ºC to 40ºC are considered.
- Five evaporation levels are studied: 5ºC, 0ºC, -5ºC, 10ºC and -15ºC.
- Steady state conditions.
- No pressure drops are considered.
- The heat losses through the environment are neglected.
- Both compressors efficiencies are correlated based on manufacturer's data, calculated as presented on Eq.(5.1) and parameters from Table 5.1.

$$\eta_V = \eta_G = a_0 + a_1 \cdot P_{suc} + a_2 \cdot P_{dis} + a_3 \cdot \left(\frac{P_{dis}}{P_{suc}}\right) + a_4 \cdot v_{suc} \quad (5.1)$$

$\dot{V}_G$ at 1450 rpm ($m^3 \cdot h^{-1}$)		Transcritical operation				Subcritical operation			
Main	**3.48**	η_V **Eq. (5.1)**		η_G **Eq. (5.1)**		η_V **Eq. (5.1)**		η_G **Eq. (5.1)**	
IMS	**1.12**	a_0	1.0473236	a_0	0.7633933	a_0	1.0350211	a_0	0.4868466
		a_1	0.0031061	a_1	-0.002098	a_1	0.0018747	a_1	-0.0086096
		a_2	-0.0029992	a_2	0.0013444	a_2	-0.001732	a_2	0.0115211
		a_3	0.0012158	a_3	-0.057138	a_3	-0.058808	a_3	-0.2686636
		a_4	-11.128188	a_4	0.5424680	a_4	-3.617390	a_4	20.8431999

Table 5.1. Performance data compressors obtained from manufacturers data.

- Useful superheating is considered of 10K at the main evaporator and 5K at the subcooler in the low-pressure line.
- Subcritical conditions are considered always when the ambient temperature is lower than 24ºC and transcritical conditions when it is over 25ºC. Between these temperatures both regimes are considered selecting the one with better energy performance.
- The approach considered in the gas-cooler is 2K for transcritical conditions due to the good thermal transfer of carbon dioxide at the supercritical region [24,25] while an approach of 5K is considered for subcritical conditions.

$$t_{gc,o} = t_{env} + \Delta t_{gc} \quad (5.2)$$

- The efficiency of the subcooler is not considered to be constant. Its evaporation temperature is fixed considering a pinch between subcooler exit temperature and the evaporation temperature of 2K for transcritical conditions and 5K for subcritical conditions.

$$t_{evap,ims} = t_{sub,o} - \Delta t_{sub} \quad (5.3)$$

- The subcooling degree considered in the subcooler, defined as Eq. (5.4), varies in order to optimize the system, as it is described in the following section.

$$SUB = t_{gc,o} - t_{sub,o} \quad (5.4)$$

- Both mass flows are related by the energy balance on the subcooler, being the mass flow of the IMS cycle defined by Eq. (5.5) when working in nominal conditions.

$$\dot{m}_{ims,nominal} = \dot{m}_{evap} \cdot \frac{(h_{gc,o} - h_{sub,o})}{(h_{evap,o,IMS} - h_{gc,o})} \tag{5.5}$$

- To obtain the desired value of subcooling degree, the IMS mass flow must be adapted by varying the compressor speed. A linear relation between the mass flow and the compressor velocity is considered to calculate the actual mass flow. The power consumption of the IMS compressor is also considered as linearly dependent on the compressor speed.

$$N = 1450 \cdot \frac{\dot{m}_{ims}}{\dot{m}_{ims,nominal}} \tag{5.6}$$

$$P_{c,ims} = P_{c,ims,nominal} \cdot \frac{N}{1450} \tag{5.7}$$

5.2.3. Second law approach. Exergy analysis

The exergy analysis of the system is performed calculating the exergy destruction in each of the components of the cycle with the aim to identify where the more irreversibilities are produced. The death state is considered as 0ºC and 1 bar. The exergy of a point is the difference between the enthalpy of the point and the enthalpy of the death state plus the product of the death state's temperature and the difference between the entropy of the point and the entropy of the death state (Eq. (3.8)).

$$e = (h - h_o) - t_o(s - s_o) \tag{5.8}$$

- Exergy destruction at the compressors is calculated as shown in Eq. (3.9) were $\dot{W}_{comp}$ is the work rate of the compressor.

$$\dot{E}x_{dest,comp} = \dot{m}_{evap}(e_i - e_o) + \dot{W}_{comp} \tag{5.9}$$

- At the subcooler, the exergy destruction of both flows taking part in the heat transfer is considered (Eq.(3.10)).

$$\dot{E}x_{dest,sub} = \dot{m}_{evap}(e_i - e_o) + \dot{m}_{ims}(e_{i,ims} - e_{o,ims}) \tag{5.10}$$

- In the expansion valves and the back-pressure, it is calculated as the product of the mass flow circulating on the device and the difference between the exergy at the inlet and outlet of the component.

$$\dot{E}x_{dest} = \dot{m}(e_i - e_o) \tag{5.11}$$

- At gas-cooler and evaporator only the exergy destruction of the CO_2 side is considered, as shown in Eq. (3.12) and Eq.(3.13) respectively.

$$\dot{E}x_{dest,gc} = \dot{m}_{CO_2}(e_i - e_o) \quad (5.12)$$

$$\dot{E}x_{dest,evap} = \dot{m}_{evap}(e_i - e_o) \quad (5.13)$$

5.3. Performance advantages of the IMS system

Subcooling at CO_2 systems has several benefits on their performance. Specifically, the mechanical subcooling cycles allow increasing the specific cooling capacity of the installation and reducing the optimum working pressure, which leads to a reduction in the specific compression work and, despite the addition of a second compressor, the overall COP of the cycle increases. Regarding the exergy losses of the system, the introduction of the subcooling also drifts in a reduction of the irreversibilities that take place in the expansion stage [8].

5.3.1. First law

Comparing the CO_2 refrigeration system with integrated mechanical subcooling to a single-stage refrigeration cycle with internal heat exchanger (IHX) from a first law analysis, the improvements of COP are clearly seen, due to the benefits named before.

Figure 5.2 shows the increment of COP obtained with the IMS compared to the cycle with IHX. As it can be seen, the increments are higher at high ambient temperatures, reaching increments of 40% for evaporation levels of -10ºC which justifies the implementation of this system in warm and hot climates, due to its improved performance.

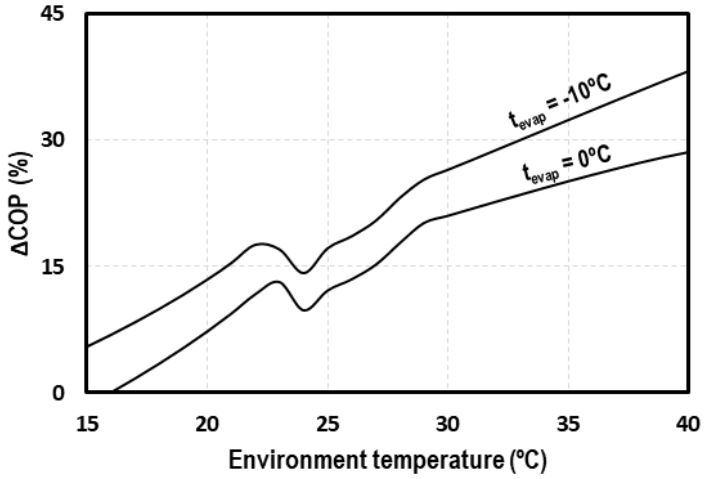

Figure 5.2. COP increments due to the use of the IMS cycle.

The comparison of the IMS to a classical CO_2 system demonstrates the potential improvements that this system can introduce to transcritical CO_2 cycles from an energy efficiency point of view.

5.3.2. Second law

In this section, an exergy destruction analysis is performed. As it is presented by Llopis et al. [8], the introduction of the subcooling avoids some of the exergy losses that take place in the throttling processes, being this benefit more important in transcritical conditions due to the reduction of the high pressure.

Figure 5.3 presents the T-s diagram of a transcritical CO_2 system with internal heat exchanger (yellow) and with integrated mechanical subcooling (orange). The effect of the subcooling can clearly be observed, moving the inlet back-pressure point to the left and thus reducing the exergy losses in that stage. The reduction of the optimum working pressure also contributes to the reduction of the irreversibilities because the temperatures of the IMS are lower.

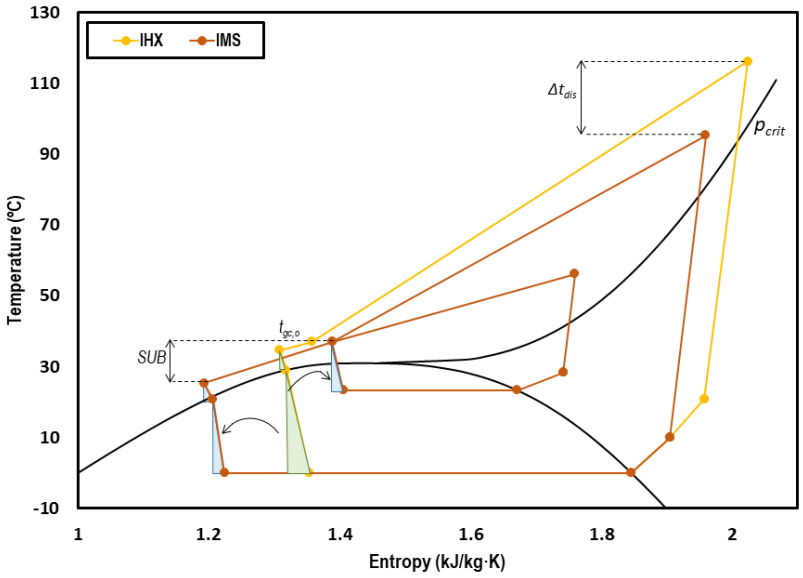

Figure 5.3. T-s diagram of a transcritical CO_2 system with IHX (yellow) and with IMS (orange) at t_{evap}=0ºC and t_{env}=35ºC.

The implementation of the IMS produces also an increment in the cooling capacity of the cycle. To compare the exergy destruction of this system to the cycle with internal heat exchanger, it is necessary to refer the exergy destruction to the cooling capacity of the analysed cycle.

Figure 5.4 represents the contribution of each of the components of the system to the exergy destruction divided by the total cooling capacity of the system. The exergy destruction on the gas-cooler represents a 56%, a 21% comes from the compressor, 7% from the expansion valve, 5% of the back-pressure and 4% corresponds to the expansion in the IMS cycle. Only 4% is produced on the IMS compressor, 2% on the subcooler and 1% on the evaporator. The main irreversibilities are produced in the gas-cooler and the compressor. However, extracting a part of the CO_2 and subcooling the rest allows reducing the irreversibilities produced on the expansion stage because the mass flow is smaller and the temperature at the entrance of the expansion device is lower. The additional compressor, the IMS expansion valve and the subcooler are elements that introduce irreversibilities to the system. But the reduction obtained because of the pressure reduction and the subcooling, leads to a total exergy destruction per cooling capacity unit lower than that produced in the system with IHX. It is for these reasons that the IMS is a very interesting system from the point of view of exergy performance for the application in warm and hot climates.

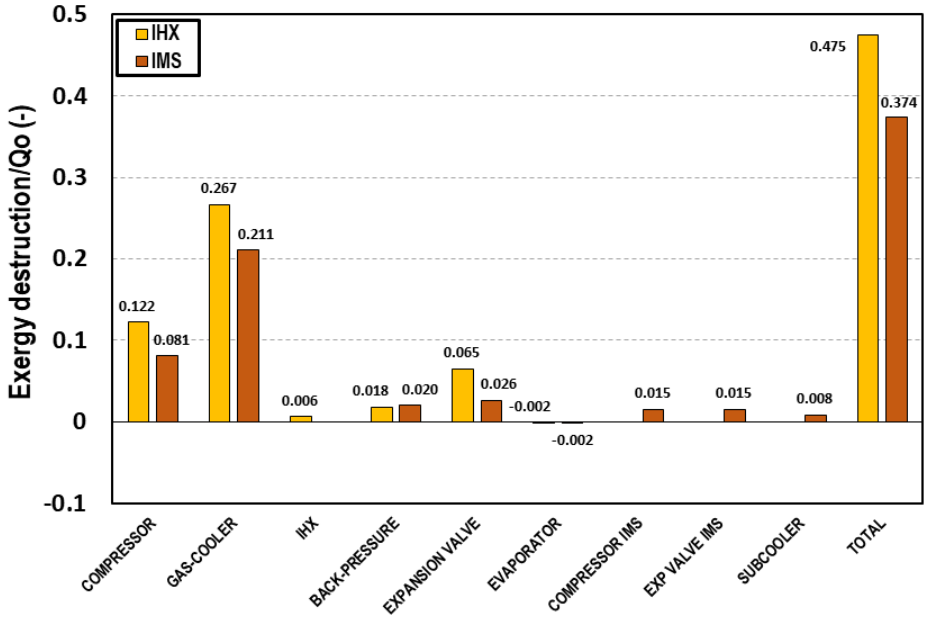

Figure 5.4. Exergy destruction in each of the cycle components at tevap=0ºC and tenv=35ºC referred to the cooling capacity for the transcritical CO2 system with IHX (yellow) and with IMS (red).

5.4. Optimum parameters

CO_2 systems must be optimized in order to maximize the efficiency of the cycle. In the following section, the existence of these optimum parameters for which the COP is

maximum is demonstrated for these cycles. The parameters that must be optimized are the discharge pressure and the subcooling degree.

COP of the system is the ratio between the cooling capacity on the main evaporator and the power consumption of both compressors as described in Eq. (5.14).

$$COP = \frac{\dot{Q}_{evap}}{P_{c,main} + P_{c,ims}} \tag{5.14}$$

Where cooling capacity is:

$$\dot{Q}_{evap} = \dot{m}_{evap}\,(h_{evap,o} - h_{sub,o}) \tag{5.15}$$

Power consumption of the main compressor is calculated as Eq. (5.16) and of the IMS compressor as Eq. (5.17).

$$P_{c,main} = \frac{\dot{m}_{evap}\,(h_{dis,s} - h_{evap,o})}{\eta_g} \tag{5.16}$$

$$P_{c,ims} = \frac{\dot{m}_{ims}\,(h_{dis,ims,s} - h_{evap,o,ims})}{\eta_{g,ims}} \tag{5.17}$$

Combining Eq. (5.5) and Eq. (5.14), Eq. (5.15), Eq. (5.16) and Eq. (5.17), Eq. (5.18) is obtained:

$$COP = \frac{(h_{evap,o} - h_{sub,o})}{\frac{h_{dis} - h_{evap,o}}{\eta_g} + \frac{h_{gc,o} - h_{sub,o}}{h_{evap,o,ims} - h_{gc,o}} \cdot \frac{h_{dis,ims} - h_{evap,o,ims}}{\eta_{g,ims}}} \tag{5.18}$$

COP depends on $h_{gc,o}$, $h_{sub,o}$, h_{dis}, $h_{dis,ims}$, $h_{evap,o}$, $h_{evap,o,ims}$, η_g and $\eta_{g,ims}$. From Eq. (5.19) to Eq. (5.24) show the dependence of each of the previous mentioned parameters.

$$h_{gc,o} = f(p_{gc}, t_{env}, \varepsilon_{gc}) \tag{5.19}$$

$$h_{sub,o} = f(p_{gc}, h_{gc,o}, SUB) \tag{5.20}$$

$$h_{dis,s} = f(p_{gc}, t_{evap}, SH, \eta_g) \tag{5.21}$$

$$h_{evap,o} = f(t_{evap}, SH) \tag{5.22}$$

$$h_{dis,s,ims} = f(p_{evap,ims}, p_{gc}, SH_{ims}) \tag{5.23}$$

$$h_{evap,o,ims} = f(p_{evap,ims}, SH) \tag{5.24}$$

$$p_{evap,ims} = f(t_{gc,o}, SUB, \varepsilon_{sub}) \tag{5.25}$$

Thus, the COP is only function of the environment temperature, the evaporation level, the gas-cooler pressure, the subcooling degree, the efficiency of the gas-cooler and subcooler, the superheating in evaporator and on the subcooler and the performance parameters of the compressors (Eq. (5.26)). Last four parameters depend on the efficiency of the components of the plant (heat exchangers and compressors);

evaporation and environment temperatures are fixed by the needs of the application and the ambient conditions. Gas-cooler pressure and the subcooling degree are the only parameters that can be modified in order to maximize COP, so these are the two parameters that must be optimized in CO_2 cycles with integrated mechanical subcooling.

$$COP = f(t_{evap}, t_{env}, P_{gc}, SUB, \varepsilon_{gc}, \varepsilon_{sub}, SH, SH_{ims}, \eta_g, \eta_{g,ims}) \quad (5.26)$$

5.4.1. Optimum pressure

All the transcritical CO_2 systems must be optimized in terms of discharge pressure but for this system with integrated mechanical subcooling, the optimum pressure is not the same as for classical CO_2 systems.

Figure 5.5 shows the COP variation for different ambient temperatures at different gas-cooler pressures. It can be observed that for all the cases it exists a gas-cooler pressure for which the COP is maximum. It is also observed that for the ambient temperature of 25ºC the optimum pressure corresponds to the critical one. This fact is due to the different temperature approach obtained between the ambient temperature and the gas-cooler exit temperature in subcritical and transcritical conditions. For this environment temperature we found that reducing the pressure is beneficial for the system but when going under the critical pressure, the temperature approach increases significantly, worsening system performance.

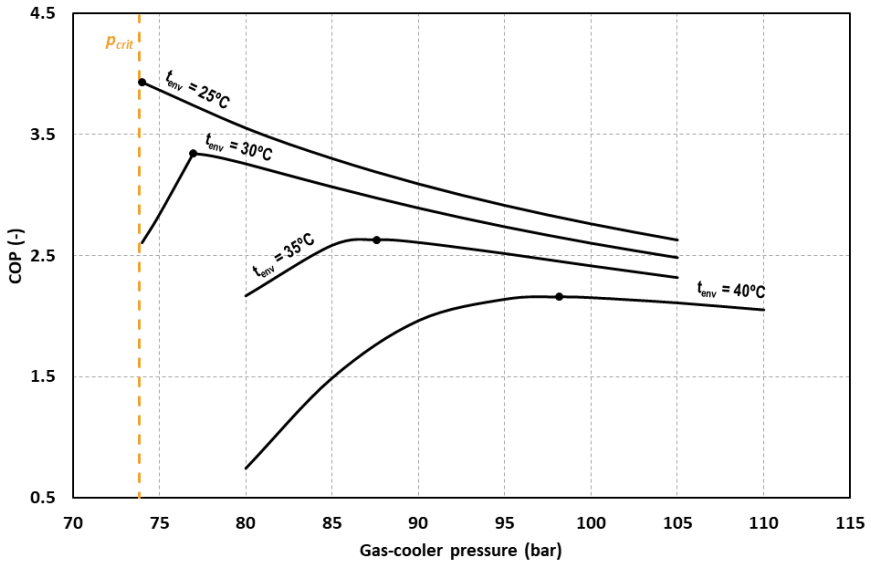

Figure 5.5. Evolution of the COP as function of the gas-cooler pressure for t_{evap}= 0ºC and different environment temperatures.

For the rest of the evaluated temperatures, working with a lower pressure than the optimum causes an important decrease in the COP value. For this reason, the system must be optimized in terms of gas-cooler pressure and the optimum working pressure must be determined.

Reducing or increasing the pressure with respect to the optimum, produces reductions in the value of the COP. For an environment temperature of 25ºC we obtain reductions of COP of 9% by increasing 5 bar the optimum gas-cooler. A reduction of 3 bars and an increment of 3 bars produces reductions of 22.0% and 2.5% for t_{env}=30ºC respectively. The same variation produces reductions of 1.7% and 0.9% for t_{env}=35ºC and of 0.9% and 0.3% for t_{env}=40ºC. It must be said that if optimum conditions cannot be reached, it is advisable to work at pressures above the optimum since it is for lower pressures when the COP of the cycle drops dramatically.

The optimum pressure is determined for all the studied conditions and presented in Figure 5.6. It can be observed that the optimum pressure is clearly related with the environment temperature but it is not much dependent on the evaporation level.

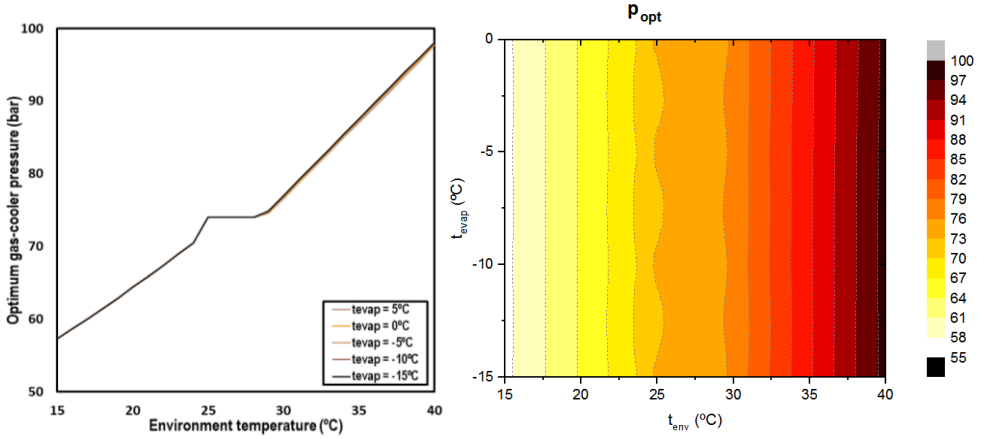

Figure 5.6. Optimum discharge pressure depending on environment temperature and the evaporation level.

When working in subcritical conditions, the optimum pressure was established by condensation, in the transition zone, the optimum pressure corresponds to the critical pressure and for transcritical regime, the optimum pressure increases linearly with the ambient temperature. The following correlations allow determining the optimum gas-cooler pressure for CO_2 systems with IMS.

$$p_{gc,opt} = p_{cond} \qquad \text{for } 15ºC \leq t_{env} < 24ºC \qquad (5.27)$$

$$p_{gc,opt} = p_{crit} \qquad \text{for } 24ºC \leq t_{env} < 29ºC \qquad (5.28)$$

$$p_{gc,opt} = 2.108 \cdot t_{env} + 13.645 \qquad \text{for } 29ºC \leq t_{env} \leq 40ºC \qquad (5.29)$$

The average error of the correlation (5.29) is 0.16 bars with a maximum error of 0.38 bars for a range of application from 29ºC ≤ t_{env} ≤40ºC and -15ºC ≤ t_{evap} ≤5ºC.

One of the interests of these systems is that the subcooling cycle allows reducing the high working pressure of the cycle. Figure 5.7 shows the optimum pressure reduction accomplished with the IMS system for transcritical CO_2 systems compared to one of the classical correlations for transcritical CO_2 systems [26]. Only the evaporations levels from -10ºC to 5ºC and gas-cooler outlet temperatures over 30ºC are compared according to the range of application of Liao's correlation.

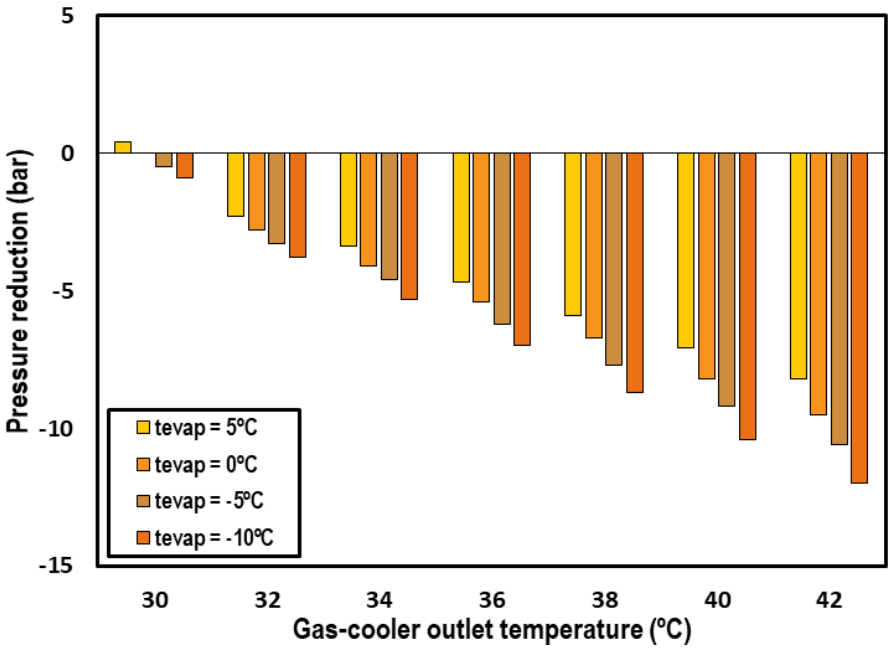

Figure 5.7. Optimum pressure reduction obtained with the use of the IMS system.

An important reduction is observed, being it more important when higher is the outlet gas-cooler temperature. The reductions reach values up to 12 bars for the highest gas-cooler outlet temperatures and lowest evaporation levels.

5.4.2. Optimum subcooling degree

The subcooling degree, presented in Eq. (5.4), is an operation parameter that must be optimized both in transcritical and subcritical conditions. Figure 5.8 shows the evolution of the COP for different environment temperatures as a function of the subcooling

degree, demonstrating that there is an optimum subcooling degree for each of the studied conditions.

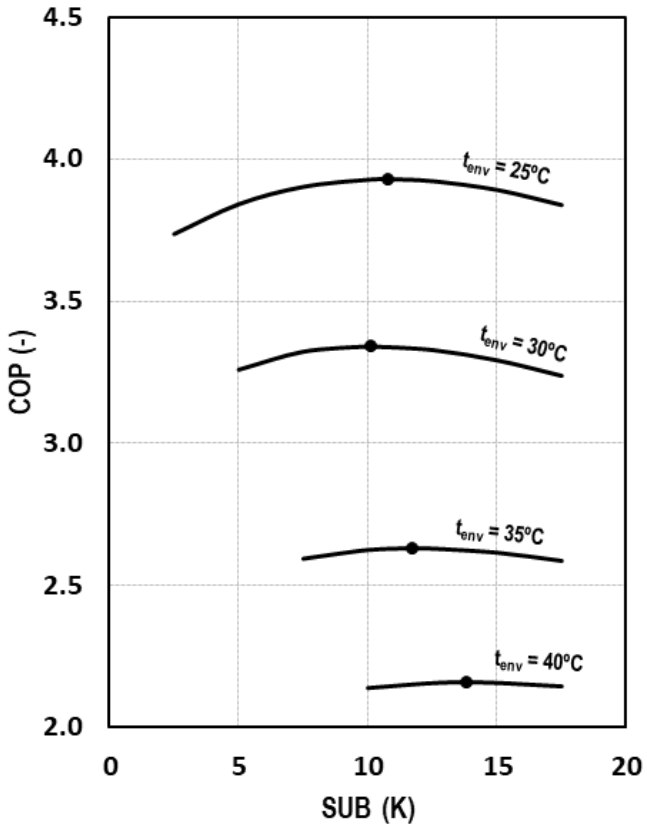

Figure 5.8. Evolution of COP depending on the subcooling degree for tevap=0ºC.

As it can be observed in Figure 5.8 and comparing these results with those of Figure 5.5, it can be stated that the influence of the subcooling on the COP is less strong than the pressure influence. For an environment temperature of 25ºC we obtain reductions of COP of 0.6% and 0.7% by increasing or decreasing 3K respectively the optimum subcooling degree. The same variation produces reductions of 0.6% and 0.4% for a decrease and increase of 2.5K at t_{env}=30ºC, of 1.4 % and 0.9% for t_{env}=35ºC and of 0.9% and 0.6% for a decrease and increase of 4K respectively at t_{env}=40ºC.

When optimizing the subcooling degree, it can be observed that it is completely dependent on the environment temperature but also on the evaporation level, obtaining higher degrees for lower evaporation temperatures and higher ambient conditions. Figure 5.9 summarizes the optimum subcooling conditions for all the outdoor temperatures and evaporation levels.

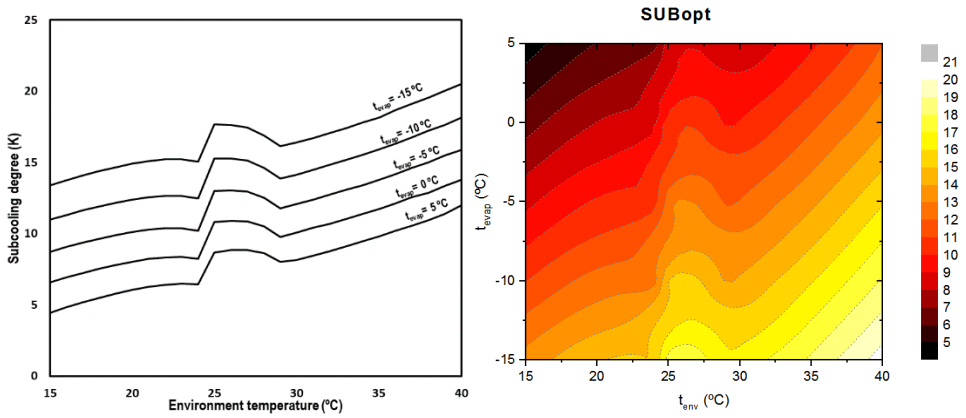

Figure 5.9. Optimum subcooling degree depending on environment and evaporation temperatures.

The optimum subcooling degree increases as the environment temperature does. There is a change in the trend in the transition zone due to the changes in the thermal properties of the CO_2 in the critical region [27] and the variation of the hypothesis between subcritical and transcritical regime.

Eq. (5.30) describes the optimum subcooling degree as a function of the environment temperature and the evaporation temperature for transcritical CO_2 systems with integrated mechanical subcooling.

$$SUB_{opt} = 2.7925 - 0.40180 \cdot t_{evap} + 0.0021 \cdot t_{evap}^2 + 0.2704 \cdot t_{env} - 0.0002 \cdot t_{env}^2 \quad (5.30)$$

The range of application of this correlation is for evaporating temperatures between -15.0ºC and 5.0ºC and environment temperatures from 15.0ºC to 40ºC with a maximum error of 1.6K.

5.5. Energy results

This section presents the main energy parameter results obtained from this study for the different evaluated conditions, always optimizing gas-cooler pressure and subcooling degree in order to obtain the maximum COP.

5.5.1. Cooling capacity

Cooling capacity is calculated as the product of the mass flow circulating on the evaporator and the enthalpy difference between the inlet and outlet of the evaporator (Eq. (5.15)). The inlet enthalpy is considered to be the same as the enthalpy at the exit of the subcooler.

Figure 5.10 shows the cooling capacity of the system for the range of studied environment temperatures and the different evaporation levels. The cooling capacity of the system is between 17.9kW and 13.1kW for t_{evap} = 5ºC, between 15.6kW and 11.3kW for t_{evap} = 0ºC, between 13.5kW and 9.7kW for t_{evap} = -5ºC, between 11.5kW and 8.2kW for t_{evap} = -10ºC and between 9.7kW and 6.9kW for t_{evap} = -15ºC. The observed trend is the same for all the evaporation levels, suffering a decrement on the capacity of the cycle as the environment temperature increases.

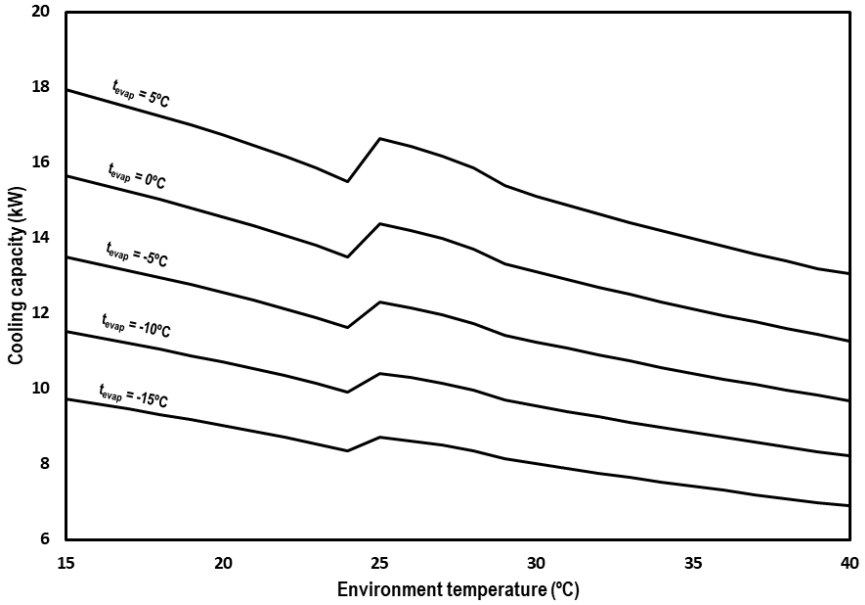

Figure 5.10. Evolution of the cooling capacity for subcritical and transcritical conditions.

The enthalpy at the exit of the subcooler can be also defined as the enthalpy at the gas-cooler outlet less the enthalpy difference produced in the subcooler, then the cooling capacity can be redefined as shown in Eq.(5.31).

$$\dot{Q}_{evap} = \dot{m}_{evap} \cdot (h_{evap,o} - h_{gc,o} + \Delta h_{sub}) \quad (5.31)$$

Expressed in another way, the cooling capacity is the sum of the cooling capacity of the cycle without subcooling plus the cooling capacity of the IMS system, as described in Eq. (5.32).

$$\dot{Q}_{evap} = \dot{m}_{evap} \cdot (h_{evap,o} - h_{gc,o}) + \dot{Q}_{IMS} \quad (5.32)$$

Figure 5.11 represents the cooling capacity contribution of the IMS system as a percentage of the total cooling capacity. It can be notice that the most important contributions of the IMS are obtained from 30ºC of ambient temperature. The

contribution always increases as the environment temperature does but the increments are more abrupt for these hottest levels, it is, for transcritical conditions. This increment in the contribution of the IMS is because is in transcritical regime where the CO_2 pure system is less performant and thus need more improvement. Analyzing the IMS contributions as a function of the evaporation level, higher contributions are obtained when lower the evaporation level is but the differences at different evaporation temperatures and a defined environment temperature are not so marked.

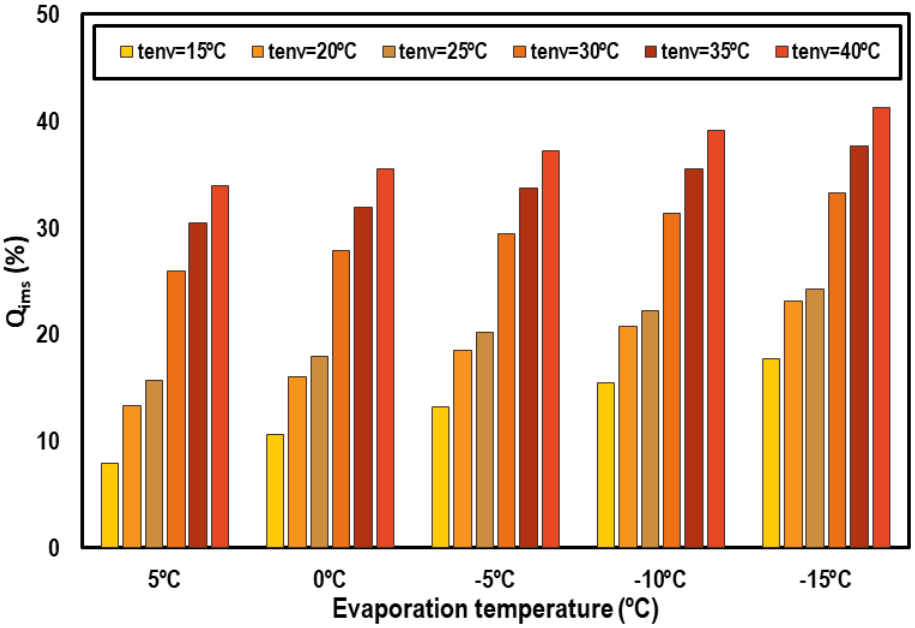

Figure 5.11. Cooling capacity contribution of the IMS system.

5.5.2. COP

Figure 5.12 shows overall COP of the system for the optimum working conditions at the different evaluated evaporation levels and range of ambient temperatures. COP values decrease from 8.13 to 4.76 for t_{evap} = 5ºC, from 6.17 to 3.94 for t_{evap} = 0ºC, from 4.92 to 3.31 for t_{evap} = -5ºC, from 4.03 to 2.79 for t_{evap} = -10ºC, from 3.34 to 2.34 for t_{evap} = -15ºC at subcritical conditions and from 4.78 to 2.48 for t_{evap} = 5ºC, from 3.93 to 2.16 for t_{evap} = 0ºC, from 3.29 to 1.89 for t_{evap} = -5ºC, from 2.79 to 1.66 for t_{evap} = -10ºC and from 2.38 to 1.45 for t_{evap} = -15ºC in transcritical regime.

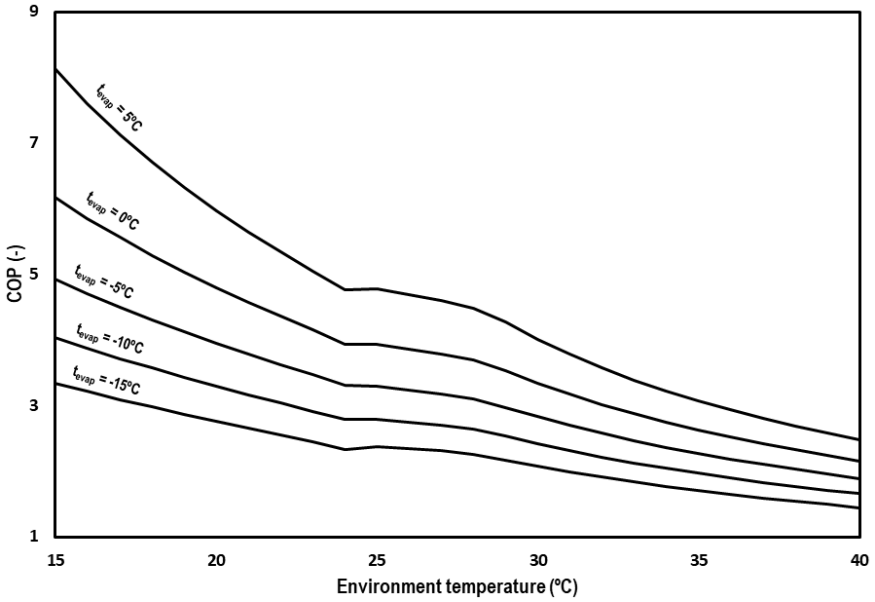

Figure 5.12. Evolution of the COP for subcritical and transcritical conditions.

In order to contrast the possible advantages of the IMS solution, the theoretical results of Chen and Gu [28] for a single-stage CO_2 transcritical system with an IHX have been contrasted with the COP values obtained in this work. The comparison is made for an environment temperature of 35ºC and evaporating levels from -10 to 5ºC. Figure 5.13 presents the COP values and the increments in relation to the system working with internal heat exchanger.

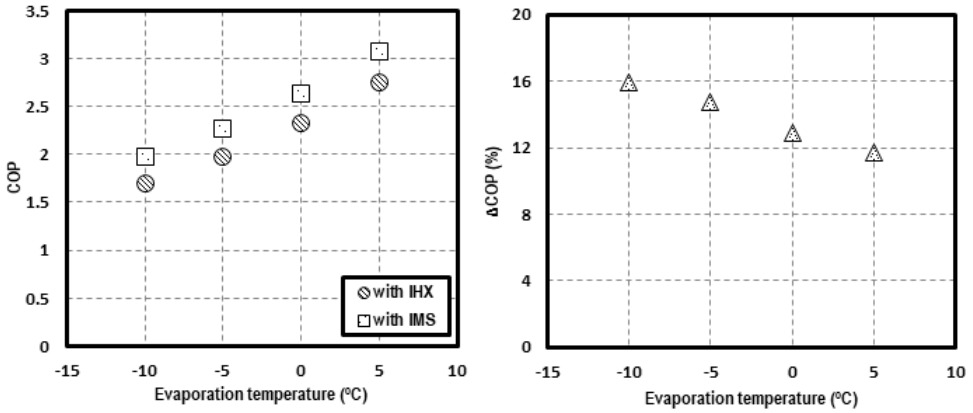

Figure 5.13. COP comparison at tenv=35ºC for a system with IHX and with IMS.

On the left, the COP of both systems is presented for different evaporating temperatures, being the COP of the CO_2 system with IMS always higher. On the right,

the increment of COP, achieved thanks to the IMS in reference to the system with IHX, is shown. It is observed that the increments are higher when lower the evaporation level is. The calculated increments are 15.9% for t_{evap} = -10ºC, 14.8% for t_{evap} = -5ºC, 12.9% for t_{evap} = 0ºC and 11.7% for t_{evap} = 5ºC.

5.6. Conclusions

In this paper the use of an integrated mechanical subcooling system for improving CO_2 refrigeration systems is studied from a theoretical approach. The study has been carried out using a simplified thermodynamic model based on assumptions as close to reality as possible.

It has been demonstrated that the COP of CO_2 refrigeration plants depend on the operating conditions, the performance of the components and the discharge pressure and subcooling degree, being these last two the only ones that can be adjusted to obtain the maximum COP in a specific plant for given operating conditions. Optimum working conditions of this type of cycle have been determined, being it necessary to optimize the system in terms of discharge pressure but also the subcooling degree performed at the exit of the gas-cooler.

The optimum working conditions have been determined both, for transcritical and subcritical conditions, for different evaporation levels (from -15.0ºC to +5ºC) and a wide range of ambient temperatures between 15.0ºC and 40.0ºC. It has been observed that the use of the IMS cycle reduces the optimum gas-cooler pressure of the system when working in transcritical regime compared to classical pressure correlations of CO2 systems. The optimum pressure is more reduced when higher are the ambient temperatures, reaching reductions over 10 bar for environment temperatures of 40ºC. At subcritical conditions, the optimum pressure corresponds to the condensation pressure. The optimum subcooling degree is also defined being higher when higher is the ambient temperature and when lower is the evaporation level.

The main energy parameters of the cycle, COP and cooling capacity, are calculated for all the studied levels obtaining values of COP from 8.13 to 2.48 for t_{evap} = 5ºC, from 6.17 to 2.16 for t_{evap} = 0ºC, from 4.92 to 1.89 for t_{evap} = -5ºC, from 4.03 to 1.66 for t_{evap} = -10ºC and from 3.34 to 1.45 for t_{evap} = -15ºC. The system presents remarkable increases in COP compared to systems with internal heat exchanger, up to 15.9% for t_{evap} = -10ºC and t_{env} = 35ºC. Cooling capacity of the system is between 17.9kW and 13.1kW for t_{evap}=5ºC, between 15.6kW and 11.3kW for t_{evap}=0ºC, between 13.5kW and 9.7kW for t_{evap}=-5ºC, between 11.5kW and 8.2kW for t_{evap}=-10ºC and between 9.7kW and 6.9kW for t_{evap}=-15ºC.

Furthermore, the cycle has also been studied from a second law approach, identifying the components of the system which present more irreversibilities. The exergy destruction in the expansion process is reduced and the components that present larger exergy destruction are gas-cooler and compressor.

Finally, as a general conclusion, we can affirm that the integrated mechanical subcooling cycle is an interesting subcooling method to improve the performance of CO_2 plants and its high pressure and subcooling degree must be optimized in order to obtain the maximum COP.

5.7. Acknowledgments

The authors thank the Ministry of Science, Innovation and Universities - Spain (project RTI2018-093501-B-C21), the Ministry of Education, Culture and Sports - Spain (grant FPU16/00151) and the Jaume I University (project UJI-B2017-06) for financing this research work.

5.8. Nomenclature

app approach, K

COP coefficient of performance

h specific enthalpy, $kJ \cdot kg^{-1}$

$\dot{m}$ mass flow rate, $kg \cdot s^{-1}$

p absolute pressure, bar

P_C compressor power consumption, kW

$\dot{Q}$ cooling capacity, kW

SH superheating, K

SUB degree of subcooling at the subcooler, K

t temperature, ºC

Greek symbols

ρ density, $kg \cdot m^{-3}$

η compressor efficiency

ε heat exchanger efficiency

Subscripts

dis compressor discharge

evap evaporation

exp expansion

gc gas-cooler

ims corresponding to the IMS cycle

in inlet

main corresponding to the main cycle

0 death state

o outlet

sub corresponding to the subcooler

suc compressor suction

5.9. References

1. European Commission. Regulation (EU) No 517/2014 of the European Parliament and of the Council of 16 April 2014 on fluorinated greenhouse gases and repealing Regulation (EC) No 842/2006. 2014.
2. United Nations. The Kyoto Protocol to the Framework Convention on Climate Change. 1997. Available at: <http://unfccc.int/essential_background/kyoto_protocol/background/items/1351.php >. 1997.
3. UNEP/TEAP. The implications to the Montreal Protocol of the inclusion of HFCs and PFCs in the Kyoto Protocol. United States, 1999.
4. Sarkar, J.; Agrawal, N. Performance optimization of transcritical CO2 cycle with parallel compression economization. International Journal of Thermal Sciences 2010, 49, 838-843, doi:10.1016/j.ijthermalsci.2009.12.001.
5. Chesi, A.; Esposito, F.; Ferrara, G.; Ferrari, L. Experimental analysis of R744 parallel compression cycle. Applied Energy 2014, 135, 274-285, doi:10.1016/j.apenergy.2014.08.087.
6. Gullo, P.; Hafner, A.; Banasiak, K.; Minetto, S.; Kriezi, E.E. Multi-ejector concept: A comprehensive review on its latest technological developments. Energies 2019, 12, doi:10.3390/en12030406.
7. Lawrence, N.; Elbel, S. Experimental investigation on control methods and strategies for off-design operation of the transcritical R744 two-phase ejector cycle.

International Journal of Refrigeration 2019, https://doi.org/10.1016/j.ijrefrig.2019.04.020, doi:https://doi.org/10.1016/j.ijrefrig.2019.04.020.
8. Llopis, R.; Nebot-Andrés, L.; Sánchez, D.; Catalán-Gil, J.; Cabello, R. Subcooling methods for CO2 refrigeration cycles: A review. International Journal of Refrigeration 2018, 93, 85-107, doi:https://doi.org/10.1016/j.ijrefrig.2018.06.010.
9. Llopis, R.; Cabello, R.; Sánchez, D.; Torrella, E. Energy improvements of CO2 transcritical refrigeration cycles using dedicated mechanical subcooling. International Journal of Refrigeration 2015, 55, 129-141, doi:http://dx.doi.org/10.1016/j.ijrefrig.2015.03.016.
10. Llopis, R.; Sanz-Kock, C.; Cabello, R.; Sánchez, D.; Torrella, E. Experimental evaluation of an internal heat exchanger in a CO2 subcritical refrigeration cycle with gas-cooler. Applied Thermal Engineering 2015, 80, 31-41, doi:http://dx.doi.org/10.1016/j.applthermaleng.2015.01.040.
11. Llopis, R.; Nebot-Andrés, L.; Cabello, R.; Sánchez, D.; Catalán-Gil, J. Experimental evaluation of a CO2 transcritical refrigeration plant with dedicated mechanical subcooling. International Journal of Refrigeration 2016, 69, 361-368, doi:10.1016/j.ijrefrig.2016.06.009.
12. Sánchez, D.; Catalán-Gil, J.; Llopis, R.; Nebot-Andrés, L.; Cabello, R.; Torrella, E. Improvements in a CO2 transcritical plant working with two different subcooling systems. In Proceedings of Refrigeration Science and Technology; pp. 1014-1022.
13. Dai, B.; Liu, S.; Sun, Z.; Ma, Y. Thermodynamic Performance Analysis of CO2 Transcritical Refrigeration Cycle Assisted with Mechanical Subcooling. In Proceedings of Energy Procedia; pp. 2033-2038.
14. Dai, B.; Liu, S.; Li, H.; Sun, Z.; Song, M.; Yang, Q.; Ma, Y. Energetic performance of transcritical CO2 refrigeration cycles with mechanical subcooling using zeotropic mixture as refrigerant. Energy 2018, 150, 205-221, doi:10.1016/j.energy.2018.02.111.
15. Bush, J.; Beshr, M.; Aute, V.; Radermacher, R. Experimental evaluation of transcritical CO2 refrigeration with mechanical subcooling. Science and Technology for the Built Environment 2017, 23, 1013-1025, doi:10.1080/23744731.2017.1289056.
16. Beshr, M.; Bush, J.; Aute, V.; Radermacher, R. Steady state testing and modeling of a CO2 two-stage refrigeration system with mechanical subcooler. In Proceedings of Refrigeration Science and Technology; pp. 893-900.
17. Catalán-Gil, J.; Llopis, R.; Sánchez, D.; Nebot-Andrés, L.; Cabello, R. Energy analysis of dedicated and integrated mechanical subcooled CO2 boosters for supermarket applications. International Journal of Refrigeration 2019, https://doi.org/10.1016/j.ijrefrig.2019.01.034, doi:https://doi.org/10.1016/j.ijrefrig.2019.01.034.
18. Nebot-Andrés, L.; Llopis, R.; Sánchez, D.; Catalán-Gil, J.; Cabello, R. CO2 with mechanical subcooling vs. CO2 cascade cycles for medium temperature commercial refrigeration applications thermodynamic analysis. Applied Sciences (Switzerland) 2017, 7, doi:10.3390/app7090955.

19. Shapiro, D. Refrigeration system with mechanical subcooling. 2009.
20. Cecchinato, L.; Chiarello, M.; Corradi, M.; Fornasieri, E.; Minetto, S.; Stringari, P.; Zilio, C. Thermodynamic analysis of different two-stage transcritical carbon dioxide cycles. International Journal of Refrigeration 2009, 32, 1058-1067, doi:https://doi.org/10.1016/j.ijrefrig.2008.10.001.
21. Qureshi, B.A.; Zubair, S.M. Mechanical sub-cooling vapor compression systems: Current status and future directions. International Journal of Refrigeration 2013, 36, 2097-2110, doi:http://dx.doi.org/10.1016/j.ijrefrig.2013.07.026.
22. Nebot-Andrés, L.; Llopis, R.; Catalán-Gil, J.; Sánchez, D.; Calleja-Anta, D.; Cabello, R. Thermodynamics analysis of CO2 refrigeration cycles working with mechanical subcooling systems. In Proceedings of 25th IIR International Congress of Refrigeration, Montreal, Canada.
23. Lemmon, E.W.; Huber, M.L.; McLinden, M.O. REFPROP, NIST Standard Reference Database 23, v.9.1. National Institute of Standards, Gaithersburg, MD, U.S.A. 2013.
24. Gullo, P.; Hafner, A.; Banasiak, K. Transcritical R744 refrigeration systems for supermarket applications: Current status and future perspectives. International Journal of Refrigeration 2018, 93, 269-310, doi:https://doi.org/10.1016/j.ijrefrig.2018.07.001.
25. Purohit, N.; Sharma, V.; Sawalha, S.; Fricke, B.; Llopis, R.; Dasgupta, M.S. Integrated supermarket refrigeration for very high ambient temperature. Energy 2018, 165, 572-590, doi:https://doi.org/10.1016/j.energy.2018.09.097.
26. Liao, S.M.; Zhao, T.S.; Jakobsen, A. A correlation of optimal heat rejection pressures in transcritical carbon dioxide cycles. Applied Thermal Engineering 2000, 20, 831-841.
27. Torrella, E.; Sánchez, D.; Llopis, R.; Cabello, R. Energetic evaluation of an internal heat exchanger in a CO2 transcritical refrigeration plant using experimental data. International Journal of Refrigeration 2011, 34, 40-49.
28. Chen, Y.; Gu, J. The optimum high pressure for CO2 transcritical refrigeration systems with internal heat exchangers. International Journal of Refrigeration 2005, 28, 1238-1249.

Chapter 5. Thermodynamic analysis of a CO_2 refrigeration cycle with integrated mechanical subcooling

Chapter 6 Experimental determination of the optimum working conditions of a transcritical CO_2 refrigeration plant with integrated mechanical subcooling.

Chapter 6. Experimental determination of the optimum working conditions of a transcritical CO_2 refrigeration plant with integrated mechanical subcooling.

6. Experimental determination of the optimum working conditions of a transcritical CO_2 refrigeration plant with integrated mechanical subcooling.

International Journal of Refrigeration 113 (2020) 266–275

Contents lists available at ScienceDirect

International Journal of Refrigeration

journal homepage: www.elsevier.com/locate/ijrefrig

Chapter adapted from the paper: Nebot-Andrés, L., Catalán-Gil, J., Sánchez, D., Calleja-Anta, D., Cabello, R., Llopis, R. Experimental determination of the optimum working conditions of a transcritical CO_2 refrigeration plant with integrated mechanical subcooling (2020) International Journal of Refrigeration, 113, p.p. 266-275. DOI: 10.1016/j.ijrefrig.2020.02.012.

Abstract

Subcooling methods for transcritical CO_2 plants are being studied in order to improve their behaviour. Among them, the Integrated Mechanical Subcooling system is one of the most promising owing that performs with high efficiency and it is a total-CO_2 system.

This work presents the experimental determination of the optimum working conditions of a transcritical CO_2 plant working with an integrated mechanical subcooling system. The plant was tested at different pressure and subcooling conditions in order to optimize the COP of the plant and determine the optimal conditions for three ambient temperatures 25.0ºC, 30.4ºC and 35.1ºC and evaporation levels between -15.6ºC and -4.1ºC.

Optimum operating conditions were determined and two correlations are proposed to determine the optimal pressure and subcooling as function the gas-cooler outlet temperature and the evaporation level.

Keywords

CO_2, Transcritical, Integrated Mechanical Subcooling, COP, Optimum conditions

Chapter 6. Experimental determination of the optimum working conditions of a transcritical CO_2 refrigeration plant with integrated mechanical subcooling.

6.1. Introduction

Carbon dioxide refrigeration systems have been the centre of effort of many of the scientific research in the recent years. The purpose of these studies was to improve the classical CO_2 systems to make them systems more competent, especially in hot climates. All these efforts have been fostered by the F-Gas Regulation (European Commission, 2014) that limits the use of refrigerants of high GWP in many of today's refrigeration applications. It is necessary to look for refrigerants with low GWP and for certain applications CO_2 is the only candidate with low GWP that ensures safety and it is non-flammable nor toxic (A1 ASHRAE classification).

Although these systems were flatly used in the northernmost countries of Europe due to their good performance in those climates, in southern Europe and other regions of the planet, where the average annual temperature is much higher, these systems suffer a significant decline in their performance.

The use of CO_2 systems with parallel compression was proposed as a way of enhancing the energetic behaviour of these systems. Sarkar and Agrawal (2010) performed the optimization of different architectures with parallel compression and quantified the COP improvements, reaching as maximum 47.3% in optimum COP employing parallel compression economization. Chesi et al. (2014) carried on an experimental study on the parallel compression cycle with flash tank but they do not reach the theoretical values of cooling capacity and COP due to several phenomena that they found in real application.

Another alternative studied in order to upgrade CO_2 systems is the use of ejectors. The latest proposals try to find solutions with variable ejectors such as the multi-ejector (Gullo et al., 2019) or the adjustable ejector (Lawrence and Elbel, 2019).

In addition to the alternatives already mentioned, the use of CO_2 in warm climates has been considered in cascade systems or combined with the dedicated mechanical subcooling. Nebot-Andrés et al. (2017) studied both alternatives for a warm climate like that of Spain. They concluded that the dedicated mechanical subcooling would offer highest energy efficiencies in overall-year operation for evaporating levels over -15ºC.

Subcooling methods define a clear line of research that is acquiring a lot of weight at this time (Yu et al., 2019). Llopis et al. (2018) compiled in a general way the effects of subcooling on CO_2 cycles and reviewed all the methods existing up to the moment to generate this subcooling and sum up the works done so far. Initially, with the most basic subcooling methods such as the internal heat exchanger (Llopis et al., 2015b), and subsequently with more complex systems such as dedicated mechanical subcooling (DMS). The dedicated mechanical subcooling has been studied in the last years, offering

important improvements for CO_2 cycles both in terms of COP and cooling capacity. The first studies, of a theoretical nature, were carried out by Llopis et al. (2015a) who studied a transcritical plant with dedicated mechanical subcooling working with R290 for different evaporation levels and heat rejection temperature. In the obtained results, an optimal working pressure was identified but the optimum subcooling degree was not considered. Despite this, the results showed increases in the overall COP that reached increments in reference to the base system without subcooling of 18.4% for t0=-30ºC, 17.9% for -5ºC and 12.3% for 5ºC.

The studies that followed this, presented data with optimized pressure and subcooling degree, so that maximum COP conditions were obtained. Dai et al. (2017) studied a R152a DMS single-stage system at optimum conditions, obtaining the most significant improvements for higher ambient temperatures and low evaporation levels, achieving an increment of 25.3% in COP for t_o=0ºC and 30ºC of ambient temperature. They also studied the performance advantages of using zeotropic mixtures in the auxiliary cycle (Dai et al., 2018) concluding that the maximum COP is directly related to the glide of the mixture due to the small heat transfer irreversibility that is generated. They obtained increments of 4.9% in COP by using a R32/R1234ze(Z) (55/45) mixture in the DMS cycle instead of pure R32.

In parallel, this system was also studied from an experimental point of view. First, Llopis et al. (2016) presented the experimentation of a CO_2 plant with and without subcooling (working with R1234yf). These tests were only optimized in terms of discharge pressure because the subcooling degree was not adapted in order to enhance the COP. However, the results presented increments in COP at the evaporation level of 0ºC of 10.9% at 24.0ºC, 22.1% at 30.2ºC and 26.1% at 40.0ºC. In addition, the measured increments in capacity were of 23.1% at 24.0 °C, 34.0% at 30.2ºC and 39.4% at 40.0ºC. Authors also corroborated the reduction of the optimal working pressure, being it reduced up to 8 bar in relation to the system working without DMS. In addition, other experimental tests have been carried out, both for single stage (Sánchez et al., 2016) and booster systems (Beshr et al., 2016; Bush et al., 2017).

The dedicated subcooling cycles have been quite studied in recent years, they being very interesting for the integration with air conditioning systems but they still are a not only-CO2 system. However, for space heating applications, a combined system using only CO_2 has been studied (Cao et al., 2019). Cao et al. presented a transcritical CO_2 heat pump combined with a subcooling system working with CO_2, obtaining increments of 15.3% in COP comparing to the standard transcritical CO_2 heat pump systems.

The integrated mechanical subcooling cycle (IMS), presented on this paper, only uses CO_2 as refrigerant for refrigeration applications. The purpose of this system is to subcool the CO_2 at the exit of the gas cooler thanks to a part of the current that is extracted from the main cycle and expanded, passing through the subcooler and recompressed until the gas-cooler entrance. The extraction of the CO_2 can be done from the exit of the gas-cooler, the exit of the subcooler and the liquid tank. The interest of this cycle is that it is simpler than the dedicated; it has fewer components, and only works with CO_2. As well as the dedicated does, this subcooling cycle produces large increments in cooling capacity and COP with respect to the base cycle (Catalán-Gil et al., 2019).

The IMS system was firstly proposed by the patent of Shapiro (2009). Cecchinato et al. (2009) evaluated the system from a theoretical point of view and obtained an increment of 17.3% in energy efficiency in relation to a basic single-stage CO_2 cycle for an evaporating level of −10°C of and a gas-cooler outlet temperature of 30°C. This cycle has certain similarities with the one presented by Sarkar and Agrawal (2010) called parallel cycle with economizer. However, Sarkar and Agrawal's cycle only includes two control elements (two expansion valves) and does not allow to optimize all the degrees of freedom, which is needed for centralized refrigeration systems.

Later, Catalán-Gil et al. (2019) analyzed the thermodynamic models of the integrated mechanical subcooling and the dedicated for CO_2 booster systems for supermarket applications, achieving annual energy consumption reductions from 2.9% to 3.4% for warm zones and from 1.3% to 2.4% for hot regions. Nebot-Andrés et al. (2019a) studies from a theoretical approach the IMS system optimizing gas-cooler pressure and the subcooling degree, reaching increments of 15.9% for −10 °C of evaporation temperature and 35ºC of environment temperature in comparison to the CO2 cycle with internal heat exchanger studied by Chen and Gu (2005). Subcooled boosters have also been studied for space heating by Song et al. who evaluated the optimal discharge pressure for these cycles (Song et al., 2018) and the optimal medium temperature (Song and Cao, 2018).

The integrated mechanical subcooling represents an important interest for the enhancement of CO_2 cycles, having a strong potential of improvement. However, this cycle has never been tested experimentally and its optimum conditions have not been determined or studied, to the knowledge of authors.

Accordingly, this work has been developed in order to determine experimentally the optimum conditions, in terms of subcooling degree and gas-cooler pressure, of an integrated mechanical subcooling system of a CO_2 refrigeration plant, working in transcritical conditions. The main objective is to identify the existence of these optimal

conditions, determine which are the needed values to obtain the best results in terms of COP and to define an expression that generalizes the optimum pressure and optimum subcooling degree for this type of systems. The results presented on this paper correspond to the evaluation of a single –stage plant at different evaporation levels, maintaining the temperature of the secondary fluid at the entrance of the evaporator (-1.3ºC, 3.8ºC and 10.0ºC) and three heat rejection temperatures (25.0ºC, 30.4ºC and 35.1ºC), determining for each test the optimum value of pressure and subcooling degree.

The optimum conditions have been determined and stated on a general correlation depending on the evaporation temperature and the temperature at the exit of the gas-cooler. The evolution of the main energy parameters is analyzed as well as the behavior of the optimum conditions of pressure and subcooling degree.

6.2. Refrigeration cycle and description of the experimental plant

This section presents the experimental installation used to evaluate the optimal conditions of the CO_2 transcritical cycle with the integrated mechanical subcooling system. The most important details of the main components of the cycle are provided and the measurement system used in the plant is described.

6.2.1. Experimental plant

The experimental plant tested in this work is shown in Figure 6.1 and its scheme in Figure 6.2. The plant is a CO_2 single-stage transcritical refrigeration system with an integrated mechanical subcooling system extracting gas at the exit of the subcooler. The main single-stage refrigeration cycle uses a semihermetic compressor with a displacement of 3.48 $m^3 \cdot h^{-1}$at 1450 rpm and a nominal power of 4 kW. The expansion is carried out by a double-stage system, composed of an electronic expansion valve (back-pressure) controlling the gas-cooler pressure, a liquid receiver between stages and an electronic expansion valve, working as thermo-static, to control the evaporating process. Evaporator and gas-cooler are brazed plate counter current heat exchangers with exchange surface area of 4.794 m^2 and 1.224 m^2, respectively. The subcooler is situated directly downstream of the gas-cooler. It is a brazed plate heat exchanger with an exchange surface area of 0.850 m^2. It works as evaporator of the mechanical subcooling system and subcools the CO_2 at the exit of the gas-cooler. The mechanical subcooling cycle is driven by a variable speed semihermetic compressor with displacement of 1.12 $m^3 \cdot h^{-1}$ at 1450 rpm. The expansion valve of the IMS cycle is electronic, working as thermostatic.

Heat dissipation in gas-cooler is done with a water loop, simulating the heat rejection level. The evaporator is supplied with another loop, working with a propylene glycol–

water mixture (60% by volume) that enables a constant entering temperature in the evaporator. Both the mass flow and the inlet temperature are controlled in these loops.

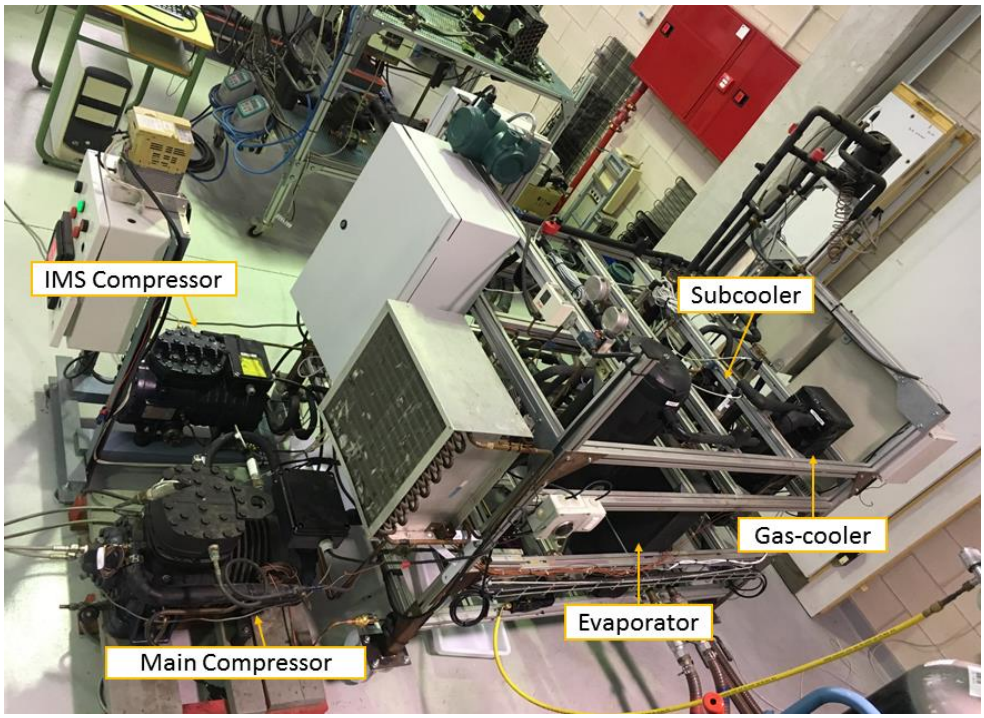

Figure 6.1. Experimental plant.

6.2.2. Measurement system

The thermodynamic properties of the working fluids are obtained thanks to the measurement system presented in Figure 6.2. All fluid temperatures are measured by 18 T-type thermocouples. The thermocouples placed at the evaporator and at the exit of gas-cooler and subcooler are immersion thermocouples. 11 pressure gauges are installed along all the circuit. CO_2 mass flow rates are measured by two Coriolis mass flow meters, as well as dissipation water flow of the gas-cooler, which is measured using another one. The flow of the other secondary fluids is measured by a magnetic volumetric flow meter. Compressors' power consumptions are measured by two digital wattmeters. The accuracies of the measurement devices are presented in Table 6.1.

Table 6.1. Accuracies and calibration range of the measurement devices.

Measured variable	**Measurement device**	**Range**	**Calibrated accuracy**
Temperature (ºC)	T-type thermocouple	-40.0 to 145.0	±0.5K
CO_2 pressure (bar)	Pressure gauge	0.0 to 160.0	±0.6% of span
CO_2 pressure (bar)	Pressure gauge	0.0 to 100.0	±0.6% of span
CO_2 pressure (bar)	Pressure gauge	0.0 to 60.0	±0.6% of span
CO_2 main mass flow rate ($kg \cdot s^{-1}$)	Coriolis mass flow meter	0.00 to 1.38	±0.1% of reading
CO_2 IMS mass flow rate ($kg \cdot s^{-1}$)	Coriolis mass flow meter	0.00 to 0.083	±0.1% of reading
Water mass flow rate ($kg \cdot s^{-1}$)	Coriolis mass flow meter	0.00 to 13.88	±0.1% of reading
Glycol volume flow rate ($m^3 \cdot h^{-1}$)	Magnetic flow meter	0.0 to 4.0	±0.25% of reading
Power consumption (kW)	Digital wattemeter	0.0 to 6.0	±0.5% of reading

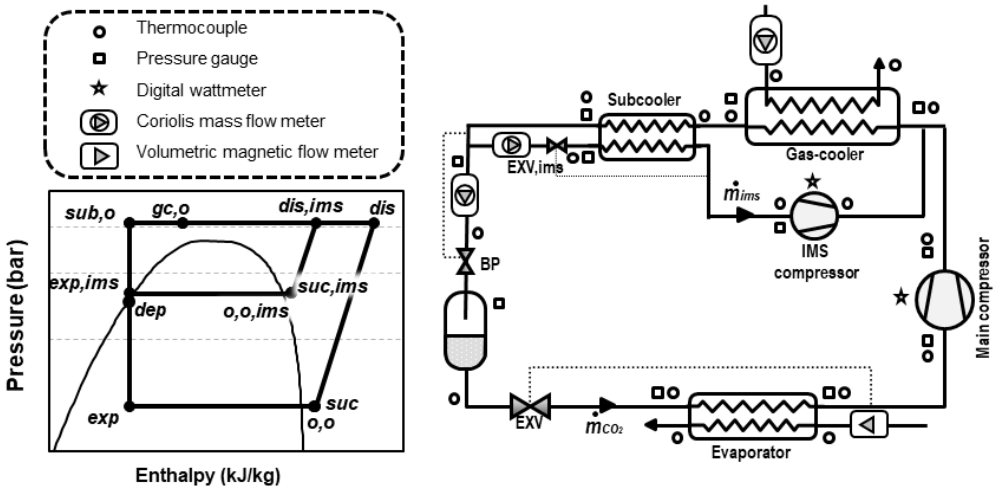

Figure 6.2. Schema of the experimental plant and the measurement system and Ph diagram of the cycle.

6.3. Experimental tests

This section contains the description of the strategy for conducting the experimental tests in order to determine the optimum conditions of the cycle for different heat rejection levels and different evaporation temperatures.

6.3.1. Test procedure

To evaluate the refrigeration plant using integrated mechanical subcooling, the system has been tested at different working conditions always operating in the transcritical region. The evaluated conditions were:

- Heat rejection level: three different temperatures: 25.0, 30.4 and 35.1°C, with maximum deviation of ±0.20°C. These levels were performed fixing the temperature of the secondary fluid (water) at the entrance of the gas-cooler and maintaining the water flow rate to 1.167 $m^3 \cdot h^{-1}$.

- Three different evaporation levels maintaining the inlet temperature of the secondary fluid in the evaporator and the flow rate. The secondary fluid is a mixture propylene glycol-water (60% by volume) and the evaluated temperatures were -1.3±0.07°C, 3.8±0.12°C and 10.1±0.23°C. The flow rate was fixed to 0.7 $m^3 \cdot h^{-1}$.

- Gas-cooler pressure was regulated with an electronic BP fixed during each test thanks to a PDI controller. Each test was performed at different pressures in order to identify the optimum one and reach the optimum COP conditions.

- Compressors: The main compressor always operated at nominal speed of 1450 rpm. The speed of the IMS compressor was varied is order to obtain the optimum subcooling degree.

- Electronic expansion valves: The electronic expansion valves were set to obtain a superheating degree in the evaporator of 10K and of 5K on the subcooler.

All the tests were carried out in steady state conditions for periods longer than 10 minutes, taking data each 5 seconds, obtaining the test point as the average value of the whole test. The measured data were used to calculate the thermodynamic properties of the points using Refprop v.9.1. (Lemmon et al., 2013).

6.3.2. Test range

Table 6.2 sumps up all the tests carried out, including the number of tests performed in each of the evaluated conditions. The range of values evaluated for the subcooling degree, the gas-cooler pressure and the main energy parameters for each test are also detailed on it.

Table 6.2. Experimental tests and range of tested conditions.

$t_{w,in}$ (ºC)	$t_{g,in}$ (ºC)	number of tests	SUB (K)	p_{gc} (bar)	COP (-)	Q_0 (kW)
25.0	-1.3	8	19.4-23.4	74.0-75.0	1.77-1.83	7.4-7.7
	3.8	8	16.1-21.4	74.5-76.0	2.02-2.12	8.7-8.9
	10.1	21	8.8-19.7	74.0-78.1	2.49-2.96	11.3-12.1
30.4	-1.3	17	10.7-24.3	78.9-89.3	1.48-1.60	6.4-7.2
	3.8	23	11.8-23.6	80.0-91.9	1.47-1.82	7.8-8.4
	10.1	19	8.6-16.2	80.2-82.2	1.92-2.10	9.1-9.6
35.1	-1.3	23	18.5-25.6	86.9-89.3	1.29-1.38	6.3-6.5
	3.8	18	3.8-18.5	84.0-90.9	1.40-1.58	6.1-7.6
	10.1	18	3.6-12.7	85.1-90.9	1.66-1.84	7.6-8.8

6.4. Optimization of the plant

In transcritical refrigeration cycles with subcooling there is an optimum working condition where the COP is maximum (Llopis et al., 2018). This point corresponds to the optimal gas-cooler pressure and the optimal subcooling degree, defined as eq. (6.1) . The subcooling degree is the difference between the temperature at the exit of the gas-cooler and the temperature at the exit of the subcooler. The tests were carried out in order to demonstrate the existence of this optimum, identify it, and then to evaluate the behaviour of the plant at optimum conditions.

$$SUB = t_{gc,o} - t_{sub,o} \tag{6.1}$$

6.4.1. Experimental COP identification

The cooling capacity of the plant is calculated as the product of the mass flow rate through the evaporator ($\dot{m}_{co2}$) and the enthalpy difference in evaporator, as shown in Eq.(6.2). The enthalpy at the evaporator inlet ($h_{0,o}$) is considered to be the same as the enthalpy at the inlet of the back-pressure valve. The COP of the system is the ratio between the cooling capacity and the sum of the power consumption of two compressors, as established in Eq. (6.3).

To obtain the maximum COP, tests have been carried out modifying pressure and subcooling values following a method similar to a Simplex algorithm. When three initial points were available, these parameters were increased or decreased following the trend of the previous points, in order to get closer and closer to the point of maximum COP. The process ended when the increments achieved between the new value and the previous one were less than 1%.

Figure 6.3 shows the measured COP for the tested condition of $t_{w,in}$ = 35.1ºC and $t_{g,in}$ = 10.0ºC, for different pressure levels and several subcooling degrees, representing the value of the COP as a function of Pgc and SUB. This colour map shows the evolution of the COP, where the existence of a maximum COP is clearly observed. Reducing or increasing pressure or subcooling degree will always reduce the obtained value of COP. As it can be seen, the influence of the pressure on the variation of the COP is higher than the influence of the subcooling degree. Increasing or reducing the pressure 1.5% has a higher impact on the COP than modifying the subcooling degree in the same percentage.

$$\dot{Q}_0 = \dot{m}_{co2} \cdot \left(h_{0,o} - h_{exp}\right) \tag{6.2}$$

$$COP = \frac{\dot{Q}_0}{P_{C,main} + P_{C,ims}} \tag{6.3}$$

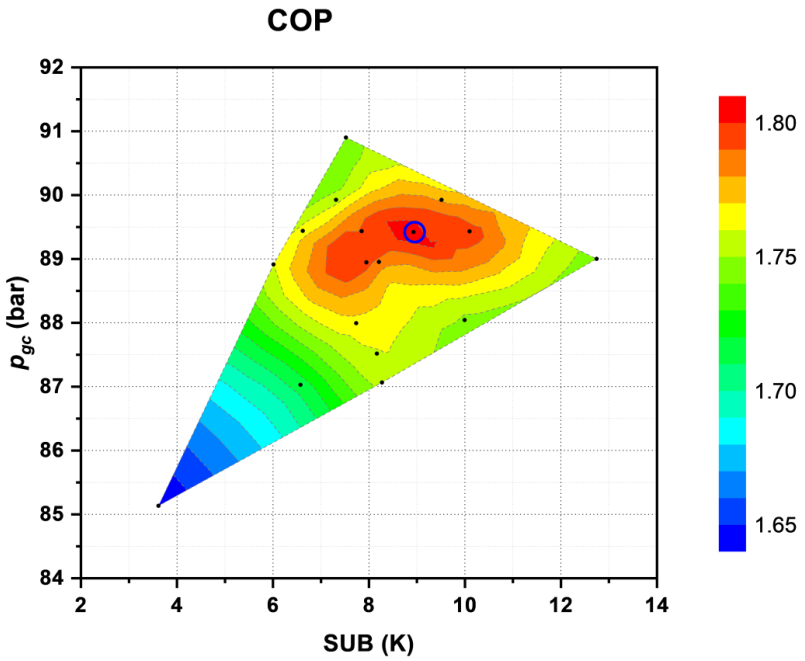

Figure 6.3. Experimental COP for $t_{w,in}$ = 35.1ºC and $t_{g,in}$ = 10.0ºC.

6.4.2. Experimental analysis of the cooling capacity

Regarding cooling capacity, calculated with Eq. (6.2), the subcooling degree increases the capacity of the plant, it being higher when higher the subcooling degree is, as it can be seen in Figure 6.4. Due to that, the optimum condition does not correspond to the point with higher cooling capacity, but the difference is not remarkable. The positive

aspect of this effect is that the capacity of the system can be adjusted by modifying the subcooling degree in order to fit the needs of the application with decrements in COP of 1.5% when increasing or decreasing 2K of subcooling.

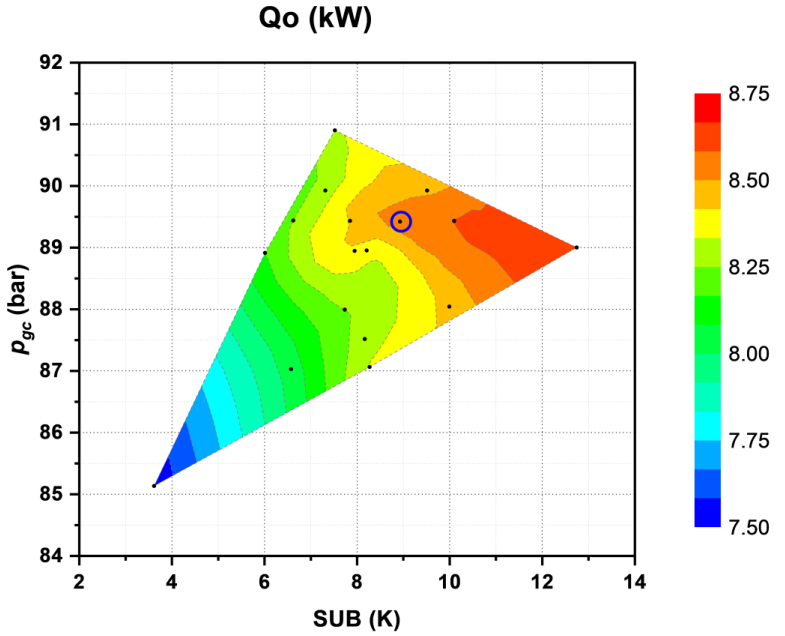

Figure 6.4. Experimental cooling capacity for $t_{w,in}$ = 35.1ºC and $t_{g,in}$ = 10.0ºC.

6.4.3. Optimum COP evaluation

Even it is not possible to determine with exactitude the exact value of the optimum COP, the experimental tests have allow to identify the region where the maximum COP is. To obtain the exact optimum COP, an interpolation of all the experimental data has been carried out. For that, all the measured values have been taken into account and referred to the subcooling degree and the gas-cooler pressure.

The data has been interpolated using the method of thin-plate spline (Bookstein, 1992), obtaining a 3D representation of the behaviour of the COP depending on the working pressure and the subcooling degree. Then, the interpolated function has been used to determine the exact position of the optimum COP values. The optimum COP values for the entire evaluation range are presented in Table 6.3, as well as the difference between this value and the maximum COP registered experimentally.

Figure 6.5 shows the interpolation at $t_{w,in}$=25.0ºC and $t_{g,in}$=1.3ºC. The blue points represent the measured experimental points and the red point represents the optimum point, obtained by the interpolation. The difference between the experimental and the

interpolated point, calculated with Eq.(6.4), is 0.34% in average and a maximum difference of 1.46% at one of the tested conditions, which means that the maximum point obtained experimentally is practically the same as the obtained by the interpolation.

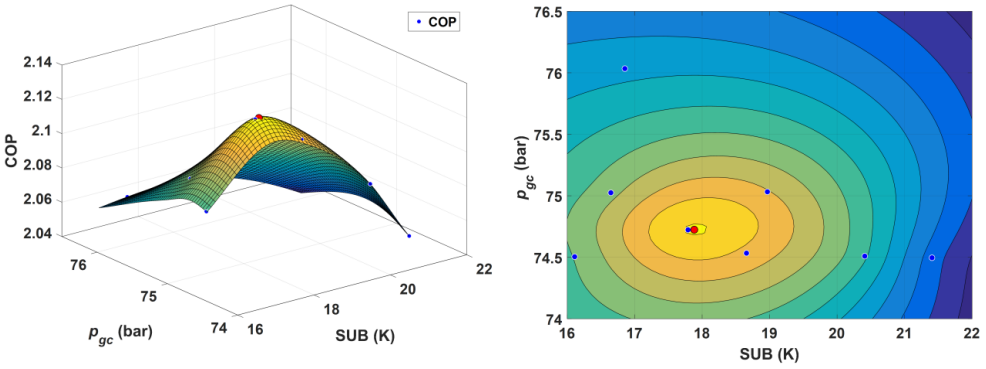

Figure 6.5. 3D and contour thin-plate spline interpolation of the COP at $t_{w,in}$=25.0ºC and $t_{g,in}$=-1.3ºC.

$$\Delta COP\ (\%) = \frac{COP_{inter} - COP_{expe}}{COP_{expe}} \cdot 100 \qquad (6.4)$$

Table 6.3. Experimental data vs interpolated results.

		Experimental data	Thin-plate spline	
Tw,in (ºC)	Tgly,in (ºC)	COP (-)	COP (-)	ΔCOP (%)
25.2	-1.4	1.866	1.868	0.11
30.5	-1.3	1.626	1.626	0.02
35.0	-1.3	1.404	1.409	0.36
25.0	3.7	2.131	2.131	0.01
30.4	3.8	1.818	1.822	0.20
35.2	3.9	1.564	1.578	0.92
24.8	9.9	2.482	2.482	0.01
30.2	9.9	2.101	2.132	1.46
35.1	10.3	1.811	1.811	0.00

6.5. Experimental results at optimum conditions

The results presented in this section correspond to the tests where the COP is maximum for each evaluated condition. The presented results are the measured data

and not the interpolated due to the minimal difference between them, as discussed in the previous section. Figure 6.6 represents the working cycle of the refrigeration system, with the most important points of measure. The red points correspond to the test conditions with the inlet glycol temperature of 10.0ºC, the green ones to the 3.8ºC and the blue ones to the -1.3ºC. The drawn cycles correspond to the water inlet temperature of 30.4ºC. For water temperatures of 25.0ºC and 35.1ºC, only the points of the exit of the gas-cooler and subcooler exit are represented.

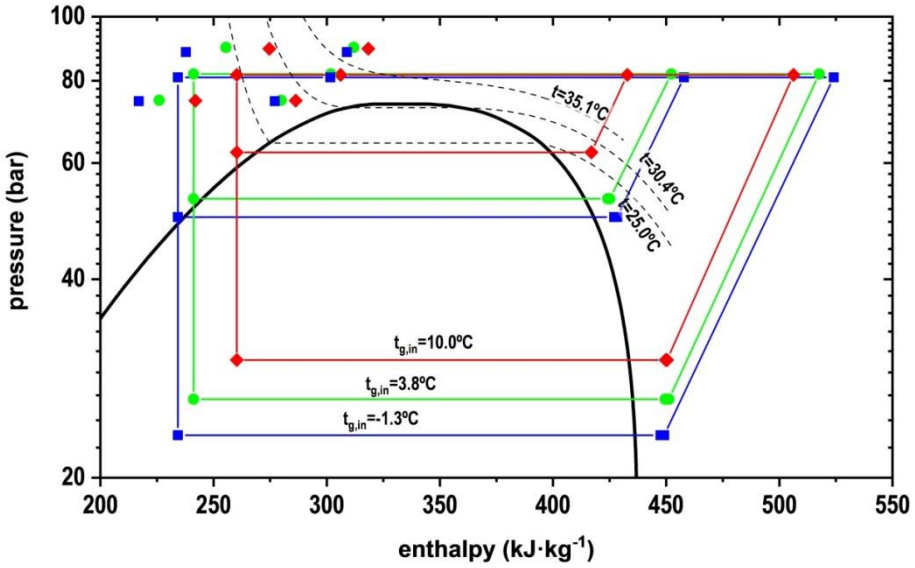

Figure 6.6. P-h diagram of the cycle at optimum working conditions for all the tests.

As it can be seen, at the water temperature level of 30.4ºC, the three gas-cooler exit points, corresponding to the three evaporation levels, are practically coincident, having them all very similar approach of temperature at gas-cooler. However, the subcooler exit points are not the same. Thus, here it is possible to observe the different optimum subcooling degree needed for each evaporation level since the subcooler outlet point is farther from the gas-cooler outlet when lower the evaporation temperature is. The same phenomenon is repeated at the water inlet temperature levels of 25.0ºC and 35.1ºC. In the diagram, it can also be observed that for a water inlet temperature condition, there is no large difference in terms of high pressure for the different evaporation levels, so the optimum gas-cooler pressure is slightly dependent on the evaporation temperature.

Table 6.4 sums up the main results. It contains the optimum COP of each tested condition, the main temperatures, the cooling capacity and power consumption of the

compressors as well as the uncertainty and the energy balances for data validation. COP, cooling capacity and working conditions are discussed in the following subsections.

The main energy parameters studied in this work are cooling capacity and COP, defined by Eq.(7.2) and Eq. (6.3), respectively. The uncertainty of these main parameters has been calculated using Moffat's method (Moffat, 1985) and the measurement devices' accuracies. The average measured uncertainty is ±0.85% in $\dot{Q}_0$ and ±0.95% in COP. The uncertainty ε(COP) and ε(Q_0) of all the results presented in this work is compiled in Table 6.4. To ensure correct measurement of the parameters in the cycle, the energy balances in evaporator, gas-cooler and subcooler have been calculated taking into account the capacity transmitted on the CO_2 side and on the secondary fluid.

Eq. (6.5) is the heat transfer at the side of the glycol. Eq. (6.6) quantifies the discrepancy between the heat transfer of the glycol and the cooling capacity on the evaporator.

$$\dot{Q}_g = \dot{V}_g \cdot \rho_g \cdot Cp_g \cdot (t_{g,in} - t_{g,o}) \tag{6.5}$$

$$\Delta\dot{Q}_{evap} = \frac{\dot{Q}_0 - \dot{Q}_g}{\dot{Q}_0} \cdot 100 \tag{6.6}$$

Eq. (6.7) corresponds to the heat transfer of the CO_2 in the gas-cooler and Eq.(6.8) in the water side. The difference between the heat transfers of each of the fluids is calculated as Eq.(6.9).

$$\dot{Q}_{gc} = (\dot{m}_{co2} + \dot{m}_{ims}) \cdot (h_{gc,in} - h_{gc,o}) \tag{6.7}$$

$$\dot{Q}_w = \dot{V}_w \cdot \rho_w \cdot C_{p,w} \cdot (t_{w,in} - t_{w,o}) \tag{6.8}$$

$$\Delta\dot{Q}_{gc} = \frac{\dot{Q}_{gc} - \dot{Q}_w}{\dot{Q}_{gc}} \cdot 100 \tag{6.9}$$

The capacity of the subcooler is calculated as Eq.(6.10) for the side corresponding to the CO_2 subcooled and Eq.(6.11) corresponds to the cooling capacity of the subcooler for the evaporation fluid. The heat transfer difference between both sides of the subcooler is calculated as Eq.(6.12).

$$\dot{Q}_{sub} = (\dot{m}_{co2} + \dot{m}_{ims}) \cdot (h_{gc,o} - h_{sub,o}) \tag{6.10}$$

$$\dot{Q}_{0,sub} = \dot{m}_{ims} \cdot (h_{sub,o} - h_{0,o,ims}) \tag{6.11}$$

$$\Delta\dot{Q}_{sub} = \frac{\dot{Q}_{0,ims} - \dot{Q}_{sub}}{\dot{Q}_{0,ims}} \cdot 100 \tag{6.12}$$

These balance differences are presented in Table 6.4. As it can be seen, the differences are quite small: 3.4% at evaporator in average, 3.8% at gas-cooler and 5.2% at subcooler. In tests number E3, E4 and E6 the discrepancies are greater than 5%. This is because the gas-cooler outlet is near the pseudocritical region where due to the variation of the isobaric heat capacity, small changes in temperature result in high measurement uncertainties (Torrella et al., 2011).

6.5.1. Maximum COP

Figure 6.7shows the evolution of the maximum measured COP for all the evaluated conditions. It can be seen a clear trend in its evolution, marked by the glycol and the water inlet temperatures. For all the glycol levels, it can be perceived that the COP is lower when lower the glycol inlet temperature is, so when lower the evaporation level is. It can be also observed that, as the water inlet temperature increases (corresponding to the heat rejection level) the COP decreases, so lower COPs are obtained when higher is the heat rejection temperature.

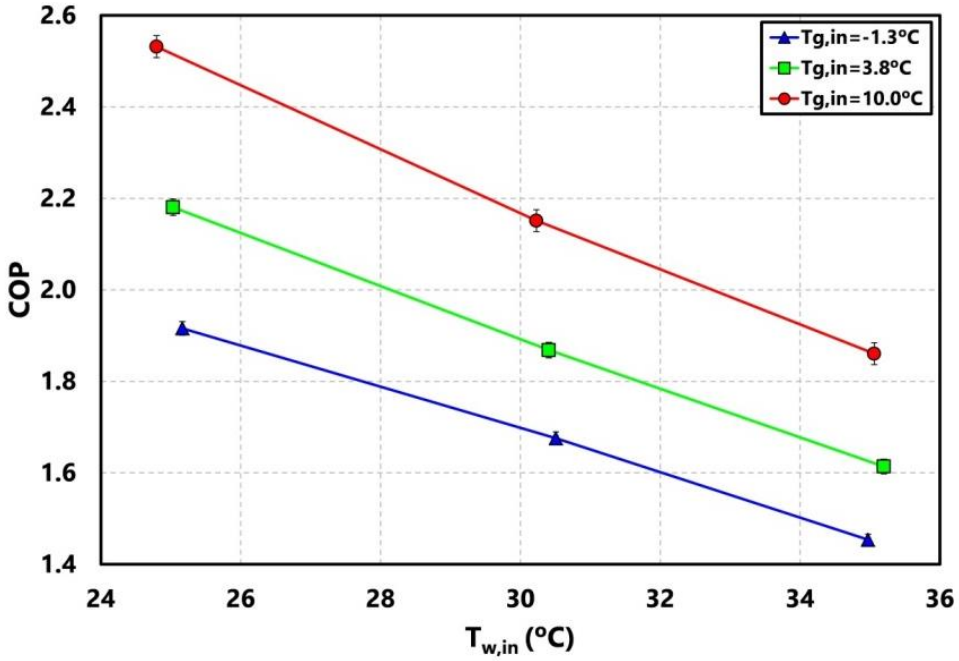

Figure 6.7. Evolution of the maximum COP for optimal conditions depending on the water inlet temperature.

The measured values go from 1.40 to 1.87 for $t_{g,in}$ = -1.3ºC, from 1.56 to 2.13 for $t_{g,in}$ = 3.8ºC and from 1.81 to 2.48 for $t_{g,in}$ = 10.0ºC.

6.5.2. Cooling capacity

The cooling capacity that the plant is capable of providing under the conditions of maximum COP is represented in Figure 6.8. A linear trend can be observed depending on the heat rejection temperature, reducing the cooling capacity of the plant as the water inlet temperature increases. Likewise, it is clearly observed how the capacity is greater when higher the evaporation level is.

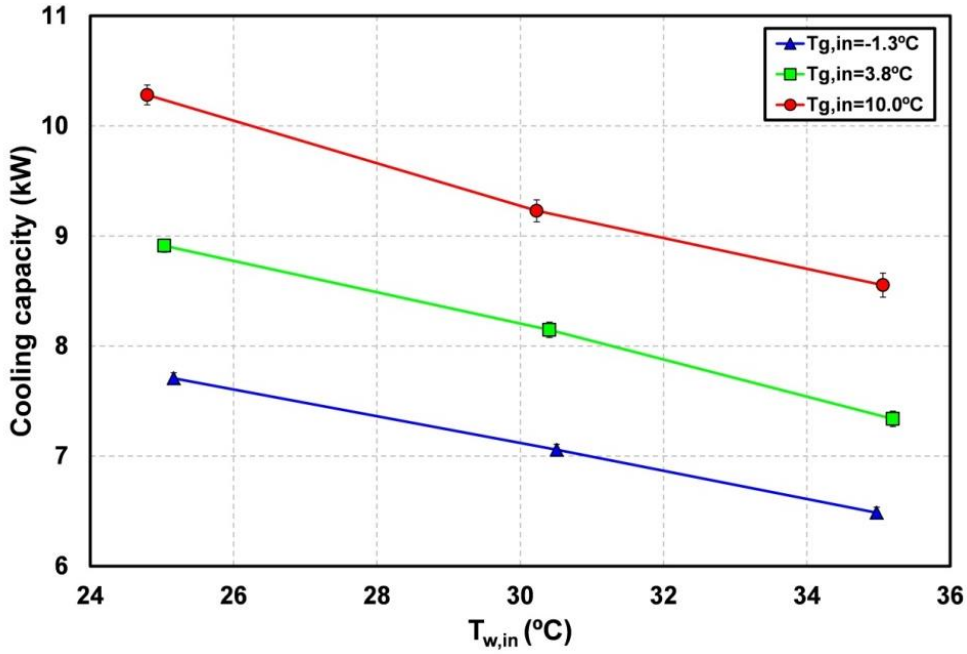

Figure 6.8. Evolution of the cooling capacity for optimal conditions depending on the water inlet temperature.

The measured values go from 6.5kW to 7.7kW for $t_{g,in}$ = -1.3ºC, from 7.3kW to 8.9kW for $t_{g,in}$ = 3.8ºC and from 8.6kW to 10.3kW for $t_{g,in}$ = 10.0ºC.

Cooling capacity can also be described as shown in Eq. (6.13), where the first term corresponds to the cooling capacity if there was not subcooling and the second to the contribution generated by the subcooling cycle. So the cooling capacity of the system can be defined as the sum of two terms, as shown by Eq. (6.14), the capacity of the system without subcooling ($\dot{Q}_{base}$) and the capacity added by the subcooler, Eq. (6.15).

$$\dot{Q}_0 = \dot{m}_{co2} \cdot \left(h_{0,o} - h_{gc,o}\right) + \dot{m}_{co2} \cdot \Delta h_{sub} \quad (6.13)$$

$$\dot{Q}_0 = \dot{Q}_{base} + \dot{m}_{co2} \cdot \Delta h_{sub} \quad (6.14)$$

$$\dot{Q}_{sub,add} = \dot{m}_{co2} \cdot \Delta h_{sub} \quad (6.15)$$

The proportion of the cooling capacity corresponding to the contribution of the subcooler represents in all cases less than a third of the total cooling capacity and goes from 2.0kW to 2.4kW. This contribution is greater the higher the water temperature and the lower the evaporation level are (when further the heat source and hot sink are). The effect of the subcooling cycle is higher at high rejection temperatures and low evaporation levels because these are the conditions where the behaviour of the plant needs to be more improved due to the reduction of the COP, as it was presented by Nebot-Andrés et al. (2019b). The contributions represent between 25.6% and 21.5% at 25.0ºC, between 31.5% and 24.1% at 30.4ºC and between 33.2 and 24.9 at 35ºC.

Figure 6.9 shows the total cooling capacity of the plant divided into the cooling capacity corresponding to the cycle without subcooling and the subcooling contribution.

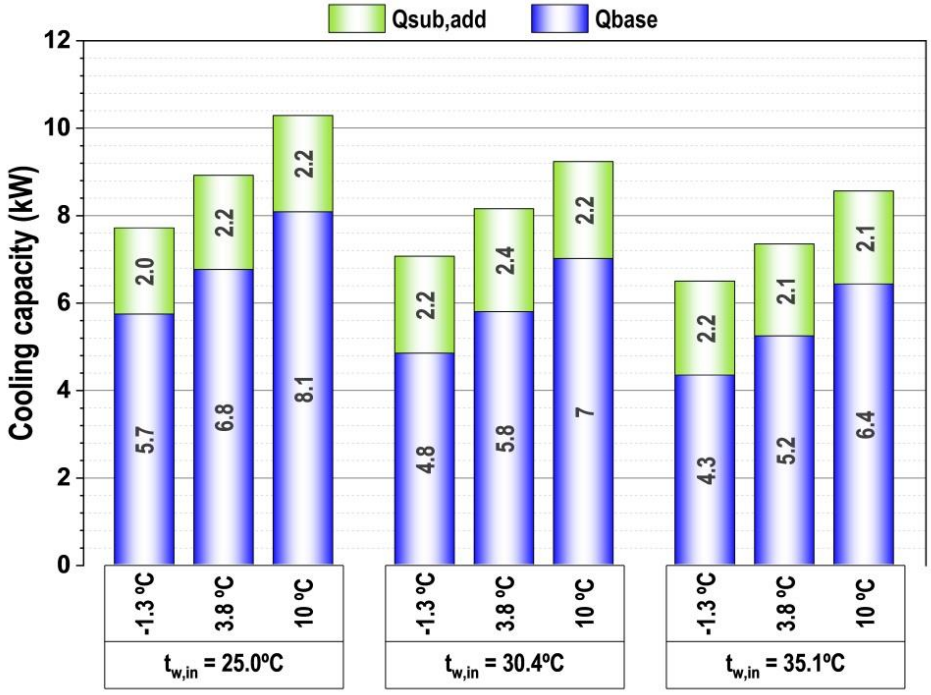

Figure 6.9. Cooling capacity broken down into base capacity and subcooler contribution.

Figure 6.10 represents the power consumption of each of the compressors of the plant for the different evaluated conditions. The increment in the power consumption due to the introduction of an additional compressor can be noticed. However, the power

consumption of the IMS compressor is much lower than those of the main compressor. In addition, as seen in the previous sections, the cooling capacity is increased in higher proportions, thus this effect is positive for the overall COP of the plant.

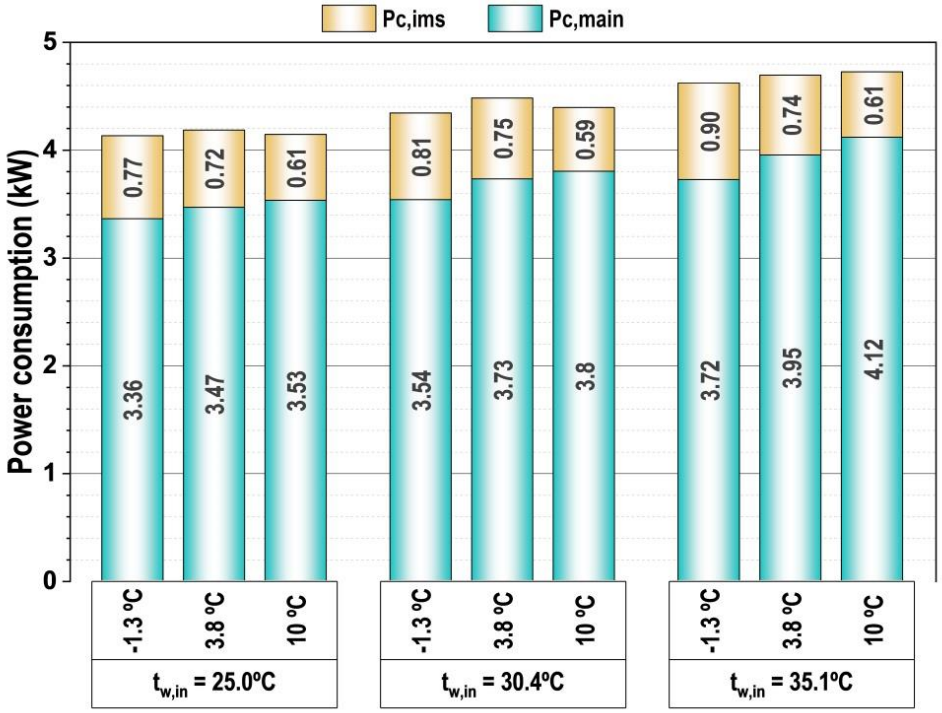

Figure 6.10. Power consumption of each of the compressors.

6.5.3. Optimum pressure

Figure 6.11 shows the optimum gas-cooler pressure value for each test condition. It can be observed that for the three glycol temperatures, the evolution of the pressure follows the same trend and also it practically does not depend on the inlet temperature at the evaporator. However, it is clearly correlated with the heat rejection level.

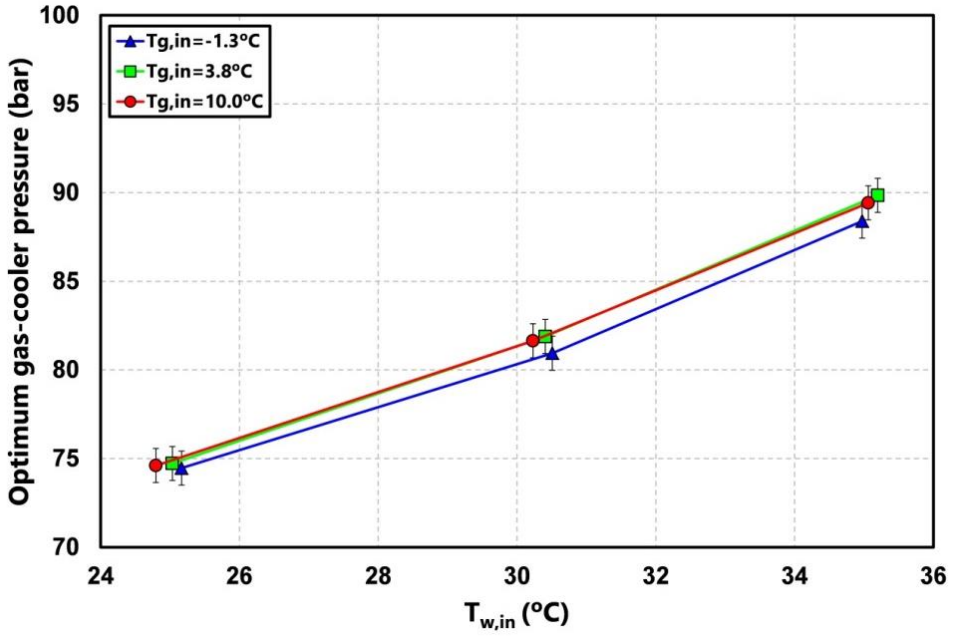

Figure 6.11. Optimum working pressure for the tested conditions.

There is a small difference for the lower glycol level but this difference is within the limits of the measurement uncertainty, therefore we can state that the optimum pressure depends more strongly on the heat rejection temperature than on the inlet temperature at the evaporator of the plant. Analyzing the influence of the heat rejection level, we can affirm that the higher the temperature is, the greater the pressure of the plant must be.

6.5.4. Optimum subcooling degree

Optimal subcooling degree is presented in Figure 6.12. We can affirm that when lower is the evaporation level, greater the degree of subcooling necessary to achieve the optimum COP must be. Analysing each of the different evaporation levels, a slight decreasing trend can be seen for the higher inlet glycol temperatures ($t_{g,in}$ = 3.8ºC and 10.0ºC) while for -1.3ºC the optimal subcooling degree decreases and then increases again. This change in trend in the evolution of the optimal subcooling degree may be because the gas-cooler outlet is near the pseudocritical zone, where CO_2 present abrupt changes in its thermophysical properties. Also, this effect was observed in the theoretical simulations presented by Nebot-Andrés et al. (2017).

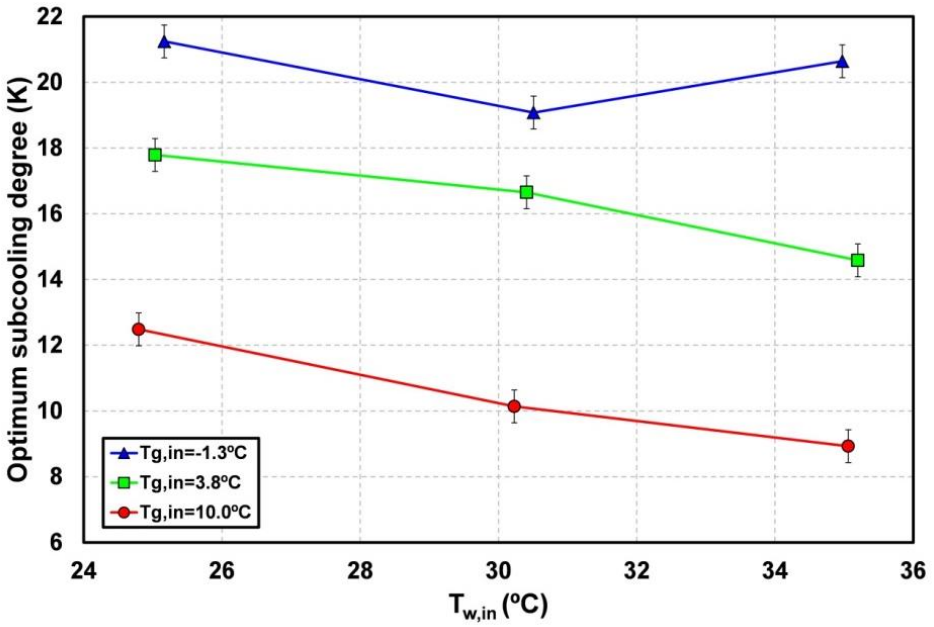

Figure 6.12.Evolution of the optimum subcooling degree for the tested conditions.

6.5.5. Correlations

In the previous sections all the results are referred to the inlet water and glycol temperatures because these were the parameters set in the test. In order to generalize more the results, in this section the optimal operating conditions are referred to the evaporation temperature and the gas-cooler outlet temperatures.

The following correlations allow calculating the optimum subcooling degree and the optimal gas-cooler pressure. They have been obtained by adjusting the values obtained experimentally by an adjustment of least-squares.

6.5.5.1. Optimum pressure

Equation (6.16) defines the optimum gas-cooler pressure as a function of the evaporation temperature and the gas-cooler outlet temperature.

$$p_{gc} = 126.5 + 0.285 \cdot t_0 - 4.537 \cdot t_{gc,o} - 0.01374 \cdot t_0 \cdot t_{gc,o} + 0.09409 \cdot t_{gc,o}^2 \quad (6.16)$$

$$27.5ºC \leq t_{gc,o} \leq 37.5ºC$$

$$-15.6ºC \leq t_0 \leq -4.1ºC$$

The range of application of this correlation is for temperatures of gas-cooler exit between 27.5ºC and 37.5ºC and evaporation temperatures between -15.6ºC and -4.1ºC. The average error of this correlation is ±0.3 bar and the maximum error ±0.6 bar.

Kauf (1999), Liao et al. (2000) and Sarkar et al. (2004) proposed correlations to determine the optimum pressure for single-stage transcritical CO2 cycles. Then, Chen and Gu (2005) proposed a correlation for transcritical carbon dioxide cycles with internal heat exchanger that provide similar results to Kauf's correlation. Also, Song et al. (2018) presented a correlation based on experimental data to obtain the optimum pressure for subcooler-based transcritical CO2 systems used as heat pump.

Figure 6.13 shows the optimum CO_2 gas-cooler pressure based on the different correlations for an evaporating level of -5ºC including the previous correlation presented in eq.(6.16). Kauf's correlation is not included because the range of application is different. It can be observed that the correlation proposed in this paper provides lower pressures for temperatures over 32ºC at the exit of gas-cooler, corroborating the optimal pressure reduction achieved with the use of subcooling cycles (Dai et al., 2018; Llopis et al., 2016).

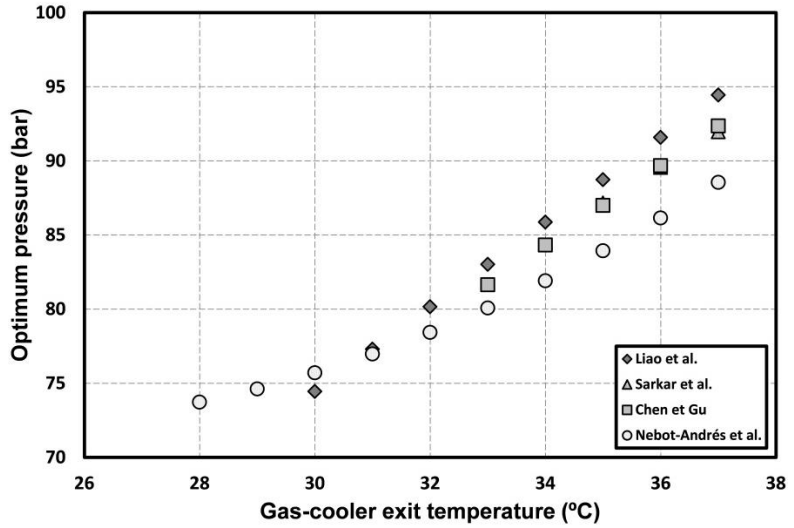

Figure 6.13. Optimum gas-cooler pressure based on different correlations (t_o=-5ºC).

Figure 6.14 shows the reduction in pressure obtained comparing the correlation of eq. (6.16) with the correlations of Liao, Sarkar and Chen. The optimum pressure of the CO_2 system with IMS is gradually reduced when higher the gas-cooler outlet temperature is, compared to a pure transcritical CO_2 cycle. A reduction of 5.9 bar is obtained for $t_{gc,o}$ =

37°C comparing to Liao's correlation. Comparing to Sarkar's expression, an average reduction of 3.3 bar is accomplished for temperatures between 35 and 37ºC. The IMS cycles also reduces the pressure of the system comparing it to cycles with internal heat exchanger, up to -3.8 bar for $t_{gc,o}$ = 37°C.

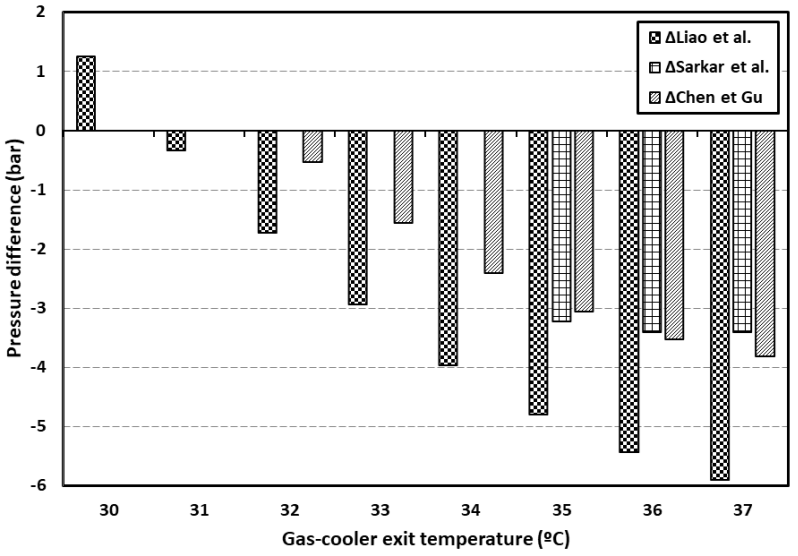

Figure 6.14. Pressure difference obtained using the IMS optimum pressure correlation.

The correlations posed by the previous authors differ significantly from the optimal pressure of the transcritical cycle with IMS; therefore, the use of the correlation in the eq.(6.16) is recommended for this type of cycles.

6.5.5.2. Optimum subcooling degree

Equation (6.17) shows the correlation between the evaporation temperature and the gas-cooler outlet temperature that defines the optimum subcooling degree needed to obtain the maximum COP when working at the optimum pressure for a CO_2 cycle with integrated mechanical subcooling.

$$SUB = 9.682 - 0.9938 \cdot t_0 - 0.1226 \cdot t_{gc,o}$$
$$27.5ºC \leq t_{gc,o} \leq 37.5ºC \quad (6.17)$$
$$-15.6ºC \leq t_0 \leq -4.1ºC$$

The range of application of this correlation is for temperatures of gas-cooler exit between 27.5ºC and 37.5ºC and for evaporating levels between -15.6ºC and -4.1ºC. The average error of this correlation is ±0.6K and the maximum error ±1.0K.

6.6. Conclusions

This paper presents for the first time the experimental optimization of a CO_2 transcritical refrigeration plant with integrated mechanical subcooling. The evaluation covered the heat rejection levels of 25.0ºC, 30.4ºC and 35.1ºC and the cold source temperatures of -1.3ºC, 3.8ºC and 10ºC at steady-state conditions. The main compressor was run at nominal speed while the velocity of the auxiliary compressor was modified in order to obtain the optimum subcooling degree. All the experimental data have been validated by comparing the energy balances in all the heat exchangers of the plant.

The experimental tests have allowed to demonstrate the existence of a maximum COP, obtained at optimum conditions of pressure and subcooling degree. All the tests were performed to obtain the optimal COP of the plant, that goes from 1.40 to 1.87 at $t_{g,in}$ = -1.3ºC, from 1.56 to 2.13 for $t_{g,in}$ = 3.8ºC and from 1.81 to 2.48 for $t_{g,in}$ = 10.0ºC and the cooling capacity from 6.5kW to 7.7kW at tg,in = -1.3ºC, from 7.3kW to 8.9kW for tg,in = 3.8ºC and from 8.6kW to 10.3kW for tg,in = 10.0ºC. On the one hand, the optimum pressure is strongly dependent on the gas-cooler outlet temperature, following a linear trend but it practically does not vary depending on the level of evaporation. On the other hand, the optimum subcooling degree is a function of the gas-cooler outlet temperature and the evaporation temperature, the subcooling being always different for each of the working levels, being higher when lower is the evaporation level.

From the experimental data, two general expressions have been stated to determine the optimum pressure and subcooling in this type of installation, only as a function of its evaporation level and the gas-cooler outlet temperature. Optimum pressure correlation differs significantly from the classical equations, so it is advisable to use the correlation presented in this paper for CO_2 transcritical cycles with integrated mechanical subcooling.

6.7. Acknowledgements

The authors thank the Ministry of Economy and Competitiveness - Spain (project ENE2014-53760-R.7), the Ministry of Education, Culture and Sports - Spain (grant FPU16/00151) and the Jaume I University (project UJI-B2017-06) for financing this research work.

6.8. Nomenclature

COP coefficient of performance

Cp specific heat capacity, $kJ \cdot kg^{-1} \cdot K^{-1}$

h specific enthalpy, $kJ \cdot kg^{-1}$

m mass flow $kg \cdot s^{-1}$

p absolute pressure, bar

Pc power consumption, kW

Q cooling capacity, kW

SUB degree of subcooling produced in the subcooler, K

t temperature, ºC

V volumetric flow, $m^3 \cdot s^{-1}$

Greek symbols

ρ density, $kg \cdot m^{-3}$

ε uncertanity

Subscripts

add addition

dis compressor discharge

exp expansion

expe experimental

g glycol

gc gas-cooler

ims corresponding to the IMS cycle

in inlet

inter interpolated

main corresponding to the main cycle

0 evaporating level

o outlet

sub corresponding to the subcooler

suc compressor suction

w water

6.9. References

Beshr, M., Bush, J., Aute, V., Radermacher, R., 2016. Steady state testing and modeling of a CO2 two-stage refrigeration system with mechanical subcooler, Refrigeration Science and Technology, pp. 893-900.

Bookstein, F.L., 1992. Principal warps: Thin-plate splines and the decomposition of deformations. IEEE Transactions on Pattern Analysis and Machine Intelligence v, 567-585.

Bush, J., Beshr, M., Aute, V., Radermacher, R., 2017. Experimental evaluation of transcritical CO2 refrigeration with mechanical subcooling. Science and Technology for the Built Environment 23, 1013-1025.

Cao, F., Cui, C., Wei, X., Yin, X., Li, M., Wang, X., 2019. The experimental investigation on a novel transcritical CO2 heat pump combined system for space heating. International Journal of Refrigeration 106, 539-548.

Catalán-Gil, J., Llopis, R., Sánchez, D., Nebot-Andrés, L., Cabello, R., 2019. Energy analysis of dedicated and integrated mechanical subcooled CO2 boosters for supermarket applications. International Journal of Refrigeration.

Cecchinato, L., Chiarello, M., Corradi, M., Fornasieri, E., Minetto, S., Stringari, P., Zilio, C., 2009. Thermodynamic analysis of different two-stage transcritical carbon dioxide cycles. International Journal of Refrigeration 32, 1058-1067.

Chen, Y., Gu, J., 2005. The optimum high pressure for CO2 transcritical refrigeration systems with internal heat exchangers. International Journal of Refrigeration 28, 1238-1249.

Chesi, A., Esposito, F., Ferrara, G., Ferrari, L., 2014. Experimental analysis of R744 parallel compression cycle. Applied Energy 135, 274-285.

Dai, B., Liu, S., Li, H., Sun, Z., Song, M., Yang, Q., Ma, Y., 2018. Energetic performance of transcritical CO2 refrigeration cycles with mechanical subcooling using zeotropic mixture as refrigerant. Energy 150, 205-221.

Dai, B., Liu, S., Sun, Z., Ma, Y., 2017. Thermodynamic Performance Analysis of CO2 Transcritical Refrigeration Cycle Assisted with Mechanical Subcooling, Energy Procedia, pp. 2033-2038.

European Commission, 2014. Regulation (EU) No 517/2014 of the European Parliament and of the Council of 16 April 2014 on fluorinated greenhouse gases and repealing Regulation (EC) No 842/2006.

Gullo, P., Hafner, A., Banasiak, K., Minetto, S., Kriezi, E.E., 2019. Multi-ejector concept: A comprehensive review on its latest technological developments. Energies 12.

Kauf, F., 1999. Determination of the optimum high pressure for transcritical CO2-refrigeration cycles. International Journal of Thermal Sciences 38, 325-330.

Lawrence, N., Elbel, S., 2019. Experimental investigation on control methods and strategies for off-design operation of the transcritical R744 two-phase ejector cycle. International Journal of Refrigeration.

Lemmon, E.W., Huber, M.L., McLinden, M.O., 2013. REFPROP, NIST Standard Reference Database 23, v.9.1. National Institute of Standards, Gaithersburg, MD, U.S.A.

Liao, S.M., Zhao, T.S., Jakobsen, A., 2000. A correlation of optimal heat rejection pressures in transcritical carbon dioxide cycles. Applied Thermal Engineering 20, 831-841.

Llopis, R., Cabello, R., Sánchez, D., Torrella, E., 2015a. Energy improvements of CO2 transcritical refrigeration cycles using dedicated mechanical subcooling. International Journal of Refrigeration 55, 129-141.

Llopis, R., Nebot-Andrés, L., Cabello, R., Sánchez, D., Catalán-Gil, J., 2016. Experimental evaluation of a CO2 transcritical refrigeration plant with dedicated mechanical subcooling. International Journal of Refrigeration 69, 361-368.

Llopis, R., Nebot-Andrés, L., Sánchez, D., Catalán-Gil, J., Cabello, R., 2018. Subcooling methods for CO2 refrigeration cycles: A review. International Journal of Refrigeration 93, 85-107.

Llopis, R., Sanz-Kock, C., Cabello, R., Sánchez, D., Torrella, E., 2015b. Experimental evaluation of an internal heat exchanger in a CO2 subcritical refrigeration cycle with gas-cooler. Applied Thermal Engineering 80, 31-41.

Moffat, R.J., 1985. Using Uncertainty Analysis in the Planning of an Experiment. Journal of Fluids Engineering 107, 173-178.

Nebot-Andrés, L., Calleja-Anta, D., Sánchez, D., Cabello, R., Llopis, R., 2019a. Thermodynamic analysis of a CO2 refrigeration cycle with integrated mechanical subcooling. Energies 13.

Nebot-Andrés, L., Llopis, R., Catalán-Gil, J., Sánchez, D., Calleja-Anta, D., Cabello, R., 2019b. Thermodynamics analysis of CO2 refrigeration cycles working with mechanical subcooling systems, 25th IIR International Congress of Refrigeration, Montreal, Canada.

Nebot-Andrés, L., Llopis, R., Sánchez, D., Catalán-Gil, J., Cabello, R., 2017. CO2 with mechanical subcooling vs. CO2 cascade cycles for medium temperature commercial refrigeration applications thermodynamic analysis. Applied Sciences (Switzerland) 7.

Sánchez, D., Catalán-Gil, J., Llopis, R., Nebot-Andrés, L., Cabello, R., Torrella, E., 2016. Improvements in a CO2 transcritical plant working with two different subcooling systems, Refrigeration Science and Technology, pp. 1014-1022.

Sarkar, J., Agrawal, N., 2010. Performance optimization of transcritical CO2 cycle with parallel compression economization. International Journal of Thermal Sciences 49, 838-843.

Sarkar, J., Bhattacharyya, S., Gopal, M.R., 2004. Optimization of a transcritical CO2 heat pump cycle for simultaneous cooling and heating applications. International Journal of Refrigeration 27, 830-838.

Shapiro, D., 2009. Refrigeration system with mechanical subcooling, https://patentimages.storage.googleapis.com/56/2a/72/a987f71d7ab41a/US7628027.pdf, United States.

Song, Y., Cao, F., 2018. The evaluation of the optimal medium temperature in a space heating used transcritical air-source CO2 heat pump with an R134a subcooling device. Energy Conversion and Management 166, 409-423.

Song, Y., Ye, Z., Wang, Y., Cao, F., 2018. The experimental verification on the optimal discharge pressure in a subcooler-based transcritical CO2 system for space heating. Energy and Buildings 158, 1442-1449.

Torrella, E., Sánchez, D., Llopis, R., Cabello, R., 2011. Energetic evaluation of an internal heat exchanger in a CO2 transcritical refrigeration plant using experimental data. International Journal of Refrigeration 34, 40-49.

Yu, B., Yang, J., Wang, D., Shi, J., Chen, J., 2019. An updated review of recent advances on modified technologies in transcritical CO2 refrigeration cycle. Energy 189, 116147.

Table 6.4. Main experimental results and uncertainty measurements.

	$t_{g,in}$ (ºC)	t_0 (ºC)	$t_{w,in}$ (ºC)	$p_{gc,o}$ (bar)	$t_{gc,o}$ (ºC)	SUB (ºC)	m_{CO2} (kg/s)	Pc_{main} (kW)	Pc_{ims} (kW)	Q_0 (kW)	$\varepsilon(Q_0)$ (kW)	$\varepsilon(Q_0)$ (%)	COP (-)	ε(COP) (-)	ε(COP) (%)		ΔQ_{evap} (%)	ΔQ_{gc} (%)	ΔQ_{sub} (%)
E1	-1.4	-15.6	25.2	74.5	27.5	21.3	0.03	3.36	0.77	7.71	0.05	0.66	1.87	0.015	0.78		-3.3	-2.5	4.4
E2	3.7	-11.2	25.0	74.7	28.1	17.8	0.04	3.47	0.72	8.91	0.06	0.73	2.13	0.018	0.84		-5.2	-3.0	3.3
E3	9.9	-5.9	24.8	74.6	29.2	12.5	0.05	3.53	0.61	10.28	0.09	0.87	2.48	0.024	0.97		-4.7	-4.9	6.6
E4	-1.3	-14.6	30.5	80.9	32.9	19.1	0.03	3.54	0.81	7.06	0.05	0.77	1.63	0.014	0.88		-2.8	-4.3	7.2
E5	3.8	-10.2	30.4	81.9	33.2	16.7	0.04	3.73	0.75	8.15	0.07	0.82	1.82	0.017	0.92		-1.8	-2.8	1.9
E6	9.9	-5.3	30.2	81.6	33.6	10.1	0.05	3.80	0.59	9.23	0.10	1.05	2.10	0.024	1.13		-6.4	-6.3	8.8
E7	-1.3	-14.5	35.0	88.4	36.1	20.6	0.03	3.72	0.90	6.49	0.05	0.76	1.40	0.012	0.86		-3.4	-3.2	5.7
E8	3.9	-9.8	35.2	89.8	36.9	14.6	0.04	3.95	0.74	7.34	0.07	0.92	1.56	0.016	1.01		-2.7	-2.7	3.4
E9	10.3	-4.1	35.1	89.4	37.5	8.9	0.05	4.12	0.61	8.55	0.11	1.25	1.81	0.024	1.32		-0.3	-4.1	5.2

Chapter 6. Experimental determination of the optimum working conditions of a transcritical CO_2 refrigeration plant with integrated mechanical subcooling.

Chapter 7 Experimental determination of the optimum working conditions of a commercial transcritical CO_2 refrigeration plant with a R-152a dedicated mechanical subcooling.

Chapter 7. Experimental determination of the optimum working conditions of a commercial transcritical CO_2 refrigeration plant with a R-152a dedicated mechanical subcooling.

7. Experimental determination of the optimum working conditions of a commercial transcritical CO2 refrigeration plant with a R-152a dedicated mechanical subcooling

International Journal of Refrigeration 121 (2021) 258–268

Contents lists available at ScienceDirect

International Journal of Refrigeration

journal homepage: www.elsevier.com/locate/ijrefrig

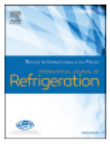

Chapter adapted from the paper: Nebot-Andrés, L., Sánchez, D., Calleja-Anta, D., Cabello, R., Llopis, R. Experimental determination of the optimum working conditions of a commercial transcritical CO_2 refrigeration plant with a R-152a dedicated mechanical subcooling (2021) International Journal of Refrigeration, 121, p.p. 258-268. DOI: 10.1016/j.ijrefrig.2020.10.002.

Abstract

Transcritical CO_2 plants combined with subcooling systems are the focus of several researches in the last years with the objective of improving their performance. Among the subcooling systems, the Dedicated Mechanical Subcooling system (DMS) is one of the most interesting because it greatly improves the overall COP and the cooling capacity of the system.

This work presents the experimental study of a transcritical CO_2 plant working with an R-152a DMS. The plant was tested at different pressure and subcooling conditions in order to determine the working conditions where the COP of the plant is maximum. The optimal operation conditions are determined for three ambient temperatures 25.0ºC, 30.4ºC and 35.1ºC and three cold sink temperatures (-1.3ºC, 3.8ºC and 10.0ºC). The measured values go from 6.5 kW to 7.3 kW for glycol inlet temperature -1.3ºC, from 7.6 kW to 8.4 kW for 3.8ºC and from 8.8 kW to 9.8 kW for 10.0ºC. Optimum COP goes from 1.51 to 1.95 for -1.3ºC, from 1.69 to 2.21 for 3.8ºC and from 1.86 to 2.52 for 10.0ºC.

Optimum gas-cooler pressure has a higher dependence on the heat rejection level, being higher when higher the heat rejection level is, but it slightly depends on the evaporation level. Optimum subcooling degree is both dependent on the water inlet temperature and on the glycol inlet temperature.

Two correlations are proposed to determine the optimal pressure and subcooling degree for the CO_2 plants working with DMS as a function of the gas-cooler outlet temperature and the evaporation level.

Keywords

CO_2, Transcritical, Dedicated Mechanical Subcooling, COP, Optimum conditions

Chapter 7. Experimental determination of the optimum working conditions of a commercial transcritical CO_2 refrigeration plant with a R-152a dedicated mechanical subcooling.

Chapter 7. Experimental determination of the optimum working conditions of a commercial transcritical CO_2 refrigeration plant with a R-152a dedicated mechanical subcooling.

7.1. Introduction

Carbone dioxide commercial refrigeration systems are getting more complex in the recent years in order to reach high energy performance, above all in hot climates. As a cause of the Montreal Protocol and the Kigali Amendment (UNEP/TEAP, 1999; United Nations, 1997) and later the F-Gas Regulation (European Commission, 2014) that restricts the use of high GWP refrigerants in almost all refrigeration applications, the CO_2 is the only low-GWP refrigerant that is safe, non-flammable and non-toxic for commercial refrigeration. Researchers' efforts are focused on improving these systems because despite the fact that they have been used in cold regions for many years, in areas where the ambient temperature is higher, they have a significant loss of efficiency, not being enough performant.

Several solutions have been proposed as the use of a parallel compressor for enhancing energy performance. Sarkar and Agrawal (2010) performed the optimization of different architectures with parallel compression and Chesi et al. (2014) carried on an experimental study on a parallel compression cycle with flash tank but they did not reach the same results found in their theoretical studies. Karampour and Sawalha (2016a) investigated key operating parameters of a supermarket located in Sweden where heating and air conditioning are integrated into the CO_2 transcritical booster system with parallel compression. During air conditioning delivery, authors found that COP of the system was 8% higher using the PC comparing with the system without PC (Karampour and Sawalha, 2016b). The use of ejectors is one of the other solutions being studied in the last years with two types of ejector, the adjustable ejector presented by Lawrence and Elbel (2019) and the multi-ejector concept (Gullo et al., 2019; Hafner A. et al., 2014).

Subcooling methods are another clear line of research that is acquiring a lot of weight at this moment (Yu et al., 2019). The main methods of subcooling were reviewed by Llopis et al. (2018). Subcooling can be performed in different ways as the use of an internal heat exchanger (Llopis et al., 2015b) or more complex methods as mechanical subcooling systems. These lasts can be integrated in the CO2 cycle, as the integrated subcooling system (IMS) or built as an auxiliary cycle, as the dedicated mechanical subcooling system (DMS). The IMS, working only with CO_2 as refrigerant, has been studied theoretically (Nebot-Andrés et al., 2019) and has an important potential of improvement with respect to the classic CO_2 cycle producing high increments in COP (Catalán-Gil et al., 2019). Nebot-Andrés et al. (2020) have experimentally tested a transcritical CO_2 refrigeration plant with IMS and demonstrate the existence of an optimum COP depending on the gas-cooler pressure and subcooling degree.

Regarding the DMS system, Llopis et al. (2015a) studied from a theoretical approach a transcritical plant with a R290 DMS for different evaporation levels and heat rejection temperatures. The results were optimized in terms of discharge pressure but the subcooling degree was not optimized. Despite this, the results showed increases in the overall COP with reference to the system without subcooling up to 18.4% for an evaporating temperature of -30ºC. After that, Dai et al. (2017) studied theoretically a R-152a DMS single-stage system at optimum conditions, obtaining significant improvements. The use of zeotropic mixtures in the DMS cycle was also studied by Dai et al. (2018) theoretically with increments in COP of 4.9% by using a R-32/R-1234ze(Z) (55/45) mixture in the DMS cycle instead of pure R-32.

Later, Catalán-Gil et al. (2019) analyzed the thermodynamic models of the IMS and the DMS for CO_2 booster systems for supermarket applications, achieving annual energy consumption reductions for tempered places from 1.5% to 2.9%, for warm between 2.9% and 3.4% and for hot from 3.0% to 5.1% in relation to the configuration with parallel compressor.

Parallel to theoretical studies, DMS was experimentally studied by Llopis et al. (2016) who tested a CO_2 plant with a R-1234yf DMS cycle. The tests were optimized in terms of gas-cooler pressure but the subcooling degree was not optimized. Despite this fact, the results showed increments in COP of 10.9% at 24.0ºC, 22.1% at 30.2ºC and 26.1% at 40.0ºC for the evaporation level of 0ºC comparing the results with the cycle without subcooling. Nebot-Andrés et al. (2018) tested a CO_2 cycle with DMS giving service to a commercial medium temperature cabinet using direct expansion and compared the energy consumption to a classic CO_2 cycle, without mechanical subcooling, and obtained reductions in energy consumption up to 7.2% for the heat rejection level of 43.6ºC. Sánchez et al. (2020) experimentally tested an R-600a dedicated mechanical subcooling system for hermetic small systems at different operating conditions and compared the results to the CO2 system with internal heat exchanger (IHX) and then developed a computational model to predict the optimal subcooling degree. Other experimental tests have been carried out with booster systems (Beshr et al., 2016; Bush et al., 2017).

The dedicated subcooling cycles have been studied for space heating applications. Song et al. (Song and Cao, 2018; Song et al., 2017; Song et al., 2018) proposed a cycle with R-134a DMS cycle for water heating purposes, allowing to increase the CO_2 COP and to increment its specific heating capacity and determined the optimum working parameters. Later, a combined system using only CO_2 has been studied (Cao et al., 2019). Cao et al. presented a transcritical CO2 heat pump combined with a subcooling

system working with CO_2, obtaining increments of 15.3% in COP comparing to the standard transcritical CO_2 heat pump systems. Dai et al. (2020) proposed a transcritical CO_2 reversible system combined with DMS for residential heating and cooling applied to a common residential building. The system annual performance is studied from the energetic, exergetic, and exergoeconomic point of view and compared to a traditional CO_2 system. The obtained improvements range from 6.23 to 22.90% in terms of annual performance factor, which demonstrates the benefits of this system.

The dedicated mechanical subcooling has been a strong option for the enhancement of CO_2 cycles in the last years. However, DMS cycles applied to transcritical refrigeration CO_2 plants have never been optimized in terms of pressure and subcooling degree in an experimental plant. Furthermore, its optimum energy parameters have not been studied experimentally, to the knowledge of authors.

This work has been developed in order to determine experimentally the optimum conditions, in terms of subcooling degree and gas-cooler pressure, of a CO_2 commercial refrigeration plant with a R-152a DMS, working in transcritical conditions. The main objective is to identify these optimal conditions, determine the parameters for which the maximum COP is obtained and to define an expression that generalizes the optimum pressure and optimum subcooling degree for this type of systems. The data presented on this paper correspond to the evaluation of a single–stage plant for different external conditions: three different temperatures of the secondary fluid at the entrance of the evaporator (-1.3ºC, 3.8ºC and 10.0ºC) and three heat rejection levels (25.0ºC, 30.4ºC and 35.1ºC). In every test, the optimum value of pressure and subcooling degree is determined and a general correlation depending on the evaporation temperature and the temperature at the exit of the gas-cooler has been stated. The evolution of cooling capacity and COP of the overall system is analyzed.

7.2. Refrigeration cycle and description of the experimental plant

This section presents the experimental plant used to evaluate the optimal conditions of the CO_2 transcritical cycle with the dedicated mechanical subcooling system presented in Figure 7.1. The main components of the cycle are detailed and the measurement system used in the plant is described.

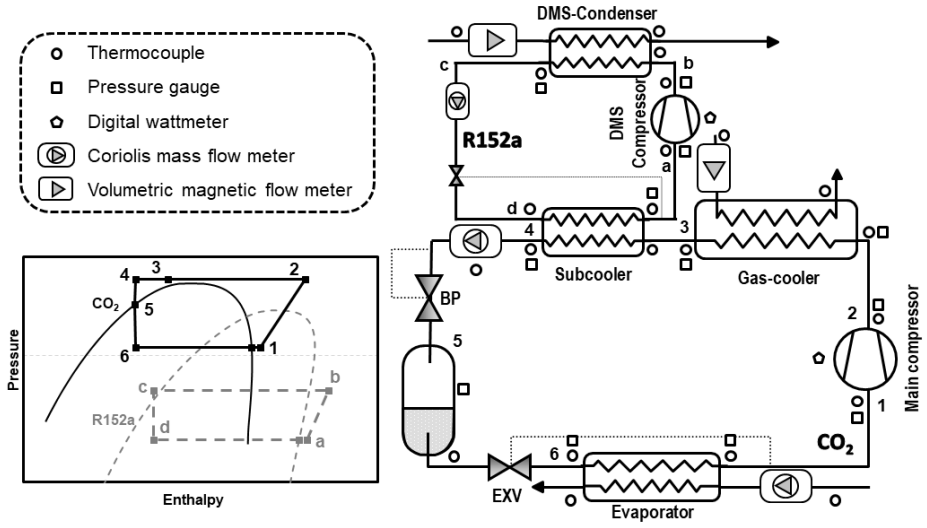

Figure 7.1. Schema of the experimental plant and the measurement system and Ph diagram of the cycle.

7.2.1. Experimental plant

Figure 7.1 shows the schema of the CO_2 single-stage transcritical refrigeration system with a dedicated mechanical subcooling system and the experimental plant is presented in Figure 7.2 and Figure 7.3. The main single-stage refrigeration cycle uses a semihermetic compressor with a displacement of 3.48 $m^3 \cdot h^{-1}$at 1450 rpm and a nominal power of 4 kW. A double-stage system carries out the expansion of the CO_2. An electronic expansion valve (back-pressure) controls the gas-cooler pressure and an electronic expansion valve, working as thermo-static, controls the evaporating process, while there is a liquid receiver between both expansion stages. Two brazed plate counter current heat exchangers are used as gas-cooler and evaporator with exchange surface area of 4.794 m^2 and 1.224 m^2, respectively. The subcooler is situated directly downstream of the gas-cooler. It is a brazed plate heat exchanger with an exchange surface area of 0.576 m^2 and it couples thermally the main cycle and the dedicated cycle.

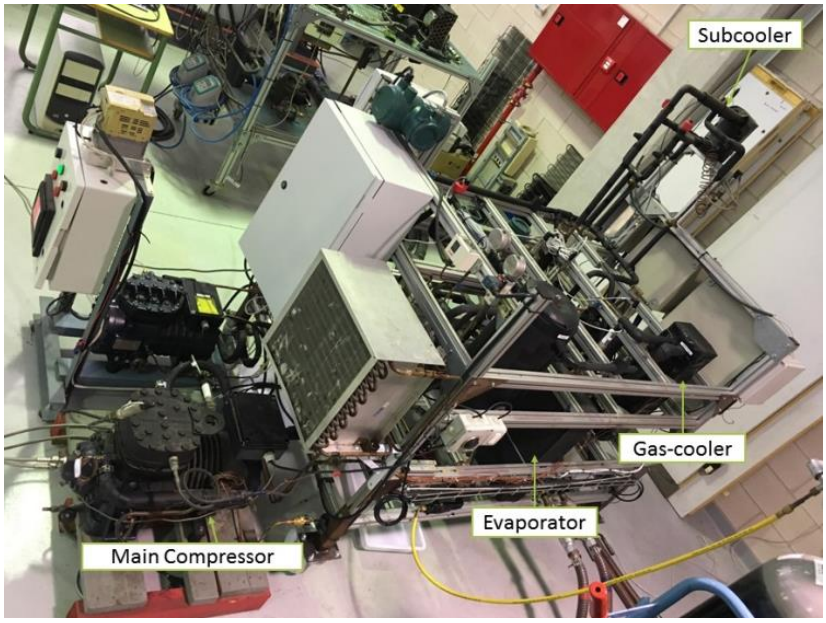

Figure 7.2. Experimental CO_2 plant.

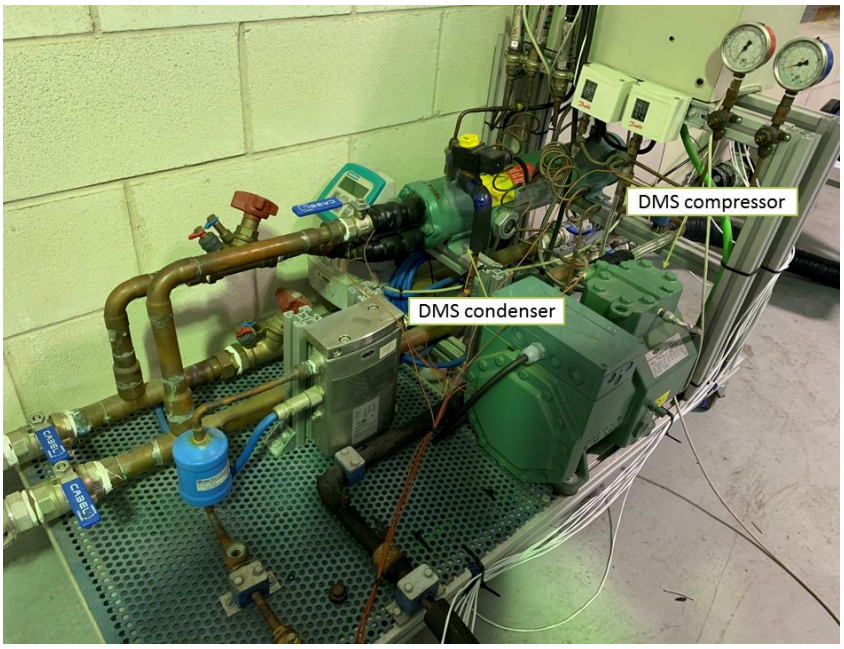

Figure 7.3. Experimental DMS cycle.

The subcooler is also the evaporator of the DMS cycle. The dedicated cycle performs the subcooling of the CO_2 and works with R-152a. Its compressor is a variable speed

semihermetic compressor with displacement of 4.06 $m^3 \cdot h^{-1}$ at 1450 rpm and nominal power of 0.7 kW. It is necessary to have a variable speed compressor in order to vary the subcooling degree. The achieved subcooling is directly related to the compressor speed, and as it has been seen in previous theoretical results (Nebot-Andrés et al., 2017), it exists an optimum subcooling degree for which the COP is maximum and it is different for each working conditions so it is necessary to have a variable speed compressor in order to better adapt to each condition.

The expansion valve of the DMS cycle is electronic, working as thermostatic and the condenser is shell-and-tube heat exchanger also used liquid recipient.

R-152a has been chosen as the refrigerant for the DMS cycle because as it has been studied by Llopis et al. (2015a), the refrigerant used in the DMS cycle has a very little influence on the overall COP as long as the COP of the auxiliary cycle is higher than the COP of the CO_2 cycle. R-152a is one of the possible refrigerants that can be used in the compressor of the plant, it is ozone-friendly, has excellent thermodynamic efficiency, and has a very low global warming potential (GWP=124), therefore it was an interesting refrigerant for this application.

Heat dissipation in gas-cooler and in DMS condenser is done with a water loop, simulating the heat rejection level. The evaporator is supplied with another loop, working with a propylene glycol–water mixture (60% by volume) that enables a constant entering temperature in the evaporator. Both the mass flow and the inlet temperature are controlled in these loops.

7.2.2. Measurement system

The measurement system of the experimental plant is presented in Figure 7.1. 22 T-type thermocouples are used to measure the temperatures of the CO_2, the R-152a and the secondary fluids. The thermocouples placed at the evaporator, the exit of gas-cooler and the exit of subcooler are immersion thermocouples. 8 pressure gauges are installed along all the CO_2 circuit and 4 are placed on the DMS cycle.

Refrigerant mass flow rates are measured by two Coriolis mass flow meters, as well as dissipation glycol flow in the evaporator. The flow of the dissipation water is measured by two magnetic volumetric flow meters to measure the flow arriving to the gas-cooler and to the DMS condenser. Compressors' power consumptions are measured by two digital wattmeters. The accuracies of the measurement devices are presented in Table 7.1.

Table 7.1. Accuracies and calibration range of the measurement devices.

Measured variable	Measurement device	nº of devices	Range	Calibrated accuracy
Temperature (ºC)	T-type thermocouple	22	-40.0 to 145.0	±0.5K
CO_2 pressure (bar)	Pressure gauge	4	0.0 to 160.0	±0.6% of span
CO_2 pressure (bar)	Pressure gauge	1	0.0 to 100.0	±0.6% of span
CO_2 pressure (bar)	Pressure gauge	3	0.0 to 60.0	±0.6% of span
DMS pressure (bar)	Pressure gauge	2	0.0 to 16.0	±0.6% of span
DMS pressure (bar)	Pressure gauge	2	0.0 to 40.0	±0.6% of span
CO_2 main mass flow rate ($kg \cdot s^{-1}$)	Coriolis mass flow meter	1	0.00 to 1.38	±0.1% of reading
DMS mass flow rate ($kg \cdot s^{-1}$)	Coriolis mass flow meter	1	0.00 to 0.05	±0.1% of reading
Water mass flow rate ($m^3 \cdot h^{-1}$)	Magnetic flow meter	2	0.0 to 5.0	±0.3% of rate
Glycol volume flow rate ($kg \cdot s^{-1}$)	Coriolis mass flow meter	1	0.0 to 13.88	±0.1% of reading
Power consumption (kW)	Digital wattemeter	2	0.0 to 6.0	±0.5% of reading

7.3. Experimental tests

The strategy for conducting the experimental tests in order to determine the optimum conditions where the COP of the cycle is maximum is presented in this section.

7.3.1. Test procedure

To evaluate the refrigeration plant using a DMS working with R-152a, the system has been tested at different environment conditions always over the transcritical point. The evaluated conditions were:

- Heat rejection level: three different temperatures: 25.0, 30.4 and 35.1°C, with maximum deviation of ±0.2°C. The heat rejection level was performed fixing the temperature of the secondary fluid (water) at the entrance of the gas-cooler and the DMS condenser and maintaining the water flow rate to 1.15 $m^3 \cdot h^{-1}$ in gas-cooler and 0.62 $m^3 \cdot h^{-1}$ in the DMS condenser.

- Three different inlet temperature of the secondary fluid in the evaporator. The secondary fluid is a mixture propylene glycol-water (60% by volume) and the

evaluated temperatures were -1.3, 3.8 and 10.1 ±0.2°C. The flow rate was fixed to 0.7 $m^3 \cdot h^{-1}$.

- Gas-cooler pressure was regulated with an electronic BP fixed during each test thanks to a PID controller. Each test was performed at different pressures in order to identify the optimum one and reach the optimum COP conditions.

- The main compressor always operated at nominal speed of 1450 rpm. The speed of the DMS compressor was varied in order to change the subcooling degree.

- The electronic expansion valves were set to obtain a superheating degree in the evaporator of 10K and of 5K on the DMS evaporator.

All the tests were carried out in steady state conditions for periods longer than 10 minutes, taking data each 5 seconds, obtaining the test point as the average value of the whole test. The measured data were used to calculate the thermodynamic properties of the points using Refprop v.9.1. (Lemmon et al., 2013).

7.3.2. Test range

All the tests performed in order to obtain the maximum COP of each condition are summed up in Table 7.2, including the number of tests performed in each of the evaluated conditions. The range of values evaluated for the subcooling degree, the gas-cooler pressure and the main energy parameters for each test are also detailed on it.

Table 7.2. Experimental tests and range of tested conditions.

$t_{w,in}$ (ºC)	$t_{g,in}$ (ºC)	number of tests	SUB (K)	p_{gc} (bar)	COP (-)	Q_0 (kW)
25.0	-1.3	11	12.4-19.3	74.9-85.0	1.74-1.97	7.2-7.4
	3.8	8	8.1-15.8	74.9-75.9	2.19-2.24	8.2-8.7
	10.1	7	10.3-11.1	74.9-75.5	2.52-2.54	9.8-9.9
30.4	-1.3	20	9.7-16.1	76.8-82.9	1.64-1.74	6.6-7.0
	3.8	7	11.4-14.1	78.9-81.8	1.91-1.95	7.7-8.0
	10.1	17	6.1-13.9	79.9-84.4	2.09-2.16	8.6-9.3
35.1	-1.3	20	3.2-20.0	79.9-93.8	1.35-1.53	5.5-6.7
	3.8	25	8.5-15.8	83.9-93.9	1.60-1.71	7.2-7.7
	10.1	19	7.3-13.1	84.9-91.9	1.81-1.88	8.4-8.9

7.4. Optimization of the plant

In CO_2 transcritical refrigeration cycles, COP is function of the gas-cooler pressure and also of the subcooling degree (Llopis et al., 2018), existing an optimal gas-cooler pressure and subcooling degree where the COP is maximum. Gas-cooler pressure can be regulated by the BP valve and the subcooling degree is modified by adjusting the DMS compressor speed. The subcooling degree is the difference between the temperature at the exit of the gas-cooler and the temperature at the exit of the subcooler as shown in Eq.(7.1).

$$SUB = t_{gc,o} - t_{sub,o} \tag{7.1}$$

Tests were carried out in order to demonstrate the existence of this optimum, identify it, and determine the optimal gas-cooler pressure and subcooling degree needed to obtain the maximum COP for each condition. Then, the behaviour of the plant at optimum conditions is evaluated.

Cooling capacity is calculated as the product of the mass flow rate through the evaporator ($\dot{m}_{co2}$) and the enthalpy difference in evaporator, as shown in Eq. (7.2). The enthalpy at the evaporator inlet ($h_{0,o}$) is considered to be the same as the enthalpy at the inlet of the back-pressure valve. The COP of the system is calculated as the ratio between the cooling capacity and the sum of the power consumption of two compressors, as established in Eq. (6.3).

$$\dot{Q}_0 = \dot{m}_{co2} \cdot \left(h_{0,o} - h_{exp}\right) \tag{7.2}$$

$$COP = \frac{\dot{Q}_0}{P_{C,main} + P_{C,DMS}} \tag{7.3}$$

7.4.1. Experimental COP identification

Tests have been performed at external fixed conditions and modifying pressure and subcooling values following a method similar to a Simplex algorithm to reach the maximum COP. After evaluating one point, another test was done changing the value of gas-cooler pressure or compressor velocity. When three initial points were available, a colour map of the COP is represented, showing the tendency to follow to reach the maximum COP. Depending on the obtained values, pressure or subcooling were increased or decreased following the trend of the previous points, in order to get closer and closer to the maximum. The process ended when the increments achieved between the new value and the previous one were less than 1%.

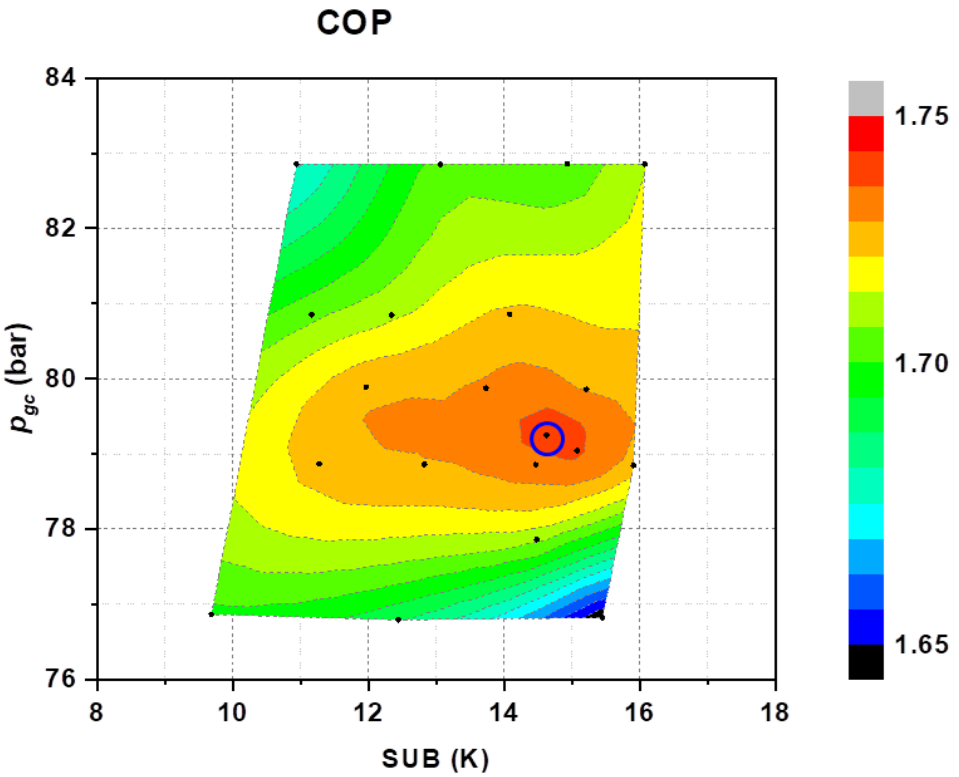

Figure 7.4. Experimental COP for $t_{w,in}$ = 30.4ºC and $t_{g,in}$ = -1.3ºC

The measured COP for the tested condition of $t_{w,in}$ = 30.4ºC and $t_{g,in}$ = -1.3ºC is shown in Figure 7.4. The COP is presented as a function of the gas-cooler pressure and subcooling degree. It can be seen the existence of a maximum COP, marked in blue, for a determined value of gas-cooler pressure and subcooling degree. Changing the pressure or the DMS compressor velocity will always decrease the value of the COP with respect to this optimum point. Reducing or increasing pressure or subcooling degree will always reduce the obtained value of COP. It can also be seen that the gas-cooler pressure has higher influence on the COP than the subcooling degree. COP is more affected by increasing or decreasing pressure than by changing the subcooling.

7.4.2. Experimental analysis of the cooling capacity

Cooling capacity is totally related to the degree of subcooling. When higher the subcooling is, higher the capacity of the overall cycle is. This phenomenon can be observed in Figure 7.5, where the cooling capacity is represented as a function of the gas-cooler pressure and subcooling degree for the condition of $t_{w,in}$ = 30.4ºC and $t_{g,in}$ = -1.3ºC. Because of that, the point where the COP is maximum does not correspond to

the highest cooling capacity, but the difference is not remarkable. Varying the DMS compressor speed, the cooling capacity can be regulated without having important decrements in COP as it has been stated in the previous sub-section.

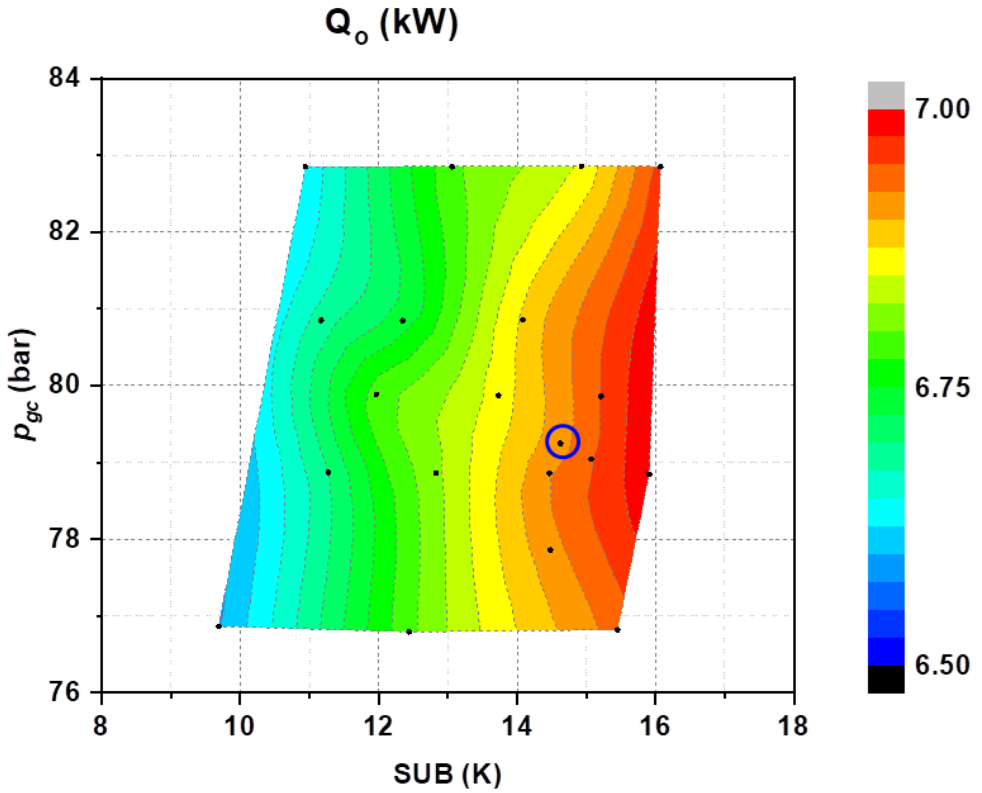

Figure 7.5. Experimental cooling capacity for $t_{w,in}$ = 30.4ºC and $t_{g,in}$ = -1.3ºC.

7.5. Experimental results at optimum conditions

The results presented in this section correspond to the tests where the COP is maximum for each evaluated condition. The main results are summed up in Table 7.3. The main temperatures, the cooling capacity, optimum COP and power consumption of the compressors are presented, as well as the uncertainty and the energy balances for data validation. The COP, cooling capacity and working conditions are discussed in the following subsections.

Figure 7.6 shows the working cycle of two of the experimental tests, corresponding to gas-cooler outlet temperature of 30.4ºC and $t_{g,in}$=-1.3ºC in blue (E2) and $t_{g,in}$=10.0ºC in red (E8), where the subcooling effect can be observed between points 3 and 4.

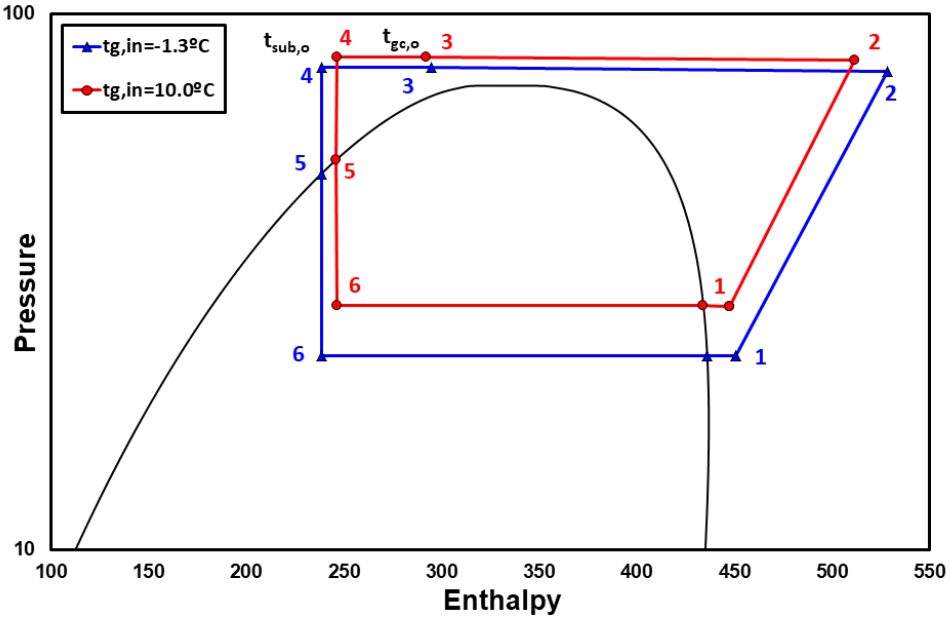

Figure 7.6. Ph Diagram of the tests $t_{gc,o}$=30.4ºC and $t_{g,in}$=-1.3ºC (blue) and $t_{g,in}$=10.0ºC (red).

The main energy parameters studied in this work are cooling capacity defined by Eq. (7.2) and COP presented in Eq.(7.3). The uncertainty of these main parameters has been calculated using Moffat's method (Moffat, 1985) and the measurement devices' accuracies, presented in Table 7.1. The average measured uncertainty is ±0.83% in $\dot{Q}_0$ and ±0.94% in COP with maximum uncertainty of ±0.94% and ±1.04% respectively. The uncertainty ε(COP) and ε(Q_0) of all the results presented in this work is compiled in Table 7.3. To ensure correct measurement of the parameters in the cycle, the energy balances in evaporator, gas-cooler, subcooler and DMS condenser have been calculated taking into account the capacity transmitted on the CO_2 side and on the secondary fluid.

Eq. (7.4) is the heat transfer at the side of the glycol. Eq. (7.5) quantifies the discrepancy between the heat transfer of the glycol and the cooling capacity on the evaporator.

$$\dot{Q}_g = \dot{V}_g \cdot \rho_g \cdot Cp_g \cdot (t_{g,in} - t_{g,o}) \tag{7.4}$$

$$\Delta\dot{Q}_{evap} = \frac{\dot{Q}_0 - \dot{Q}_g}{\dot{Q}_0} \cdot 100 \tag{7.5}$$

Eq. (7.6) corresponds to the heat transfer of the CO_2 in the gas-cooler and Eq. (7.7) in the water side. The difference between the heat transfers of each of the fluids is calculated as Eq. (7.8).

$$\dot{Q}_{gc} = \dot{m}_{co2} \cdot (h_{gc,in} - h_{gc,o}) \tag{7.6}$$

$$\dot{Q}_{w,gc} = \dot{V}_{w,gc} \cdot \rho_w \cdot C_{p,w} \cdot (t_{w,in,DMS} - t_{w,o,DMS}) \tag{7.7}$$

$$\Delta\dot{Q}_{gc} = \frac{\dot{Q}_{gc} - \dot{Q}_{w,gc}}{\dot{Q}_{gc}} \cdot 100 \tag{7.8}$$

The capacity of the subcooler is calculated as Eq. (7.9) for the side corresponding to the CO_2 subcooled and Eq. (7.10) corresponds to the cooling capacity of the subcooler for the R-152a. The heat transfer difference between both sides of the subcooler is calculated as Eq. (7.11).

$$\dot{Q}_{sub} = \dot{m}_{co2} \cdot (h_{gc,o} - h_{sub,o}) \tag{7.9}$$

$$\dot{Q}_{0,DMS} = \dot{m}_{DMS} \cdot (h_{exp,DMS} - h_{0,o,DMS}) \tag{7.10}$$

$$\Delta\dot{Q}_{sub} = \frac{\dot{Q}_{0,DMS} - \dot{Q}_{sub}}{\dot{Q}_{0,DMS}} \cdot 100 \tag{7.11}$$

The heat transfer on the DMS condenser is calculated as Eq. (7.12) for the side corresponding to the R-152a and the heat transfer on the water side is calculated by Eq. (7.13). The heat transfer difference between both sides of the DMS condenser is calculated as Eq. (7.14).

$$\dot{Q}_{k,DMS} = \dot{m}_{R-152a} \cdot (h_{k,in,DMS} - h_{k,o,DMS}) \tag{7.12}$$

$$\dot{Q}_{w,DMS} = \dot{V}_{w,DMS} \cdot \rho_w \cdot C_{p,w} \cdot (t_{w,in,DMS} - t_{w,o,DMS}) \tag{7.13}$$

$$\Delta\dot{Q}_{k,DMS} = \frac{\dot{Q}_{k,DMS} - \dot{Q}_{w,DMS}}{\dot{Q}_{k,DMS}} \cdot 100 \tag{7.14}$$

These balance differences are presented in Table 7.3. As it can be seen, the differences are quite small: 2.7% at evaporator in average, 3.1% at gas-cooler, 2.4% at subcooler and 4.9% at the DMS condenser. In tests number E1 the discrepancies are greater than 5%. This is because the gas-cooler pressure is near the critical pressure and there is partial condensation so the temperature at the exit of the gas-cooler implies large uncertainty in enthalpy computation.

7.5.1. Maximum COP

The evolution of the optimum COP for all the evaluated conditions is presented in Figure 7.7. It can be seen that it depends on the glycol and the water inlet temperatures. For all the glycol levels, it can be perceived that the COP is lower when lower the glycol inlet temperature is, so when lower the evaporation level is. It can also be noticed that the COP is lower when higher the water inlet temperature is. This temperature corresponds to the heat rejection level, so lower COPs are obtained when higher is the heat rejection temperature. The measured values go from 1.51 to 1.95 for $t_{g,in}$ = -1.3ºC, from 1.69 to 2.21 for $t_{g,in}$ = 3.8ºC and from 1.86 to 2.52 for $t_{g,in}$ = 10.0ºC.

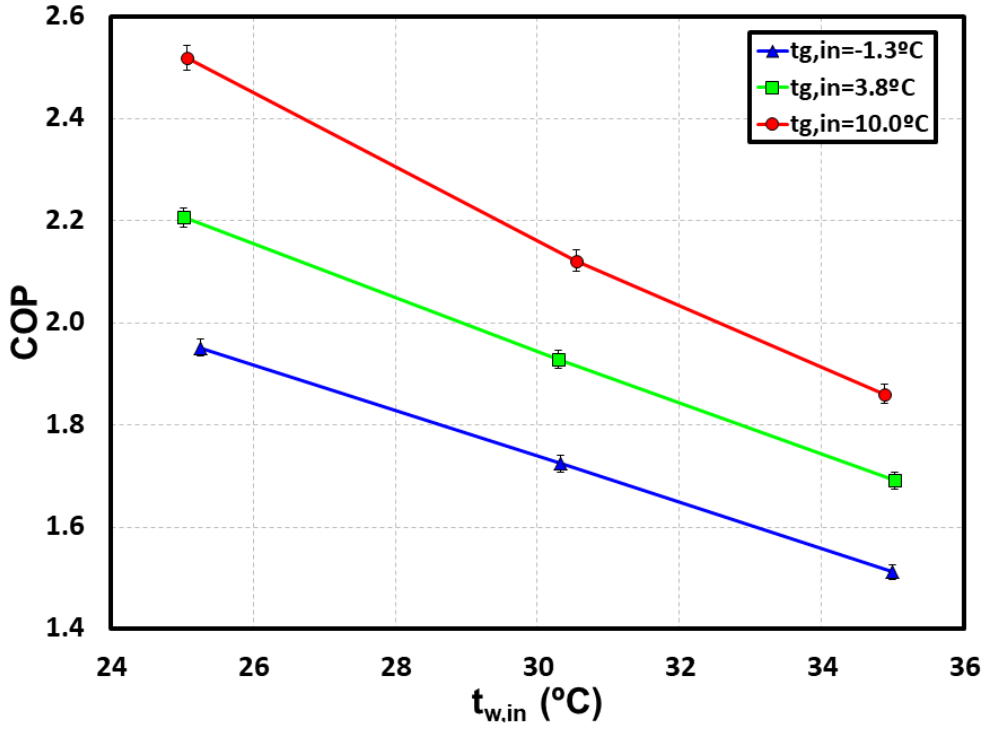

Figure 7.7. Evolution of the maximum COP for optimal conditions depending on the water inlet temperature.

7.5.2. Cooling capacity

Figure 7.8 shows the cooling capacity obtained for the conditions where the COP is maximum. It depends on the heat rejection temperature, being reduced when the water inlet temperature increases. Likewise, it is clearly observed how the capacity is greater when higher the evaporation level is.

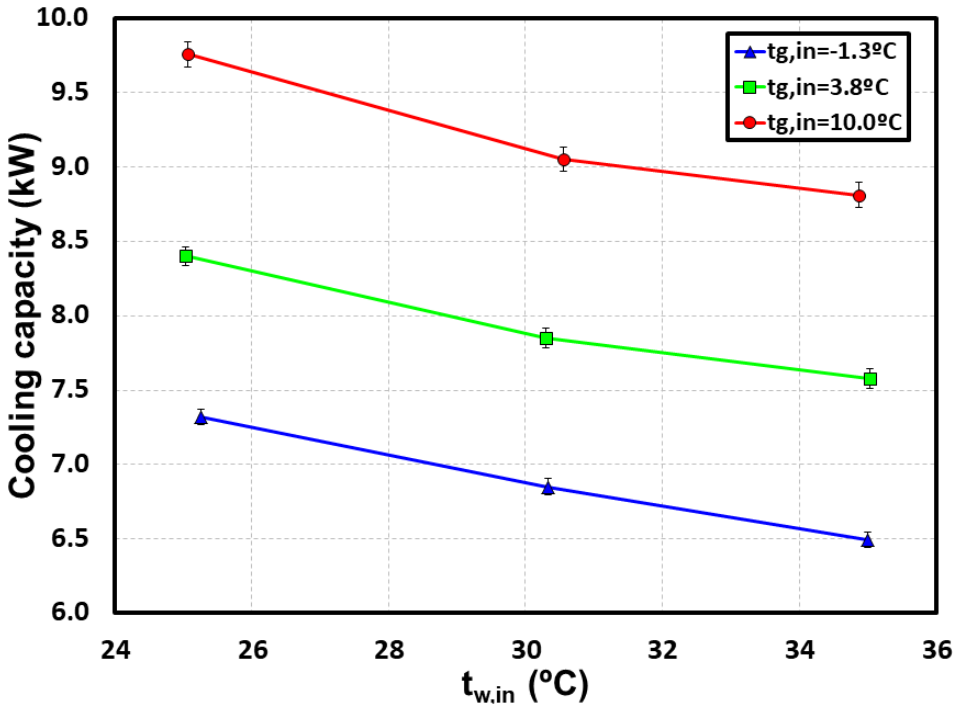

Figure 7.8. Evolution of the cooling capacity for optimal conditions depending on the water inlet temperature.

The measured values go from 6.5 kW to 7.3 kW for $t_{g,in}$ = -1.3ºC, from 7.6 kW to 8.4 kW for $t_{g,in}$ = 3.8ºC and from 8.8 kW to 9.8 kW for $t_{g,in}$ = 10.0ºC.

Cooling capacity increases when the evaporation level is higher because at higher evaporation levels, the compression ratio is lower and there is an increase of the evaporator mass flow rate due to the higher density at compressor inlet and higher volumetric efficiency, leading to a higher cooling capacity.

By adding the subcooling system, the cooling capacity of the plant is increased, as it is described in the previous section. Thus, cooling capacity can be divided into two terms, the cooling capacity that the simple CO_2 cycle would give under the studied conditions and the capacity provided by the DMS. Cooling capacity can be calculated as shown in Eq.(7.15), where the two terms are clearly separated. The first term corresponds to the cooling capacity if there was not subcooling ($\dot{Q}_{base}$) and the second corresponds to the contribution generated by the DMS cycle. So the cooling capacity of the system can be defined as the sum of both terms, as shown by Eq.(7.16), the capacity of the base

system without subcooling and the subcooler cooling capacity, Eq.(7.17), directly related to the subcooling degree.

$$\dot{Q}_0 = \dot{m}_{co2} \cdot \left(h_{0,o} - h_{gc,o}\right) + \dot{m}_{co2} \cdot \Delta h_{sub} \quad (7.15)$$

$$\dot{Q}_0 = \dot{Q}_{base} + \dot{m}_{co2} \cdot \Delta h_{sub} \quad (7.16)$$

$$\dot{Q}_{sub,add} = \dot{m}_{co2} \cdot \Delta h_{sub} \quad (7.17)$$

Figure 7.9 shows the cooling capacity divided into the cooling capacity of the cycle without subcooling and subcooler cooling capacity.

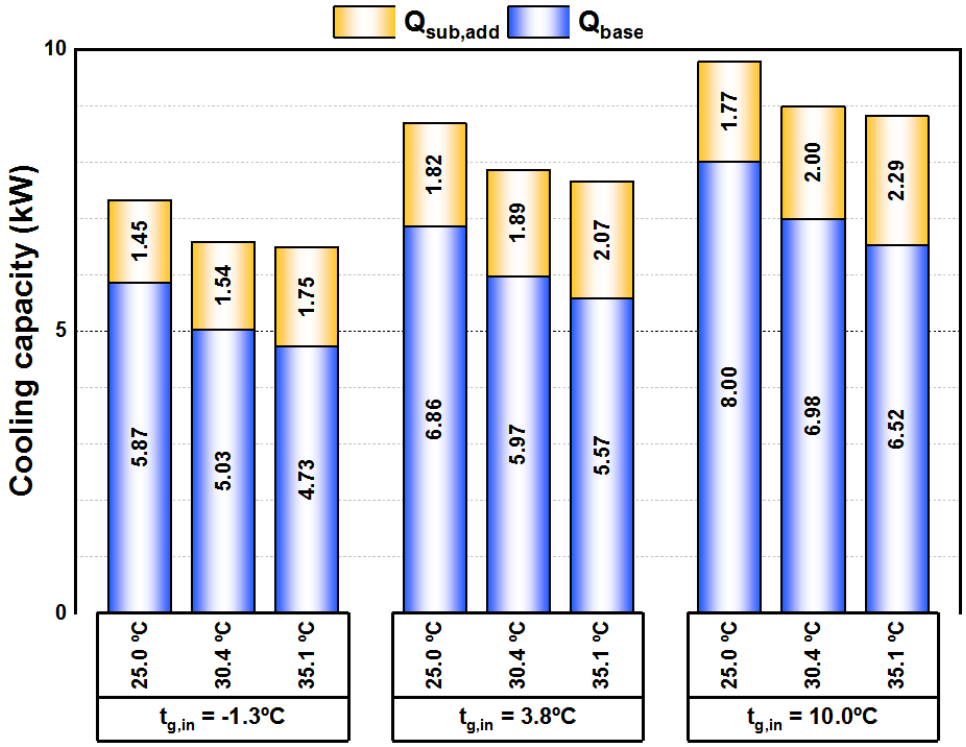

Figure 7.9. Cooling capacity broken down into base capacity and subcooler contribution.

The cooling capacity of the DMS is between 1.45 kW and 2.29 kW for all the studied cases, corresponding to less than the third part of the total cooling capacity. It can be observed that the contribution of the DMS is higher when lower the evaporation level is and also higher when higher the water inlet temperature is. The biggest contribution as a proportion of the total cooling capacity is for of $t_{w,in}$ = 35.1ºC and $T_{g,in}$ =-1.3ºC, where it represents a 27.2%, because this is the condition where further the heat source and hot sink are and a higher improvement is needed.

7.5.3. Optimum pressure

The optimum gas-cooler pressures are presented in Figure 7.10. It can be observed that for the three inlet glycol temperatures, the evolution of the pressure follows the same trend and also it practically does not depend on the inlet temperature at the evaporator. However, it is clearly correlated with the heat rejection level, being it higher when higher the water inlet temperature is.

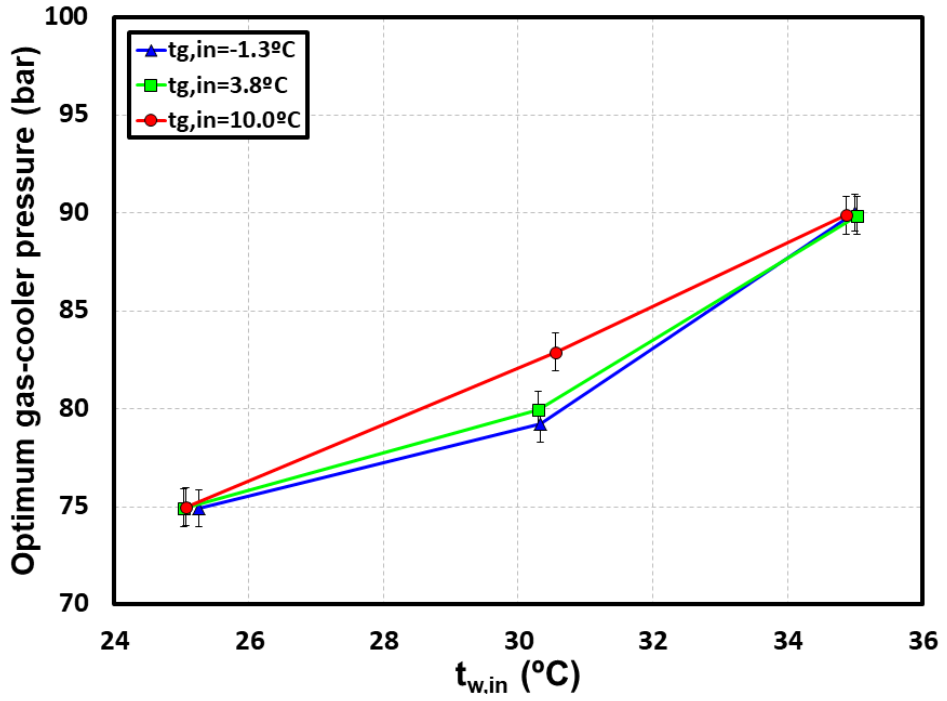

Figure 7.10. Optimum working pressure for the tested conditions.

There is a small difference for the glycol level of 10.0ºC and water inlet temperature of 30.4ºC, where the measured pressure is slightly higher from that of the other glycol conditions. This difference is practically within the limits of the measurement uncertainty. Despite this, we can affirm that the optimum pressure is only a function of the heat rejection level and it does not depend on the glycol inlet temperature.

7.5.4. Optimum subcooling degree

Figure 7.11 presents the optimal subcooling degree for the evaluated conditions. It can be seen that for high heat rejection levels, the subcooling needed is higher. In addition, the subcooling degree is higher when lower the glycol inlet temperature is. This fact is due to the lower efficiency of CO_2 at high temperatures, being these levels where it is most necessary to improve their behaviour. Besides, we also observe that for low levels

of evaporation we need more subcooling because the COP is lower at these conditions, needing more improvement (Nebot-Andrés et al., 2017).

Analysing the subcooling at 30.4ºC of water temperature, we can observe a slight change in the trend. This change in trend in the evolution of the optimal subcooling degree may be because the gas-cooler outlet is near the pseudocritical zone, where CO_2 present abrupt changes in its thermophysical properties. Also, this effect was observed in the experimental study of the transcritical CO_2 cycle with integrated mechanical subcooling (Nebot-Andrés et al., 2020) and in the previous theoretical studies (Nebot-Andrés et al., 2019; Nebot-Andrés et al., 2017).

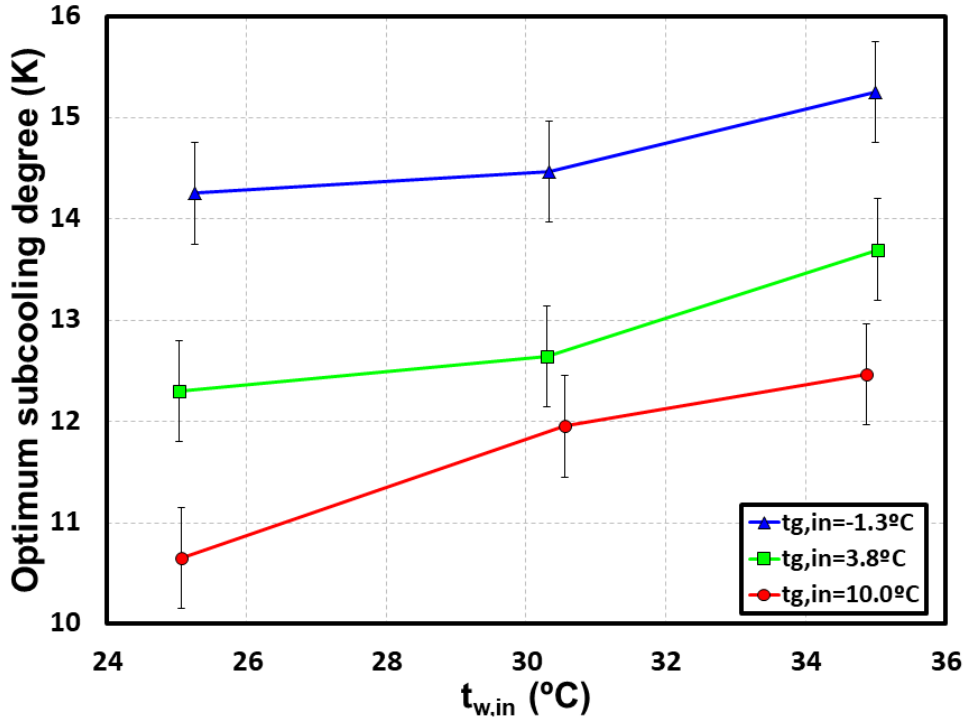

Figure 7.11.Evolution of the optimum subcooling degree for the tested conditions.

7.5.5. Correlations

The experimental tests of this study have permitted to determine the optimum conditions to operate a CO_2 transcritical refrigeration plant with DMS in order to reach maximum efficiency. In order to generalize the results, this section presents two correlations to determine the optimum pressure and subcooling. These correlations are

function of the evaporating level of the CO_2 plant and the gas-cooler outlet temperature, to make the parametrization more general.

Both correlations are obtained by adjusting the experimental values by an adjustment of least-squares.

7.5.5.1. Optimum pressure

The optimum gas-cooler pressure is presented by Eq.(7.18) and it defines the optimum pressure as a function of the gas-cooler outlet temperature and the evaporation temperature.

$$p_{gc} = 184.6 + 0.6872 \cdot t_0 - 8.18 \cdot t_{gc,o} - 0.02203 \cdot t_0 \cdot t_{gc,o} + 0.1543 \cdot t_{gc,o}^2 \quad (7.18)$$

The range of application of this correlation is for temperatures of gas-cooler exit between 26.0ºC and 36.0ºC and evaporation temperatures between -15.5ºC and -5.9ºC. The average error of this correlation is ±0.6 bar and the maximum error ±1.5 bar.

7.5.5.2. Optimum subcooling degree

The optimum subcooling degree is defined by the Eq.(7.19) shows as a function of the evaporation temperature and the gas-cooler outlet temperature. This correlation shows the optimum subcooling degree needed to obtain the maximum COP when working at the optimum pressure for a CO_2 cycle with dedicated mechanical subcooling.

$$SUB = 1.632 + 0.2244 \cdot t_{gc,o} - 0.4012 \cdot t_o \quad (7.19)$$

The range of application of this correlation is for temperatures of gas-cooler exit between 26.0ºC and 36.0ºC and for evaporating levels between -15.5ºC and -5.9ºC. The average error of this correlation is ±0.3K and the maximum error ±0.7K.

7.6. Conclusions

This paper presents for the first time the experimental optimization of a CO_2 transcritical refrigeration plant with a R-152a dedicated mechanical subcooling. The evaluation covered the heat rejection levels of 25.0ºC, 30.4ºC and 35.1ºC and the cold source temperatures of -1.3ºC, 3.8ºC and 10.0ºC at steady-state conditions. The plant was tested with the main compressor running at nominal speed and the DMS compressor working at different speeds, in order to modify the subcooling degree. The reliability of the measurements has been verified by calculating the energy balances in all the heat exchangers of the plant.

The main conclusions of this study are:

- The experimental tests permit to demonstrate the existence of a maximum COP for this type of CO_2 plant with subcooling, related to the gas-cooler pressure and subcooling degree.

- In all the tests, the optimum conditions have been identified, evaluating COP and cooling capacity of the system. Regarding cooling capacity, the measured values go from 6.5 kW to 7.3 kW for $t_{g,in}$ = -1.3ºC, from 7.6 kW to 8.4 kW for $t_{g,in}$ = 3.8ºC and from 8.8 kW to 9.8 kW for $t_{g,in}$ = 10.0ºC. Optimum COP go from 1.51 to 1.95 for $t_{g,in}$= -1.3ºC, from 1.69 to 2.21 for $t_{g,in}$ = 3.8ºC and from 1.86 to 2.52 for $t_{g,in}$ = 10.0ºC.

- The parameters that must be optimized, gas-cooler pressure and subcooling degree, have been determined and studied to obtain two general correlations that define the optimum parameters needed to optimize the COP.

- The optimum gas-cooler pressure has a higher dependence on the heat rejection level, being higher when higher the heat rejection level is, but it slightly depends on the evaporation level.

- The optimum subcooling degree is both dependent on the water inlet temperature and on the glycol inlet temperature.

Further future research is needed to analyze deeper the behavior of the system and to be able to quantify the improvements achieved thanks to the use of the DMS cycle.

7.7. Acknowledgements

The authors thank the Ministerio de Educación, Cultura y Deporte (Spain) grant FPU16/00151; the Ministerio de Ciencia y Tecnología (Spain) project RTI2018-093501-B-C21, and the Jaume I University (Spain), project UJI-B2019-56 for financing this research work. Authors also thank Gabriele Toffoletti from Udine University for his help in performing the experimental tests.

7.8. Nomenclature

BP back-pressure valve

COP coefficient of performance

Cp specific heat capacity, $kJ \cdot kg^{-1} \cdot K^{-1}$

EXV electronic expansion valve

h	specific enthalpy, $kJ \cdot kg^{-1}$
m	mass flow $kg \cdot s^{-1}$
p	absolute pressure, bar
Pc	power consumption, kW
Q	cooling capacity, kW
SUB	degree of subcooling produced in the subcooler, K
t	temperature, ºC
V	volumetric flow, $m^3 \cdot s^-$

Greek symbols

ρ	density, $kg \cdot m^{-3}$
ε	uncertanity

Subscripts

add	addition
base	referring to the CO_2 cycle without subcooling
dis	compressor discharge
DMS	corresponding to the DMS cycle
evap	referring to the evaporator
exp	expansion
g	glycol
gc	gas-cooler
k	referring to the condenser
in	inlet
main	corresponding to the main cycle
0	evaporating level

o	outlet
R-152a	refrigerant R-152a
sub	corresponding to the subcooler
w	water

7.9. References

Montreal Protocol on Substances That Deplete the Ozone Layer, 1987. United Nations (UN), New York, NY, USA (1987 with subsequent amendments). .

Beshr, M., Bush, J., Aute, V., Radermacher, R., 2016. Steady state testing and modeling of a CO2 two-stage refrigeration system with mechanical subcooler, Refrigeration Science and Technology, pp. 893-900.

Bush, J., Beshr, M., Aute, V., Radermacher, R., 2017. Experimental evaluation of transcritical CO2 refrigeration with mechanical subcooling. Science and Technology for the Built Environment 23, 1013-1025.

Cao, F., Cui, C., Wei, X., Yin, X., Li, M., Wang, X., 2019. The experimental investigation on a novel transcritical CO2 heat pump combined system for space heating. International Journal of Refrigeration 106, 539-548.

Catalán-Gil, J., Llopis, R., Sánchez, D., Nebot-Andrés, L., Cabello, R., 2019. Energy analysis of dedicated and integrated mechanical subcooled CO2 boosters for supermarket applications. International Journal of Refrigeration.

Chesi, A., Esposito, F., Ferrara, G., Ferrari, L., 2014. Experimental analysis of R744 parallel compression cycle. Applied Energy 135, 274-285.

Dai, B., Liu, S., Li, H., Sun, Z., Song, M., Yang, Q., Ma, Y., 2018. Energetic performance of transcritical CO2 refrigeration cycles with mechanical subcooling using zeotropic mixture as refrigerant. Energy 150, 205-221.

Dai, B., Liu, S., Sun, Z., Ma, Y., 2017. Thermodynamic Performance Analysis of CO2 Transcritical Refrigeration Cycle Assisted with Mechanical Subcooling, Energy Procedia, pp. 2033-2038.

Dai, B., Zhao, X., Liu, S., Yang, Q., Zhong, D., Hao, Y., Hao, Y., 2020. Energetic, exergetic and exergoeconomic assessment of transcritical CO2 reversible system combined with dedicated mechanical subcooling (DMS) for residential heating and cooling. Energy Conversion and Management 209.

European Commission, 2014. Regulation (EU) No 517/2014 of the European Parliament and of the Council of 16 April 2014 on fluorinated greenhouse gases and repealing Regulation (EC) No 842/2006.

Gullo, P., Hafner, A., Banasiak, K., Minetto, S., Kriezi, E.E., 2019. Multi-ejector concept: A comprehensive review on its latest technological developments. Energies 12.

Hafner A., Hemmingsen A. K. T., Ven A. van de, 2014. R744 refrigeration system configurations for supermarkets in warm climates, 3rd IIR International Conference

on Sustainability and the Cold Chain. Proceedings. International Institute of Refrigeration, London, UK.

Karampour, M., Sawalha, S., 2016a. Integration of heating and air conditioning into a CO2 trans-critical booster system with parallel compression Part I: Evaluation of key operating parameters using field measurements, Refrigeration Science and Technology, pp. 323-331.

Karampour, M., Sawalha, S., 2016b. Integration of heating and air conditioning into a CO2 trans-critical booster system with parallel compression part II: Performance analysis based on field measurements, Refrigeration Science and Technology, pp. 332-340.

Lawrence, N., Elbel, S., 2019. Experimental investigation on control methods and strategies for off-design operation of the transcritical R744 two-phase ejector cycle. International Journal of Refrigeration.

Lemmon, E.W., Huber, M.L., McLinden, M.O., 2013. REFPROP, NIST Standard Reference Database 23, v.9.1. National Institute of Standards, Gaithersburg, MD, U.S.A.

Llopis, R., Cabello, R., Sánchez, D., Torrella, E., 2015a. Energy improvements of CO2 transcritical refrigeration cycles using dedicated mechanical subcooling. International Journal of Refrigeration 55, 129-141.

Llopis, R., Nebot-Andrés, L., Cabello, R., Sánchez, D., Catalán-Gil, J., 2016. Experimental evaluation of a CO2 transcritical refrigeration plant with dedicated mechanical subcooling. International Journal of Refrigeration 69, 361-368.

Llopis, R., Nebot-Andrés, L., Sánchez, D., Catalán-Gil, J., Cabello, R., 2018. Subcooling methods for CO2 refrigeration cycles: A review. International Journal of Refrigeration 93, 85-107.

Llopis, R., Sanz-Kock, C., Cabello, R., Sánchez, D., Torrella, E., 2015b. Experimental evaluation of an internal heat exchanger in a CO2 subcritical refrigeration cycle with gas-cooler. Applied Thermal Engineering 80, 31-41.

Moffat, R.J., 1985. Using Uncertainty Analysis in the Planning of an Experiment. Journal of Fluids Engineering 107, 173-178.

Nebot-Andrés, L., Calleja-Anta, D., Sánchez, D., Cabello, R., Llopis, R., 2019. Thermodynamic analysis of a CO2 refrigeration cycle with integrated mechanical subcooling. Energies 13.

Nebot-Andrés, L., Catalán-Gil, J., Sánchez, D., Calleja-Anta, D., Cabello, R., Llopis, R., 2020. Experimental determination of the optimum working conditions of a transcritical CO2 refrigeration plant with integrated mechanical subcooling. International Journal of Refrigeration 113, 266-275.

Nebot-Andrés, L., Llopis, R., Catalán-Gil, J., Sánchez, D., Cabello, R., 2018. Energy evaluation of the mechanical subcooling impact on a CO2 DX-system in a commercial MT cabinet, Refrigeration Science and Technology, pp. 173-181.

Nebot-Andrés, L., Llopis, R., Sánchez, D., Catalán-Gil, J., Cabello, R., 2017. CO2 with mechanical subcooling vs. CO2 cascade cycles for medium temperature commercial refrigeration applications thermodynamic analysis. Applied Sciences (Switzerland) 7.

Sánchez, D., Catalán-Gil, J., Cabello, R., Calleja-Anta, D., Llopis, R., Nebot-Andrés, L., 2020. Experimental Analysis and Optimization of an R744 Transcritical Cycle Working with a Mechanical Subcooling System. Energies 13, 3204.

Sarkar, J., Agrawal, N., 2010. Performance optimization of transcritical CO2 cycle with parallel compression economization. International Journal of Thermal Sciences 49, 838-843.

Song, Y., Cao, F., 2018. The evaluation of the optimal medium temperature in a space heating used transcritical air-source CO2 heat pump with an R134a subcooling device. Energy Conversion and Management 166, 409-423.

Song, Y., Li, D., Cao, F., Wang, X., 2017. Investigation of the optimal intermediate water temperature in a combined r134a and transcritical CO2 heat pump for space heating. International Journal of Refrigeration 79, 10-24.

Song, Y., Ye, Z., Wang, Y., Cao, F., 2018. The experimental verification on the optimal discharge pressure in a subcooler-based transcritical CO2 system for space heating. Energy and Buildings 158, 1442-1449.

UNEP/TEAP, 1999. The implications to the Montreal Protocol of the inclusion of HFCs and PFCs in the Kyoto Protocol, United States.

United Nations, 1997. The Kyoto Protocol to the Framework Convention on Climate Change. 1997. Available at: <http://unfccc.int/essential_background/kyoto_protocol/background/items/1351.php >.

Yu, B., Yang, J., Wang, D., Shi, J., Chen, J., 2019. An updated review of recent advances on modified technologies in transcritical CO2 refrigeration cycle. Energy 189, 116147.

Table 7.3. Main experimental results and uncertainty measurements.

	$t_{g,in}$	t_0	$t_{w,in}$	$p_{gc,o}$	$t_{gc,o}$	SUB	m_{CO2}	Pc_{main}	Pc_{dms}	Q_0	$\varepsilon(Q_0)$	$\varepsilon(Q_0)$	COP	ε(COP)	ε(COP)	ΔQ_{evap}	ΔQ_{gc}	ΔQ_{sub}	$\Delta Q_{h,dms}$
	(ºC)	(ºC)	(ºC)	(bar)	(ºC)	(ºC)	($kg \cdot s^{-1}$)	(kW)	(kW)	(kW)	(kW)	(%)	(-)	(-)	(%)	(%)	(%)	(%)	(%)
E1	-1.2	-15.5	25.3	74.9	26.0	14.3	0.03	3.37	0.38	7.32	0.05	0.71	1.95	0.016	0.84	-8.9	-5.7	-4.5	-8.5
E2	-1.1	-14.8	30.3	79.2	31.6	14.5	0.03	3.51	0.46	6.85	0.05	0.80	1.72	0.016	0.91	-4.0	2.4	0.6	8.7
E3	-1.3	-14.1	35.0	90.0	35.3	15.3	0.03	3.80	0.50	6.50	0.05	0.81	1.51	0.014	0.93	2.9	2.0	0.0	6.4
E4	3.7	-12.0	25.0	74.9	26.4	12.3	0.04	3.43	0.38	8.40	0.06	0.76	2.21	0.019	0.88	2.6	-3.4	-4.7	-5.0
E5	3.6	-11.5	30.3	79.9	31.6	12.6	0.04	3.58	0.49	7.85	0.07	0.84	1.93	0.018	0.95	0.2	-3.3	4.9	-1.3
E6	3.8	-10.4	35.0	89.9	35.6	13.7	0.04	3.95	0.53	7.58	0.07	0.87	1.69	0.017	0.98	-1.0	0.9	2.0	6.6
E7	9.9	-7.7	25.1	75.0	27.4	10.7	0.05	3.49	0.38	9.76	0.08	0.85	2.52	0.024	0.96	0.0	-4.4	-2.8	-5.0
E8	10.11	-7.3	30.2	83.1	31.7	11.7	0.05	3.78	0.45	9.12	0.08	0.86	2.16	0.021	0.97	-2.9	-3.3	-0.3	-1.1
E9	10.1	-5.9	34.9	89.9	36.0	12.5	0.05	4.07	0.66	8.81	0.08	0.94	1.86	0.019	1.04	2.0	-2.1	1.3	1.3

Chapter 7. Experimental determination of the optimum working conditions of a commercial transcritical CO_2 refrigeration plant with a R-152a dedicated mechanical subcooling.

Chapter 8 Experimental determination of the optimum intermediate and gas-cooler pressures of a commercial transcritical CO_2 refrigeration plant with parallel compression

Chapter 8. Experimental determination of the optimum intermediate and gas-cooler pressures of a commercial transcritical CO_2 refrigeration plant with parallel compression.

8. Experimental determination of the optimum intermediate and gas-cooler pressures of a commercial transcritical CO_2 refrigeration plant with parallel compression

Applied Thermal Engineering 189 (2021) 116671

Contents lists available at ScienceDirect

Applied Thermal Engineering

journal homepage: www.elsevier.com/locate/apthermeng

Chapter adapted from the paper: Nebot-Andrés, L., Sánchez, D., Calleja-Anta, D., Cabello, R., Llopis, R. Experimental determination of the optimum intermediate and gas-cooler pressures of a commercial transcritical CO_2 refrigeration plant with parallel compression (2021) Applied Thermal Engineering, 189, 116671. DOI: 10.1016/j.applthermaleng.2021.116671.

Abstract

CO_2 systems used in refrigeration are becoming more complex with the aim of improving their energy performance. Parallel compression is one of the implemented solutions to enhance the performance of the plants. However, an optimization process is required to operate this system at high performance and its operation is subjected to physical limitations in real plants.

This work presents the experimental optimization of a transcritical CO_2 plant working with parallel compression. The plant is tested at different discharge pressures and different secondary compressor speeds in order to optimize the COP of the plant and determine the optimal conditions for three gas-cooler exit temperatures 27.5ºC, 32.5ºC and 37.5ºC and three evaporation levels: -15.0ºC, -10.0ºC and -5.0ºC.

The optimal working conditions that can be achieved in a real plant have been determined, obtaining COP from 1.71 to 2.63 for -5.0ºC, from 1.50 to 2.22 for -10.0ºC and from 1.25 to 1.84 for -15.0ºC. Cooling capacity ranges from 8.94 kW to 11.34 for -5.0ºC, from 7.71 kW to 9.47 kW for -10.0ºC and from 6.22 kW to 7.76 kW for -15.0ºC. The trends observed in theoretical results have been corroborated and the optimum gas-cooler and intermediate pressures have been determined and discussed.

Keywords

Carbon dioxide, COP, energy improvement, parallel compression, optimization

Chapter 8. Experimental determination of the optimum intermediate and gas-cooler pressures of a commercial transcritical CO_2 refrigeration plant with parallel compression.

8.1. Introduction

Centralized Commercial refrigeration has undergone several technological advances in recent years that have been driven by different regulations that restrict the use of certain refrigerants in these facilities. First advances were driven by the Montreal Protocol, the Kyoto Protocol and the subsequent Kigali Amendment [1]. After the F-Gas regulation [2], CO_2 is the only gas that meets the limitations and can be used in these plants in safety conditions since it is neither toxic nor flammable. Although it is a perfect fluid to meet legislative restrictions, its performance in basic systems is not as good as that of other fluorinated gases.

Researcher's efforts have been focused on improving the performance of CO_2 systems in order to make them more competitive. Several research lines have been studied, as the use of ejectors [3-5], the subcooling methods [6] as the internal heat exchanger [7], the dedicated mechanical subcooling [8-11] and the integrated mechanical subcooling [12], the combination with other systems [13-15] and the parallel compression [16]. This latter is one of the most implemented solutions in commercial refrigeration.

Sawalha et al. [17] investigated the refrigeration performance of three CO_2 transcritical solutions based on field measurements and saw that transcritical booster systems with gas removal from the intermediate vessel have the highest total COP at that moment. Later, authors studied the integration of heating and air conditioning into a CO_2 transcritical booster system with parallel compression in a Swedish supermarket and obtained an increment of 8% on the total COP comparing with the system without PC [13, 18].

Gullo el al. [19], compared several supermarket configurations, including the parallel compression, located in cities with warm climates. They found that all the enhanced configurations obtained a comparable energy saving to the one of the cascade system for the studied locations.

Tsamos et al. [20] compared four different CO_2 refrigeration system configurations for the weather conditions of London, UK, and Athens, Greece. They found the CO_2 booster with parallel compressor to be the most energy efficient system for moderate and warm climates. Energy efficiency improvement over the conventional CO_2 booster was of 5.0% for the warm climate and 3.6% for the moderate climate.

The parallel compression is widely applied in booster systems for supermarket applications and combined with other systems as heat recovery [21]. The parallel compression is also combined with ejectors in European food retail industry [22].

However, there are not many studies that analyze the behavior of the parallel compression and its improvement applied to a simple cycle. In supermarket boosters with PC only the heat rejection pressure is controlled, since the pressure of the receiver is maintained around 35 bars [23].

Sarkar and Agrawal [16] performed a theoretical optimization study of a transcritical CO_2 refrigeration cycle with parallel compression economization, comparing three different techniques: parallel compression economization alone, parallel compression economization with recooler and multistage compression with flash gas bypass. They obtained an increment of 47.3% in terms of COP thanks to the parallel compression economization.

Minetto et al. [24] performed a theoretical investigation of a transcritical refrigerating CO_2 cycle with parallel compression and found benefits on the COP and cooling capacity when compared with the traditional cycle. Moreover, the optimum intermediate pressure is lower and the gas-cooler pressure is also lower than the optimal one for the traditional cycle.

Later, Chesi et al. [25] performed an experimental analysis of a CO_2 parallel compression cycle in flash tank configuration. In the first part, the authors carried out a theoretical study to define the limitations of the system and later performed the experimental tests but without optimizing the intermediate pressure. The tests were performed with a fixed parallel compressor speed, so the intermediate pressure is not optimized and the maximum improvements have not been reached.

Bella and Kaemmer [26] presented the experimental evaluation of a reciprocating prototype working with CO_2 with parallel compression. The compressor is a semi-hermetic four cylinders compressor with one compression chamber. Authors highlighted the influence of the intermediate pressure on the efficiency of the compressor and the system. They also found that the compressor shows a degradation in performance when the intermediate pressure increases.

Literature shows that there are no experimental studies in which the two working pressures are optimized at the same time, since in booster systems the tank pressure remains constant and Chesi et al. [25] also limit this variable.

The objective of this work is to determine experimentally the optimum conditions of CO_2 refrigeration plant with parallel compression, working in transcritical conditions. The main objective is to identify the existence of these optimal conditions and determine which are the needed pressures, gas-cooler pressure and intermediate pressure, to obtain the maximum COP of the installation. The results presented on this paper

correspond to the evaluation of the plant at three different evaporation levels (-15.0ºC, -10.0ºC and -5.0ºC) and three gas-cooler exit temperatures (27.5ºC, 32.5ºC and 37.5ºC), determining for each test the optimum values of gas-cooler and intermediate pressures. The applicability of this study focuses on medium temperature (MT) applications or in the high temperature cycle of a booster cycle.

Optimum conditions have been determined and stated on a general expression depending on the evaporation temperature and the temperature at the exit of the gas-cooler. The evolution of the main energy parameters is analyzed as well as the behavior of the optimum working conditions.

8.2. Refrigeration cycle and description of the experimental plant

The transcritical refrigeration plant with parallel compressor is presented in this section. The scheme of the plant and the Ph diagram of the cycle are shown in Figure 8.1. The refrigeration system is made up of two compressors: a main compressor and a secondary compressor (PC) that extracts vapour from the tank and recompresses it at the gas-cooler inlet. From the vessel, saturated liquid is extracted and expanded until the evaporator. The aim of the secondary compressor is to reduce the intermediate pressure (p_i) in order to increase the specific cooling capacity of the evaporator.

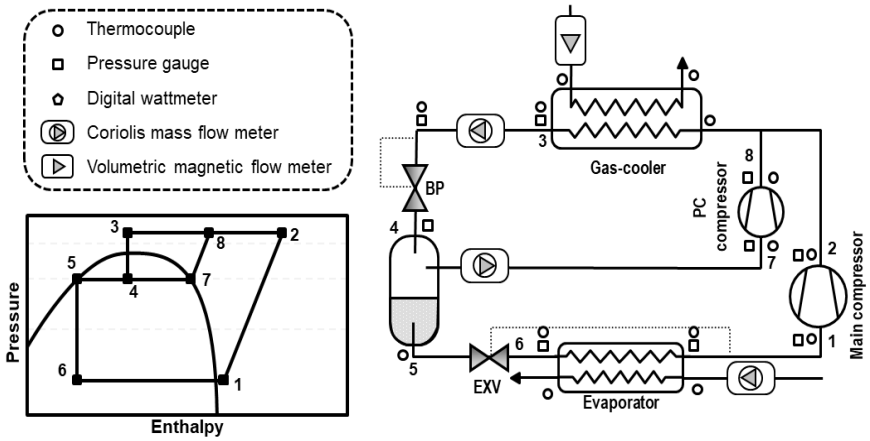

Figure 8.1. Schematic of the experimental plant and the measurement system and Ph diagram of the cycle.

Although the use of the PC has benefits in the behaviour of the cycle, it must also be taken into account that the presence of an additional compressor represents an increase in power consumption. Therefore, a compromise must be found between the power consumption and the intermediate pressure, for which the use of the PC enhances the COP.

8.2.1. Experimental plant

The schematic figure of the plant tested in this work is shown in Figure 8.1, and the experimental plant in Figure 8.2. The plant is a CO_2 single-stage transcritical refrigeration system with a parallel compressor system, extracting gas from the vessel. The main single-stage refrigeration cycle uses a semihermetic compressor with a displacement of 3.48 $m^3 \cdot h^{-1}$at 1450 rpm and a nominal power of 4 kW. The expansion is carried out by a double-stage system, composed of an electronic expansion valve (back-pressure) controlling the gas-cooler pressure, a liquid receiver between stages and an electronic expansion valve that controls the degree of superheat in the evaporator. Evaporator and gas-cooler are brazed plate counter current heat exchangers with exchange surface area of 4.794 m^2 and 1.224 m^2, respectively. The parallel compressor is a variable speed semihermetic compressor with displacement of 1.12 $m^3 \cdot h^{-1}$ at 1450 rpm.

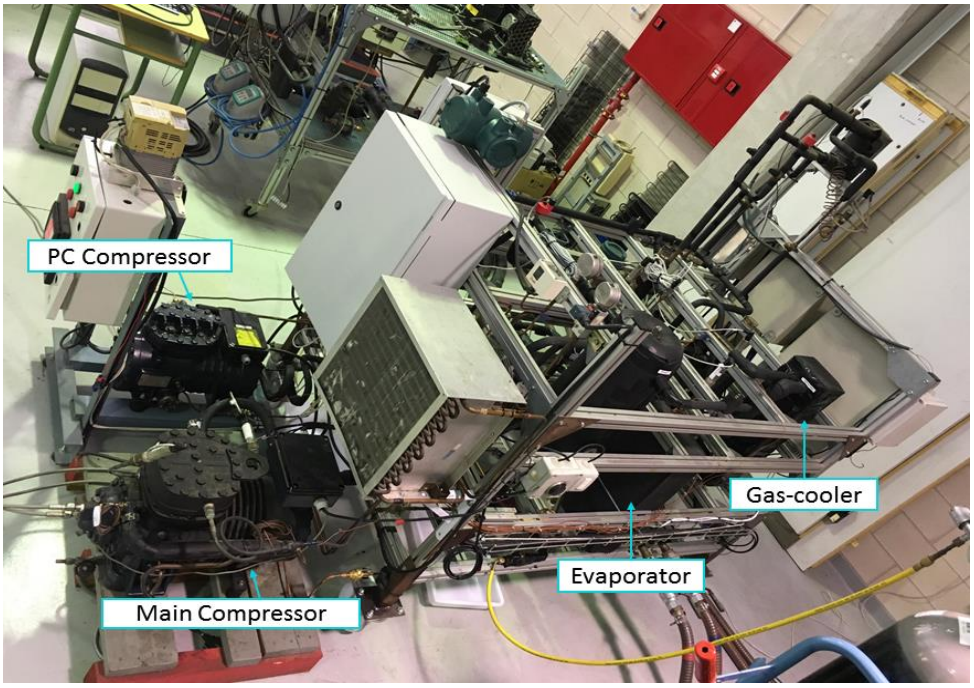

Figure 8.2. Experimental CO_2 plant.

Heat dissipation in gas-cooler is done with a water loop, simulating the heat rejection level. The evaporator is supplied with another loop, working with a propylene glycol–water mixture (60% by volume). Both the mass flow and the inlet temperature of the two secondary fluids can be controlled in these loops.

8.2.2. Measurement system

The thermodynamic properties of the working fluids are obtained thanks to the measurement system presented in Figure 8.1. All fluid temperatures are measured by 18 T-type thermocouples. The majority of the thermocouples are surface thermocouples but the ones placed at the evaporator, the exit of gas-cooler and subcooler are immersion thermocouples. Pressures are measured with 11 pressure gauges installed along all the circuit. CO_2 mass flow rates are measured by two Coriolis mass flow meters, as well as dissipation flow on the evaporator, which is measured by another Coriolis mass flow meter. The water flow of the gas-cooler dissipation is measured using a magnetic volumetric flow meter. Power consumptions of the compressors are measured by two digital watt meters. The accuracies of the measurement devices are presented in Table 8.1.

Table 8.1. Accuracies and calibration range of the measurement devices.

Measured variable	**Measurement device**	**Range**	**Calibrated accuracy**
Temperature (ºC)	T-type thermocouple	-40.0 to 145.0	±0.5K
CO_2 pressure (bar)	Pressure gauge	0.0 to 160.0	±0.6% of span
CO_2 pressure (bar)	Pressure gauge	0.0 to 100.0	±0.6% of span
CO_2 pressure (bar)	Pressure gauge	0.0 to 60.0	±0.6% of span
CO_2 main mass flow rate ($kg \cdot s^{-1}$)	Coriolis mass flow meter	0.00 to 1.38	±0.1% of reading
CO_2 PC mass flow rate ($kg \cdot s^{-1}$)	Coriolis mass flow meter	0.00 to 0.083	±0.1% of reading
Water mass flow rate ($m^3 \cdot h^{-1}$)	Magnetic flow meter	0.0 to 4.0	±0.25% of reading
Glycol volume flow rate ($kg \cdot s^{-1}$)	Coriolis mass flow meter	0.00 to 13.88	±0.1% of reading
Power consumption (kW)	Digital watt meter	0.0 to 6.0	±0.5% of reading

8.3. Experimental tests

The strategy for conducting the experimental tests in order to determine the optimum conditions is presented in this section.

8.3.1. Test procedure

To evaluate the refrigeration CO_2 plant working with parallel compressor, the system has been tested at different evaporation levels and different gas-cooler outlet temperatures. The evaluated conditions are:

- Three different evaporation temperatures: -5.0, -10.0 and -15.0ºC with maximum measured deviation of ±0.20°C. The evaporation level is maintained

adjusting the inlet temperature of the secondary fluid and the flow rate. The secondary fluid is a mixture propylene glycol-water (60% by volume).

- Three different gas-cooler exit temperatures: 27.5, 32.5 and 37.5°C, with maximum measured deviation of ±0.20°C. The heat rejection was performed with the secondary fluid (water) that can be controlled in terms of flow rate and inlet temperature.
- Gas-cooler pressure was regulated with an electronic Back-Pressure (BP). The pressure is fixed during each test and it is controlled thanks to a PID controller. Each test was performed at different pressures in order to identify the optimum one and reach the optimum COP conditions.
- Compressors: The main compressor always operated at nominal speed of 1450 rpm. The speed of the PC compressor was varied to modify the intermediate pressure.
- Electronic expansion valve: The electronic expansion valve of the evaporator was set to obtain a superheating degree in the evaporator of 10K.

Tests were carried out in steady state conditions for periods longer than 10 minutes, taking data each 5 seconds, obtaining the test point as the average value of the whole test. The measured data was used to calculate the thermodynamic properties of the cycle points using Refprop v.9.1. [27].

8.3.2. Test range

Table 8.2 sums up the range of evaluated conditions for all the test including intermediate and gas-cooler pressures, COP and cooling capacity. The number of tests carried out for each evaluated condition is also included on the table, with a total number of tests of 152.

Table 8.2. Experimental tests and range of tested conditions.

$t_{gc,o}$ (ºC)	t_o (ºC)	number of tests	P_i (bar)	P_{gc} (bar)	COP (-)	Q_0 (kW)
27.5	-5.0	19	44.3-49.0	75.4-76.1	2.57-2.63	11.0-11.5
	-10.0	14	35.0-46.5	75.0-79.9	1.99-2.22	9.0-9.8
	-15.0	13	33.2-43.6	74.4-80.9	1.67-1.84	7.4-8.2
32.5	-5.0	12	44.3-64.4	79.7-94.9	1.87-2.24	8.5-10.6
	-10.0	24	43.1-60.5	78.5-84.9	1.58-1.84	7.4-8.9
	-15.0	12	42.1-54.0	77.4-80.9	1.49-1.58	6.4-7.2
37.5	-5.0	21	49.1-67.2	90.1-97.0	1.62-1.71	7.7-9.7
	-10.0	19	46.7-67.4	86.8-91.9	1.34-1.50	6.1-8.1
	-15.0	18	44.8-58.4	85.9-90.8	1.12-1.26	5.7-6.5

8.4. Optimization of the plant

The cooling capacity of the cycle is calculated as the product of the CO_2 mass flow rate and the enthalpy difference between the exit and the entrance of the evaporator, as stated in Eq.(8.1). The enthalpy at the entrance of the evaporator is considered to be the same as the enthalpy at the exit of the vessel, before the expansion valve, as shown in Eq. (8.2). This enthalpy is calculated with the value of the pressure in the liquid tank and considering saturated liquid. To guarantee consistency of calculations, it was verified in each test that the refrigerant at the exit of the vessel was saturated liquid, as it can be seen in Figure 8.3.

$$\dot{Q}_0 = \dot{m}_0 \cdot (h_{0,o} - h_{0,in}) \tag{8.1}$$

$$h_{0,in} = h_{dep,liq} = f(P_i, x = 0) \tag{8.2}$$

$$h_{0,o} = f(P_{0,o}, t_{0,o}) \tag{8.3}$$

Figure 8.3. CO_2 liquid level in the vessel.

The COP of the plant is evaluated as the ratio between the cooling capacity and the power consumption of both compressors:

$$COP = \frac{\dot{Q}_0}{Pc_{main} + Pc_{PC}} \tag{8.4}$$

8.4.1. Determination of the optimum COP

CO_2 transcritical cycles can be performed at maximum efficiency by optimizing the gas-cooler pressure but, when having a parallel compressor, it is also necessary to optimize the intermediate pressure [28]. In CO_2 cycles with parallel compression, lower intermediate pressures increase the specific cooling capacity of the system but also the compression ratio and mass flow of the PC compressor are higher.

The tests have been performed in order to identify the maximum COP. First, three points are tested for different gas-cooler and intermediate pressures, always values close to those obtained in previous theoretical studies. Then, the three first tested points are represented in a graph and from there; a colour map is formed by these three points, similar to that presented in Figure 8.4. The intermediate pressure or gas-cooler pressure values are modified in the direction where the COP increases as it is indicated in the contour map. This procedure is followed, obtaining new COP points until the maximum COP is clearly identified. Both gas-cooler pressure and intermediate pressure can be modified independently according to the needs of each tested condition. New points are added to the colour map and the process ends when the increments achieved between the new COP value and the previous one are less than 1%.

Figure 8.4 shows the COP for the evaporating temperature of -5.0ºC and a gas-cooler outlet temperature of 27.5ºC. COP is presented as a function of the gas-cooler and the intermediate pressures. The optimum point has been marked with a blue circle. It corresponds to an intermediate pressure of 46.0 bar and 75.4 bar in gas-cooler. It can be seen that as the intermediate pressure increases or decreases with respect to the optimum, the COP decreases. Similar trend is observed regarding the gas-cooler pressure, when gas-cooler pressure increases, the COP decreases. Gas-cooler pressures under 74.4 bar have not been tested because the aim of this work is only to evaluate the system in transcritical conditions.

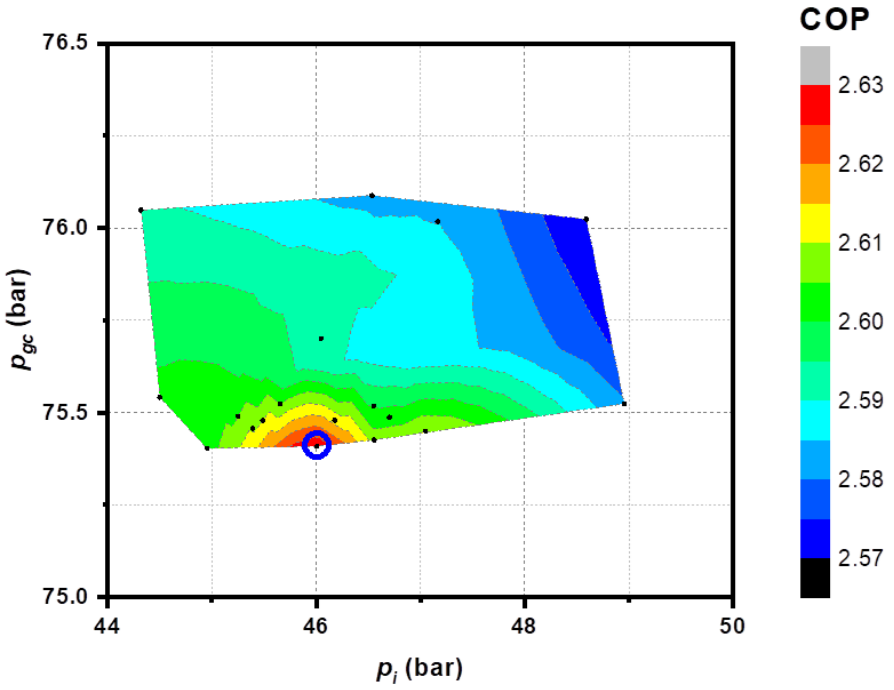

Figure 8.4.COP as a function of gas-cooler and intermediate pressure for t_0 =-5.0ºC $t_{gc,o}$=27.5ºC.

As it can be seen in Figure 8.4 and later in Figure 8.6, the effect of the gas-cooler pressure in the COP is higher than the effect of the intermediate pressure. Modifying the pressure with respect to its optimal value, we can see that the COP decreases. As illustrative data, observing Figure 8.4 and Figure 8.6 we can see that a variation of 5 bars in the intermediate pressure has less effect on the COP than a variation of 5 bar in the gas-cooler pressure, where the COP would suffer a more important reduction.

Cooling capacity is inversely related to the intermediate pressure. When higher the intermediate pressure is, lower the cooling capacity is. Conversely, cooling capacity is not much dependent on the gas-cooler pressure. As it can be seen in Figure 8.5, for a fixed intermediate pressure, cooling capacity remains the same regardless of the gas-pressure. However, this phenomenon only occurs when analysing very small gas-cooler variations. This is because the influence of the intermediate pressure on the cooling capacity is much higher than the influence of gas-cooler pressure. Analysing a higher range of gas-cooler pressures has an effect on the cooling capacity of the plant.

The evolution of the cooling capacity as a function of both pressures can be seen in the Figure 8.5. The colour map shows the evolution of the cooling capacity for t_0 =-5.0ºC

and $t_{gc,o}$=27.5ºC. The point corresponding to the maximum COP obtained in Figure 8.4 is marked in blue.

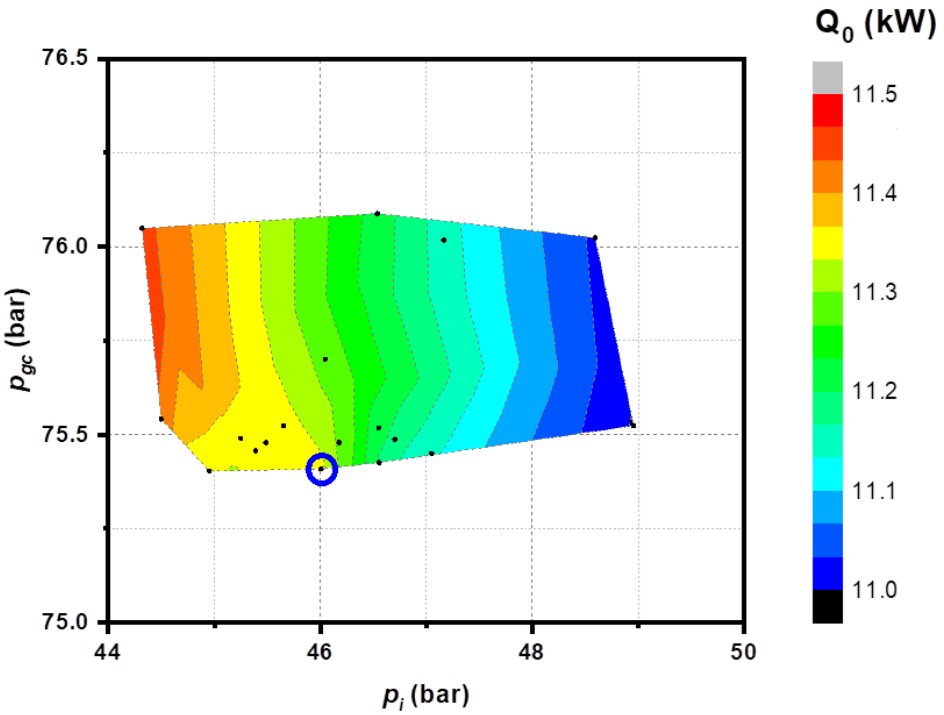

Figure 8.5. Cooling capacity for t_0 =-5.0ºC $t_{gc,o}$=27.5ºC.

From this moment on, all the data presented are obtained following the process above described and correspond to the optimum point of each of the studied test conditions.

8.4.2. Physical limitations of the plant

During the experimental evaluation of the plant, some physical limits have been detected. As previously mentioned, gas-cooler pressure is regulated thanks to the backpressure valve. For each gas-cooler outlet and evaporator temperatures, there is a lower gas-pressure limit from which it is impossible to make pressure go lower. As it can be seen in Figure 8.6, this low limit is different depending on the gas-cooler outlet temperature. It can be seen that the optimum point is located at this low limit. When higher the gas-cooler outlet temperature is, higher the limit pressure is. The evaporator level has little influence on this parameter as it will be presented later in Figure 8.10, where the optimum gas-cooler pressures are represented.

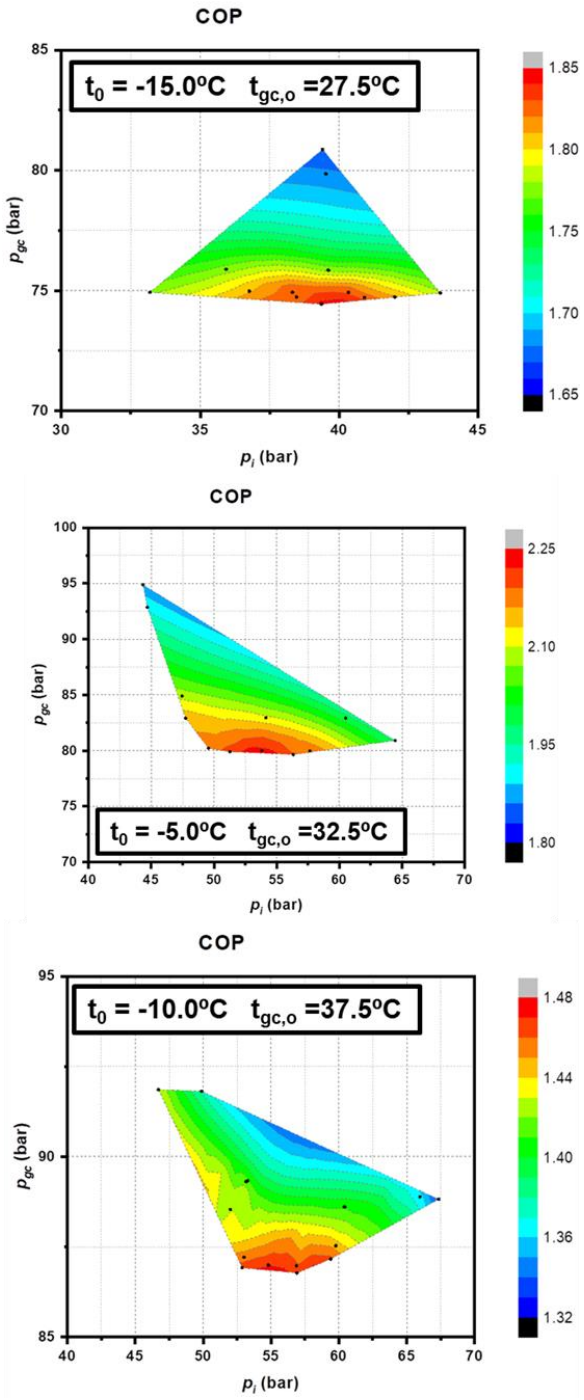

Figure 8.6. COP evolution for for t_0 =-15.0ºC and $t_{gc,o}$=27.5ºC; t_0 =-5.0ºC and $t_{gc,o}$=32.5ºC and t_0 =-10.0ºC and $t_{gc,o}$=37.5ºC.

The reason for that phenomenon is the mass balance in the liquid tank. As mentioned in the previous section, saturated liquid must be extracted from the lower part of the tank and saturated vapor from the upper part to ensure the correct operation of the system. Also, the system should be evaluated in steady-state conditions; otherwise, the mass balance in the tank (Eq.(8.5)) is not verified.

Hazarika [29] studied the receiver influence in CO_2 air-conditioning two-stage expansion unit. Authors found that higher the size of the receiver is, higher will be the range of refrigerant charge over which the liquid portion changes from 0 to 100% in the receiver. Thus, for a specific size of receiver, the refrigerant charge should be maintained within the range to keep the receiver partially filled with liquid during operation. This means that if the refrigerant charge is lower than the lower limit of that range, we cannot ensure the presence of liquid in the tank. And if the refrigerant charge is higher than the upper limit of that range, we would have 100% liquid in the tank. Working within the limits of this refrigerant charge range ensures that the tank pressure will remain constant regardless of the refrigerant charge. For the experimental tests presented in this work, the refrigerant charge has been maintained and also corroborated that it is inside the correct range for the real liquid receiver.

Chesi et al. [25] demonstrated that for a given condition ($t_{g,co}$, p_{gc} and t_0) and given conditions of the compressors, there is only one possible intermediate pressure that ensures both conditions stated in the previous paragraph, because after expanding from the gas-cooler exit and entering to the vessel, the CO_2 quality changes when the intermediate pressure is varied. As presented by some authors [24, 25], the intermediate pressure of this cycle is influenced by the compressor volumetric flow ratio. It means that the intermediate pressure is affected by the range of compressors volumetric ratio that the plant can realize. This determines the operability limits of parallel compression cycle by the choice of the compressors.

That is why the physical limits of the system depend on the gas-cooler conditions but also on the sizes and performances of the compressors.

To verify the energy balance in the liquid tank and the mass balance, ensuring steady-state conditions, there is only on intermediate pressure that reaches the equilibrium for these conditions. The lower pressure limit may be caused due to the fact that the BP valve is completely open and it is not capable of transferring as much flow as it arrives from the gas-cooler and therefore it is not possible to lower the pressure in the discharge line any further.

The mass balance in the vessel is stated in Eq.(8.5). As it can be seen in Figure 8.1, the mass flow entering the vessel ($\dot{m}_4$) is the sum of the mass flow through the evaporator ($\dot{m}_5$) and the mass flow suctioned by the parallel compressor ($\dot{m}_7$).

$$\dot{m}_4 = \dot{m}_5 + \dot{m}_7 \tag{8.5}$$

As previously mentioned, in steady-state conditions, the flow extracted through the lower part of the tank is saturated liquid and the flow extracted through the upper part is saturated vapour, so the mass flows can be defined as:

$$\dot{m}_5 = \dot{m}_4 \cdot (1 - x_4) \tag{8.6}$$

$$\dot{m}_7 = \dot{m}_4 \cdot x_4 \tag{8.7}$$

Thus, the ratio between the mass flow through the PC and the total mass flow can be determined as:

$$\frac{\dot{m}_7}{\dot{m}_4} = \frac{\dot{m}_4 \cdot x_4}{\dot{m}_4} = x_4 \tag{8.8}$$

As demonstrated in Eq. (8.8) the proportion of mass flow going into the parallel compressor is the vapour quality at the vessel, so it is completely dependent on the intermediate pressure.

Figure 8.7 shows the ratio between the mass flows (Eq. (8.8)) as a function of the evaporating level and gas-cooler outlet temperature. It can be observed that when higher the t_0 is lower the PC mass flow ratio is. As it will be seen in the following section, when evaporation temperature decreases, the intermediate pressure is lower and the difference between intermediate pressure and gas-cooler pressure increases which lead to a higher x_4.

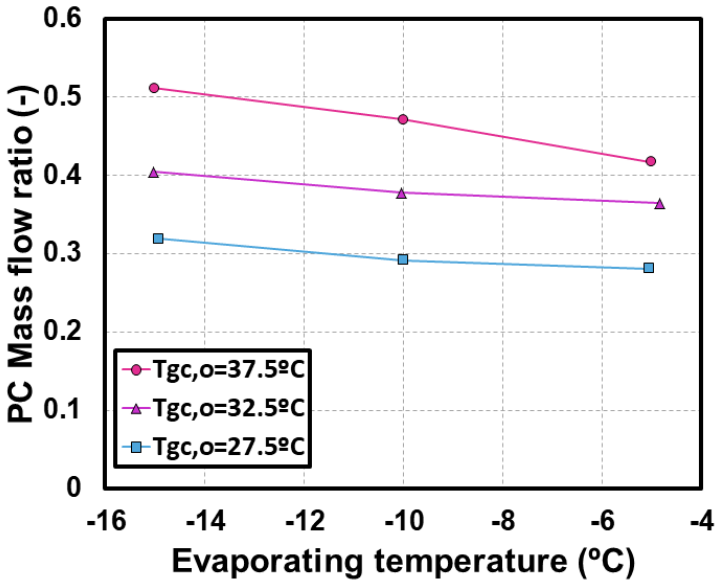

Figure 8.7. PC Mass flow ratio.

Also, for higher $t_{gc,o}$, the PC mass flow ratio is also higher because for high gas-cooler temperatures, optimum gas-cooler increases while the optimum intermediate pressure decreases when the evaporation temperature decreases. These trends corroborate the theoretical optimization presented by Sarkar and Agrawal [16].

8.5. Experimental results at optimum conditions

In this section, the main results are presented for the evaluated conditions: the optimum COP, the cooling capacity and the optimum pressures. The presented results correspond to the experimental points where the highest COP is obtained, which are the optimum conditions. The most important parameters of these tests are summed up in Table 8.3 as well as the uncertainty of the COP and cooling capacity, which has been calculated using Moffat's method [30]. The measurement devices' accuracies are presented in Table 8.1. The average measured uncertainty is ±1.24% in $\dot{Q}_0$ and ±1.31% in COP with maximum uncertainty of ±1.40% and ±1.46% respectively. Main operation parameters of the compressors are also included in Table 8.3 as the volumetric efficiency and the frequency of the IMS compressor. As it can be seen, all the main compressor's overall efficiencies are between 52% and 60% while the overall efficiencies of the parallel compressor are between 48% and 56%, always running below the nominal frequency of 50Hz.

8.5.1. Maximum COP and cooling capacity

Optimum COP is presented in Figure 8.8 for the three evaporating temperatures as a function of the gas-cooler outlet temperature. As it can be seen, COP is higher when higher the evaporation level is, and it is lower when higher the gas-cooler outlet temperature is. The measured COP is 2.63 at $t_{gc,o}$=27.5ºC, 2.24 at $t_{gc,o}$=32.5ºC and 1.71 at $t_{gc,o}$=37.5ºC for the evaporating level of t_0=-5.0ºC. For the evaporating level of t_0=-10.0ºC, the measured COP is 2.22 at $t_{gc,o}$=27.5ºC, 1.84 at $t_{gc,o}$=32.5ºC and 1.50 at $t_{gc,o}$=37.5ºC and for the evaporating level of t_0=-15.0ºC 1.84, 1.58 and 1.25 respectively.

Figure 8.9 shows the cooling capacity of the points with maximum COP. The cooling capacity follows the same trend as the COP, being higher when higher the evaporation level is and when lower the gas-cooler outlet temperature is. The cooling capacity is 11.34 kW at $t_{gc,o}$ =27.5ºC, 10.13 kW at $t_{gc,o}$ =32.5ºC and 8.94 kW at $t_{gc,o}$=37.5ºC for the evaporating level of t_0=-5.0ºC. For the evaporating level of t_0=-10.0ºC, the measured cooling capacity is 9.47 kW at $t_{gc,o}$ =27.5ºC, 8.28 kW at $t_{gc,o}$=32.5ºC and 7.71 kW at $t_{gc,o}$ =37.5ºC and for the evaporating level of t_0=-15.0ºC 7.76 kW, 6.94 kW and 6.22 kW respectively.

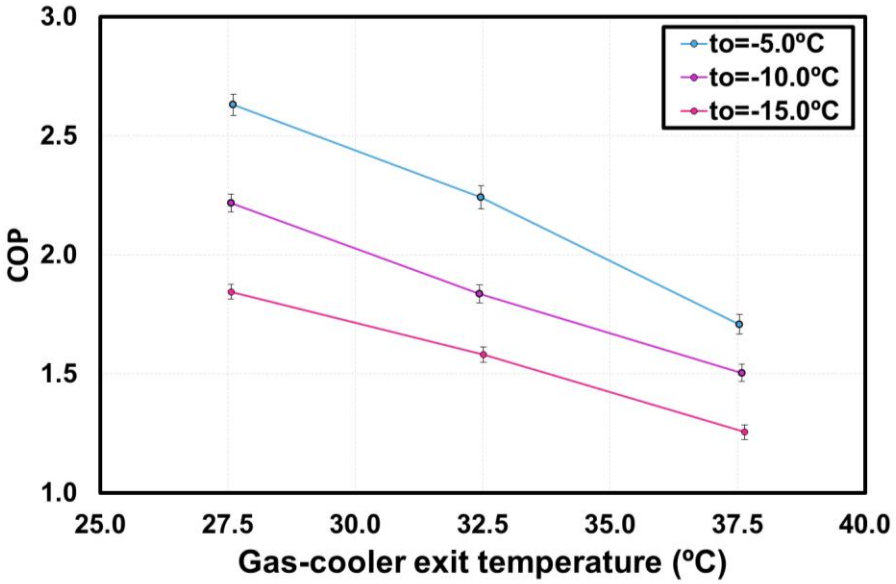

Figure 8.8. Optimum COP evolution.

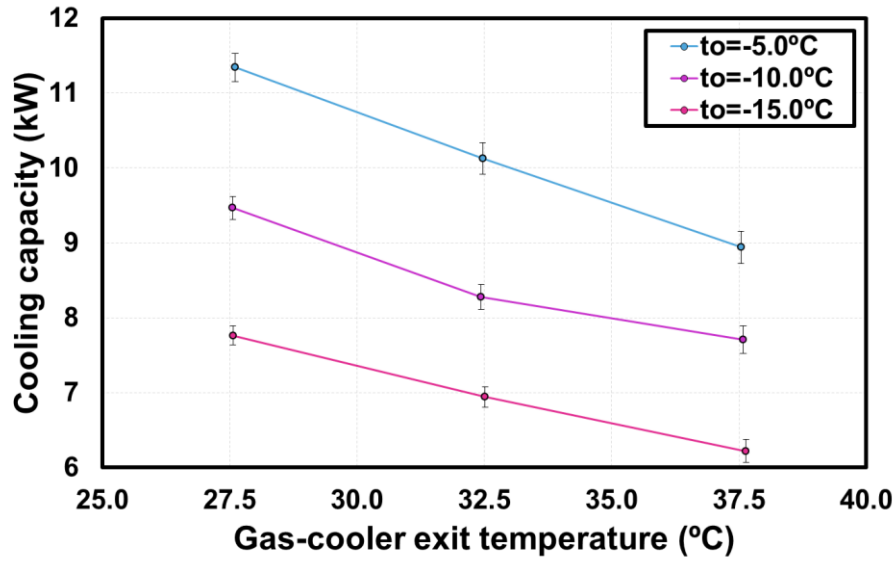

Figure 8.9. Evolution of the cooling capacity.

8.5.2. Optimum pressures

The COP of the plant depends on the gas-cooler pressure but also on the intermediate pressure that is the pressure of the liquid tank. Gas-cooler pressure can be regulated thanks to the back-pressure valve and the pressure in the vessel should be regulated by the parallel compressor's speed.

Figure 8.10 shows the optimum gas-cooler pressure and the optimum intermediate pressures. As it can be seen, gas-cooler pressure strongly depends on the gas-cooler outlet temperature, being higher when higher the temperature is but it practically does not depend on the evaporation level.

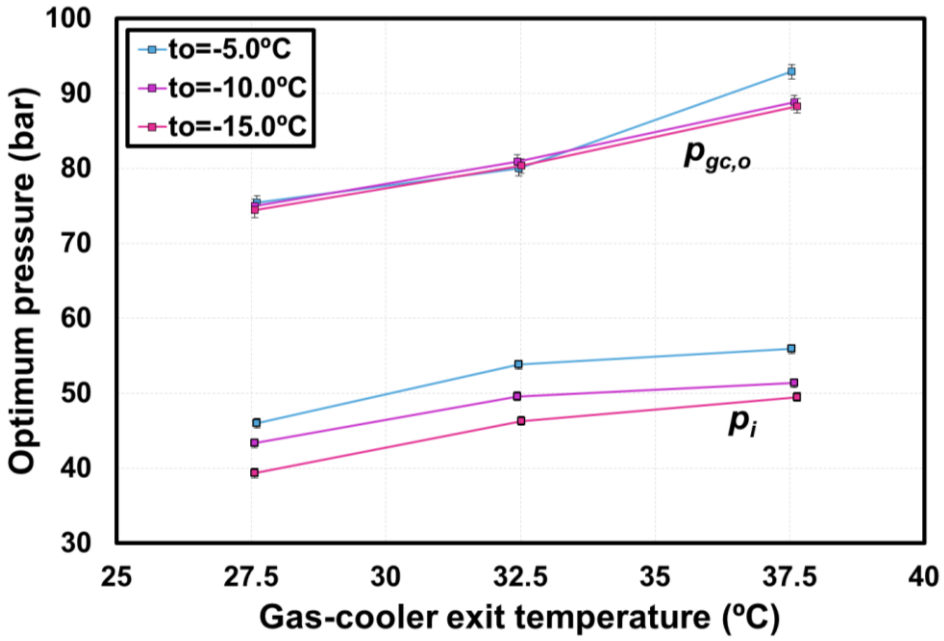

Figure 8.10. Optimum gas-cooler and intermediate pressures.

The obtained gas-cooler pressures have the same trend as the pressures obtained by Sarkar and Agrawal [16]. It is dependent on the gas-cooler temperature and it is higher when higher the temperature is. Also, as presented by Sarkar and Agrawal, it is practically independent on the evaporation level. When regarding the highest evaporation level (E1 in Table 8.3), a slight influence of the evaporation temperature on the discharge pressure can be observed. This coincides with the operating limits of the system, presented by Chesi et al. [25], where the gas-cooler pressure increases for high ambient temperatures for the highest evaporation levels.

The intermediate pressure has a different trend. It depends both on the gas-cooler outlet temperature and the evaporating temperature as it can be seen in Figure 8.10. The pressure is higher when higher the evaporation temperature and the gas-cooler outlet temperature are. The obtained trends on the intermediate pressure are also observed in the theoretical study of the CO_2 cycle with parallel compression performed by Sarkar and Agrawal [16].

In the following section the correlations to obtain both pressures are presented. They are also compared to the correlations proposed by Sarkar and Agrawal [16] in their theoretical study.

8.5.5. Correlations

The following correlations are obtained from the experimental data and they allow calculating the optimal working pressures to obtain maximum COP depending on the evaporation and gas-cooler outlet temperature conditions. Correlations have been obtained using an adjustment of least-squares.

8.5.5.1. Optimum gas-cooler pressure

Gas-cooler pressure's correlation is defined in Eq. (8.9) and it is a function of the gas-cooler outlet temperature and the evaporation temperature.

$$p_{gc} = 101.3 - 3.064 \cdot t_{gc} - 1.1 \cdot t_0 + 0.0762 \cdot t_{gc}^2 + 0.0392 \cdot t_{gc} \cdot t_0 \qquad (8.9)$$

The range of application of this correlation is for temperatures of gas-cooler exit between 27.5 °C and 37.5 °C and evaporation temperatures between −15.0 °C and −5.0 °C. The root-mean-square deviation of the correlation is 1.213 bar.

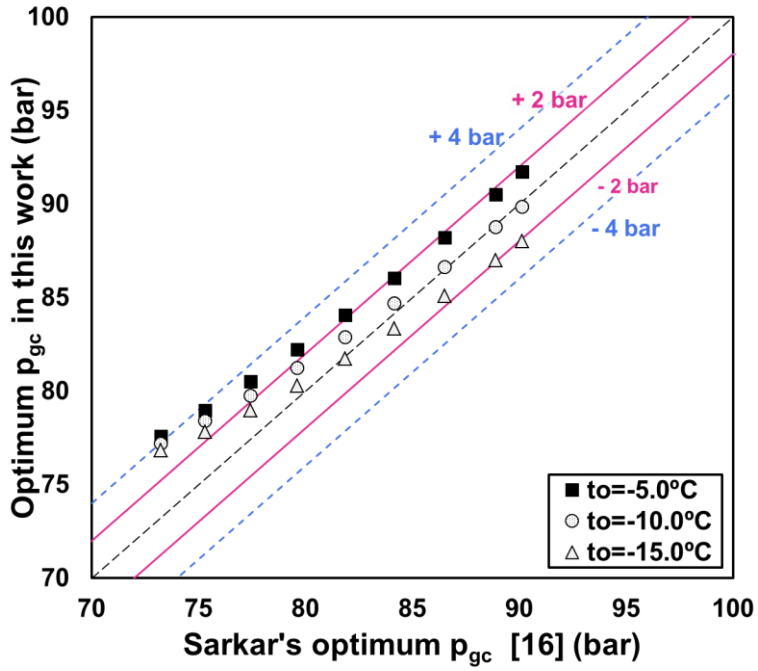

Figure 8.11. Comparison of the optimum gas-cooler pressure obtained by Sarkar's correlation [16] with the optimum pressures obtained experimentally.

Figure 8.11 shows the comparison of the optimum gas-cooler pressure obtained by the correlation proposed in Eq.(8.9) with the correlation proposed by Sarkar and Agrawal [16] for different evaporation temperatures and a range of gas-cooler exit temperatures between 30 and 37ºC, where both correlations can be applied. As it can be observed, both pressures are quite similar but those corresponding to the lower temperatures have a slightly higher discrepancy (up to 4 bar for $t_{gc,o}$ = 30ºC). Even so, we can affirm that the trend obtained by Sarkar and Agrawal [16] is experimentally corroborated with the results presented in this work.

8.5.5.2. Optimum intermediate pressure

The optimum intermediate pressure can be calculated with Eq.(8.10). The range of application of this correlation is for evaporation temperatures between –15.0 °C and –5.0 °C and temperatures of gas-cooler exit between 27.5 °C and 37.5 °C. The root-mean-square deviation of the correlation is 0.6761 bar.

$$p_i = -74.87 + 7.175 \cdot t_{gc} + 0.7716 \cdot t_0 - 0.0962 \cdot t_{gc}^2 - 0.0027 \cdot t_0 \cdot t_{gc} \qquad (8.10)$$

8.6. Conclusions

The experimental optimization of a CO_2 transcritical refrigeration plant with parallel compression is presented in this work. The evaluation covered three evaporating levels (-5.0ºC, -10.0ºC and -15.0ºC) and the gas-cooler exit temperatures of 27.5ºC, 32.5ºC and 37.5ºC at steady-state conditions. The main compressor worked at nominal speed while the parallel compressor's speed has been modified in order to obtain the optimum intermediate pressure.

The results obtained in this work corroborate the trends presented in the theoretical optimization of Sarkar and Agrawal [16]. Also, the tank pressure limit has been demonstrated experimentally.

The experimental tests have allowed to demonstrate the existence of a maximum COP, obtained for the optimum conditions of gas-cooler and intermediate pressures, that varies depending on the test conditions. The optimum COP goes from 1.71 to 2.63 for the evaporating temperature of -5.0ºC, from 1.50 to 2.22 for the evaporating temperature of -10.0ºC and from 1.25 to 1.84 for -15.0ºC. The cooling capacity from 8.94 kW to 11.34 kW for the evaporating temperature of -5.0ºC, from 7.71 kW to 9.47 kW for -10.0ºC and from 6.22 kW to 7.76 kW for -15.0ºC. The optimum pressure is strongly dependent on the gas-cooler outlet temperature, being higher when higher the temperature is, whereas it practically does not depend on the level of evaporation for the evaluated evaporation temperatures. On the other hand, the optimum intermediate pressure depends on both, the gas-cooler outlet temperature and the evaporation

temperature, being higher when higher the evaporation level and the gas-cooler outlet temperature are.

Two general expressions have been stated from the experimental data to determine the optimum gas-cooler and intermediate pressures for CO_2 single-stage transcritical refrigeration plants with parallel compression, only depending on the evaporation level and the gas-cooler outlet temperature. The correlation obtained to determine the gas-cooler pressure is compared to the correlation proposed by Sarkar and Agrawal [16] corroborating experimentally the trends presented in Sarkar and Agrawal's theoretical study.

Furthermore, further research is needed to study the physical limitations that have been found in the experimental operation of this plant.

8.7. Acknowledgements

The authors thank the Ministerio de Educación, Cultura y Deporte (Spain) grant FPU16/00151; the Ministerio de Ciencia y Tecnología (Spain) project RTI2018-093501-B-C21, and the Jaume I University (Spain), project UJI-B2019-56 for financing this research work.

8.8. Nomenclature

BP back-pressure valve

COP coefficient of performance

BP back-pressure valve

COP coefficient of performance

h specific enthalpy, $kJ \cdot kg^{-1}$

$\dot{m}$ mass flow rate $kg \cdot s^{-1}$

MT medium temperature

p absolute pressure, bar

Pc power consumption, kW

PID proportional–integral–derivative controller

Q cooling capacity, kW

t temperature, ºC

Greek symbols

ε uncertanity

x vapour quality

Subscripts

dep corresponding to the liquid tank

dis compressor discharge

gc gas-cooler

i intermediate

in inlet

main corresponding to the main cycle

0 evaporating level

o outlet

PC corresponding to the parallel compressor

w water

8.9. References

[1] UNEP/TEAP, The implications to the Montreal Protocol of the inclusion of HFCs and PFCs in the Kyoto Protocol, in, United States, 1999.

[2] European Commission, Regulation (EU) No 517/2014 of the European Parliament and of the Council of 16 April 2014 on fluorinated greenhouse gases and repealing Regulation (EC) No 842/2006., (2014).

[3] Hafner A., Hemmingsen A. K. T., Ven A. van de, R744 refrigeration system configurations for supermarkets in warm climates, in: 3rd IIR International Conference on Sustainability and the Cold Chain. Proceedings, International Institute of Refrigeration, London, UK, 2014.

[4] N. Lawrence, S. Elbel, Experimental investigation on control methods and strategies for off-design operation of the transcritical R744 two-phase ejector cycle, International Journal of Refrigeration, (2019).

[5] N. Lawrence, S. Elbel, Experimental study on control methods for transcritical CO2 two-phase ejector systems at off-design conditions, in: Refrigeration Science and Technology, 2016, pp. 511-518.

[6] R. Llopis, L. Nebot-Andrés, D. Sánchez, J. Catalán-Gil, R. Cabello, Subcooling methods for CO2 refrigeration cycles: A review, International Journal of Refrigeration, 93 (2018) 85-107.
[7] J. Rigola, N. Ablanque, C.D. Pérez-Segarra, A. Oliva, Numerical simulation and experimental validation of internal heat exchanger influence on CO2 trans-critical cycle performance, International Journal of Refrigeration, 33 (2010) 664-674.
[8] R. Llopis, L. Nebot-Andrés, R. Cabello, D. Sánchez, J. Catalán-Gil, Experimental evaluation of a CO2 transcritical refrigeration plant with dedicated mechanical subcooling, International Journal of Refrigeration, 69 (2016) 361-368.
[9] L. Nebot-Andrés, D. Sánchez, D. Calleja-Anta, R. Cabello, R. Llopis, Experimental determination of the optimum working conditions of a commercial transcritical CO2 refrigeration plant with a R-152a dedicated mechanical subcooling, International Journal of Refrigeration, (2020).
[10] J. Bush, M. Beshr, V. Aute, R. Radermacher, Experimental evaluation of transcritical CO2 refrigeration with mechanical subcooling, Science and Technology for the Built Environment, 23 (2017) 1013-1025.
[11] M. Beshr, J. Bush, V. Aute, R. Radermacher, Steady state testing and modeling of a CO2 two-stage refrigeration system with mechanical subcooler, in: Refrigeration Science and Technology, 2016, pp. 893-900.
[12] L. Nebot-Andrés, J. Catalán-Gil, D. Sánchez, D. Calleja-Anta, R. Cabello, R. Llopis, Experimental determination of the optimum working conditions of a transcritical CO2 refrigeration plant with integrated mechanical subcooling, International Journal of Refrigeration, 113 (2020) 266-275.
[13] M. Karampour, S. Sawalha, Integration of heating and air conditioning into a CO2 trans-critical booster system with parallel compression Part I: Evaluation of key operating parameters using field measurements, in: Refrigeration Science and Technology, 2016, pp. 323-331.
[14] C. Aprea, A. Greco, A. Maiorino, The application of a desiccant wheel to increase the energetic performances of a transcritical cycle, Energy Conversion and Management, 89 (2015) 222-230.
[15] A. Arora, N.K. Singh, S. Monga, O. Kumar, Energy and exergy analysis of a combined transcritical CO2 compression refrigeration and single effect H2O-LiBr vapour absorption system, International Journal of Exergy, 9 (2011) 453-471.
[16] J. Sarkar, N. Agrawal, Performance optimization of transcritical CO2 cycle with parallel compression economization, International Journal of Thermal Sciences, 49 (2010) 838-843.
[17] S. Sawalha, M. Karampour, J. Rogstam, Field measurements of supermarket refrigeration systems. Part I: Analysis of CO2 trans-critical refrigeration systems, Applied Thermal Engineering, 87 (2015) 633-647.
[18] M. Karampour, S. Sawalha, Integration of heating and air conditioning into a CO2 trans-critical booster system with parallel compression part II: Performance analysis based on field measurements, in: Refrigeration Science and Technology, 2016, pp. 332-340.

[19] P. Gullo, B. Elmegaard, G. Cortella, Energy and environmental performance assessment of R744 booster supermarket refrigeration systems operating in warm climates, International Journal of Refrigeration, 64 (2016) 61-79.
[20] K.M. Tsamos, Y.T. Ge, I. Santosa, S.A. Tassou, G. Bianchi, Z. Mylona, Energy analysis of alternative CO2 refrigeration system configurations for retail food applications in moderate and warm climates, Energy Conversion and Management, 150 (2017) 822-829.
[21] A. Polzot, P. D'Agaro, G. Cortella, Energy Analysis of a Transcritical CO2 Supermarket Refrigeration System with Heat Recovery, Energy Procedia, 111 (2017) 648-657.
[22] P. Gullo, K. Tsamos, A. Hafner, Y. Ge, S.A. Tassou, State-of-the-art technologies for transcritical R744 refrigeration systems – a theoretical assessment of energy advantages for European food retail industry, Energy Procedia, 123 (2017) 46-53.
[23] J. Catalán-Gil, D. Sánchez, R. Llopis, L. Nebot-Andrés, R. Cabello, Energy evaluation of multiple stage commercial refrigeration architectures adapted to F-gas regulation, Energies, 11 (2018).
[24] S. Minetto, L. Cecchinato, M. Corradi, E. Fornasieri, C. Zilio, A. Schiavon, Theoretical and experimental analysis of a CO2 refrigerating cycle with two-stage throttling and suction of the flash vapour by an auxiliary compressor, in: IIR International conference on thermophysical properties and transfer processes of refrigerants, Vicenza (Italy), 2005.
[25] A. Chesi, F. Esposito, G. Ferrara, L. Ferrari, Experimental analysis of R744 parallel compression cycle, Applied Energy, 135 (2014) 274-285.
[26] B. Bella, N. Kaemmer, Experimental Performance of Carbon Dioxide Compressor with Parallel Compression, in: DKV-Tagung, Aachen (Germany), 2011.
[27] E.W. Lemmon, M.L. Huber, M.O. McLinden, REFPROP, NIST Standard Reference Database 23, v.9.1. National Institute of Standards, Gaithersburg, MD, U.S.A., (2013).
[28] L. Cecchinato, M. Chiarello, M. Corradi, E. Fornasieri, S. Minetto, P. Stringari, C. Zilio, Thermodynamic analysis of different two-stage transcritical carbon dioxide cycles, International Journal of Refrigeration, 32 (2009) 1058-1067.
[29] M.M. Hazarika, Studies on a CO2 based summer air conditioning system with single and multiple expansion valves, in: Department of mechanical engineering Vol. Doctor of Philosophy, Indian Institute of Technology Kharagpur, 2020, pp. 158.
[30] R.J. Moffat, Using Uncertainty Analysis in the Planning of an Experiment, Journal of Fluids Engineering, 107 (1985) 173-178.

Table 8.3. Main experimental results and uncertainty measurements.

	t_0 (ºC)	$t_{sc,o}$ (ºC)	$t_{w,in}$ (ºC)	$p_{sc,o}$ (bar)	p_i (bar)	$\dot{m}_0$ (kg·s^{-1})	P_{CO2} (kW)	P_{CPC} (kW)	$\dot{Q}_0$ (kW)	$\varepsilon(\dot{Q}_0)$ (%)	COP (-)	ε(COP) (%)	η_{main} (-)	η_{PC} (-)	f_{PC} (Hz)
E1	-5.0	37.5	35.6	92.9	55.9	0.05	4.20	1.04	8.94	1.40	1.71	1.46	0.56	0.56	38
E2	-10.0	37.6	35.6	88.8	51.4	0.04	3.90	1.23	7.71	1.27	1.50	1.33	0.55	0.55	45
E3	-15.0	37.6	36.3	88.3	49.5	0.03	3.69	1.27	6.22	1.23	1.25	1.29	0.52	0.53	45
E4	-4.8	32.5	28.0	80.0	53.8	0.05	3.74	0.78	10.13	1.34	2.24	1.41	0.59	0.52	35
E5	-10.0	32.4	29.7	80.9	49.6	0.04	3.66	0.85	8.28	1.25	1.84	1.32	0.56	0.51	34
E6	-15.0	32.5	30.2	80.3	46.3	0.03	3.50	0.89	6.94	1.19	1.58	1.26	0.54	0.52	35
E7	-5.0	27.6	23.7	75.4	46.0	0.05	3.56	0.76	11.34	1.20	2.63	1.28	0.60	0.52	32
E8	-10.0	27.6	24.3	75.0	43.3	0.04	3.51	0.77	9.47	1.16	2.22	1.24	0.57	0.48	31
E9	-14.9	27.6	24.8	74.4	39.4	0.03	3.38	0.83	7.76	1.13	1.84	1.20	0.54	0.49	33

Chapter 9 Experimental evaluation of zeotropic refrigerants in a dedicated mechanical subcooling system in a CO_2 cycle.

Chapter 9. Experimental evaluation of zeotropic refrigerants in a dedicated mechanical subcooling system in a CO_2 cycle

9. Experimental evaluation of zeotropic refrigerants in a dedicated mechanical subcooling system in a CO_2 cycle.

International Journal of Refrigeration 128 (2021) 287–298

Contents lists available at ScienceDirect

International Journal of Refrigeration

journal homepage: www.elsevier.com/locate/ijrefrig

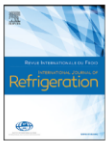

Chapter adapted from the paper: Llopis, R., Toffoletti, G. Nebot-Andrés, L., Cortella, G. Experimental evaluation of zeotropic refrigerants in a dedicated mechanical subcooling system in a CO_2 cycle. (2021) International Journal of Refrigeration, 128, pp. 287-298. DOI: 10.1016/j.ijrefrig.2021.05.028.

Abstract

Use of zeotropic blends in the dedicated mechanical subcooling system of a CO_2 refrigeration system was suggested as a possible improvement due to matching of evaporating temperature with CO_2 temperature profile during subcooling. This work has verified this possibility and has determined theoretically the best performing compositions of R-600, R-32 and CO_2 with the base fluid R-152a. Then, the mixtures have been tested experimentally in a lab-test bench for constant heat load temperature for three heat rejection temperatures (25.1, 30.3 and 35.1ºC). Optimum conditions are measured (subcooling degree and heat rejection) and a COP increase of 1.4% has been obtained. The work, for the optimum conditions, analyses the operating parameters of the cycles and focus specially on the thermal parameters of the subcooler. It has been verified that the use of zeotropic mixtures allows to reduce irreversibilities in the cycle, as pointed out theoretically by Dai et al. (2018).

Keywords

CO_2, mechanical subcooling, R-152a, zeotropic, refrigeration

Chapter 9. Experimental evaluation of zeotropic refrigerants in a dedicated mechanical subcooling system in a CO_2 cycle

9.1. Introduction

Subcooling has been recognised during the last years as a useful technology to enhance the performance of refrigeration cycles. Subcooling, as reviewed by Park et al. (2015) for subcritical cycles, consists in chilling the liquid at the exit of the condenser, thus incrementing the refrigerating effect and, in general, improving the coefficient of performance. However, when subcooling is used in transcritical systems the benefits of this method are taken to an extreme, as analysed by Llopis et al. (2018). In transcritical cycles the decoupling between pressure and temperature in the supercritical region makes it possible to reduce the enthalpy of the refrigerant at the inlet of the first expansion stage and at the same time to cut down the optimum heat rejection pressure. The combination of both outcomes increases the refrigerating effect and at the same time reduces the compression ratio and thus diminishes the power consumption of the compressor, resulting in large increments on capacity and COP. Specifically, using internal heat exchangers increments up to 12% in COP have been measured (Torrella et al., 2011), using economizers up to 21% (Cavallini et al., 2005) and using thermoelectric subcoolers up to 9.9% (Sánchez et al., 2020).

Concretely, one of the most appealing methods is the subcooling based on an external vapour compression cycle, known as dedicated mechanical subcooler (DMS) (Bertelsen and Haugsdal, 2015; Llopis et al., 2015). In this case the subcooling is provided at the exit of the condenser/gas-cooler using an auxiliary vapour compression cycle with a heat exchanger (subcooler) where a different refrigerant evaporates. The main characteristic of this system is that both cycles, the main and the auxiliary, perform heat rejection at the same temperature level. Initial experimental tests in single-stage plants measured capacity and COP improvements of 55.7% and 30.3% respectively using R-1234yf as refrigerant in the DMS (Llopis et al., 2016) only with the optimization of the heat rejection pressure. Later, with an updated version of the plant and using R-152a in the DMS (Nebot-Andrés et al., 2021), they demonstrated the existence of optimum working parameters and determined them, heat rejection pressure and subcooling degree, which are the two main variables to control in this cycle. In relation to the application of the DMS to CO2 booster systems, authors have only found the experimental work of Bush et al. (2017), who tested a lab-scale plant with R-134a in the DMS, measuring a COP improvement of 9.5%. Nonetheless, the use of the DMS with booster systems has been analysed with different approaches (Bush et al., 2018; Catalán-Gil et al., 2019; Catalán-Gil et al., 2020; D'Agaro et al., 2020; Gullo et al., 2016). The general conclusion of these investigations is that the application of the DMS cycle to booster systems is as more beneficial as higher the heat rejection temperature (or environment temperature) is. In fact, Catalán-Gil et al. (2019) predicts, for a medium-sized supermarket, annual reductions of electricity consumption between 2.9 to 3.4% in

warm regions and from 3.0 to 5.1% in hot zones. In addition, Dai et al. (2019) have also verified from a theoretical approach that the DMS system is also useful to improve the performance of heat pumps for residential heating, with predicted COP increments up to 24.4% (Dai et al., 2020).

The mentioned researches have performed the evaluation of the cycles using pure fluids as refrigerants in the DMS. As Dai et al. (2017) and Nebot-Andrés et al. (2017) point out, the optimum subcooling degree in CO_2 transcritical cycles is relatively high, reaching values as high as 16.5ºC (to=5ºC, tenv=30ºC). This large subcooling implies a poor temperature match between CO_2 and the refrigerant when a pure fluid is used as refrigerant in the subcooler. It implies the operation at a low evaporation temperature in the DMS cycle and thus a reduction of the overall thermal efficiency of the cycle combination. In an attempt to enhance even more the combination of a DMS and a transcritical CO_2 cycle, Dai et al. (2018) launched a hypothesis about the use of zeotropic refrigerant mixtures with matching glide in the DMS cycle, to reduce the temperature difference in the subcooler and thus to improve the performance of the combination. With a thermodynamic model with pressure dependent overall efficiencies of the compressors and using Refprop 9.1 (Lemmon et al., 2013), they evaluated the performance of zeotropic binary combinations in the DMS. They selected R-32 as based fluid and then evaluated theoretically mixtures with R-290, R-1234yf, R-152a, R-1234ze(E), R-600a and R-1234ze(Z). They determined the optimum working conditions for each refrigerant mixture and concluded that theoretically the COP of a DMS-CO_2 cycle can be improved, and that the optimum heat rejection pressure is further reduced compared to the case of a pure refrigerant. In Dai's study they found that the mixture R-32 with R-152a promised the best results in comparison with the use of R-152a as pure fluid, reaching an increment in COP of about 6.5%. However, Dai's hypothesis has not been verified experimentally for the moment, to the best knowledge of the authors.

Accordingly, this work aims to verify Dai's hypothesis, that is, to corroborate that the use of zeotropic refrigerants in the DMS brings about increments in COP and reductions of heat rejection pressure. This evaluation, to the best knowledge of the authors has not been performed experimentally yet. To accomplish it, first we have adapted Dai's thermodynamic model with the newest version of Refprop 10 (Lemmon E. W. et al., 2018) and the experimental efficiency correlations of tested compressors. Then, we have selected the best performing binary mixtures using R-152a as reference fluid. And finally, using an available test bench (Llopis et al., 2016), three zeotropic mixtures have been evaluated in the DMS taking R-152a as reference for three heat rejection levels and one evaporating condition. For the optimum conditions, it has been verified that Dai's hypothesis is true, but that there are different trends that must be considered.

Thus, this work discusses the experimental evaluation of Dai's hypothesis, quantifies the improvement, and points out the aspects that must be considered for future implementations of the DMS cycle.

9.2. Thermodynamic selection of zeotropic blends

9.2.1. Thermodynamic model

To select the binary mixtures for the experimental evaluation, the thermodynamic model suggested by Dai et al. (2018) has been adapted to the existing experimental plant (Figure 9.2). The first modification is the introduction in the model of the overall efficiencies of the compressors, which were obtained from experimental campaigns. Eq. (9.1) corresponds to the efficiency of the CO_2 compressor (Sánchez et al., 2014) and Eq. (9.2) to the DMS compressor working with R-1234yf (Llopis et al., 2016).

$$\eta_{G,CO2} = 0.736 - 0.052 \cdot k \tag{9.1}$$

$$\eta_{G,DMS} = 0.632 - 0.037 \cdot k \tag{9.2}$$

Then, the simulating conditions were adapted to the known performance of the plant, they being:

- Approach temperature in gas-cooler of 1.5K, since the plant is a water-to-water system.
- Approach temperature in subcooler of 5K.
- Approach temperature in the DMS condenser of 8K.
- DMS condenser subcooling degree of 2K.
- Superheating degree in CO_2 evaporator of 10K and in subcooler of 6K.

Finally, using the model, the COP of the CO_2 transcritical cycle with the DMS system (Eq. (9.3)) was optimized in terms of subcooling degree and heat rejection pressure at a water inlet temperature to the gas-cooler and DMS condenser of 35ºC and at an evaporating temperature of -14ºC, which were the experimental conditions with the R-152a evaluation (Nebot-Andrés et al., 2021).

$$COP = \frac{\dot{Q}_o}{P_{C,CO2} + P_{C,DMS}} \tag{9.3}$$

The optimization covered binary mixtures of R-152a with R-32, R-600 and CO_2 in steps of 10% of mass fraction variation. For each fluid and at each operating condition, an optimization to find the best combination of gas-cooler pressure and subcooling degree was performed, with the aim to quantify the best energy efficiency. The COP at such conditions is named 'optimum COP'. Refprop 10 was used to evaluate the thermophysical properties of the fluids (Lemmon E. W. et al., 2018).

9.2.2. Theoretical results

Figure 9.1 summarizes the optimum overall COP values with the different evaluated refrigerant mixtures at a water inlet temperature of 35ºC and an evaporating level of -14ºC. With R-152a the maximum COP reaches 1.527, whereas for the mixtures it varies depending on the R-152a mass fraction. First, it needs to be mentioned that for the existing plant and for the mixture R-152a/R-32 the COP does not present a maximum value, as observed in the theoretical results of Dai et al. (2018); and furthermore, this binary mixture does not overperform the base fluid. Second, the mixture of R-152a/CO_2 presents a maximum value, but lower in terms of efficiency to the base fluid. Finally, the unique binary combination that offers COP improvements in relation to the base fluid is R-600/R-152a, which presents a maximum at 1.534. Thus, at least with one mixture the theoretical model indicates that there is room for improvement.

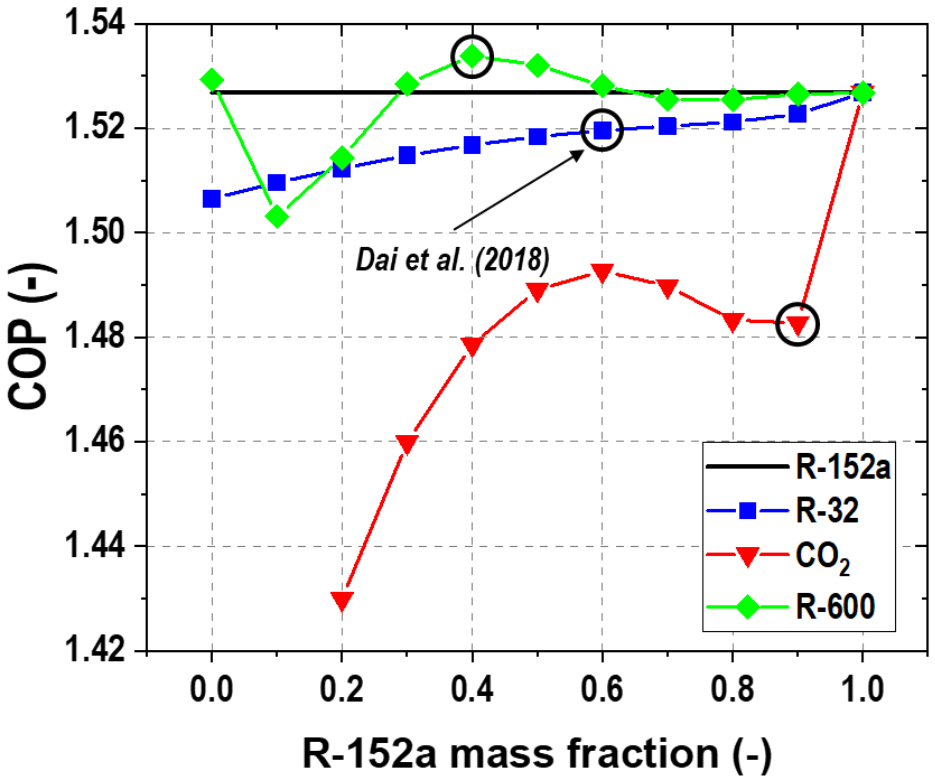

Figure 9.1. Optimum theoretical COP at t_o=-14ºC and $t_{w,in}$=35ºC, as a function of R-152a mass fraction.

9.2.3. Selected refrigerant mixtures

According to the simulations, we decided to test experimentally three binary mixtures in the DMS, whose main characteristics are reflected in Table 9.1, obtained for a CO_2

evaporation temperature of -14ºC, a CO_2 condensing temperature of 50ºC, RU = 5K and SUB=2K.

- R-152a: Selected as the reference fluid for the DMS, since it was completely tested in a previous investigation (Nebot-Andrés et al., 2021).
- R-600/R-152a [60/40%]: it was selected from the theoretical simulation (Figure 9.1) as the best performing mixture. It was prepared in our lab using n-butane with purity of 99.9% and R-152a at 99.9%, with an uncertainty in the mass composition below 0.1%. This fluid presents lower phase-change temperatures than R-152a, 18% higher specific volume, 14% reduced volumetric cooling capacity, 2% lower COP_{DMS} and a moderate effective glide in the subcooler of 5.1K.
- R-152a/R-32 [60/40%]: Although it does not obtain good theoretical results, it was considered as suggested by (Dai et al., 2018), since it was the best proportion for the combination of R-152a and R-32 in their study. Presence of R-32 increases the phase-change temperatures, the suction volume is 31% lower, the COP_{DMS} is similar and it presents 5.9K effective glide in the evaporator. The mixture was prepared in the lab with a mass uncertainty below 0.1%.
- R-152a/CO_2 [90/10%]: Finally, although not obtaining good results, this mixture was selected to investigate the effect of using a high-effective-glide fluid in the subcooler. Proportion of CO_2 was limited to 10% to be able to operate with the existing plant. In this case, with 12.3K glide in the subcooler, the mixture presents 35% higher volumetric cooling capacity, 3% higher COP_{DMS} and 17% reduced specific suction volume. The mixture was prepared in the lab using CO_2 with 99.9% purity. The uncertainty of the composition is below 0.1%.

Mixture preparation was made in our lab using high purity fluids. Composition uncertainty is below 0.1% in mass.

As mentioned above all the mixtures have been simulated in the theoretical model using Refprop 10 using the standard mixing coefficients, which could lead to uncertainty in evaluating thermophysical properties since they are new defined mixtures. The model, therefore, is not able to supply the necessary accuracy to define the exact behaviour of the mixtures in the system giving rise to the need of an experimental approach.

9.3. Experimental test bench

9.3.1. Test bench description

To evaluate the zeotropic binary mixtures a research plant previously built was used (Figure 9.2). This plant is composed of a single-stage CO_2 compression cycle, with a double-stage expansion system, that incorporates brazed-plate subcooler (0.576 m^2). Both, back-pressure and expansion valves are electronic and allow controlling the heat rejection pressure and the degree of superheat in the evaporator. The subcooling is provided coupling thermally another single-stage vapour compression system through the subcooler, in which the DMS refrigerant evaporates. This cycle is composed of a semi-hermetic compressor (4.06 $m^3 \cdot h^{-1}$ at 1450 rpm), a shell-and-tube condenser and an electronic expansion valve that is customized for each refrigerant.

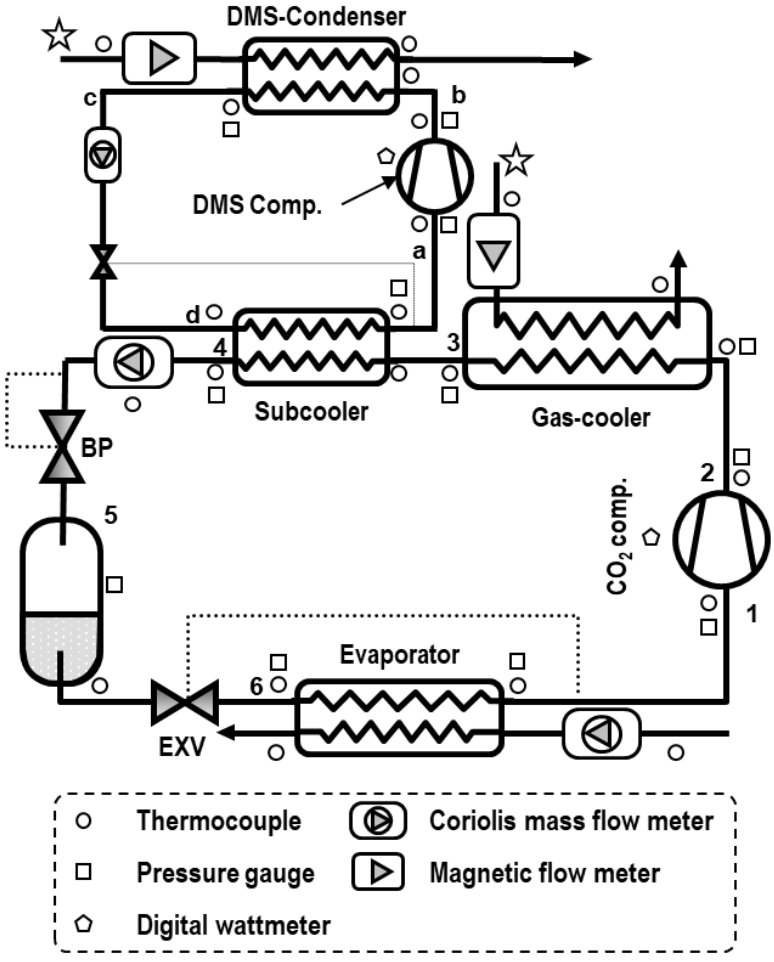

Figure 9.2. Scheme of the experimental test bench.

Heat dissipation in gas-cooler and DMS condenser is performed with a water loop, allowing the volumetric flow and inlet temperature to be controlled. The heat load is provided with a loop working with a propylene-glycol mixture, also allowing to regulate the volumetric flow and inlet temperature.

The plant is fully instrumented with pressure gauges, thermocouples, Coriolis and volumetric flow meters and digital wattmeters. A complete description of the plant and measurement system is detailed in Nebot-Andrés et al. (2021) work.

9.3.2. Experimental procedure

The experimental tests were conducted in steady-state conditions according to the following constraints:

- Heat rejection: system was evaluated for all the mixtures at three water dissipation temperatures of 25.1, 30.3 and 35.1ºC. This temperature was warranted (±0.2K) at the inlet of the DMS condenser and at the inlet of the gas-cooler (see stars in Figure 9.2). The volumetric flow of water was of 1.16 $m^3 \cdot h^{-1}$ at the gas-cooler and of 0.61 $m^3 \cdot h^{-1}$ at the DMS condenser.
- Heat load: the plant was tested only at one evaporating condition, that fixed using an inlet temperature of the glycol-mixture in the evaporator at -1.2ºC ± 0.2K, with constant volumetric flow rate of 0.71 ± 0.02 $m^3 \cdot h^{-1}$.
- Heat rejection pressure: it was regulated with the electronic back-pressure using an own PID controller implemented in the monitoring system.
- Subcooling degree: the subcooling degree in the subcooler was regulated with speed variation of the DMS compressor. The CO_2 compressor was always kept at nominal speed (1450rpm).
- Degree of superheat: In the CO_2 evaporator 10K and in subcooler 5K were maintained.

In order to obtain the optimum conditions of the subcooled CO_2 transcritical cycle, the plant was subjected to optimization of heat rejection pressure and subcooling degree with the method proposed by Nebot-Andrés et al. (2020). The optimum COP value was obtained from cooling capacity calculation, Eq. (9.4), and the direct measurements of compressor power consumption, according to Eq.(9.3). In Figure 9.3, it can be observed the optimization process as function of gas-cooler pressure and subcooling degree (Eq. (9.5)), where the black points correspond to the experimental measurements. The optimum conditions determination ended when the COP value from a point to another changed less than 1%.

$$\dot{Q}_o = \dot{m}_{CO2} \cdot \left(h_{O,out} - h_{exp}\right) \tag{9.4}$$

$$SUB = t_{sub,in} - t_{sub,out} \tag{9.5}$$

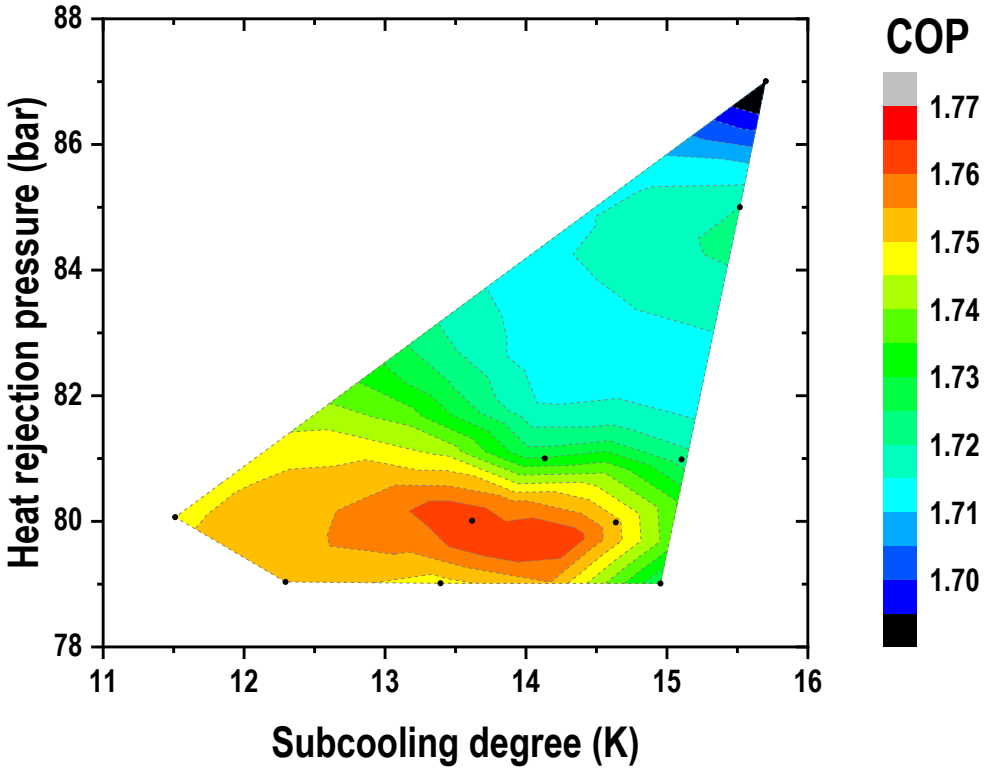

Figure 9.3. Experimental optimization of CO_2 – R600/R152a [60/40] at $t_{w,in}$=30.3ºC.

9.3.3. Data validation

Considering the calibrated accuracy of the measurement devices, which are described in the work of Nebot-Andrés et al. (2021), the uncertainties of cooling capacity, Eq. (9.4), and COP, Eq.(9.3), were evaluated using Moffat's method (1985), reaching maximum uncertainties of 0.84% and 0.95%, respectively. Furthermore, the heat transfer balance in subcooler was considered to check experimentally the consistency of measurements and to contrast that the evaluation of thermodynamic properties of mixtures with Refprop does not introduce large computation errors. Table 9.2 reflects the percentage deviation between the heat transferred by CO_2 and the mixture in the subcooler, reaching maximum deviations of 3.7%, which are considered good for the purpose of this investigation.

9.4. Results

Although the experimental campaign covered multiple steady-state conditions for each external condition, at different heat rejection pressures and different subcooling degrees, this section focuses only on the optimum conditions.

9.4.1. Optimum conditions

Optimum conditions, in terms of COP, Eq.(9.3), for the three heat rejection levels and for the four refrigerants used in the DMS cycle are summarized in Figure 9.4. It can be observed that a zeotropic mixture is able to overperform the reference fluid (R-152a). Concretely, the energy improvement achieved by the mixture R-600/R-152a [60/40] is between 1.1 to 1.4% higher than with R-152a. However, the two other refrigerant blends present COP reductions. R-152a/R-32 [60/40] mixture presents an overall COP decrease between 4.1 to 5% and the R-152a/CO_2 [90/10] mixture a COP cut between 5.6 to 7.9%.

Although the test conditions are different, the measured trends (Figure 9.4) coincide with the theoretical simulations summarized in Figure 9.1. Thus, it is demonstrated experimentally that it is possible to improve the performance of a dedicated mechanical subcooling system by the use of a zeotropic mixture in the auxiliary cycle, as suggested by Dai et al. (2018).

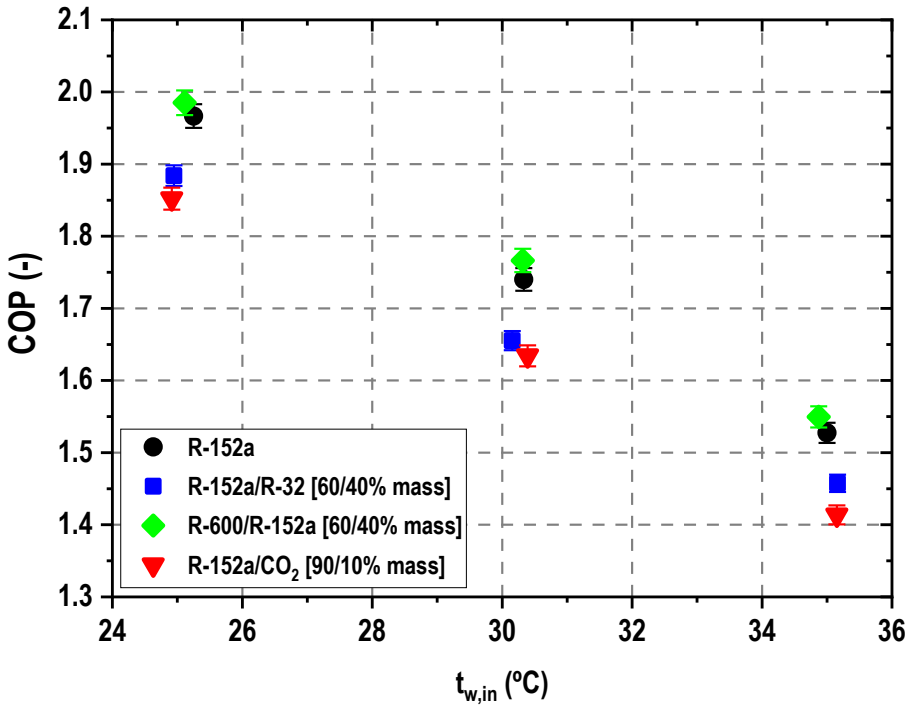

Figure 9.4. Optimum experimental COP at $t_{g,in}$ = -1.25ºC.

At optimum conditions (Figure 9.4), the partial contribution to the cooling capacity of each refrigeration cycle is presented in Figure 9.5, where $\dot{Q}_{sub}$ represents the enhancement of capacity due to the subcooling, Eq.(9.6), and $\dot{Q}_{base}$ the capacity provided by the CO_2 cycle, Eq. (9.7).

$$\dot{Q}_{sub} = \dot{m}_{CO2} \cdot \left(h_{sub,out} - h_{gc,out}\right) \tag{9.6}$$

$$\dot{Q}_{base} = \dot{Q}_O - \dot{Q}_{sub} \tag{9.7}$$

On the one side, as it can be observed in Figure 9.5, the contribution corresponding to the base cycle is similar for each test condition between the different DMS refrigerants. Small variations of this parameter are linked to the different optimum heat rejection pressures, which are lower as higher the subcooling degree is (see Table 9.2). At reduced heat rejection pressures, the capacity provided by the CO_2 itself is lower. However, large differences are found in the partial contribution to the cooling capacity provided by the subcooler, Eq.(9.6). For the mixture R-152a/R-32 [60/40] this contribution is between 16.2 and 41.1% higher than with the use of R-152a at optimum conditions, for R-600/R-152a [60/40] ranges between -5.1 to -7.1% and for R-152a/CO_2 [90/10] from 0.4 to 9.1%. These variations are not directly correlated with the VCC_{DMS} parameter (Table 9.1). Nonetheless, it is important to note that the use of the DMS cycle always intensifies the capacity provided by the cycle.

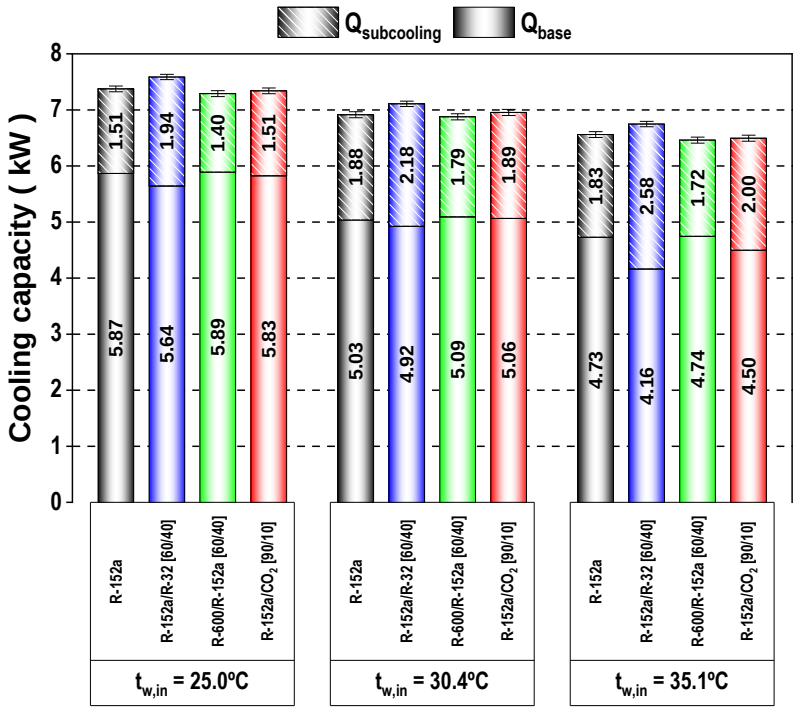

Figure 9.5. Cooling capacity at optimum condition at $t_{g,in}$ = -1.25ºC.

On the other side, the contribution to the power consumption of each compressor is presented in Figure 9.6. It is observed that the power consumption of the CO_2 compressor remains similar between all the refrigerants unlike R-152a/R-32 [60/40] with $t_{w,in}$=35.1°C that, due to the large optimum subcooling degree, allows the CO_2 cycle to work at a lower optimum pressure; on the contrary there are large differences at all conditions with the auxiliary compressor. In this case, refrigerants with high VCC_{DMS} (R-152/R-32 and R-152a/CO_2) show greater cooling capacity and thus have larger power consumption in the DMS compressor. It is worth focusing on the R-600/R-152a [60/40] mixture, that presents a very low power consumption in the DMS compressor, it being between 8.9 and 11.2% in relation to the power absorbed by the CO_2 one and between 15.2 and 21.0% lower than that absorbed with the use of R-152a in the DMS cycle. The behaviour of R-600/R-152a [60/40] mixture and thus the optimum conditions when working coupled to the CO_2 cycle are bounded to the high COP_{DMS} values achieved by the mixture (Table 9.2) which are higher than the values reached with R-152a. Although theoretical COP_{DMS} are higher for R-152a than for R-600/R-152a [60/40] mixture (see Table 9.1), the experimental COP_{DMS} have an opposite trend, because the working conditions (blend phase-change temperatures) vary, as it is analysed in the following section.

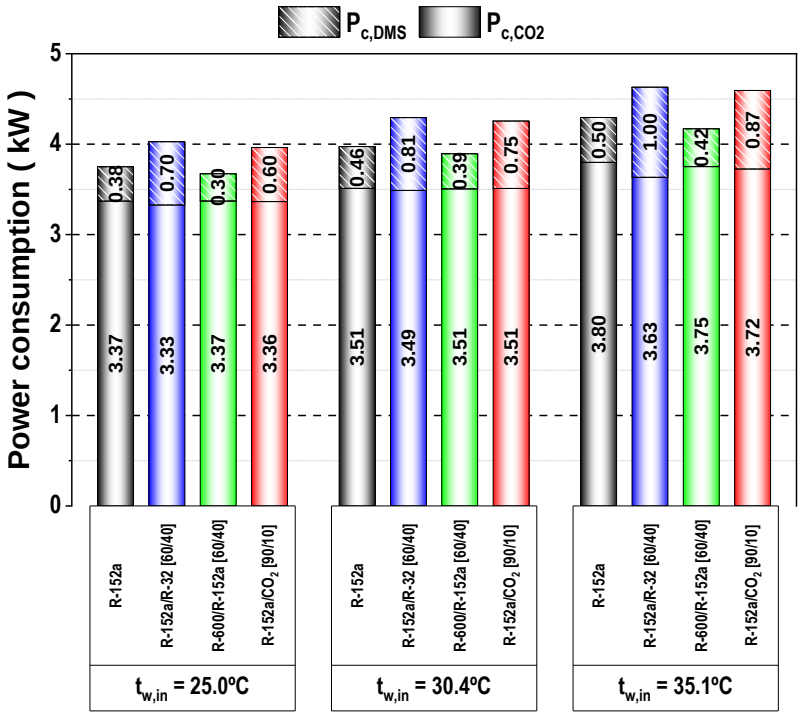

Figure 9.6. Power consumption at optimum condition at $t_{g,in}$ = -1.25ºC.

9.4.2. Operating parameters

As mentioned before, the optimum working condition of the dedicated subcooling cycle, in terms of heat rejection pressure and subcooling degree, is different between the different refrigerant blends. This section analyses closely the working conditions of each combination at dissipation water inlet temperature of 35.1ºC.

Figure 9.7 to Figure 9.10 represent the *t-s* diagram of the different refrigerants, where the estimated temperature profiles in the subcooler are highlighted. For the sake of a graphical representation, they are considered linear without affecting the conclusions of this investigation. Figure 9.11 illustrates the phase-change temperatures of the DMS refrigerant. Furthermore, Table 9.3 summarizes the key parameters of the most representative elements of the plant.

As it can be observed in Figure 9.8 to Figure 9.10, the use of a zeotropic refrigerant mixture in the DMS cycle introduces a temperature difference through the phase-change temperature. During condensation the temperature decreases, whereas during the evaporation increases. The temperature change or effective glide in the evaporator, Eq. (9.8), depends upon the components of the blend.

$$Glide_{e,O,DMS} = t_{O,v,DMS,out} - t_{O,DMS,in} \quad (9.8)$$

Analysing results of Table 9.3, it is observed that the mixture R-600/R-152a presents the highest effective glide in the subcooler. R152a/CO_2, whose total glide is higher, does not have a large effective glide in the subcooler, since the main change in temperature during the phase-change is produced at lower vapour quality conditions (see isobar in Figure 9.10), which are out of the operation of the subcooler.

The best temperature match between R-600/R-152a [60/40] and the CO_2 temperature profile along the subcooler influence the rest of parameters of the subcooler (Table 9.3). The thermal effectiveness of subcooler, Eq. (9.9), reaches even higher values than with the use of a pure fluid; the pinch at the exit/inlet of the subcooler, Eq. (9.10), reaches lower values than with R-152a; and the logarithmic mean temperature difference, Eq. (9.11), also reaches lower values than with the reference fluid. For the rest of the blends, which do not have a good temperature match with CO_2, the parameters of the subcooler are worse than with the use of R-152a. Thus, as suggested by Dai et al. (2018), if the refrigerant mixture has a good matching glide with CO_2 temperature profiles, the performance of the system can be improved. It should be noted that the subcooler size was fixed, thus, if the subcooler is resized for each mixture the results could change.

In relation to working temperatures (Figure 9.11), it can be observed that for the blends R-152a/R32 and R-152a/CO_2 the difference between condensation and evaporation temperature increases due to the low thermal performance of the subcooler (Table 9.3). However, for the mixture R-600/R-152a this difference decreases, and what is more important, the thermal improvement in the subcooler makes the evaporating temperature in the subcooler to be higher and thus, it allows the DMS cycle to work with higher COP_{DMS} values, resulting in a net increment of the COP of the combination, as seen in Figure 9.4.

$$\varepsilon_{sub} = \frac{t_{gc,out} - t_{sub,out}}{t_{gc,out} - t_{O,DMS,in}} \tag{9.9}$$

$$\Delta t_{sub} = t_{DMS,out} - t_{O,DMS,in} \tag{9.10}$$

$$\Delta t_{lmtd} = \frac{\left(t_{DMS,out} - t_{O,DMS,in}\right) - \left(t_{gc,out} - t_{O,v,DMS,out}\right)}{ln\left(\frac{t_{DMS,out} - t_{O,DMS,in}}{t_{gc,out} - t_{O,v,DMS,out}}\right)} \tag{9.11}$$

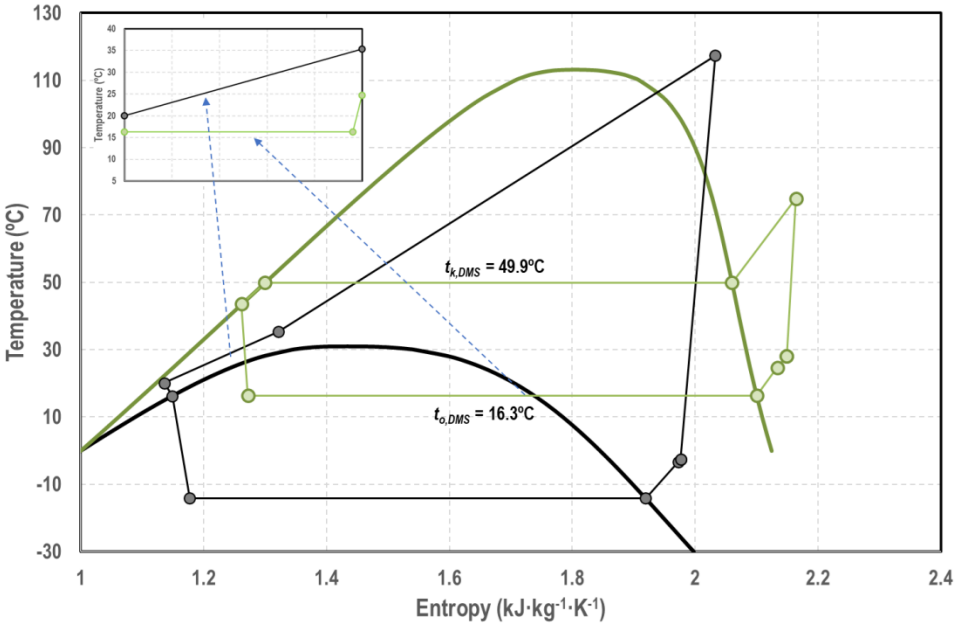

Figure 9.7. t-s diagram of CO_2 – R152a at $t_{w,in}$=35.1ºC and $t_{g,in}$ =-1.25ºC.

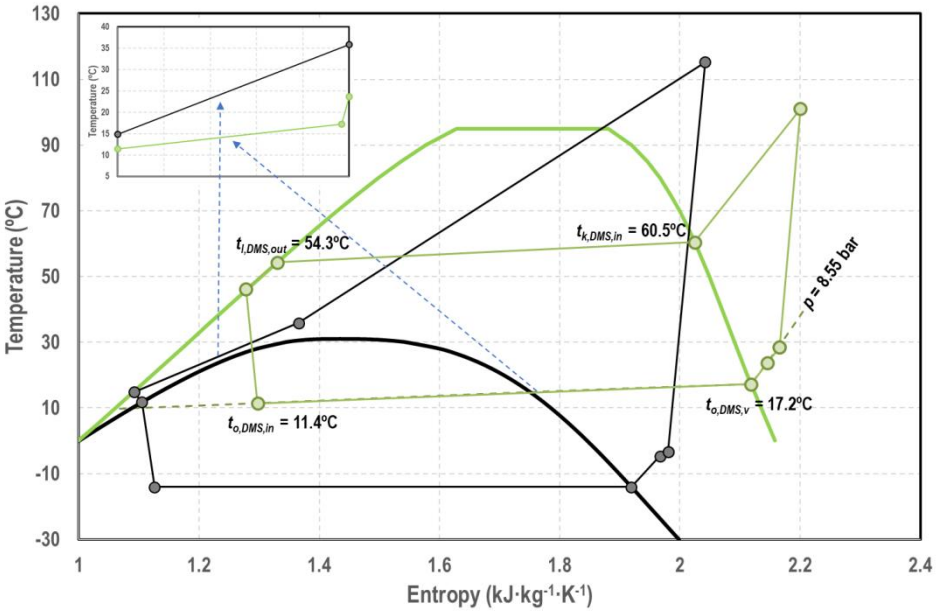

Figure 9.8. t-s diagram of CO_2 – R152a/R-32 [60/40] at $t_{w,in}$=35.1ºC and $t_{g,in}$ =-1.25ºC.

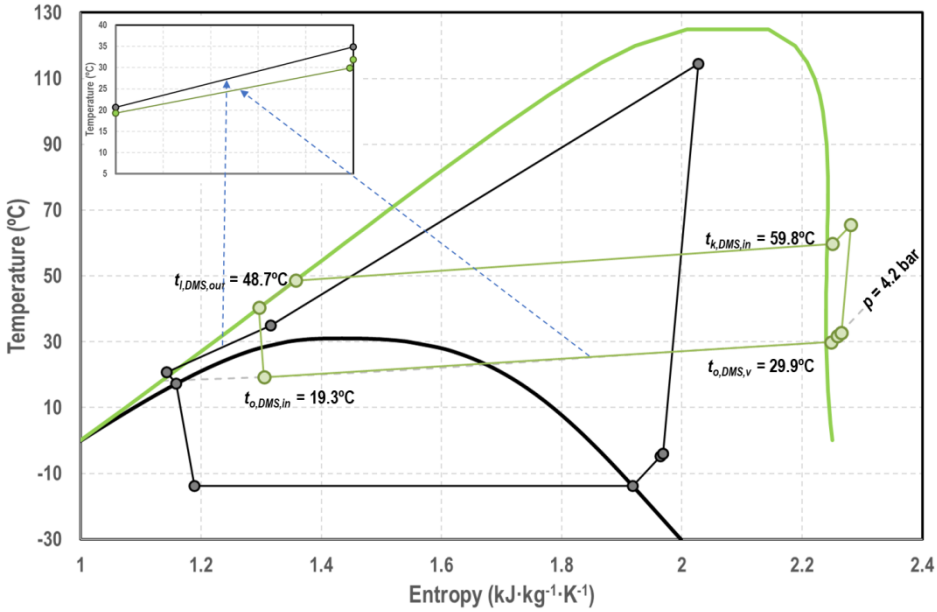

Figure 9.9. t-s diagram of CO_2 – R-600/R-152a [60/40] at $t_{w,in}$=35.1ºC and $t_{g,in}$ =-1.25ºC.

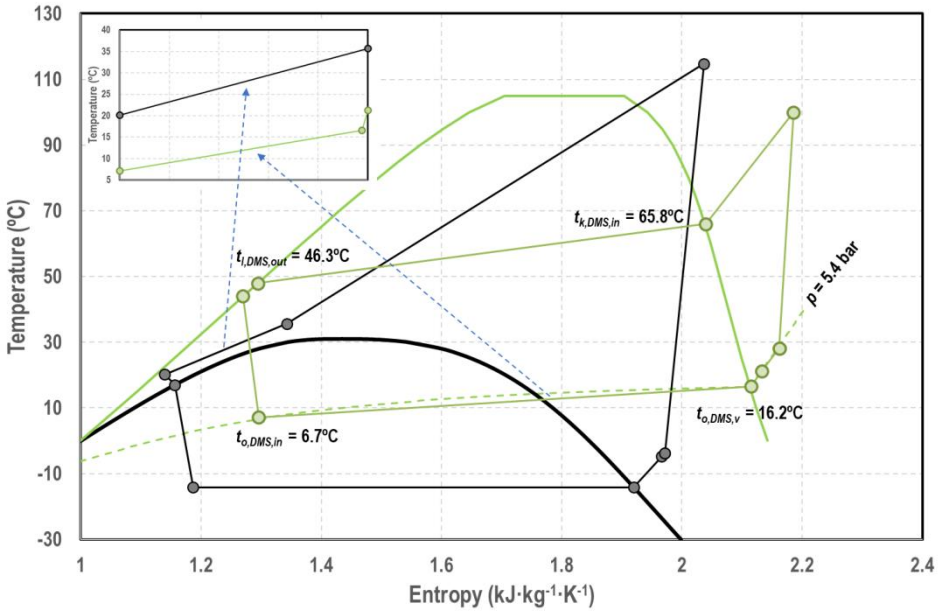

Figure 9.10. t-s diagram of CO_2 – R-152a/R-CO_2 [90/10] at $t_{w,in}$=35.1°C and $t_{g,in}$ =-1.25°C.

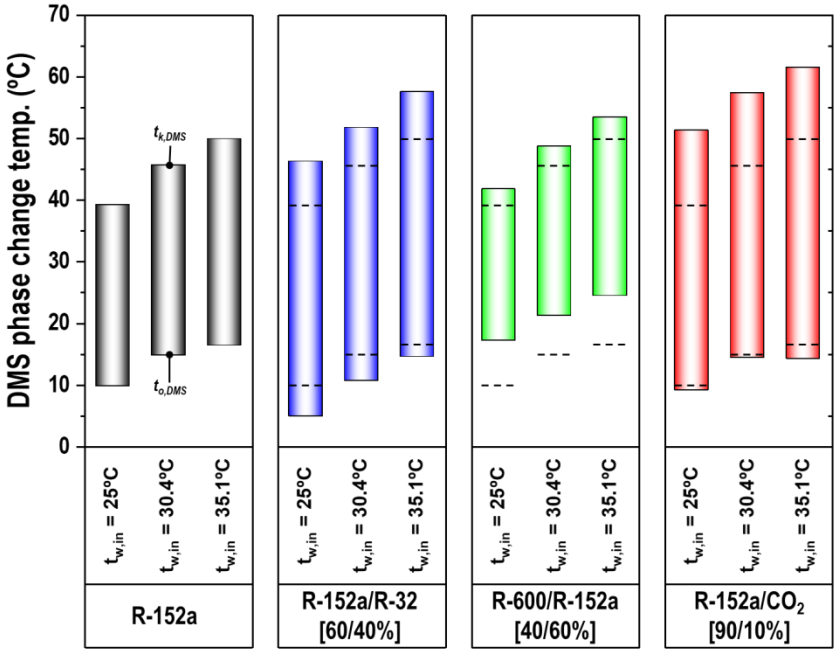

Figure 9.11. Phase change temperatures of DMS cycle at optimum conditions at $t_{g,in}$=-1.25°C.

Finally, to illustrate the energy improvement achieved using zeotropic blends in the DMS cycle, irreversibilities in subcooler, Eq. (9.12) have been evaluated. They are presented in a normalized form in Figure 9.12. To normalize the irreversibilities, total exergy destruction in the subcooler has been divided by the cooling capacity of the CO_2 cycle, Eq. (9.4), and by the death state temperature, which has been considered to be -14ºC.

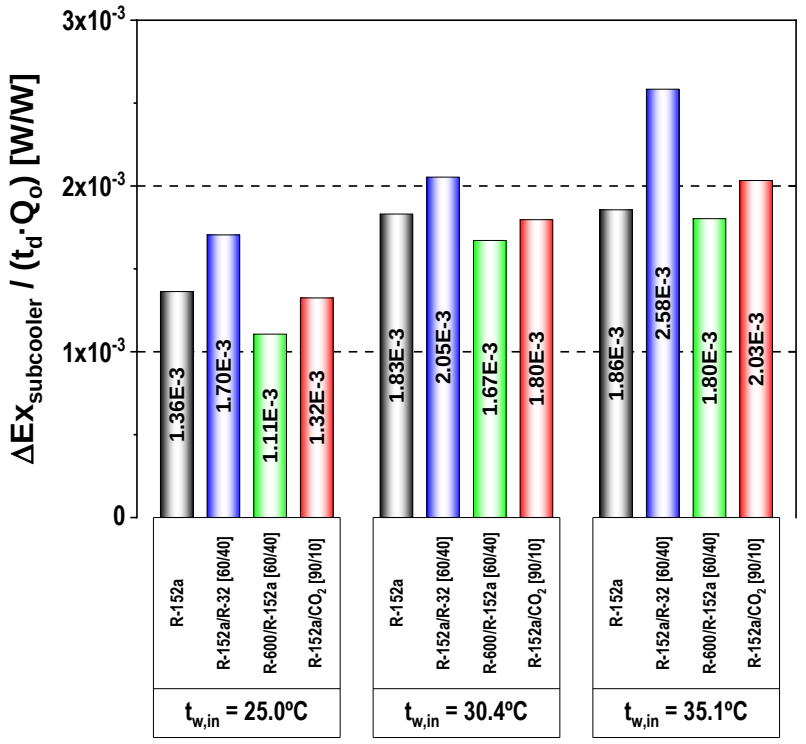

Figure 9.12. Normalized exergy destruction in subcooler at $t_{g,in}$=-1.25ºC.

$$\Delta\dot{E}_{X,sub} = t_d \cdot \left[\dot{m}_{CO2} \cdot \left(s_{sub,out} - s_{sub,in}\right) + \dot{m}_{DMS} \cdot \left(s_{DMS,in} - s_{DMS,out}\right)\right] \quad (9.12)$$

Figure 9.12 reflects that a good matching glide with CO_2 temperature profile in subcooler allows to reduce the irreversibilities in the subcooler. In this case, the blend R-600/R-152a [60/40] presents a reduction of irreversibilities in relation to R-152a from -2.9 to 18.9%. In addition, also mixture R-152a/CO_2 [90/10] reduces irreversibilities in some operating conditions.

9.5. Conclusions

In this work the possibility to enhance the performance of a transcritical CO_2 refrigeration plant using a dedicated mechanical subcooling system with zeotropic refrigerant mixtures has been addressed theoretically and experimentally.

Using Dai et al. (2018) model adapted to an existing test plant, the performance of three blends composed of R-32, R-600 or CO_2 with the base fluid R-152a has been evaluated. It has been observed that, theoretically, it is possible obtain higher COP values in relation to the use of pure fluids. However, trends presented by Dai et al. (2018) have not been seen in the simulations. The difference, which cause cannot be defined, could be associated to the different used overall compressor efficiencies and with the update of Refprop, which differ from the previous works. Theoretical simulation has identified the blend R-600/R-152a [60/40%] as the best performing one, with theoretical COP improvements up to 0.46%.

Three refrigerant blends, R-152a/R32 [60/40%], R-600/R-152a [60/40%] and R-152a/CO_2 [90/10%] have been tested experimentally against the operation with R-152a as refrigerant in the dedicated subcooling system. The evaluation was made at fixed conditions of the secondary fluids and covered three heat rejection levels, achieved varying the water inlet temperature to gas-cooler and DMS condenser (25.1, 30.3 and 35.1ºC). Experimental campaign has identified the optimum conditions, in terms of subcooling degree and heat rejection pressure, of the plant.

It has been verified that the mixture R-600/R-152a [60/40%] is able to enhance the COP of the plant, with COP increments between 1.1 and 1.4%. In addition, the mixture R-152a/CO_2 [90/10%], which has good matching temperature profiles in the subcooler, could also improve the performance of the plant if the subcooler was resized. However, the other mixtures did not show good performance. The experimental results indicated that the improvements are higher for blends with low volumetric cooling capacity. At optimum conditions, these mixtures work with a moderate subcooling degree and have low power consumption in the auxiliary compressor. Furthermore, as suggested by Dai et al. (2018), the mixtures which effective glide matches with the CO_2 temperature evolution in the subcooler, enhance the thermal performance of the subcooler. Consequently, the evaporating level in the subcooler with the mixture can be higher than with the pure fluid and enhance the performance of the auxiliary cycle and thus of the cycle combination.

Finally, it needs to be mentioned that the use of zeotropic blends in the subcooler allows reducing the irreversibilities in this heat exchanger, which agrees with Dai's work.

9.6. Acknowledgements

Authors gratefully acknowledge the Ministry of Science, Innovation and Universities of Spain (RTI2018-093501-B-C21) and Ministerio de Educación, Cultura y Deporte (Spain) grant FPU16/00151 for financing this research work. The research leading to these results has also received funding from the MIUR of Italy within the framework of the

PRIN2017 project «The energy flexibility of enhanced heat pumps for the next generation of sustainable buildings (FLEXHEAT)», grant 2017KAAECT.

9.7. Nomenclature

BP	Back pressure valve
COP	coefficient of performance
$\dot{E}_X$	exergy, kW
Glide	phase-change temperature difference at constant pressure, K
GWP	global warming potential at 100 years
h	specific enthalpy, kJ·kg^{-1}
h_{fg}	latent heat of phase-change, kJ·kg^{-1}
k	compression ratio
$\dot{m}$	refrigerant mass flow, kg·s^{-1}
M	molar mass, g·mol^{-1}
p	pressure, bar
P_C	compressor power consumption, kW
$\dot{Q}_o$	cooling capacity of the CO_2 cycle, kW
RU	superheating degree, K
s	specific entropy, kJ·kg^{-1}·K^{-1}
SUB	CO_2 subcooling degree in subcooler, K
t	temperature, ºC
v	specific volume, m^3·kg^{-1}
V	volumetric flow rate, m^3·kg^{-1}
VCC	volumetric cooling capacity, kW·m^{-3}

Greek symbols

η_G	compressor overall efficiency

ε thermal effectiveness

Subscripts

base refers to CO_2 cycle without subcooling

d death state level

DMS refers to the dedicated mechanical cycle

e effective

CO2 refers to the CO_2 cycle

g refers to glycol as secondary fluid in CO_2 evaporator

gc gas-cooler

in inlet

K refers to condensing level

l refers to saturated liquid

lmtd logarithmic mean temperature difference

O refers to the evaporating level

out outlet

sub subcooler

v refers to saturated vapour

w refers to water as secondary fluid for heat rejection

9.8. References

Bertelsen, S.K., Haugsdal, S.B., 2015. Design and measurement of a CO2 refrigeration system with integrated propane subcooler at high air temperature operations, Department of Energy and Process Engineering. Norwegian University of Science and Technology, Trondheim, Norway.

Bush, J., Aute, V., Radermacher, R., 2018. Transient simulation of carbon dioxide booster refrigeration system with mechanical subcooler in demand response operation. Science and Technology for the Built Environment 24, 687-699.

Bush, J., Beshr, M., Aute, V., Radermacher, R., 2017. Experimental evaluation of transcritical CO2 refrigeration with mechanical subcooling. Science and Technology for the Built Environment, 1-13.

Catalán-Gil, J., Llopis, R., Sánchez, D., Nebot-Andrés, L., Cabello, R., 2019. Energy analysis of dedicated and integrated mechanical subcooled CO 2 boosters for supermarket applications. International Journal of Refrigeration 101, 11-23.

Catalán-Gil, J., Nebot-Andrés, L., Sánchez, D., Llopis, R., Cabello, R., Calleja-Anta, D., 2020. Improvements in CO2 booster architectures with different economizer arrangements. Energies 13.

Cavallini, A., Cecchinato, L., Corradi, M., Fornasieri, E., Zilio, C., 2005. Two-stage transcritical carbon dioxide cycle optimisation: A theoretical and experimental analysis. International Journal of Refrigeration 28, 1274-1283.

D'Agaro, P., Coppola, M.A., Cortella, G., 2020. Effect of dedicated mechanical subcooler size and gas cooler pressure control on transcritical CO2 booster systems. Applied Thermal Engineering, 116145.

Dai, B., Liu, S., Li, H., Sun, Z., Song, M., Yang, Q., Ma, Y., 2018. Energetic performance of transcritical CO 2 refrigeration cycles with mechanical subcooling using zeotropic mixture as refrigerant. Energy 150, 205-221.

Dai, B., Liu, S., Sun, Z., Ma, Y., 2017. Thermodynamic Performance Analysis of CO2 Transcritical Refrigeration Cycle Assisted with Mechanical Subcooling. Energy Procedia 105, 2033-2038.

Dai, B., Qi, H., Liu, S., Ma, M., Zhong, Z., Li, H., Song, M., Sun, Z., 2019. Evaluation of transcritical CO2 heat pump system integrated with mechanical subcooling by utilizing energy, exergy and economic methodologies for residential heating. Energy Conversion and Management 192, 202-220.

Dai, B., Zhao, X., Liu, S., Yang, Q., Zhong, D., Hao, Y., Hao, Y., 2020. Energetic, exergetic and exergoeconomic assessment of transcritical CO2 reversible system combined with dedicated mechanical subcooling (DMS) for residential heating and cooling. Energy Conversion and Management 209, 112594.

Gullo, P., Elmegaard, B., Cortella, G., 2016. Energy and environmental performance assessment of R744 booster supermarket refrigeration systems operating in warm climates. International Journal of Refrigeration 64, 61-79.

Lemmon E. W., I.H., B., L., H.M., O., M.M., 2018. NIST Standard Reference Database 23: Reference Fluid Thermodynamic and Transport Properties-REFPROP, Version 10.0, National Institute of Standards and Technology.

Lemmon, E.W., Huber, M.L., McLinden, M.O., 2013. REFPROP, NIST Standard Reference Database 23, v.9.1. National Institute of Standards, Gaithersburg, MD, U.S.A.

Llopis, R., Cabello, R., Sánchez, D., Torrella, E., 2015. Energy improvements of CO2 transcritical refrigeration cycles using dedicated mechanical subcooling. International Journal of Refrigeration 55, 129-141.

Llopis, R., Nebot-Andrés, L., Cabello, R., Sánchez, D., Catalán-Gil, J., 2016. Experimental evaluation of a CO2 transcritical refrigeration plant with dedicated mechanical subcooling. International Journal of Refrigeration 69, 361-368.

Llopis, R., Nebot-Andrés, L., Sánchez, D., Catalán-Gil, J., Cabello, R., 2018. Subcooling methods for CO2 refrigeration cycles: A review. International Journal of Refrigeration 93, 85-107.

Moffat, R.J., 1985. Using Uncertainty Analysis in the Planning of an Experiment. Journal of Fluids Engineering 107, 173-178.

Nebot-Andrés, L., Catalán-Gil, J., Sánchez, D., Calleja-Anta, D., Cabello, R., Llopis, R., 2020. Experimental determination of the optimum working conditions of a transcritical CO2 refrigeration plant with integrated mechanical subcooling. International Journal of Refrigeration 113, 266-275.

Nebot-Andrés, L., Llopis, R., Sánchez, D., Catalán-Gil, J., Cabello, R., 2017. CO2 with Mechanical Subcooling vs. CO2 Cascade Cycles for Medium Temperature Commercial Refrigeration Applications Thermodynamic Analysis. Applied Sciences 7, 955.

Nebot-Andrés, L., Sánchez, D., Calleja-Anta, D., Cabello, R., Llopis, R., 2021. Experimental determination of the optimum working conditions of a commercial transcritical CO2 refrigeration plant with a R-152a dedicated mechanical subcooling. International Journal of Refrigeration 121, 258-268.

Park, C., Lee, H., Hwang, Y., Radermacher, R., 2015. Recent advances in vapor compression cycle technologies. International Journal of Refrigeration 60, 118-134.

Sánchez, D., Aranguren, P., Casi, A., Llopis, R., Cabello, R., Astrain, D., 2020. Experimental enhancement of a CO2 transcritical refrigerating plant including thermoelectric subcooling. International Journal of Refrigeration.

Sánchez, D., Patiño, J., Sanz-Kock, C., Llopis, R., Cabello, R., Torrella, E., 2014. Energetic evaluation of a CO2 refrigeration plant working in supercritical and subcritical conditions. Applied Thermal Engineering 66, 227-238.

Torrella, E., Sánchez, D., Llopis, R., Cabello, R., 2011. Energetic evaluation of an internal heat exchanger in a CO2 transcritical refrigeration plant using experimental data. International Journal of Refrigeration 34, 40-49.

Table 9.1. Selected refrigerants for experimental evaluation and ideal-single-stage cycle performance data of the DMS at t_o=-14ºC, t_k=50ºC, RU=5K and SUB=2K.

Refrigerant [mass comp.]	M ($g \cdot mol^{-1}$)	$GWP_{5,AR}$ (-)	p_o (bar)	p_k (bar)	v_{suc} ($m \cdot kg^{-1}$)	h_{fo} ($kJ \cdot kg^{-1}$)	VCC_{DMS} ($kJ \cdot m^{-3}$)	COP_{DMS} (-)	$Glide_O$ [K]	$Glide_k$ [K]
R-152a	66.1	137	4.39	11.77	0.075	291.1	3142	7.03	0.0	0.0
R-152a/R-32 [60/40%]	59.6	353	6.97	18.31	0.051	302.9	4776	6.79	5.9	6.5
R-600/R-152a [60/40%]	61.1	55	4.05	10.60	0.089	308.8	2697	6.87	5.1	5.9
R-152a/CO_2 [90/10%]	62.9	123	5.63	15.38	0.062	327.0	4257	7.25	12.3	19.9

Table 9.2. Summary of test conditions, main cycle and DMS cycle indicators at optimum working conditions.

	Test conditions				Cycle indicators				DMS cycle indicators			
	$t_{w,in}$ (°C)	$V_{w,ec,in}$ ($m^3 \cdot h^{-1}$)	$V_{w,DMS,in}$ ($m^3 \cdot h^{-1}$)	$t_{ev,in}$ (°C)	$V_{v,in}$ ($m^3 \cdot h^{-1}$)	COP (-)	Q_o (kW)	p_{ec} (bar)	SUB (K)	ε_{sub} (%)	COP_{DMS} (-)	$Q_{o,DMS}$ (kW)	$(Q_{o,DMS} - Q_{SUB})/Q_{SUB} * 100$ (%)
R-152a	25.3	1.10	0.62	-1.2	0.70	1.97	7.4	74.9	14.3	87.5	3.98	1.5	-2.6
	30.3	1.15	0.63	-1.1	0.72	1.74	6.9	79.2	14.5	85.7	4.07	1.9	-2.8
	35.0	1.19	0.61	-1.3	0.73	1.53	6.6	90.0	15.3	80.4	3.69	1.8	-3.6
R-152a/R-32 [60/40]	24.9	1.16	0.60	-1.4	0.71	1.88	7.6	74.9	20.0	82.0	2.78	1.9	-1.1
	30.2	1.15	0.62	-1.2	0.71	1.66	7.1	79.9	19.9	83.5	2.71	2.2	-3.5
	35.2	1.15	0.60	-1.3	0.71	1.46	6.7	85.8	21.0	86.0	2.59	2.6	-1.8
R-600/R-152a [60/40]	25.1	1.18	0.61	-1.2	0.72	1.99	7.3	74.9	12.5	75.0	4.65	1.4	-3.2
	30.3	1.16	0.62	-1.2	0.71	1.77	6.9	79.8	13.6	76.0	4.60	1.8	-3.2
	34.9	1.15	0.63	-1.2	0.71	1.55	6.5	89.4	14.2	78.9	4.11	1.7	-2.6
R-152a/CO_2 [90/10]	24.9	1.16	0.60	-1.2	0.71	1.85	7.3	74.9	14.0	60.7	2.53	1.5	-1.9
	30.4	1.16	0.59	-1.3	0.71	1.63	7.0	79.9	15.0	63.7	2.54	1.9	-3.3
	35.2	1.16	0.59	-1.2	0.70	1.41	6.5	87.9	15.5	57.1	2.30	2.0	-3.7

Table 9.3. Performance operating parameters of key elements at optimum conditions

	$t_{w,in}$ (ºC)	$\eta_{G,CO2}$ (-)	$\eta_{G,DMS}$ (-)	t_{CO2} (-)	t_{DMS} (-)	$Glide_{e,o,DMS}$ (K)	ε_{sub} (%)	Δt_{sub} (K)	Δt_{lmtd} (K)
R-152a	25.3	55.0	43.2	3.3	2.4	-	87.5	2.0	6.8
	30.3	54.2	49.1	3.5	2.5	-	85.7	2.4	7.4
	35.0	53.7	48.5	3.8	2.6	-	80.4	3.7	9.4
R-152a/R-32 [60/40]	24.9	54.5	45.2	3.4	3.4	5.1	67.0	9.9	16.2
	30.2	53.6	45.6	3.5	3.2	5.4	66.6	10.0	16.1
	35.2	53.3	47.9	3.7	3.2	5.6	67.9	9.9	16.5
R-600/R-152a [60/40]	25.1	54.8	30.4	3.3	2.1	10.9	87.5	1.8	2.5
	30.3	54.5	44.8	3.4	2.3	10.7	87.7	1.9	3.2
	34.9	53.5	47.1	3.8	2.3	10.6	91.0	1.4	2.8
R-152a/CO_2 [90/10]	24.9	54.6	42.4	3.3	3.6	8.4	61.1	8.9	11.5
	30.4	54.6	47.6	3.5	3.5	8.5	64.1	8.4	11.3
	35.2	53.5	49.4	3.7	3.9	7.8	57.4	11.5	15.0

Chapter 10 Experimental assessment of different extraction points for the integrated mechanical subcooling system of a CO_2 transcritical plant

Chapter 10. Experimental assessment of different extraction points for the integrated mechanical subcooling system of a CO_2 transcritical plant

10. Experimental assessment of different extraction points for the integrated mechanical subcooling system of a CO_2 transcritical plant

Chapter adapted from the paper: Nebot-Andrés, L., Calleja-Anta, D., Fossi C., Sánchez, D., Cabello, R. Llopis, R. Experimental assessment of different extraction points for the integrated mechanical subcooling system of a CO_2 transcritical plant. (2022) International Journal of Refrigeration, Available online 6 January 2022.

Abstract

Subcooling systems are positioned in recent years as one of the best solutions to improve the efficiency of transcritical CO_2 cycles. Specifically, the integrated mechanical subcooling cycle allows the improvement of these systems only using CO_2 as a refrigerant. This integrated cycle can be designed with three different architectures: extracting the CO_2 from the gas-cooler outlet, from the subcooler outlet or from the liquid tank. In this work, the three configurations are experimentally analysed and the main differences between them are studied. An experimental plant has been tested at three heat rejection levels (25.0, 30.4 and 35.1ºC) and a fixed temperature of the secondary fluid at the evaporator inlet of 3.8ºC. The results show that from an energy efficiency point of view, all the configurations have practically the same COP, with certain variations in the cooling capacity and the greatest differences in the cycles are found in the subcooler..

Keywords

Experimental comparative, subcooling, Integrated mechanical subcooling, Transcritical CO_2

Chapter 10. Experimental assessment of different extraction points for the integrated mechanical subcooling system of a CO_2 transcritical plant

Chapter 10. Experimental assessment of different extraction points for the integrated mechanical subcooling system of a CO_2 transcritical plant

10.1. Introduction

Carbon dioxide has been positioned as one of the only refrigerants that can be used in centralized commercial refrigeration, due to the restrictions imposed by F-gas (European Commission, 2014). The use of CO_2 allows direct emissions to be reduced, but its low performance at high temperatures makes indirect emissions an added problem. That is why the refrigeration sector seeks to develop technologies that improve the efficiency of classic CO_2 systems (Gullo et al., 2018; Karampour and Sawalha, 2018). These solutions go through the design of more complex plants where systems such as the parallel compressor (Nebot-Andrés et al., 2021a; Sarkar and Agrawal, 2010) or the ejector (Gullo et al., 2019; Lawrence and Elbel, 2019) are used to improve the COP of the facilities. Mechanical subcooling methods have become one of the most popular strategies in recent years for the improvement of CO_2 refrigeration cycles (Llopis et al., 2018). After the use of the internal heat exchanger (IHX) as a way of improvement of cooling capacity and COP in CO_2 transcritical cycles (Rigola et al., 2010), the use of the dedicated mechanical subcooling (DMS) became popular as a method to improve the COP and the cooling capacity of said system (Catalán-Gil et al., 2019; Cortella et al., 2021; Nebot-Andrés et al., 2021b). The DMS bases its operation on the use of an auxiliary cycle, thermally coupled to the main cycle through a heat exchanger, called subcooler. This cycle, thanks to the subcooling that it produces in the CO_2 at the outlet of the gas-cooler, manages to reduce the optimum working pressure as well as increase the specific cooling capacity (Llopis et al., 2015). On the contrary, this cycle works with a refrigerant other than CO_2. The DMS was first tested experimentally by Llopis et al. (2016) reaching increments up to 30.3% on COP compared to the base cycle even though the degree of subcooling was not optimized. Later, its optimum operation parameters were determined by Nebot-Andrés et al. (2021b).

With the aim of working with purely CO_2 cycles, the concept of integrated mechanical subcooling (IMS) was born, where the subcooling of the CO_2 at the outlet of the gas-cooler is carried out with a flow of CO_2 extracted from the main stream and evaporated through the subcooler. The most studied configuration performs this extraction from the gas-cooler exit (Nebot-Andrés et al., 2019), passing through an expansion valve and carrying out the evaporation process inside the subcooler, to be recompressed by the secondary compressor and reintroduced into the main stream. The advantage of this configuration is that only the CO_2 flow that is going to reach the evaporator is subcooled, therefore a smaller subcooler is necessary. However, it is also possible to carry out this cycle in two other configurations: extracting from the tank's liquid exit or extracting from the subcooler outlet.

Chapter 10. Experimental assessment of different extraction points for the integrated mechanical subcooling system of a CO_2 transcritical plant

As all subcooling methods working on transcritical CO_2 plants, two operating parameters must be optimized. They are the gas-cooler pressure and also the subcooling degree. The experimental determination of the optimum working conditions of the integrated mechanical subcooling was first determined by Nebot-Andrés et al. (2020). The evaluated configuration was the one with the extraction from the subcooler exit. The optimum COP values were also determined in this work. Although this configuration was analysed, the other two have never been experimentally tested and therefore it has not been possible to determine which of them is better.

The objective of this work is to experimentally compare the three possible configurations of the IMS and determine which of them is more convenient for its application. For this, the three configurations have been tested for three different heat rejection levels ($t_{w,in}$ = 25.0, 30.4 and 35.1ºC) and one cold level ($t_{gly,in}$ = 3.8ºC) in a single compression refrigeration plant with a two-stage expansion system.

10. 2. Integrated mechanical subcooling configurations and experimental procedure

In this section, the three possible configurations of the Integrated Mechanical Subcooling system are presented and described. Also the description of the experimental plant is included and the test procedure is explained.

10.2.1. Cycle configurations

The three configurations of the IMS are presented in Figure 10.1. The cycle with extraction from the gas-cooler outlet (GCO) is represented as point A in Figure 10.1 and the ph diagram in Figure 10.2, the extraction from the exit of the subcooler as point B in Figure 10.1 (SCO) and Figure 10.3 and from the liquid tank (TNK) as point C in Figure 10.1 and Figure 10.4.

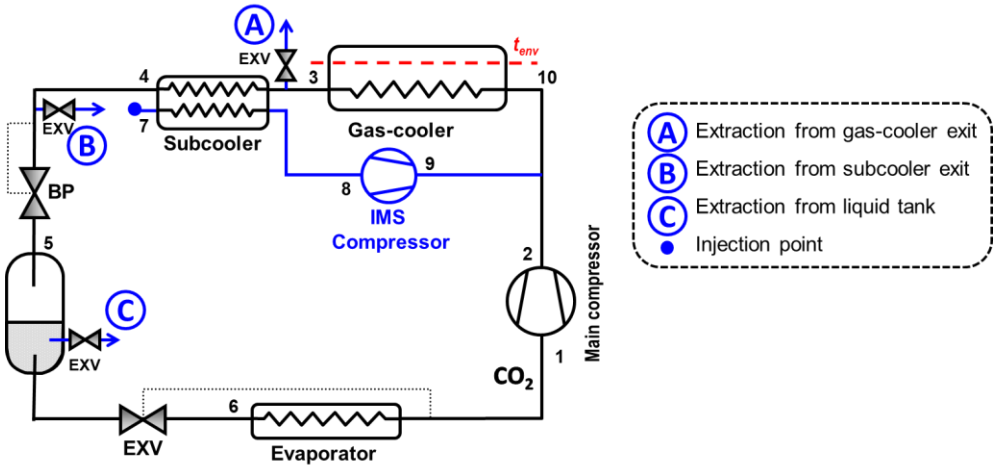

Figure 10.1. Configuration plant

As it can be seen, the main difference among the cycles is the extraction point. The rest of the cycle, marked in blue, is similar. An electronic expansion valve produces the expansion of the extracted mass flow and its evaporation is performed in the subcooler, to later be recompressed through the IMS compressor and reinjected in the discharge line.

The different extraction points have a direct effect on the heat exchanged in the subcooler. Said exchange is calculated as shown in Eq.(10.1): it is the product of the mass flow transferred by the IMS compressor and the enthalpy difference between the inlet and outlet of the subcooler.

$$\dot{Q}_{sub} = \dot{m}_{IMS} \cdot (h_8 - h_7) \quad (10.1)$$

$$h_8 = f(T_8, p_8) \quad (10.2)$$

$$h_7 = h_{gc,o} = f(T_3, p_3) \quad \text{for GCO configuration} \quad (10.3)$$

$$h_7 = h_{sub,o} = f(T_4, p_4) \quad \text{for SCO configuration} \quad (10.4)$$

$$h_7 = h_{tnk,o} = f(P_5, x = 0) \quad \text{for TNK configuration} \quad (10.5)$$

The outlet enthalpy (h_8) is calculated in the same way for all three configurations: from the temperature and pressure at the outlet of the subcooler, as shown in Eq. (10.2), although its value will depend on the degree of subcooling and the working pressure. On the other hand, the input enthalpy depends on the extraction point, which is different in every case.

For the GCO configuration, considering isenthalpic expansion, the inlet enthalpy is equal to the enthalpy at the exit of the gas-cooler; Eq. (10.3), for the SCO configuration, the inlet enthalpy is equal to the enthalpy at the exit of the subcooler, Eq.(10.4) and for the TNK configuration, the inlet enthalpy is equal to the enthalpy at the exit of the vessel, saturated-liquid, Eq.(10.5).

Neither the enthalpy difference is the same for the three configurations nor the flow transferred by the compressor, since it will depend on the rotation speed. Therefore, the behaviour of each configuration will depend on the heat exchanged in the subcooler and at the same time in the part of the flow diverted by the IMS.

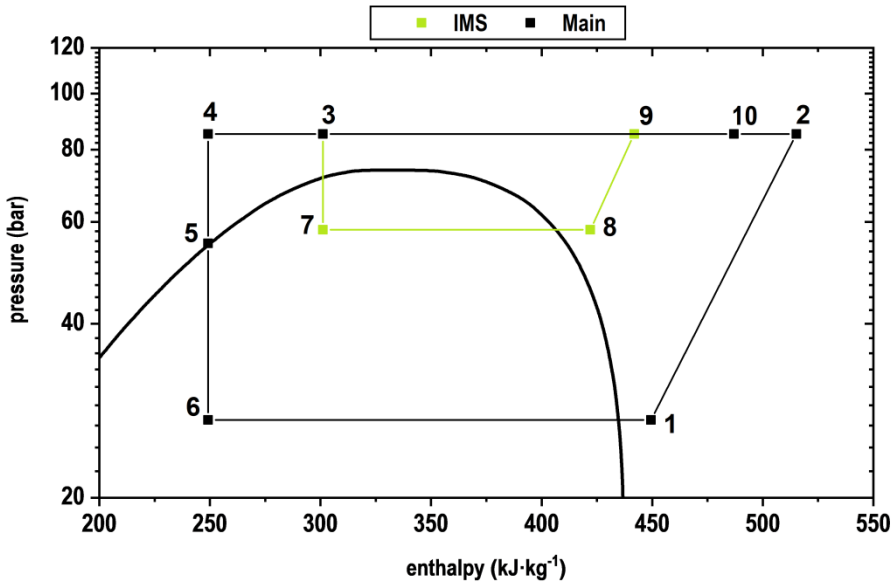

Figure 10.2. Ph Diagram of GCO configuration ($t_{w,in}$ = 30.4ºC).

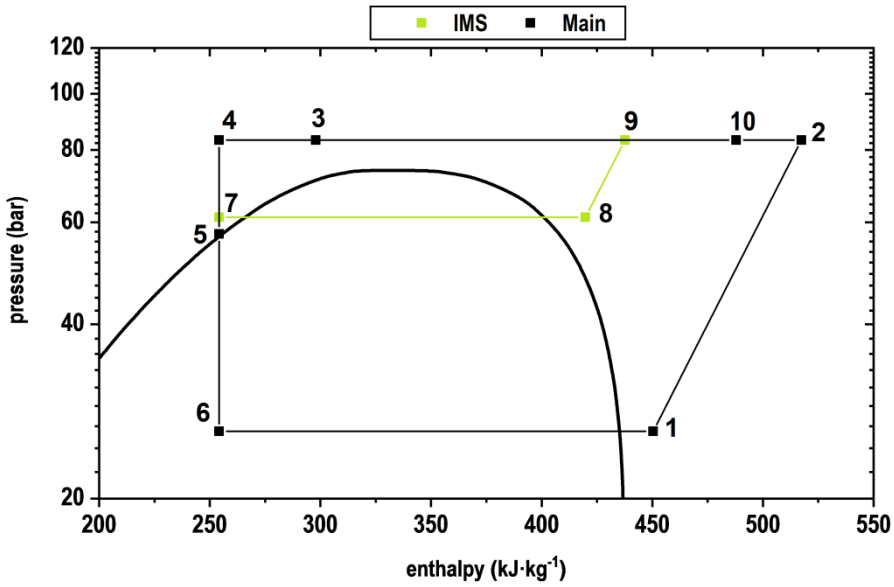

Figure 10.3. Ph Diagram of SCO configuration ($t_{w,in}$ = 30.4ºC).

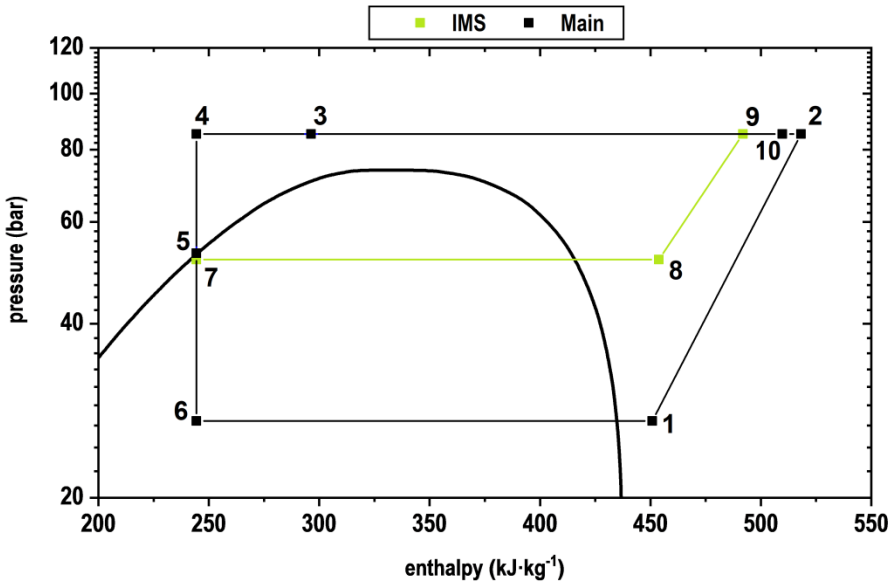

Figure 10.4. Ph Diagram of TNK configuration ($t_{w,in}$ = 30.4ºC).

10.2.2. Description of the plant and measurement system

The experimental plant tested in this work is presented in Nebot-Andrés et al. (2020). The plant is a CO_2 single-stage transcritical refrigeration system with an integrated mechanical subcooling system. The plant allows testing the three configurations: extracting gas at the exit of the subcooler (SCO), from the exit of the gas-cooler (GCO) and from the liquid tank (TNK). The main single-stage refrigeration cycle uses a semi-hermetic compressor with a displacement of 3.48 $m^3 \cdot h^{-1}$ at 1450 rpm and a nominal power of 4 kW. The expansion is carried out by a double-stage system, composed of an electronic expansion valve (back-pressure) controlling the gas-cooler pressure, a liquid receiver between stages and an electronic expansion valve, working as thermo-static, to control the evaporating process. Evaporator and gas-cooler are brazed plate counter-current heat exchangers with exchange surface area of 4.794 m^2 and 1.224 m^2, respectively. The subcooler is situated directly downstream of the gas-cooler. It is a brazed plate heat exchanger with an exchange surface area of 0.850 m^2. It works as the evaporator of the mechanical subcooling system for all configurations and subcools the CO_2 at the exit of the gas-cooler. The IMS cycle is driven by a variable speed semihermetic compressor with displacement of 1.12 $m^3 \cdot h^{-1}$ at 1450 rpm. The expansion valve of the IMS cycle is electronic, working as thermostatic, controlling the superheat in the evaporator of the subcooler. Heat dissipation in gas-cooler is done with a water loop, simulating the heat rejection level. The evaporator is supplied with another loop,

working with a propylene glycol–water mixture (60% by volume) that enables a constant entering temperature in the evaporator. Both the mass flow and the inlet temperature are controlled in these loops.

All fluid temperatures are measured by T-type thermocouples and pressure gauges that are installed along all the circuit. CO_2 mass flow rates are measured by Coriolis mass flow meters, as well as the secondary fluids. Compressors' power consumptions are measured by two digital wattmeters. The accuracies of the measurement devices can be consulted in Nebot-Andrés et al. (2020).

10.2.3. Test procedure

The description of the experimental tests procedure is detailed in this section. To evaluate the refrigeration plant using the different configurations of the integrated mechanical subcooling, each configuration has been tested at identical working conditions, always operating in the transcritical region. The evaluated conditions were:

- Heat rejection level: three different temperatures: 25.0, 30.4 and 35.1 °C, with maximum deviation of ±0.20 °C. These levels were performed fixing the temperature of the secondary fluid (water) at the entrance of the gas-cooler and maintaining the water flow rate to 1.17 m^3h^{-1}.
- One inlet temperature of the secondary fluid in the evaporator: 3.8 ±0.12 °C. The flow rate was fixed to 0.7 m^3h^{-1}.
- Gas-cooler pressure was regulated with an electronic BP fixed during each test thanks to a PDI controller. For each condition, tests were performed at different pressures in order to identify the optimum one and reach the optimum COP conditions, as done in previous experiments with this plant. The optimization process can be consulted in detail in Nebot-Andrés et al. (2020).
- Compressors: The main compressor always operated at nominal speed of 1450 rpm. The speed of the IMS compressor was varied in order to obtain the optimum subcooling degree.
- Electronic expansion valves: The electronic expansion valves were set to obtain a superheating degree in the evaporator of 10 K and of 10 K on the subcooler. Useful superheating the evaporator and also in the subcooler of SCO and GCO has been ensured. However, it was not possible to ensure this in the TNK configuration because the pressure drop in the valve was too small.

All the tests were carried out in steady state conditions for periods longer than 10 min, taking data each 5s, obtaining the test point as the average value of the whole test. The measured data were used to calculate the thermodynamic properties of the points using Refprop v.9.1. (Lemmon et al., 2013).

10.2.4. Physical limitations

This section presents some of the drawbacks that have been detected when testing the cycles and that deviate their behaviour from the results obtained in theoretical studies.

CO_2 can be subcooled as long as we are in the transcritical zone. If the plant works below the critical point, the CO_2 condenses inside the subcooler. In some of the tests, it has been observed that working at pressures close to the critical pressure (even if they are higher), the CO_2 partially condenses in the subcooler, and although the speed of the IMS compressor increases, it is not possible to increase the degree of subcooling, which is around 2 K.

The cooling capacity exchanged in the subcooler, shown in Figure 10.12, varies between 8% and 22% between the tests depending on the configuration when looking at optimum conditions. But going lower from a certain pressure, out of optimal conditions, depending on the test condition and the tested configuration, the subcooling does not vary significantly with the variation of the compressor speed. In these areas where subcooling cannot be carried out properly, the COP of the system goes down, therefore it is necessary to slightly increase the pressure in order to achieve the desired subcooling and with it the increase in COP.

The Figure 10.5 represents the subcooling degree as a function of the pressure for a fixed rotation speed (40Hz) for the GCO configuration. It can be seen how the subcooling degree drops significantly from 82 bar and when it reaches 93 bar it tends to a horizontal asymptote. This trend is observed in the three studied configurations. This is due to the fact that the gas-cooler outlet temperature is very close to the pseudocritical temperature, where the Cp grows drastically and therefore we are not able to produce a large subcooling for the same cooling capacity.

The gas-cooler outlet temperature and the pseudocritical temperature (Liao and Zhao, 2002) can be observed in Figure 10.6. As it can be seen, for the lowest pressures, both temperatures are very close, coinciding with the points where the achieved subcooling is low (Figure 10.5). However, around 83 bar, the gas-cooler outlet temperature moves away from the pseudocritical and it is from this pressure that the trend of the subcooling degree changes. In conclusion, for the correct operation of the subcooling system, the gas-cooler outlet temperature must be far from the pseudocritical temperature. All the optimal points presented in the following section meet this condition.

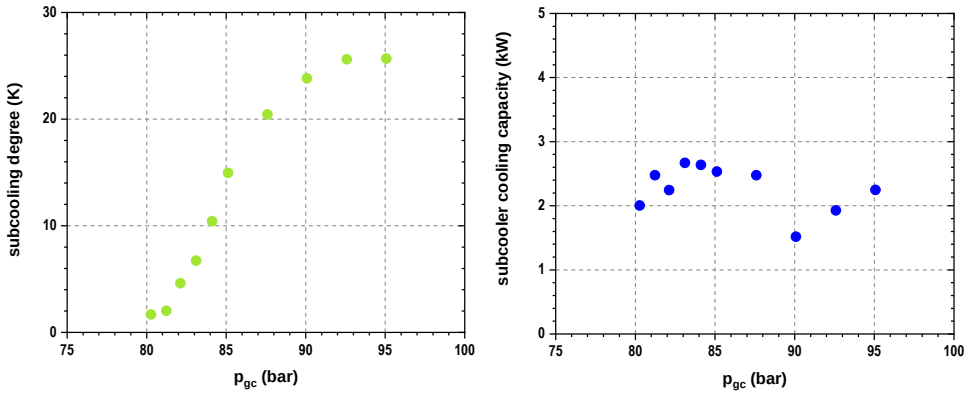

Figure 10.5. Subcooling degree and subcooler cooling capacity for GCO vs gas-cooler pressure (40Hz, $t_{w,in}$ = 30.4ºC) .

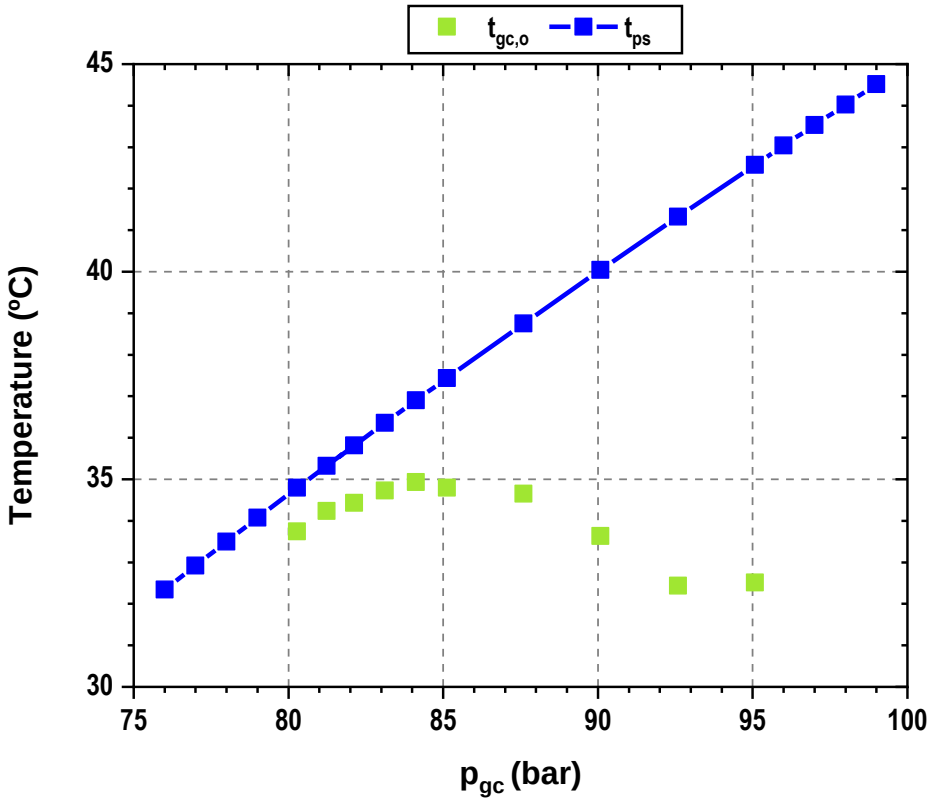

Figure 10.6. Gas-cooler outlet temperature and pseudocritical temperature for GCO vs gas-cooler pressure (40Hz, tw,in = 30.4ºC).

As mentioned in section 10.2.3, for the TNK configuration it has not been possible to ensure the superheating in the subcooler, due to the small pressure difference in the valve. In previous theoretical studies made by the authors, it has been found that the optimum point for the TNK configuration is obtained when the suction pressure of the IMS compressor is equal to the tank pressure. This cannot be achieved, as it can be seen in Figure 10.4, because the expansion valve needs to be installed as security device, to avoid liquid entering the auxiliary compressor, impairing the behaviour of this configuration. This is one inconvenient of this configuration.

10.3. Main energy results

All the points presented in this section correspond to the optimum points (optimum subcooling degree and optimum gas-cooler pressure), identified as explained in Nebot-Andrés et al. (2020). Main results as the cooling capacity, calculated as Eq.(10.6), the COP, as Eq. (10.7), and the optimum parameters are presented in Table 10.2. The uncertainties are calculated using Moffat's method (Moffat, 1985) and they are also included in Table 10.2.

$$\dot{Q}_0 = \dot{m}_0 \cdot \left(h_{suc} - h_{sub,o}\right) \quad (10.6)$$

$$COP = \frac{\dot{Q}_0}{Pc_{main} + Pc_{IMS}} \quad (10.7)$$

3.1. Optimum COP

Figure 10.7 shows the maximum COP obtained for each configuration at all the tested conditions. As it can be seen, the tendency in COP is exactly the same and the measured COP values are practically the same. It can be observed that for the water inlet conditions of 25.0ºC and 35.1ºC, the COP values can be considered identical since the differences between them are included within the measurement uncertainty. Considering the water inlet of 30ºC, slight differences can be seen in the COP, which do not exceed 2%. These differences may be due to the proximity to the pseudocritical temperature.

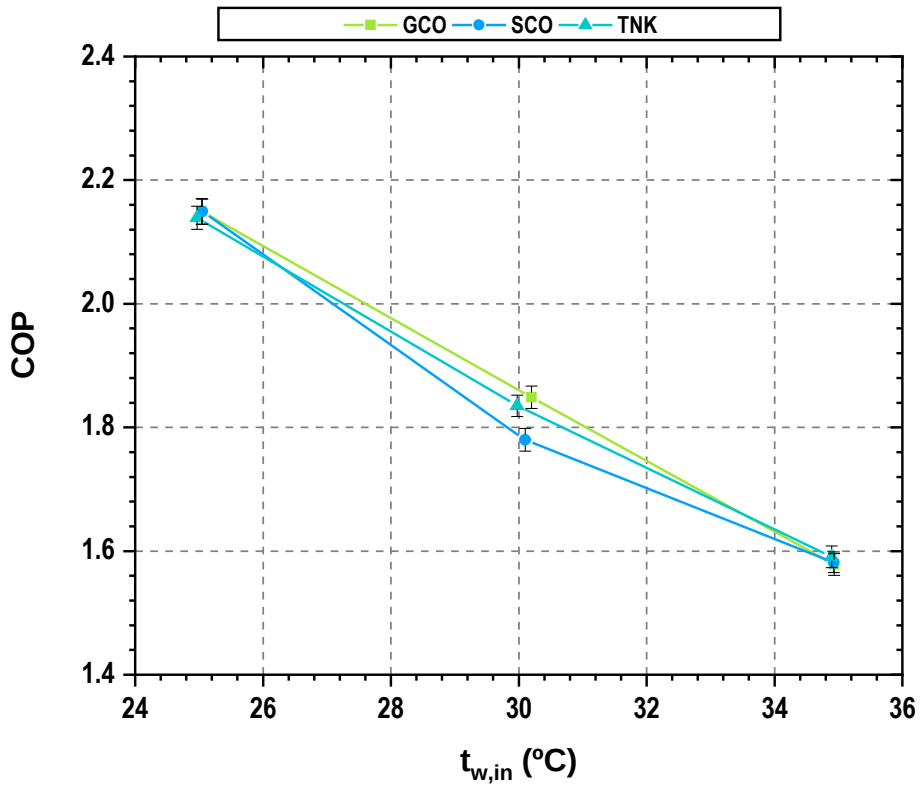

Figure 10.7. Evolution of the COP of the different configurations depending on the water inlet temperature.

3.2. Cooling capacity

As it can be seen in Figure 10.8, the cooling capacity decreases when the inlet temperature in the gas-cooler increases. More important differences can be seen in this parameter than in the analysis of the COP. The system that provides the greatest cooling capacity is the configuration with extraction from the tank, as can be seen in the graph. In addition, it is also important to note that this configuration provides the cooling capacity in a more constant way.

The GCO configuration provides a slightly lower cooling capacity. In addition, this configuration suffers a more abrupt drop at high temperatures. The biggest differences are found in the SCO configuration. Although for the points of 25ºC and 35ºC, the trend is very similar, for 30ºC, the cooling capacity drops significantly. This is due to its direct relationship with the degree of subcooling. The higher the subcooling is for a given condition of heat sink temperature and evaporation level, the higher the overall cooling capacity is. As will be seen later, the optimal subcooling degree for this configuration at

this operating point is lower than that obtained in the other configurations. This phenomenon is due to the proximity to the pseudocritical temperature and the sensitivity of the CO_2 heat transfer parameters in this area. This phenomenon was also observed theoretically (Nebot-Andrés et al., 2019). Increasing the subcooling degree will increase the cooling capacity but will imply a reduction in COP too.

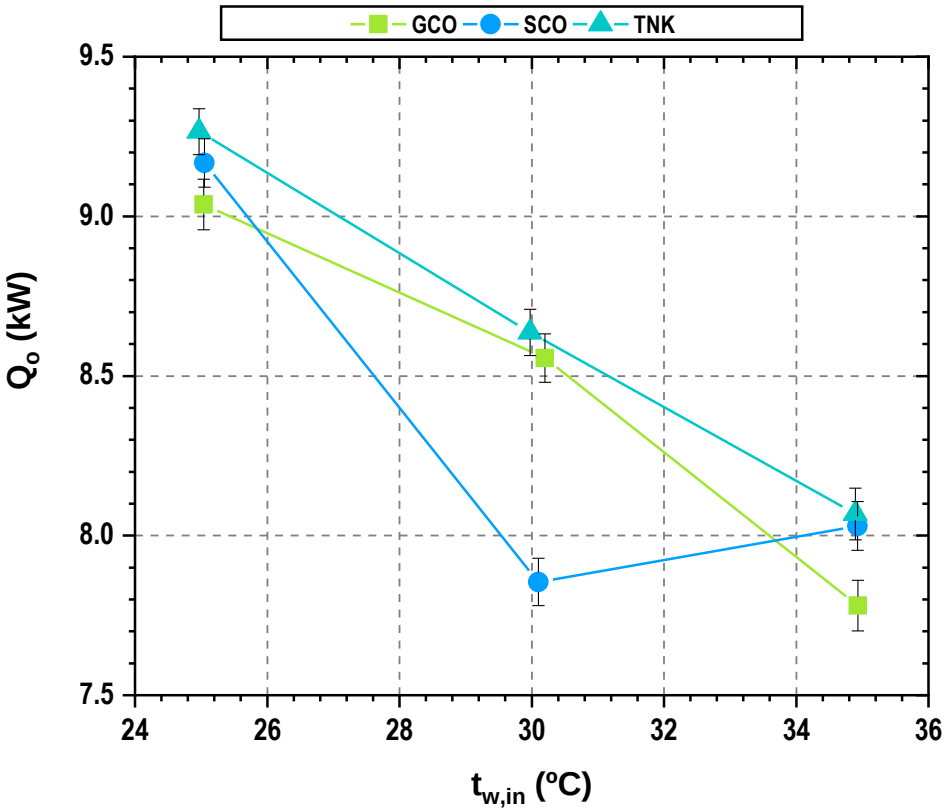

Figure 10.8. Evolution of the cooling capacity of the different configurations depending on the water inlet temperature.

10.4. Optimum operation parameters

This section presents the optimal operating parameters necessary to achieve the maximum COP values.

10.4.1. Optimum pressure

Regarding the optimal gas-cooler pressures, for each configuration, a similar behaviour is obtained for the three configurations. It is observed how it gets higher when the water inlet temperature to the gas-cooler increases. Optimal pressures are represented in Figure 10.9. As it can be observed, optimum pressure is practically the same for the

three configurations tested. A slight difference can be seen for the SCO configuration at 30ºC, but this difference is within the measurement uncertainty, so we can conclude that the optimal pressure is independent of the CO_2 extraction point. When the water inlet temperature is close to 25ºC, the optimum pressure is practically the critical pressure, while for higher temperatures, this pressure increases, until 95 bar for water inlet temperatures of 35ºC.

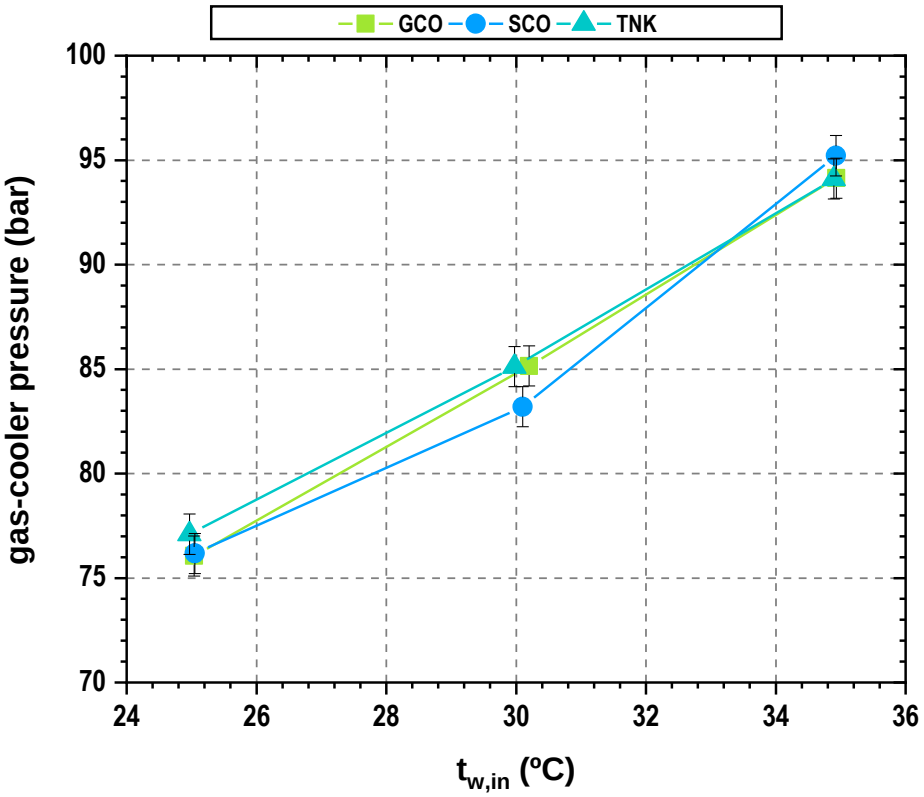

Figure 10.9. Gas-cooler optimum pressures.

4.2. Optimum subcooling degree

Figure 10.10 shows the optimum subcooling degree for each configuration, calculated as Eq.(10.8). As it can be seen, depending on the extraction point, the subcooling degree has a different trend. Regarding the TNK configuration, subcooling is lower when higher the water inlet temperature is. For the GCO configuration, the subcooling degree first increases and then decreases and for the SCO it follows the opposite trend.

$$SUB = t_{gc,o} - t_{sub,o} \tag{10.8}$$

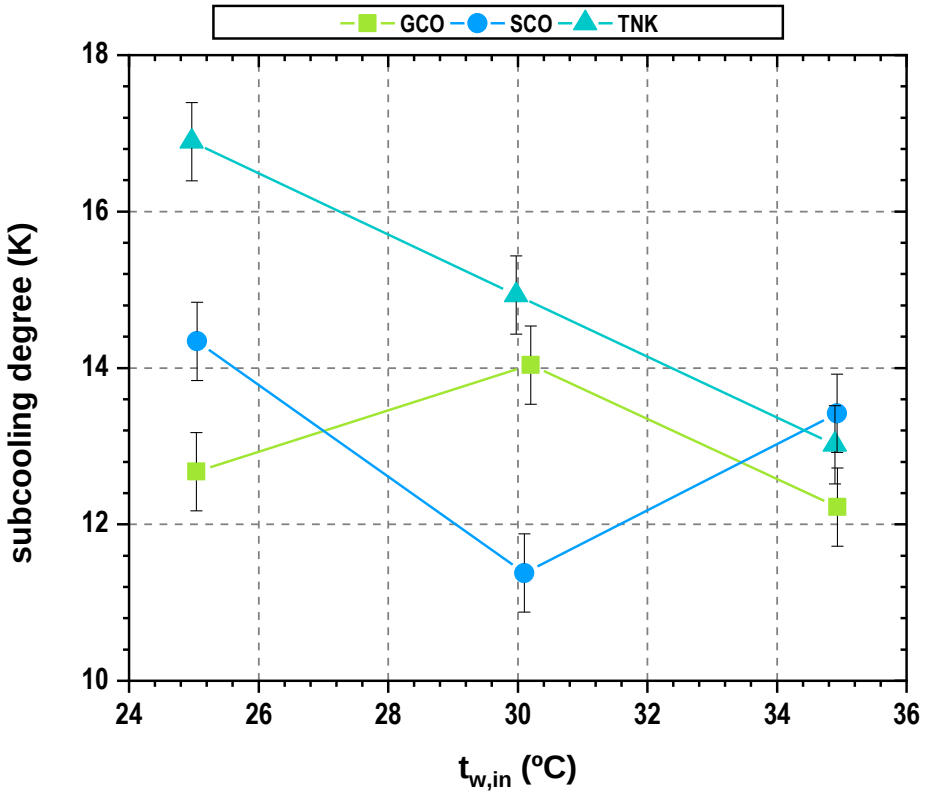

Figure 10.10. Optimum subcooling degree for each configuration.

These differences in trends are due to the gas-cooler outlet conditions, which are close to the critical point and this causes large variations in the properties of the fluid. The specific heat of the CO_2 both at the inlet and outlet of the subcooler can be seen in Figure 10.11. As it can be seen, for the TNK configuration at the inlet of the subcooler, Cp has lower values compared to the other configurations and it has an growing trend with the increment of the pressure, while the other configurations have a higher Cp but its tendency is decreasing. Regarding the outlet of the subcooler, the Cp of the three configurations has the same trend, very stable, and very similar values. With this it is seen that the main differences are marked by the subcooler inlet point, which also causes differences in the optimal subcooling degree. A lower Cp, as in the case of the TNK configuration at 25.0ºC, implies higher subcooling. However, it should be mentioned that the cross of the pseudocritical region happens inside the gas-cooler for all the configurations.

Subcooling in GCO configuration first increases and then decreases. For 25.0ºC the subcooling degree is quite small because the extraction point, after the gas-cooler exit,

is near the pseudocritical temperature and thus it is more difficult to perform the subcooling, as explained in section 2.4. On the contrary, this phenomenon is observed for the SCO configuration at 30.4ºC, since when extracting from the subcooler outlet, it is at this temperature where the system operates closer to the pseudocritical temperature.

From Figure 10.10 it could be thought that it is not necessary to control the subcooling degree, but that each configuration has a different optimum does not mean that the control of this parameter is not important. In previous studies (Nebot-Andrés et al., 2020), the sensitivity of this parameter was analysed and it was concluded that the COP is more sensitive to gas-cooler pressure but that subcooling degree is also very important.

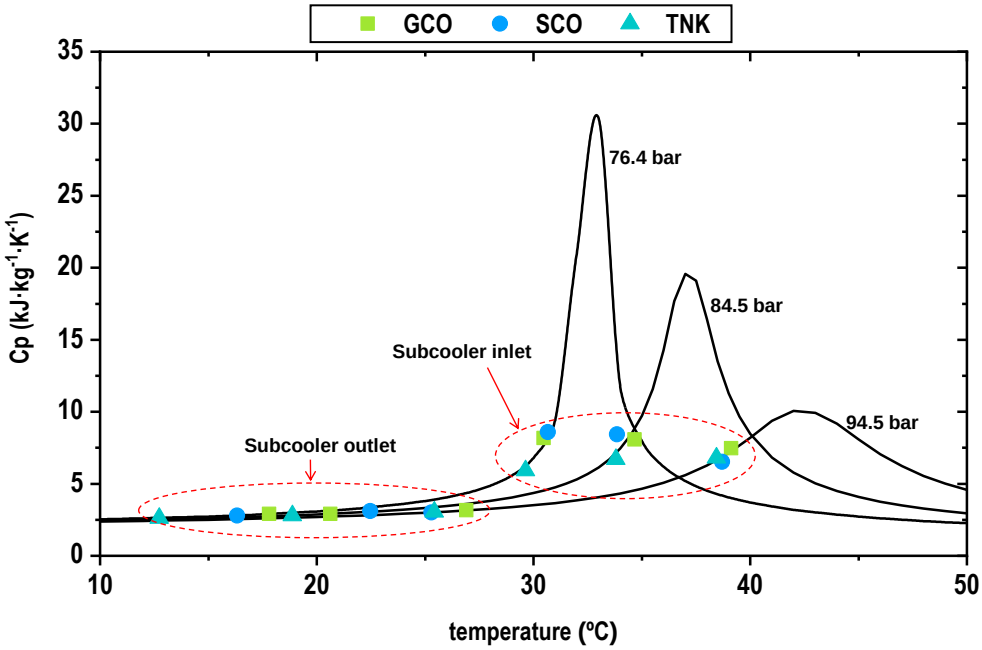

Figure 10.11. Cp at inlet and outlet of the subcooler.

10.4.3. Behaviour of the subcooler

One of the most important components of the integrated mechanical subcooling cycle is the subcooler. In this work, where three possible architectures are analysed, the same heat exchanger is used for all three, thus being the same exchange surface in all cases. As seen in the previous section, although the optimal pressure conditions are the same for the three cycles, there are significant differences in the optimal subcooling degree. It is therefore necessary to analyse the behaviour of the subcooler for each of the cases.

Figure 10.12 shows the cooling capacity of each of the configurations divided into the cooling capacity provided by the subcooler and the cooling capacity provided by the base cycle. The green bars show the subcooler cooling capacity for each of the optimum points, calculated as Eq. (10.1). The cooling capacity of the base cycle is the cooling capacity of the cycle if it was not subcooled, so calculated as stated in Eq.(10.9). As it can be clearly seen, each configuration requires different cooling capacity in the subcooler. The TNK configuration has the highest subcooler cooling capacity, being this fairly constant throughout the three test conditions. The SCO configuration exchanges lesser and the GCO configuration is the one with the least exchange. Specifically, the cooling capacity of the GCO configuration is 47% lower than the TNK.

$$\dot{Q}_{base} = \dot{Q}_0 - \dot{Q}_{sub} \tag{10.9}$$

As it can be seen, as the cooling capacity in the subcooler is higher for the TNK configuration and the overall cooling capacity is very similar for the three configurations, so the TNK has lower cooling capacity coming from the base cycle. Contrary, the 75% of the cooling power of the GCO configuration comes from the base cycle and the subcooler only represents around 25% of the contribution. A big difference between the configurations is seen. In the TNK configuration, the subcooler represents more than 50% of the cooling capacity, while in GCO it represents only 25%. This has a direct impact on the size of the heat exchanger.

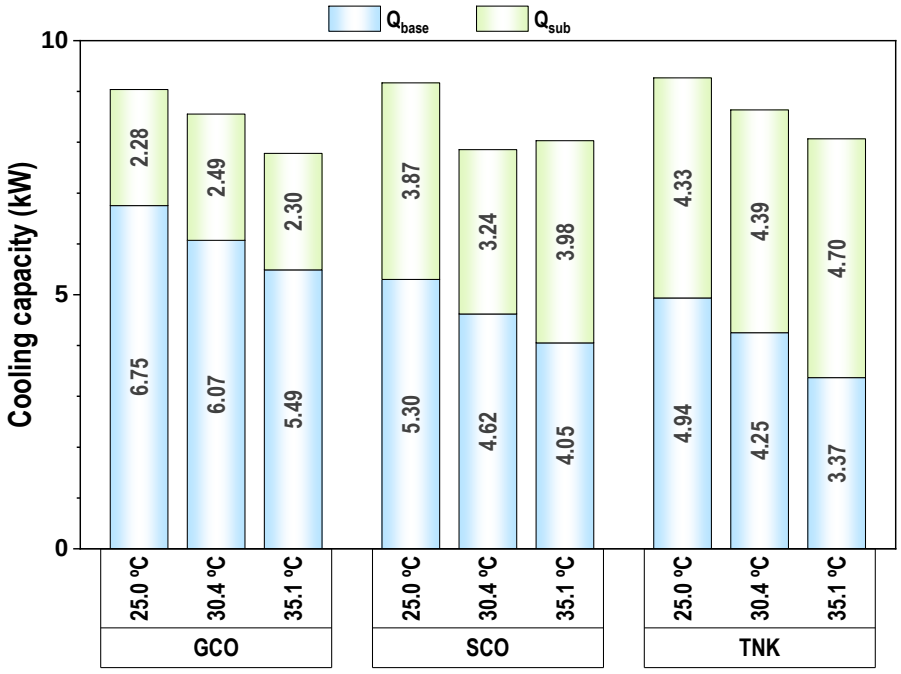

Figure 10.12. Cooling capacity divided into subcooler capacity and base cycle capacity.

Figure 10.13 shows the evaporation temperature at the subcooler. As it can be seen, the three configurations follow an upward trend, the evaporation temperature being higher the higher the water temperature is. SCO and GCO have quite similar evaporation temperatures, between 1 and 2K difference between them. It is the TNK configuration that presents the greatest differences, with an evaporation temperature between 5 and 6K lower than the other two. This is due to the fact that this temperature will always be limited by the pressure of the tank (equivalent to the maximum evaporating temperature in the subcooler) in the TNK configuration, being therefore lower than the other two configurations that do not have this limitation.

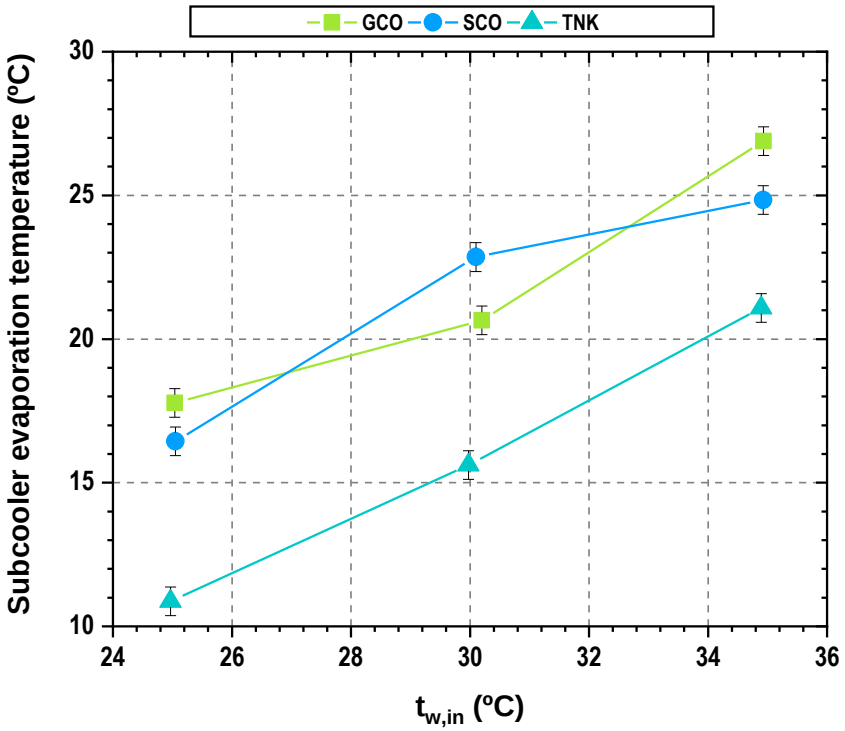

Figure 10.13. Subcooler cooling capacity (left) and subcooler evaporation temperature (right).

Comparing SCO and GCO at 30.5ºC a slight difference in the evaporation temperature is also found. This is related to the subcooling degree. Thermal effectiveness of the subcooler is the practically the same for both configurations at this point but this is the point where maximum differences in the subcooling degree are obtained. The heat transfer in the subcooler depends both in the inlet and outlet temperatures of the subcooler (so on the subcooling degree) and the evaporation level on the subcooler. So, for 30.5ºC, if the temperatures at the exit of the subcooler are analysed, 20.1ºC are

measured for GCO configuration and 21.7ºC for SCO, which is a difference of 1.6 K. Regarding the evaporation level, it is seen that the behaviour is coherent: for the GCO evaporation temperature is around 21ºC and for the SCO is around 23ºC, higher than for GCO.

Figure 10.14 shows the thermal effectiveness of the subcooler (ε_{sub}) and its uncertainty. The thermal effectiveness is calculated as stated in Eq. (10.10). As can be seen in the figure, for GCO and SCO the efficiency is very high, because the cooling capacity is lower, and therefore the exchange area is better used. In many of the tests, the measured efficiency is near to 100% due to the measurement uncertainty of the thermocouples. It can be concluded that this efficiency will be high, although never equal to 100%. Regarding the TNK configuration, the efficiency of the subcooler is lower, decreasing when water temperature increases. This is because the evaporation temperature is lower and therefore the temperature pinch in the subcooler is higher than in the other configurations.

$$\varepsilon_{sub} = \frac{t_{gc,o} - t_{sub,o}}{t_{gc,o} - t_{0,sub}} = \frac{SUB}{t_{gc,o} - t_{0,sub}} \tag{10.10}$$

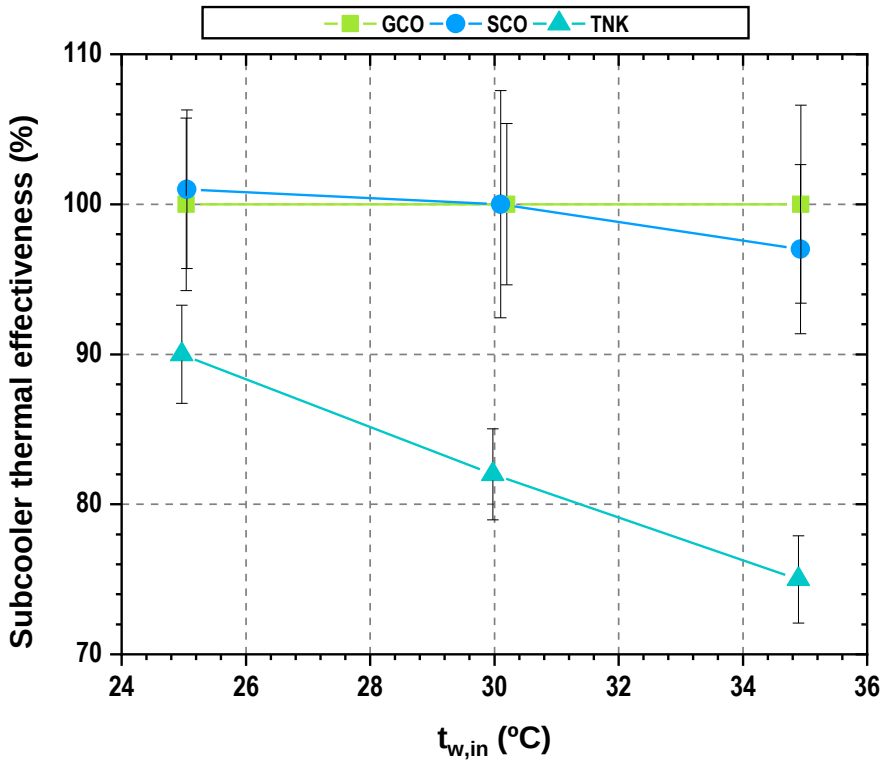

Figure 10.14. Subcooler thermal effectiveness.

10.4.4. Behaviour of the IMS compressor

As mentioned in the previous sections, the IMS system bases its operation on the use of an auxiliary compressor that recompresses to gas-cooler pressure a part of the CO_2 mass flow that has been evaporated in the subcooler. The operation of this compressor is very particular since it must adapt its rotational speed to obtain a specific subcooling degree for which the plant's COP is maximum.

Table 10.1 sums up the main operating parameters of the IMS compressor for the optimal points that have been obtained experimentally and presented in the previous section. The presented parameters are the rotation frequency, the compression ratio, the overall and volumetric performances and the suction temperature. As can be seen in the table, the compression ratios of all the tests of configurations GCO and SCO are very low and specifically less than 1.5 for some test cases. These compression ratios are outside the operating range of the compressors, which should work over a compression ratio of 1.5. Regarding the frequency, we observe that all the optimal points are achieved with very low frequencies, in some cases lower than 30Hz. For this type of plant, a smaller compressor should therefore be implemented, but the one used is the smallest existing of this type of compressors. Regarding the volumetric efficiency, the IMS compressor operates with values between 40 and 50% and the global efficiency's values are also quite low. Finally, another operating parameter that needs to be highlighted is the temperature obtained in the suction of the compressor, which, as can be seen in Table 10.1, is always higher than the compressor suction temperature limit, which is 10ºC.

	$t_{w,in}$ (ºC)	IMS compressor				
		η_{glo}	η_{vol}	τ	f_{IMS} (Hz)	t_{suc} (ºC)
GCO	25.0	0.61	0.41	1.40	25	22.0
	30.2	0.73	0.49	1.46	30	24.9
	34.9	0.66	0.50	1.40	30	31.0
SCO	25.1	0.73	0.50	1.45	30	20.7
	30.1	0.68	0.41	1.36	25	27.3
	34.9	0.69	0.48	1.49	30	29.1
TNK	25.0	0.67	0.45	1.68	30	27.4
	30.0	0.81	0.45	1.65	30	33.1
	34.9	0.65	0.47	1.60	30	38.1

Table 10.1. IMS compressor's main parameters.

In Figure 10.15 the application limits of this particular compressor in terms of gas-cooler pressure and evaporation temperature can be seen (DORIN, 2018). The experimental

data measured in the plant for the IMS compressor are shown in coloured points. As can be clearly seen, although the pressure levels are correct, the evaporation temperature of the IMS cycle is too high, falling outside the compressor operation boundary.

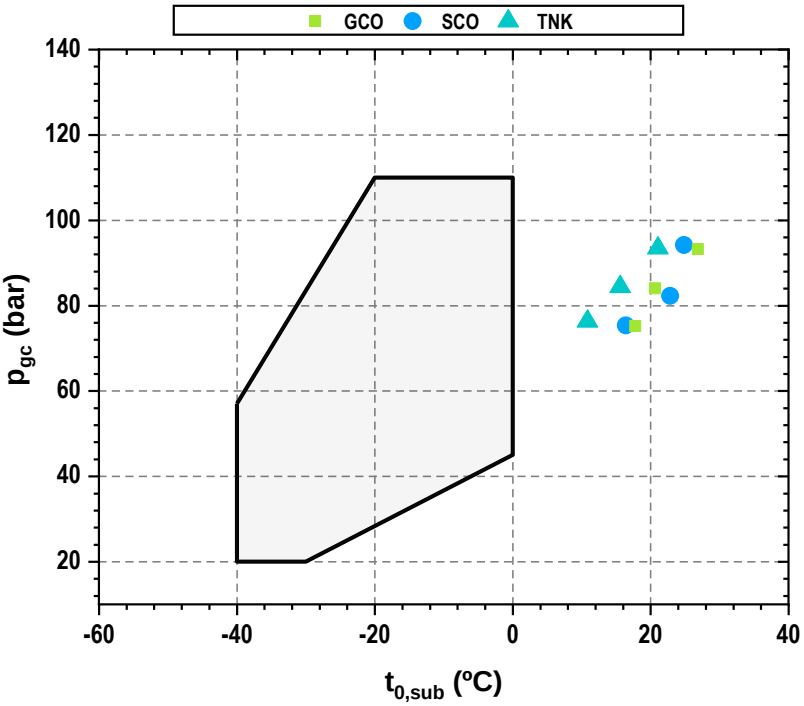

Figure 10.15. Application limits of the IMS compressor and experimental points of operation.

Although the IMS system is a very interesting system for its application in transcritical CO_2 cycles, at this time there is no CO_2 compressor specifically designed to work in the optimal system conditions, since they require very high suction temperatures, small sizes and low compression rates.

10.5. Conclusions

The experimental comparison of a CO_2 transcritical refrigeration plant working with integrated mechanical subcooling (IMS) with three different architectures is presented in this work. The difference between the configurations lies in the extraction point from which the expansion will take place in the IMS. The three possible extraction points are: the gas-cooler outlet (GCO), the subcooler outlet (SCO) or from the liquid tank (TNK). The comparison covered three heat rejection temperatures (25.0ºC, 30.4ºC and 35.1ºC)

at steady-state conditions for optimum conditions where the COP is maximum for each configuration.

The results obtained show that there are no significant differences in the energetic behaviour of the three configurations, being that the COP of all of them is very similar for all conditions. Despite this, it is in the GCO configuration where higher COP values have been measured. Regarding the cooling capacity of the overall system, it is seen that it is the TNK configuration the one that presents the highest cooling capacity values. This is due to the fact that this is the configuration that presents higher values of optimal subcooling degree, a parameter directly related to the increments in the cooling capacity.

In this study it is observed that the main difference between the configurations resides in the subcooler. The optimal subcooling degree, the thermal effectiveness of the subcooler, its evaporation temperature and also the cooling capacity exchanged in this heat exchanger have been analysed in this work. It has been seen that all these parameters are different for each of the configurations. From the analysis of these parameters, it can be concluded that the SCO and GCO configurations need a smaller subcooler since they present greater thermal effectiveness and the heat they must exchange is also much lower. This also implies a lower cost when assembling said cycle.

From this experimental work it can be concluded that the IMS cycle is a very versatile system for the improvement of transcritical CO_2 cycles since it can be designed in three different ways without having noticeable losses in its energetic performance. However, there is room for improvement since, the auxiliary compressor works outside its operability range. Therefore, the design of compressors adapted to this application would be interesting. The best configuration is the extraction from the gas-cooler outlet since the three configurations present similar energetic behaviour but it requires much lower cooling capacity in the subcooler.

10.6.Acknowledgements

The authors thank the Ministerio de Ciencia y Tecnología (Spain) project RTI2018-093501-B-C21, the Ministerio de Educación, Cultura y Deporte (Spain), grant FPU16/00151 and the Jaume I University (Spain), project UJI-B2019-56 and grant PREDOC/2019/19 for financing this research work.

10.7. Author contributions statements

L.N. developed the idea, performed the tests and wrote the manuscript. D.C. and C.F. helped to perform the tests. R. Ll. supervised the work and made final proofreading. D.S. and R.C. helped to get funds.

10.8. Nomenclature

COP coefficient of performance

Cp specific heat capacity, $kJ \cdot kg^{-1} \cdot K^{-1}$

GCO extraction from gas-cooler outlet configuration

$\dot{m}$ mass flow, $kg \cdot s^{-1}$

p absolute pressure, bar

Pc power consumption, kW

$\dot{Q}$ cooling capacity, kW

SUB degree of subcooling produced in the subcooler, K

SCO extraction from subcooler outlet configuration

t temperature, ºC

TNK extraction from liquid tank configuration

Greek symbols

ε uncertainty

ρ density, $kg \cdot m^{-3}$

f frequency, Hz

τ compression ratio

Subscripts

gly propylene glycol–water mixture

gc gas-cooler

IMS corresponding to the IMS cycle

in	inlet
main	corresponding to the main cycle
0	evaporating level
o	outlet
ps	pseudocritical
sub	corresponding to the subcooler
suc	compressor suction
tkn	corresponding to the liquid tank
w	water

10.9. References

Catalán-Gil, J., Llopis, R., Sánchez, D., Nebot-Andrés, L., Cabello, R., 2019. Energy analysis of dedicated and integrated mechanical subcooled CO 2 boosters for supermarket applications. International Journal of Refrigeration 101, 11-23.

Cortella, G., Coppola, M.A., D'Agaro, P., 2021. Sizing and control rules of dedicated mechanical subcooler in transcritical CO2 booster systems for commercial refrigeration. Applied Thermal Engineering 193.

DORIN, 2018. CO2 SEMI-HERMETIC COMPRESSORS, CD SERIES. CO2 TRANSCRITICAL APPLICATION. OFFICINE MARIO DORIN S.p.A., Italy.

European Commission, 2014. Regulation (EU) No 517/2014 of the European Parliament and of the Council of 16 April 2014 on fluorinated greenhouse gases and repealing Regulation (EC) No 842/2006.

Gullo, P., Hafner, A., Banasiak, K., 2018. Transcritical R744 refrigeration systems for supermarket applications: Current status and future perspectives. International Journal of Refrigeration 93, 269-310.

Gullo, P., Hafner, A., Banasiak, K., Minetto, S., Kriezi, E.E., 2019. Multi-ejector concept: A comprehensive review on its latest technological developments. Energies 12.

Karampour, M., Sawalha, S., 2018. State-of-the-art integrated CO2 refrigeration system for supermarkets: A comparative analysis. International Journal of Refrigeration 86, 239-257.

Lawrence, N., Elbel, S., 2019. Experimental investigation on control methods and strategies for off-design operation of the transcritical R744 two-phase ejector cycle. International Journal of Refrigeration 106, 570-582.

Lemmon, E.W., Huber, M.L., McLinden, M.O., 2013. REFPROP, NIST Standard Reference Database 23, v.9.1. National Institute of Standards, Gaithersburg, MD, U.S.A.

Liao, S.M., Zhao, T.S., 2002. Measurements of heat transfer coefficients from supercritical carbon dioxide flowing in horizontal mini/micro channels. Journal of Heat Transfer 124, 413-420.

Llopis, R., Cabello, R., Sánchez, D., Torrella, E., 2015. Energy improvements of CO2 transcritical refrigeration cycles using dedicated mechanical subcooling. International Journal of Refrigeration 55, 129-141.

Llopis, R., Nebot-Andrés, L., Cabello, R., Sánchez, D., Catalán-Gil, J., 2016. Experimental evaluation of a CO2 transcritical refrigeration plant with dedicated mechanical subcooling. International Journal of Refrigeration 69, 361-368.

Llopis, R., Nebot-Andrés, L., Sánchez, D., Catalán-Gil, J., Cabello, R., 2018. Subcooling methods for CO2 refrigeration cycles: A review. International Journal of Refrigeration 93, 85-107.

Moffat, R.J., 1985. Using Uncertainty Analysis in the Planning of an Experiment. Journal of Fluids Engineering 107, 173-178.

Nebot-Andrés, L., Calleja-Anta, D., Sánchez, D., Cabello, R., Llopis, R., 2019. Thermodynamic analysis of a CO2 refrigeration cycle with integrated mechanical subcooling. Energies 13.

Nebot-Andrés, L., Catalán-Gil, J., Sánchez, D., Calleja-Anta, D., Cabello, R., Llopis, R., 2020. Experimental determination of the optimum working conditions of a transcritical CO2 refrigeration plant with integrated mechanical subcooling. International Journal of Refrigeration 113, 266-275.

Nebot-Andrés, L., Sánchez, D., Calleja-Anta, D., Cabello, R., Llopis, R., 2021a. Experimental determination of the optimum intermediate and gas-cooler pressures of a commercial transcritical CO2 refrigeration plant with parallel compression. Applied Thermal Engineering 189.

Nebot-Andrés, L., Sánchez, D., Calleja-Anta, D., Cabello, R., Llopis, R., 2021b. Experimental determination of the optimum working conditions of a commercial transcritical CO2 refrigeration plant with a R-152a dedicated mechanical subcooling. International Journal of Refrigeration 121, 258-268.

Rigola, J., Ablanque, N., Pérez-Segarra, C.D., Oliva, A., 2010. Numerical simulation and experimental validation of internal heat exchanger influence on CO2 trans-critical cycle performance. International Journal of Refrigeration 33, 664-674.

Sarkar, J., Agrawal, N., 2010. Performance optimization of transcritical CO2 cycle with parallel compression economization. International Journal of Thermal Sciences 49, 838-843.

Table 10.2. Main experimental results and uncertainty measurements of the optimum conditions.

	t_0 (ºC)	$t_{w,in}$ (ºC)	$p_{gc,o}$ (bar)	$t_{gc,o}$ (ºC)	SUB (ºC)	$\dot{m}_0$ (kg/s)	$P_{c,main}$ (kW)	$P_{c,IMS}$ (kW)	$\dot{Q}_0$ (kW)	$\varepsilon(\dot{Q}_0)$ (%)	COP (-)	ε(COP) (%)
GCO	-9.1	25.0	76.1	30.2	12.7	0.04	3.60	0.61	9.04	0.87	2.15	0.98
	-8.8	30.2	85.1	34.1	14.0	0.04	3.89	0.74	8.56	0.89	1.85	0.98
	-7.9	34.9	94.1	38.1	12.2	0.04	4.16	0.77	7.78	1.02	1.58	1.10
SCO	-9.2	25.0	76.2	30.2	14.3	0.04	3.60	0.67	9.17	0.83	2.15	0.93
	-10.3	30.1	83.2	33.1	11.4	0.04	3.78	0.63	7.85	0.95	1.78	1.04
	-7.7	34.9	95.2	37.4	13.4	0.04	4.24	0.83	8.03	0.95	1.58	1.05
TNK	-9.5	25.0	77.1	29.5	16.9	0.04	3.56	0.77	9.27	0.77	2.14	0.88
	-9.0	30.0	85.1	33.4	14.9	0.04	3.88	0.82	8.64	0.84	1.84	0.94
	-7.5	34.9	94.1	37.7	13.0	0.04	4.20	0.88	8.07	1.00	1.59	1.09

Chapter 11 Experimental assessment of dedicated and integrated mechanical subcooling systems vs parallel compression in transcritical CO_2 refrigeration plants

Chapter 11. Experimental assessment of dedicated and integrated mechanical subcooling systems vs parallel compression in transcritical CO_2 refrigeration plants

11. Experimental assessment of dedicated and integrated mechanical subcooling systems vs parallel compression in transcritical CO_2 refrigeration plants

Chapter adapted from the paper: Nebot-Andrés, L., Calleja-Anta, D., Sánchez, D., Cabello, R. Llopis, R. Experimental assessment of dedicated and integrated mechanical subcooling systems vs parallel compression in transcritical CO_2 refrigeration plants. (2022) Energy Conversion and Management, Available online 2 December 2021, 115051

Abstract

Mechanical subcooling systems, both dedicated and integrated, have attracted lot of attention in the recent years due to their great potential to improve transcritical CO_2 refrigeration systems. Numerous studies have theoretically determined the COP increments that these systems can offer compared to classic systems and experimental works have evaluated the optimum working conditions for each individual system. However, they have not been contrasted experimentally. In this work, the dedicated and integrated mechanical subcooling systems are experimentally contrasted to the parallel compression one, which is considered as base system. The optimum energy performance of the three systems is contrasted for three heat rejection levels: 25.0ºC, 30.4ºC and 35.1ºC. The experimental tests show increments in COP of 4.1% at 25.0ºC, 7.2% at 30.4ºC and 9.5% at 35.1ºC thanks to the use of the integrated mechanical subcooling and of 7.8%, 13.7% and 17.5% respectively when using the dedicated. It is concluded that the dedicated mechanical subcooling system is the best system, however the integrated mechanical subcooling also performed better than the reference system.

Keywords

CO_2, dedicated mechanical subcooling, energy improvements, integrated mechanical subcooling, parallel compressor

Chapter 11. Experimental assessment of dedicated and integrated mechanical subcooling systems vs parallel compression in transcritical CO_2 refrigeration plants

Chapter 11. Experimental assessment of dedicated and integrated mechanical subcooling systems vs parallel compression in transcritical CO_2 refrigeration plants

11.1. Introduction

The growing need to mitigate global warming has had an important impact on the refrigeration sector, which in recent years, and driven by different regulations, as the F-Gas [1], has taken a leap towards the use of less harmful refrigerants and the improvement of the systems with the aim of reducing their indirect emissions. In centralized commercial refrigeration, carbon dioxide, CO_2, is the unique refrigerant that meets GWP limitations and is also safe. On the contrary, despite being a fluid that solves the problem of direct emissions, this refrigerant requires complex architectures to be energy efficient and thus avoid excessive indirect emissions.

The reduction of the coefficient of performance (COP) of classical CO_2 systems when ambient temperature is high has forced to seek solutions to improve their performance. Although there are different alternatives, the use of the parallel compressor (PC) was one of the first proposals and it can already be considered as the state-of-the-art system in recent years, as described by Karampour and Sawalha [2]. Bell [3] proposed the use of the parallel compressor to improve the efficiency of the CO_2 cycles and thus compete at the level of the halocarbon refrigerants, obtaining improvements by more than 10% compared to the standard carbon dioxide cycle. The benefits on the COP and cooling capacity were also reported by Minetto et al. [4] who performed a theoretical investigation of a transcritical CO_2 cycle with parallel compression and found that the optimum intermediate pressure and the gas-cooler pressure are lower than for the traditional cycle Sarkar and Agrawal [5] optimized the CO_2 transcritical cycle with parallel compressor, reaching COP increments up to 47.3% compared to the base system Chesi et al. [6] carried out a theoretically study to define the operation limits of their experimental test and then carried out the experimental test of a CO_2 cycle with PC without optimizing the intermediate pressure, performed with a fixed parallel compressor speed and concluded that to achieve the maximum theoretical COP it is highly recommended to use compressors whose volumetric flow ratio can be modified. Gullo et al. [7] performed the advanced exergy analysis of a CO_2 booster refrigeration system with parallel compression considering its application for a typical European supermarket and concluded that the parallel compressor is largely improvable by bringing down the irreversibilities of the remaining components. Andreasen et al. [8] developed a data-driven model of a refrigeration booster system with parallel compression and ejectors where the parallel compressor was used to control the tank pressure and validated the model with data from a CO_2 system with negligible deviations. Wang et al. [9] carried out the thermodynamic evaluation of a CO_2 parallel compression refrigeration system with subcooler and compared its performance to the baseline parallel compression system, obtaining COP increments of 8.4% by average. The optimum operation of a single stage CO_2 transcritical refrigeration plant with parallel

compressor where evaluated experimentally by Nebot-Andrés et al. [10], determining the gas-cooler and intermediate optimum pressures.

In recent years, various lines of research have been developed with the aim to further improve the performance of these systems. Some of these lines of work are the use of ejectors for warm climates [11], whether the multi-ejector [12] or the two-phase ejector, focusing on the control strategies [13], expanders [14], combination with other systems as desiccant wheels [15], gas removal from the intermediate vessel [16] or combination with vapour absorption system [17] or subcooling [18]. Focusing on the latter, different systems that allow the subcooling of the CO_2 at the outlet of the gas-cooler have been developed. One of the most promising is the mechanical subcooling. This can be dedicated (DMS), where the support cycle can work with any other refrigerant, or integrated (IMS), when it only uses CO_2.

The proposal to use a dedicated mechanical subcooling system began to gain momentum when Llopis et al. [19] proposed a theoretical study of the benefits of using the DMS versus a simple CO_2 system achieving increments in COP and cooling capacity even if the operation parameters were not optimized. As a result of this study, Llopis et al. [20] carried out an experimental test of this system, only optimizing the gas-cooler pressures and experimentally corroborated the improvements presented by the DMS system. Later, Nebot-Andrés et al. [21] compared the use of the DMS versus the CO_2 cascade system and concluded that for evaporation levels greater than -15ºC the energy performance of the DMS system overcomes the cascade configuration. The optimum working conditions, gas-cooler pressure and subcooling degree, were determined experimentally by Nebot-Andrés et al. [22].

Dai et al. [23] proposed the use of zeotropic mixtures as possible refrigerants for the DMS cycle, to enhance the overall performance by taking advantage of the glide temperature of the mixture in the subcooler in order to improve the heat exchange performance. Llopis et al. [24] experimentally tested Dai's theory obtaining an additional 1.4% improvement in COP with respect to the pure fluid with the mixture R-600/R-152a [60/40%].

D'Agaro et al. [25] studied the effect of dedicated mechanical subcooler size and gas cooler pressure control on transcritical CO_2 booster systems and compared the DMS system to the parallel compression and subcooling performed through a water chiller dedicated to HVAC, being the DMS the most effective solution. The importance of optimizing the operation parameters of the DMS while considering costs has been reported by Cortella et al. [26]. They performed a thermoeconomic analysis of a

commercial refrigeration plant and found that the DMS's size is more crucial at hot climates.

Liu et al. [27] presented the thermal performance of a two-stage compression transcritical CO_2 refrigeration system with R290-DMS and they found that the two-throttling and two-stage compression high-pressure mechanical subcooling system has the best performance over the other three proposed systems. Miran et al. [28] studied the DMS for a transcritical refrigeration cycle using CO_2, N_2O and ethane as refrigerants of the main cycle from an energy, exergy and exergoeconomic point of view. The CO_2 system shows the best economic performance. By comparing it with and the cycle without subcooling, it can be concluded that DMS improves performance more than the increment of the cost per unit. The increment in COP is 30.74%, while the unit product cost increment is 9.04%, concluding that the subcooling is an effective and economical way of performance improvement. This solution has being studied also for its combination with ejector presenting significant advantages compared with the transcritical CO2 ejector cycle with a thermoelectric subcooling system. Increments in COP reach up to 10.27% at an environmental temperature of 35ºC and evaporation temperature of -5ºC [29].

Dedicated mechanical subcooling is also being implemented for space heating applications. Dai et al. [30] found a reduction of annual primary energy consumption up to 8.65% in comparison with baseline CO_2 system when using the DMS for heating/cooling. It also improves by up to 6.23 - 22.90% the annual performance factor of CO_2 system and the annual exergy efficiency is promoted by 7.25 - 24.79% compared with traditional CO_2 systems [31]. Cheng et al. [32] proposed to combine the advantages of transcritical with DMS and cascade systems reaching improvements in China of at most 8.7% and 19.4% in the whole heating season compared to transcritical system with DMS and cascade system, respectively, working separately. Song et al. [33] investigated the effect of the medium-temperature in a DMS for CO_2 heat pumps and demonstrated the existence of an optimal temperature.

In parallel, the use of IMS was proposed for the first time applied to CO_2 in the patent of Kantchev and Lesage [34] with the aim of enhancing the COP. This system has been evaluated theoretically reaching up to a 17.3% in COP at -10ºC of evaporation temperature and 30ºC at the gas-cooler exit [35]. Nebot-Andrés et al. [36] performed a thermodynamic analysis of the IMS cycle optimizing gas-cooler pressure and subcooling degree. Later, they evaluated and determined the operating parameters experimentally [37].

These systems have proven to have strong potential and the theoretical improvements obtained are significant. Catalán-Gil et al. [38] evaluated theoretically energy improvements offered by dedicated and integrated mechanical subcooling systems in CO_2 booster for supermarket applications compared to the booster with parallel compressor. The mechanical subcooling systems offered annual energy reductions up to 5.1% at hot climates.

However, the optimized performance of these systems has never been contrasted from an experimental basis. The objective of this work is to present the experimental evaluation of mechanical subcooling cycles, both integrated and dedicated, versus the cycle with parallel compression in a laboratory installation for different heat rejection levels (25.0ºC, 30.4ºC and 35.1ºC) and experimentally quantify the improvements that these systems entail.

11.2. Methods

This section presents the experimental installation and the evaluated transcritical cycles tested at optimum conditions. The most important components of the parallel compression cycle, the dedicated mechanical subcooling and the integrated mechanical subcooling are provided and the measurement system used in the plant is described.

In Figure 11.1 the diagram of the cycles analyzed in this work is presented. The main CO_2 cycle is represented in black, common to all the studied cycles, and the auxiliary cycles are represented in blue.

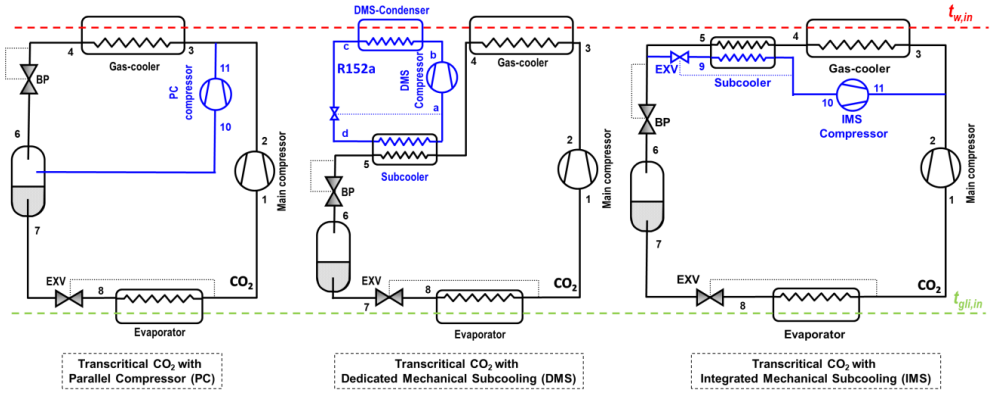

Figure 11.1. Configuration plant

On Figure 11.1 left, the cycle with parallel compression (PC) is depicted. It is a simple compression cycle with two expansion stages between which is the liquid reservoir. The auxiliary PC cycle draws vapor from the liquid tank; it is recompressed through the

auxiliary compressor and reinjected in the main cycle at the gas-cooler inlet. Parallel compression reduces the vessel pressure and thus increments the specific cooling capacity of the cycle.

Figure 11.1 (center) shows the CO_2 cycle with the dedicated mechanical subcooling system (DMS). This cycle has a heat exchanger located after the gas-cooler that is used to subcool the CO_2. This subcooler thermally connects the main cycle with the support cycle, a simple vapor compression cycle, which works with R-152a and is responsible for subcooling the CO_2. DMS also increments the specific cooling capacity, but at the same time, reduces the optimum heat rejection pressure in the main cycle.

Finally, in Figure 11.1 (right) the cycle with integrated mechanical subcooling (IMS) is presented. In this configuration is sought to subcool the CO_2 at the exit of the gas-cooler thanks to the CO_2 itself: a part of this being expanded and evaporated through the subcooler to be later compressed and reinjected in the main cycle through the auxiliary compressor. Like the DMS, the IMS enhances the specific cooling capacity and reduces the optimum heat rejection pressure.

11.2.1. Experimental plant

The three systems have been tested in the same experimental installation, where different valves allow testing each configuration separately, the main elements being common to the three cycles: evaporator, gas-cooler, expansion system and main compressor. The main compressor is a semihermetic compressor with a displacement of 3.48 $m^3 \cdot h^{-1}$ at 1450 rpm and a nominal power of 4 kW. The expansion is carried out by a double-stage system, composed of an electronic expansion valve (back-pressure) controlling the gas-cooler pressure, a liquid receiver between stages and an electronic expansion valve, working as thermo-static, to control the evaporating process. Evaporator and gas-cooler are brazed plate heat exchangers with exchange surface area of 4.794 m^2 and 1.224 m^2, respectively

For the auxiliary compressors, PC and IMS use the same compressor, a variable speed semihermetic compressor with displacement of 1.12 $m^3 \cdot h^{-1}$ at 1450 rpm and the compressor of the DMS cycle is a variable speed semihermetic compressor with displacement of 4.06 $m^3 \cdot h^{-1}$ at 1450 rpm.

The subcoolers are brazed plate counter current heat exchangers with exchange surface area of 0.850 m^2 for the IMS and 0.576 m^2 for the DMS. The experimental CO_2 installation is shown in Figure 11.2 and the DMS cycle in Figure 11.3.

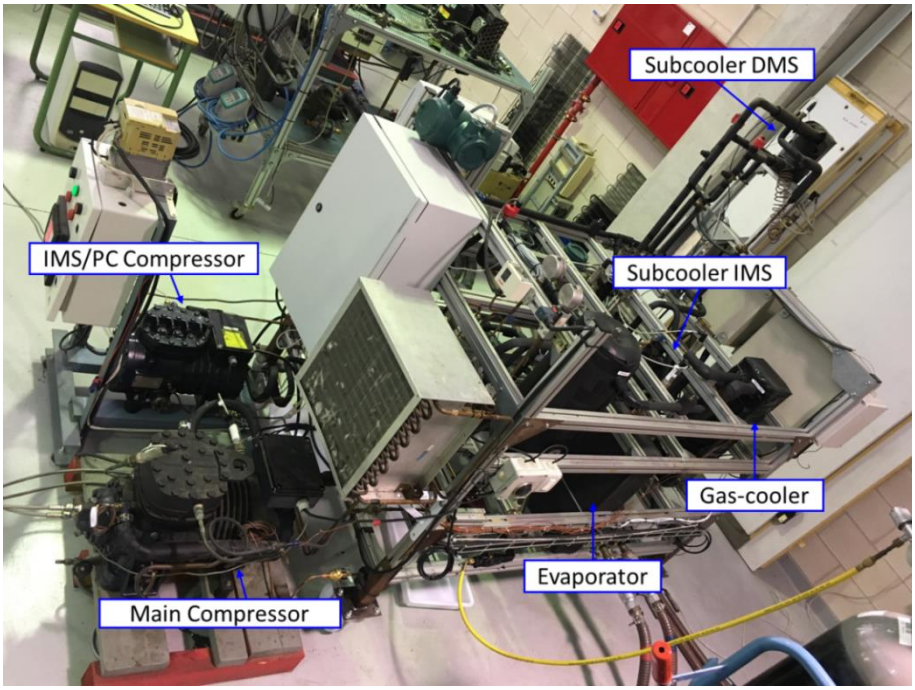

Figure 11.2. Experimental CO_2 plant.

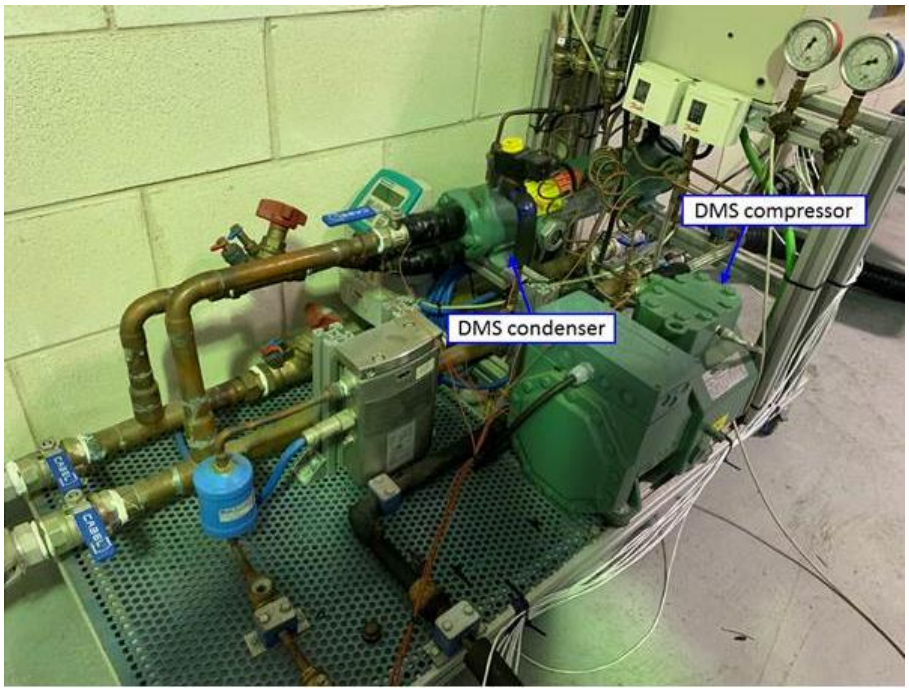

Figure 11.3. Experimental DMS cycle.

Heat dissipation in gas-cooler and the DMS condenser is done with a water loop, simulating the heat rejection level. The evaporator is supplied with another loop, working with a propylene glycol–water mixture (60% by volume) that enables a constant entering temperature in the evaporator. Both the mass flow and the inlet temperature are controlled in these loops.

11.2.2. Measurement system

The thermodynamic properties of the working fluids are obtained thanks to the measurement system presented in Figure 11.4. All fluid temperatures are measured by T-type thermocouples and pressure gauges are installed along all the circuit and CO_2 mass flow rates are measured by two Coriolis mass flow meters. The mass flow of R-152a is measured by another Coriolis mass flow meter. The flow of the propylene glycol–water mixture is measured by a Coriolis mass flow meter and the water flow rate by a magnetic volumetric flow meter and a Coriolis mass flow meter. Compressors' power consumptions are measured by digital wattmeters. The accuracies of the measurement devices are presented in Table 11.1.

Table 11.1. Accuracies and calibration range of the measurement devices.

Measured variable	**Measurement device**	**Range**	**Calibrated accuracy**
Temperature (ºC)	T-type thermocouple	-40.0 to 145.0	±0.5K
CO_2 pressure (bar)	Pressure gauge	0.0 to 160.0	±0.96 bar
CO_2 pressure (bar)	Pressure gauge	0.0 to 100.0	±0.6 bar
CO_2 pressure (bar)	Pressure gauge	0.0 to 60.0	±0.36 bar
DMS pressure (bar)	Pressure gauge	0.0 to 16.0	±0.096 bar
DMS pressure (bar)	Pressure gauge	0.0 to 40.0	±0.24 bar
CO_2 main mass flow rate ($kg \cdot s^{-1}$)	Coriolis mass flow meter	0.00 to 1.38	±0.1% of reading
CO_2 IMS/PC mass flow rate ($kg \cdot s^{-1}$)	Coriolis mass flow meter	0.00 to 0.083	±0.1% of reading
DMS mass flow rate ($kg \cdot s^{-1}$)	Coriolis mass flow meter	0.00 to 0.05	±0.1% of reading
Water mass flow rate ($m^3 \cdot h^{-1}$)	Magnetic flow meter	0.0 to 5.0	±0.3% of rate
Glycol volume flow rate ($kg \cdot s^{-1}$)	Coriolis mass flow meter	0.0 to 13.88	±0.1% of reading
Power consumption (kW)	Digital wattemeter	0.0 to 6.0	±0.5% of reading

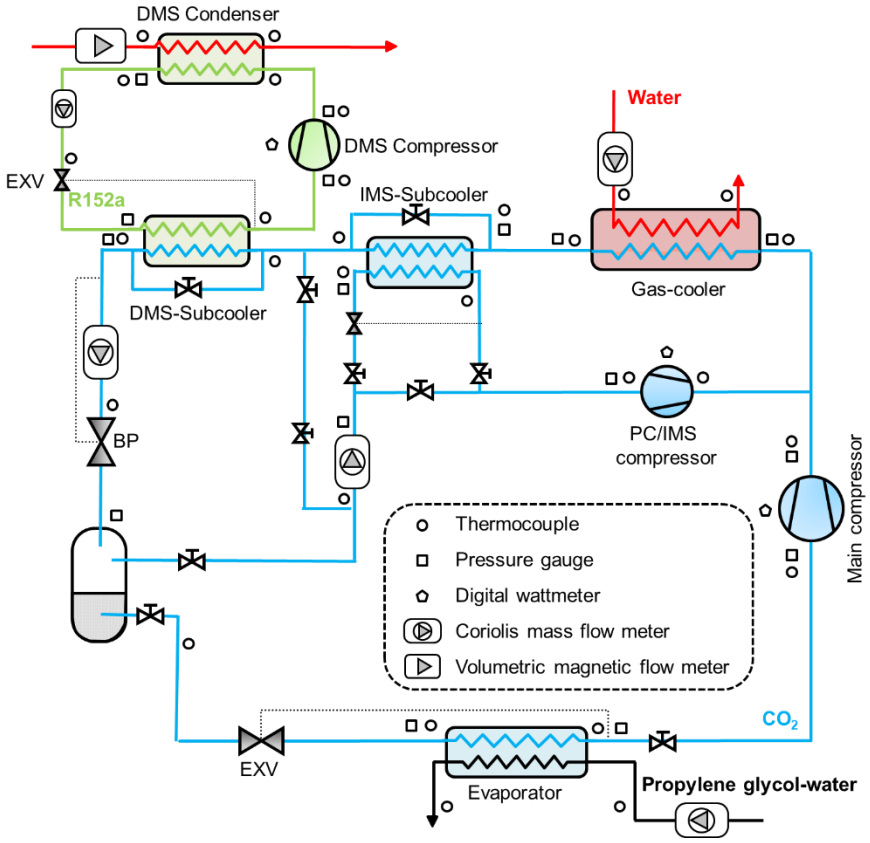

Figure 11.4. Schema of the plant and acquisition system interface.

11.2.3. Comparison methods

This section contains the description of the strategy for conducting the experimental tests in order to determine the optimum conditions of each cycle and then being able to make the comparison between the evaluated cycles.

To compare the three configurations, one evaporating condition is evaluated for three different heat rejection levels, always operating in the transcritical region. The evaluated conditions were:

- Heat rejection level: three different temperatures: 25.0, 30.4 and 35.1°C, with maximum deviation of ±0.20°C. These levels were performed fixing the inlet temperature of the secondary fluid (water) to the gas-cooler for a constant water flow rate of 1.77 $m^3 \cdot h^{-1}$. For the DMS, this mass flow is divided in two currents in order to feed the gas-cooler and the DMS-condenser, 1.17 and 0.6 respectively. Evaluated temperatures are within the possible range of the experimental plant. Lowest heat rejection temperature was 25ºC. For lower

values the plant should operate in subcritical condition, but the installation is only able to perform in transcritical conditions. Maximum heat rejection temperature was 35ºC, since is the limit of the heat dissipation system in the laboratory.

- One heat load condition: the inlet temperature of the secondary fluid in the evaporator is maintained for all the tests to 3.8ºC and the flow rate was fixed to 0.7 $m^3 \cdot h^{-1}$.
- Gas-cooler pressure was regulated with an electronic BP fixed during each test thanks to a PDI controller. Plant was subjected to an experimental optimization procedure to determine the maximum COP, which is the optimum condition. Pressure was varied within 74 to 100 bar. The optimum condition also depended on other parameters as the subcooling degree, the vessel pressure and the heat rejection level.
- Compressors: The main compressor always operated at nominal speed of 1450 rpm. The speeds of the auxiliary compressors were varied in order to obtain the optimum subcooling degree or optimum intermediate pressure. These parameters were also optimized experimentally.
- Electronic expansion valves: The electronic expansion valves were set to obtain a superheating degree in the evaporator of 10K and of 5K on the subcoolers.

All the tests were carried out in steady state conditions for periods longer than 10 minutes, taking data each 5 seconds, obtaining the test point as the average value of the whole test. The measured data were used to calculate the thermodynamic properties of the points using Refprop v.9.1. [39].

The procedure followed to identify the optimum COP is described in detail by Nebot-Andrés et al. [37].

11.3. Results and discussion

This section presents the main energy parameters measured in the tests. All the data presented correspond to the optimal points at which the COP is maximum for each of tested condition. The results are presented in Table 11.6 as well as the uncertainty measurements (u), calculated using Moffat's method [40] and described below.

Cooling capacity is calculated as product of the CO_2 mass flow rate in the evaporator and the enthalpy difference between the outlet and the inlet of the evaporator, as shown by Eq. (11.2).

$$\dot{Q}_0 = \dot{m}_0 \cdot (h_{0,out} - h_{0,in}) \quad (11.1)$$

The $h_{0,out}$ is calculated from pressure and temperature measurements at the evaporator outlet. The $h_{0,in}$ is calculated as the enthalpy at the inlet of the back pressure for the DMS and the IMS systems (Eq. (11.2)), while for the PC system, it is calculated

considering the pressure at the liquid tank and saturated condition (Eq.(11.3)). It was verified visually than at the exit of the vessel CO_2 was in liquid condition.

$$h_{0,in} = f(P_{MS,out}, T_{MS,out}) \tag{11.2}$$

$$h_{0,in} = f(P_{vess}, x = 0) \tag{11.3}$$

The COP of the systems is calculated as shown in Eq. (11.4), considering the power consumption of the main compressor and the auxiliary one.

$$COP = \frac{\dot{Q}_0}{P_{C,main} + P_{C,aux}} \tag{11.4}$$

The cooling capacity uncertainty is defined as shown in Eq. (11.5)-(11.8).

$$u_{\dot{Q}_0} = \sqrt{\left(\frac{\partial \dot{Q}_0}{\partial \dot{m}_0} \cdot u_{\dot{m}_0}\right)^2 + \left(\frac{\partial \dot{Q}_0}{\partial h_{0,out}} \cdot u_{h_{0,out}}\right)^2 + \left(\frac{\partial \dot{Q}_0}{\partial h_{0,in}} \cdot u_{h_{0,in}}\right)^2} \tag{11.5}$$

$$\frac{\partial \dot{Q}_0}{\partial \dot{m}_{co2}} = (h_{0,out} - h_{0,in}) \tag{11.6}$$

$$\frac{\partial \dot{Q}_0}{\partial h_{0,out}} = \dot{m}_0 \tag{11.7}$$

$$\frac{\partial \dot{Q}_0}{\partial h_{0,in}} = -\dot{m}_0 \tag{11.8}$$

The uncertainty of $h_{0,out}$ is calculated, using Moffat's Method [40] as described by Aprea et al. [41]:

$$h_{0,out} = f(P_{0,out}, T_{0,out}) \tag{11.9}$$

$${h_{0,out}}^{p+} = f\left(P_{0,out} + u\left(P_{0,out}\right), T_{0,out}\right) \tag{11.10}$$

$${h_{0,out}}^{p-} = f(P_{0,out} - u\left(P_{0,out}\right), T_{0,out}) \tag{11.11}$$

$${h_{0,out}}^{t+} = f(P_{0,out}, T_{0,out} + u\left(T_{0,out}\right)) \tag{11.12}$$

$${h_{0,out}}^{t-} = f(P_{0,out}, T_{0,out} - u\left(T_{0,out}\right)) \tag{11.13}$$

$$I^p = \frac{\left|{h_{0,out}}^{p+} - h_{0,out}\right| + \left|{h_{0,out}}^{p-} - h_{0,out}\right|}{2} \tag{11.14}$$

$$I^t = \frac{\left|{h_{0,out}}^{t+} - h_{0,out}\right| + \left|{h_{0,out}}^{t-} - h_{0,out}\right|}{2} \tag{11.15}$$

$$u_{h_{0,out}} = \sqrt{{I^p}^2 + {I^t}^2} \tag{11.16}$$

In the same way, the uncertainty of $h_{0,in}$ is calculated, considering Eq. (11.2) and (11.3) depending on the analysed system. The uncertainty of the measurement devices used to calculate COP and cooling capacity uncertainties are presented in Table 11.1.

The uncertainty of the measured COP is also calculated as previously described, being the error in COP defined as follows:

$$u_{COP} = \sqrt{\left(\frac{\partial COP}{\partial \dot{Q}_0} \cdot u_{\dot{Q}_0}\right)^2 + \left(\frac{\partial COP}{\partial P_{C,CO2}} \cdot u_{P_{C,main}}\right)^2 + \left(\frac{\partial COP}{\partial P_{C,IMS}} \cdot u_{P_{C,aux}}\right)^2} \quad (11.17)$$

$$\frac{\partial COP}{\partial \dot{Q}_0} = \frac{1}{P_{C,main} + P_{C,aux}} \quad (11.18)$$

$$\frac{\partial COP}{\partial P_{C,main}} = -\frac{\dot{Q}_0}{\left(P_{C,main} + P_{C,aux}\right)^2} \quad (11.19)$$

$$\frac{\partial COP}{\partial P_{C,aux}} = -\frac{\dot{Q}_0}{\left(P_{C,main} + P_{C,aux}\right)^2} \quad (11.20)$$

The uncertainty of all the presented results in this work is compiled in Table 11.6.

11.3.1. COP

The COP values measured and their uncertainty for each condition in the three cycles are presented in Figure 11.5. As it can be observed, the lowest COPs are obtained for the cycle with parallel compressor, being the cycle with the DMS the one with highest performance at all the evaluated temperatures.

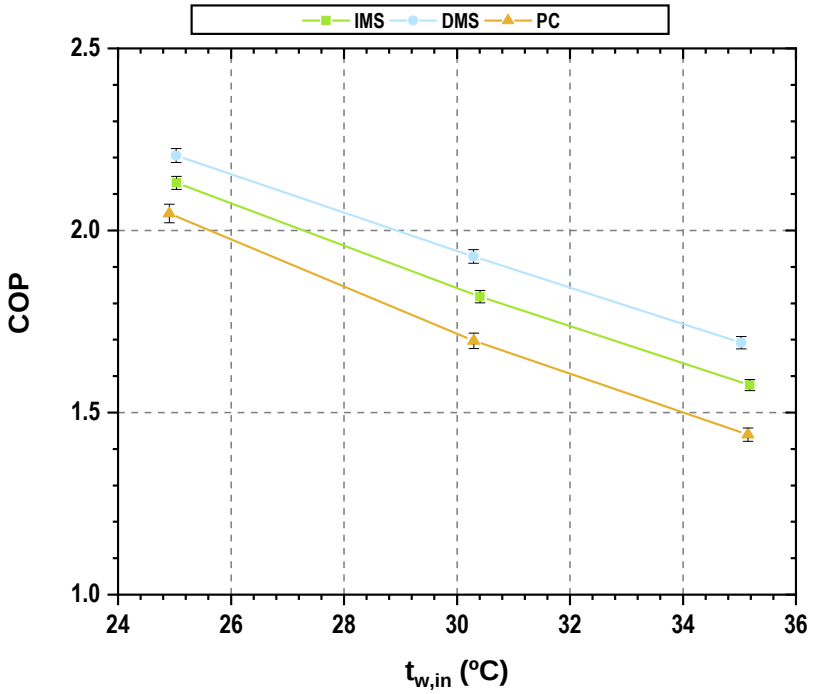

Figure 11.5. Evolution of the maximum COP for optimal conditions vs. the gas-cooler water inlet temperature.

The increments in COP obtained by the cycles with mechanical subcooling compared to the cycle with PC, calculated as Eq. (11.21), are presented in Figure 11.6. The increments obtained by the IMS are 4.1% at 25.0ºC, 7.2% at 30.4ºC and 9.5% at 35.1ºC. As for the improvements achieved with the DMS, they are superior and are 7.8%, 13.7% and 17.5% respectively. The COP of the DMS is 3.5%, 6.1% and 7.4% higher than the IMS for the analysed temperatures.

$$\Delta COP\ (\%) = \frac{COP_{MS} - COP_{PC}}{COP_{PC}} \tag{11.21}$$

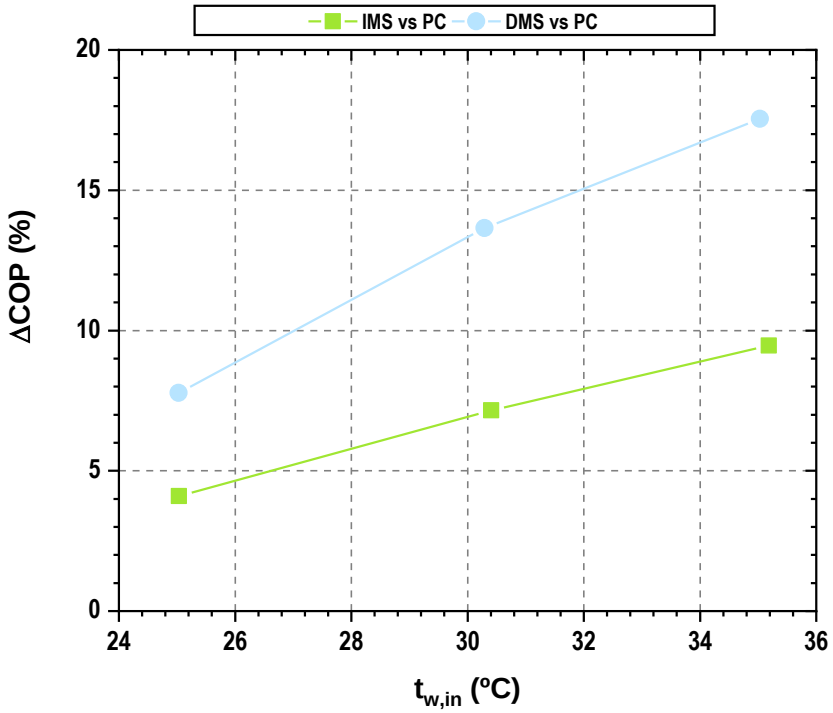

Figure 11.6. COP increments of the mechanical subcooling systems referred to the parallel compression.

11.3.2. Cooling capacity

Analyzing the cooling capacity of the cycles for their optimal operating conditions, the cycle with parallel compression is the one that provides the greatest cooling capacity, but the capacity of the DMS and IMS lower. Figure 11.7 shows the cooling capacity of each of the cycles and its uncertainty. It can be seen how the IMS's cooling capacity is practically the same as the PC and it is the cooling capacity of the DMS cycle the one that is slightly lower for the evaluated conditions, 4.1% lower in average.

It should be emphasized that the three cycles have the possibility of adapting the cooling capacity depending on the needs of each application simply by varying the rotational speed of the auxiliary compressor. However, if capacity is modified by compressor speed adjustment, the COP will suffer a penalty, since the plant will be out of optimum conditions operation.

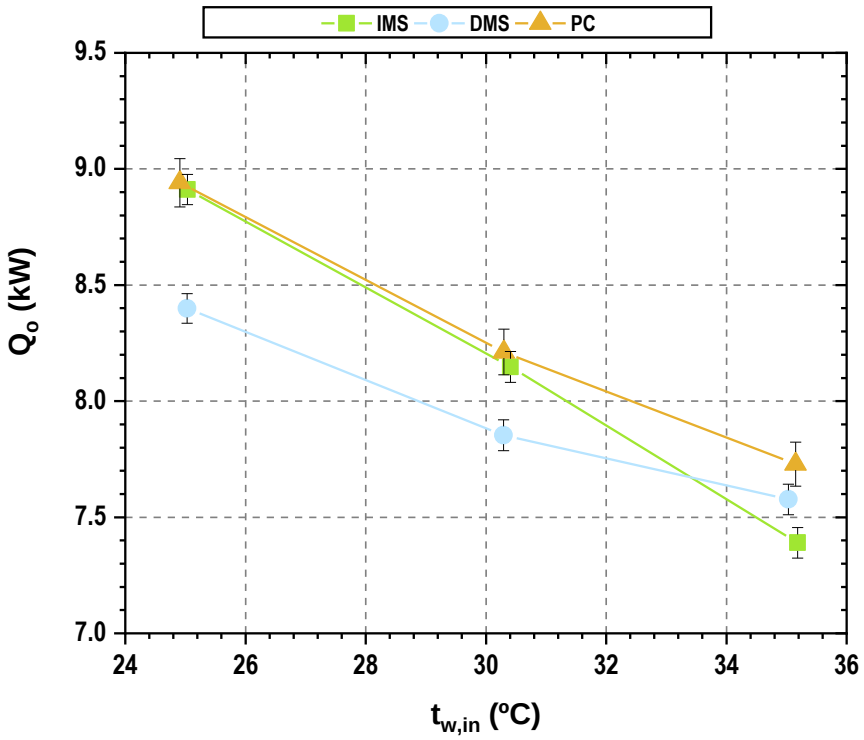

Figure 11.7. Evolution of the maximum cooling capacity for optimal conditions vs. gas cooler water inlet temperature.

11.3.3. Optimum operation parameters

The optimum operating conditions to obtain maximum COP are presented in Table 11.6. Gas-cooler pressure must be optimized in the three architectures. For the PC cycle also the intermediate pressure should be optimized while in the subcooling systems is the subcooling degree the parameter that must be optimized.

Optimum gas-cooler pressures are shown in Figure 11.8. As it can be seen, the optimum pressures for the DMS and the IMS are quite similar while the optimal pressures of the PC are significantly higher. This difference in the optimum gas-cooler pressure is caused by the subcooling of the CO_2 since it allows to reduce the optimal working pressure [19]. Comparing the optimum pressures, the DMS system allows a

reduction of the optimum pressure of 2.7 bar for 25.0ºC, 8.2 bar for 30.4ºC and 9.2 bar for 35.1ºC. The IMS reaches reductions of 2.9 bar, 6.3 bar and 11.2 bar respectively.

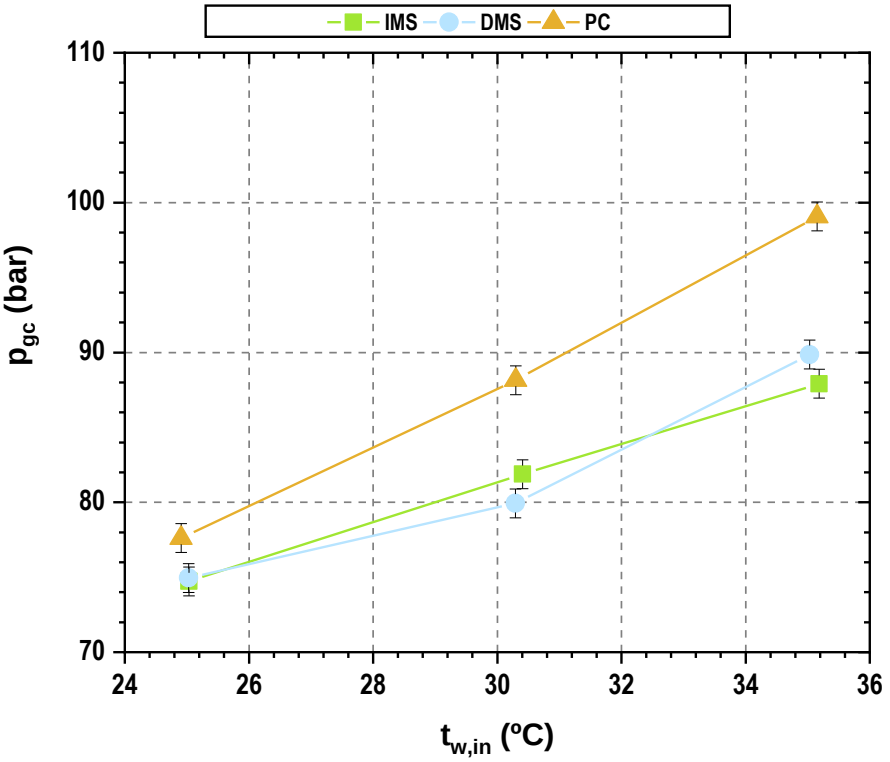

Figure 11.8. Optimum working pressures.

11.3.4. Cycles performance

As presented so far, mechanical subcooling cycles represent an energetic improvement of the performance of the CO_2 cycle with parallel compression. This section presents an analysis of the operation of the compressors as well as the heat exchangers to understand the reason for this energy improvement.

Figure 11.9 shows the p-h diagram of the PC cycle (orange), the DMS (blue) and IMS (green) for 30.4ºC of water inlet temperature at optimum conditions. It can be observed that the three solutions implemented in each cycle allow increasing the specific cooling capacity, it being higher for the PC. The optimal pressure reduction can also be easily appreciated, so that the specific compression work of cycles with mechanical subcooling is less than that of the cycle with PC. Regarding the specific compression work of the auxiliary compressor, it can be seen how this is much higher for the PC cycle than for the IMS, due to two reasons: higher discharge pressure (+6.2 bar) and lower suction pressure (- 3.2 bar).

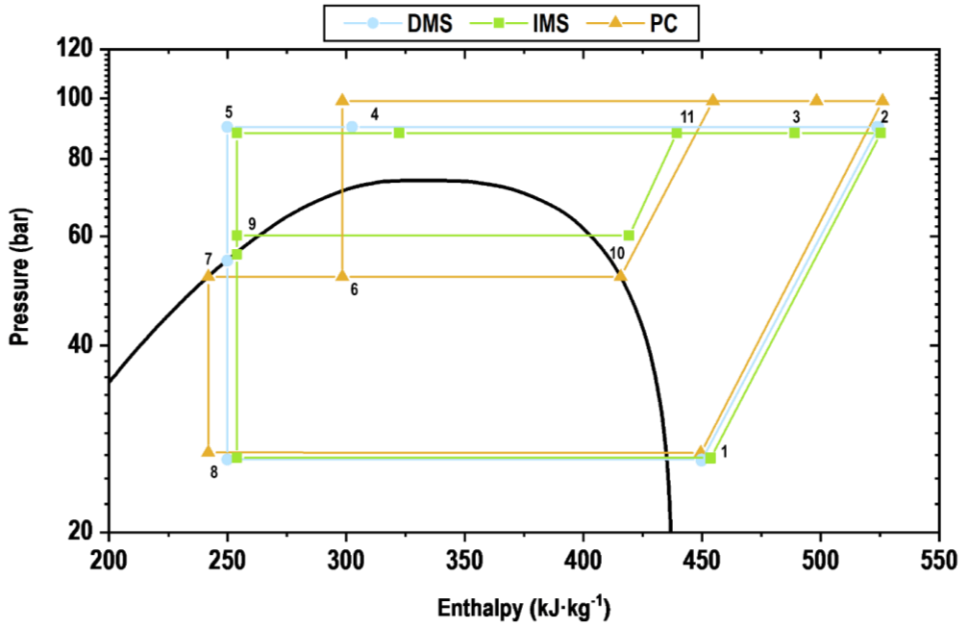

Figure 11.9. p-h diagram for water inlet temperature of 30.4ºC.

11.3.4.1. Compressors performance

As it has been seen, the optimum conditions cause the same compressor to work differently depending on the cycle. It is therefore necessary to analyze the efficiencies of the compressors as well as their compression ratio.

Figure 11.10 shows the power consumption of the main compressor (blue) and the auxiliary one (green). As it can be seen, the cycle with PC is always the one with the highest consumption, both of the main and the secondary compressors. This implies that even though the cycle has a slightly higher cooling capacity, its COP is lower. The power consumed by the main compressor is higher because the compression ratio is higher than that of the other cycles (Table 11.2), while the transferred flow is practically the same (Table 11.6).

Comparing the main compressor of the IMS and the DMS, the power consumption of the main compressor is practically the same. The greatest differences are observed in the consumption of the secondary compressor, being the auxiliary compressor of the DMS the one that consumes considerably less than that of the IMS, -38.9% in average, with the highest difference at 25.0ºC.

Table 11.2 shows the compression ratio, the volumetric efficiency and the global efficiency of the main compressor and the auxiliary compressor for all the optimum points. Regarding the main compressor, the PC system has the highest compression

ratio and the IMS the lowest. The global efficiency is higher for the DMS system and also the volumetric efficiency, while the PC has the worst efficiencies, due to the highest compression ratio.

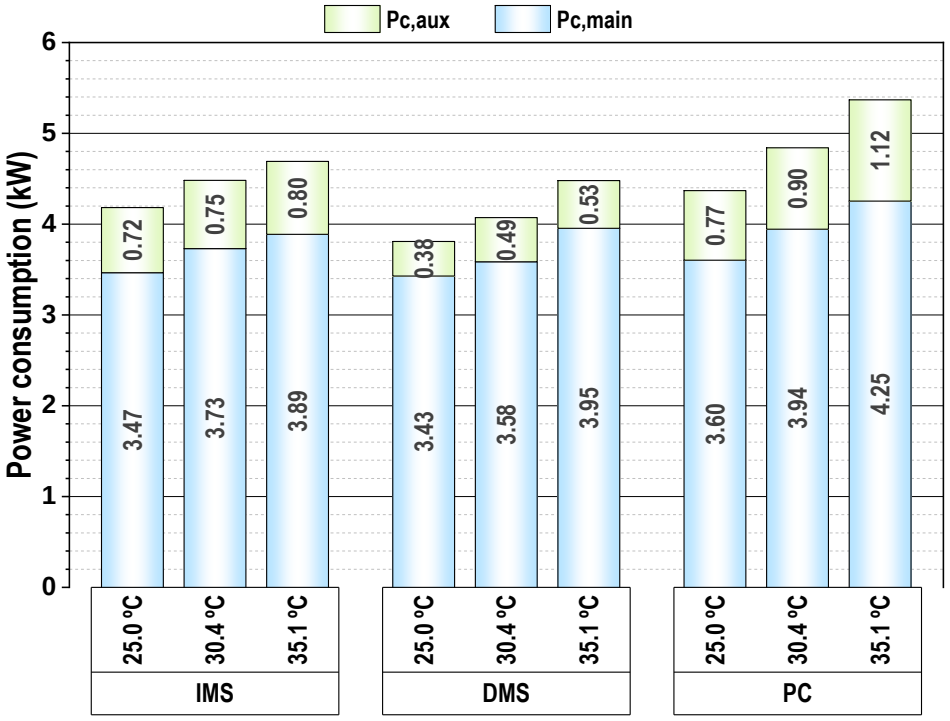

Figure 11.10. Power consumption of the main compressor and the auxiliary compressor for each system.

Regarding the auxiliary compressor, if the operation of the IMS system and the PC system are compared, using the same compressor, it is seen that the IMS presents better efficiencies in general, except for 25.0ºC. Analyzing the compression ratio, for the IMS they are lower, being close to the work limit and in one of the cases even lower than 1.5, not recommended by the manufacturer. Suction temperatures are also outside the application limits of the manufacturer, greater than the limit in both systems. The DMS system also works with relatively low volumetric efficiencies, like the other systems and as it can be seen in the table, all the auxiliary compressors work at low frequencies to achieve the optimal subcooling degree, which would require the use of smaller compressors for this plant.

Table 11.2. Compressors efficiencies and compression ratios.

		Main compressor			Auxiliary compressor				
	$T_{w,in}$ (ºC)	τ (-)	η_{vol} (-)	η_{glo} (-)	τ (-)	η_{vol} (-)	η_{glo} (-)	T_{suc} (ºC)	f (Hz)
IMS	25.0	2.9	0.67	0.72	1.7	0.44	0.68	13.9	28
	30.4	3.1	0.64	0.72	1.5	0.47	0.77	20.3	29
	35.2	3.3	0.61	0.72	1.4	0.56	0.92	26.1	33
DMS	25.0	3.0	0.66	0.75	2.4	0.42	0.57	22.4	30
	30.3	3.2	0.64	0.73	2.4	0.49	0.60	26.3	35
	35.0	3.4	0.62	0.72	2.5	0.49	0.63	29.3	35
PC	24.9	3.0	0.67	0.75	1.7	0.45	0.85	12.4	30
	30.3	3.4	0.63	0.70	1.8	0.43	0.76	14.4	30
	35.2	3.7	0.59	0.68	1.9	0.50	0.75	15.9	35

11.3.4.2. Heat exchangers thermal effectiveness

What the three systems presented in this work have in common is the use of an additional compressor as part of their upgrade cycle. Apart from this, the three cycles analyzed share the main exchangers: the evaporator and the gas-cooler.

The main effects in the evaporator of using a mechanical subcooling system or a parallel compressor are observed in the vapor quality at the evaporator inlet, what is totally related to the heat exchanger performance. As it can be observed in Table 11.3, the lowest vapor quality is achieved with the IMS system for 25.0ºC while when water inlet temperature goes up, is the PC the one that achieves lower vapor quality.

Table 11.3. Evaporator temperatures and thermal effectiveness of the evaporator.

	$T_{w,in}$ (ºC)	T_0 (ºC)	$x_{in,evap}$ (-)	ε (-)
IMS	25.0	-11.2	0.199	0.69
	30.4	-10.2	0.251	0.77
	35.2	-10.1	0.300	0.71
DMS	25.0	-11.9	0.224	0.76
	30.3	-11.5	0.269	0.76
	35.0	-10.4	0.286	0.79
PC	24.9	-10.9	0.213	0.79
	30.3	-10.2	0.237	0.72
	35.2	-9.5	0.249	0.73

Also the difference in the behavior of the systems can be observed in the evaporation temperature, where despite the fact that the three systems have the same glycol temperature at the evaporator inlet, the PC works at higher evaporation temperatures. This is directly related to the cooling capacity that the systems have under the tested

conditions, since the PC has a greater cooling capacity and therefore can slightly raise its evaporation level.

Regarding evaporator thermal effectiveness, it can be observed that for 25.0ºC, the PC is the system with highest evaporator efficiency. At higher temperatures, best performance of the evaporator is obtained with the DMS.

The gas-cooler is the exchanger that most influences the energetic behavior of these systems. The COP of transcritical systems is totally related to the gas-cooler outlet temperature, so for a fixed dissipation temperature, the behavior of this exchanger is a key parameter. As it can be seen in

Table 11.4, the DMS is the system that achieves a lower approach in the gas-cooler, the approach being the difference between the gas-cooler outlet temperature and the water inlet temperature, as expressed in Eq. (11.22).

$$APP = T_{gc,out} - T_{w,in} \tag{11.22}$$

Table 11.4. Gas-cooler temperatures and thermal effectiveness.

	$T_{w,in}$ (ºC)	$T_{gc,in}$ (ºC)	$T_{gc,out}$ (ºC)	APP (ºC)	ε (-)	$\dot{m}_{gc}$ (kg/s)
IMS	25.0	82.0	28.1	3.1	0.95	0.056
	30.4	85.0	33.2	2.8	0.95	0.061
	35.2	83.4	37.4	2.2	0.95	0.068
DMS	25.0	93.9	26.4	1.3	0.98	0.039
	30.3	98.5	31.6	1.3	0.98	0.038
	35.0	108.4	35.6	0.6	0.99	0.038
PC	24.9	82.3	29.1	4.2	0.93	0.059
	30.3	89.5	32.2	1.9	0.97	0.058
	35.2	95.7	36.9	1.8	0.97	0.061

DMS is also the system that achieves better efficiencies in the gas-cooler. These phenomena are due to the fact that the gas-cooler in this system transfers a lower CO_2 mass flow ($\dot{m}_{gc}$), since the auxiliary cycle is independent of the main cycle. As consequence gas-cooler outlet temperature is lower for the DMS system with leads to better energy performance. In a real system it implies than the heat exchanger area of the gas-cooler using DMS could be reduced in relation to the other architectures. Despite this difference, the basis for comparison is adequate since the thermal effectiveness of the gas-cooler only varies by around 3% between systems.

Main subcooler's performance parameters for optimal operation points are presented in Table 11.5. The subcooler is a heat exchanger that is only present in the IMS and in the DMS systems. Furthermore, as it has been seen in the description of the cycles, it is not the same heat exchanger for both systems, since in the IMS is a CO_2-CO_2 heat exchanger and for the DMS it is CO_2-R152a. As it has been seen for the optimum operation parameters, the IMS needs a higher subcooling degree so the cooling capacity of the subcooler of the IMS is higher, almost double the capacity.

The CO_2 mass flow passing through the subcooler ($\dot{m}_{CO2}$) is quite larger for the IMS because all the CO_2 is being subcooled since the expansion of the IMS mass flow ($\dot{m}_{0,MS}$) is carried out after the subcooler. This also makes the required cooling capacity to be higher in the subcooler.

The mass flow in the evaporator side is quite larger for the CO_2 (IMS) than for the R152a (DMS) and the efficiencies are better for the IMS system than for the DMS, as it has higher heat exchange area. Although the thermal effectiveness of the DMS subcooler is lower than the IMS, it does not affect to the energy improvements.

The mass flows and the optimum subcooling degree make the energy needs of the IMS subcooler higher, which entails the use of a larger heat exchanger. This favors the DMS, which achieves better overall performance with a smaller heat exchanger.

Table 11.5. Main subcooler performance parameters.

	$T_{w,in}$ (ºC)	SUB (ºC)	$T_{0,MS}$ (ºC)	$\dot{m}_{0,MS}$ (kg/s)	$\dot{m}_{CO2}$ (kg/s)	ε (-)	$\dot{Q}_{sub}$ (kW)
IMS	25.0	16.1	10.0	0.016	0.056	0.89	3.04
	30.4	15.1	16.7	0.022	0.061	0.91	3.66
	35.2	14.4	22.1	0.031	0.068	0.94	4.68
DMS	25.0	12.3	10.9	0.006	0.039	0.80	1.54
	30.3	12.6	16.1	0.008	0.038	0.82	1.89
	35.0	13.7	18.6	0.008	0.038	0.80	2.00

11.4. Conclusions

The experimental comparison of a CO_2 transcritical refrigeration plant working with parallel compression, dedicated mechanical subcooling (DMS) and integrated mechanical subcooling (IMS) is presented in this work. The comparison covered three heat rejection temperatures (25.0ºC, 30.4ºC and 35.1ºC) at steady-state conditions and optimizing the working parameters of each system.

The results obtained in this work corroborated the tendencies obtained in theoretical studies where the IMS and the DMS systems entrain an improvement of energy performance when comparing to the parallel compressor system (PC).

The experimental tests shown increments in COP of 4.1% at 25.0ºC, 7.2% at 30.4ºC and 9.5% at 35.1ºC thanks to the use of the IMS and of 7.8%, 13.7% and 17.5% respectively when using the DMS. The two systems therefore perform better than the reference system but it is the DMS that provides the greatest benefits. In terms of cooling capacity, there are no notable differences, this being slightly lower for cycles with mechanical subcooling. In any case, this cooling capacity can be adapted to the needs by modifying the degree of subcooling, and moving away from the optimal COP point. Both mechanical subcooling systems allow working at gas-cooler pressures lower than the optimum of the cycle with parallel compression, a fact that also benefits these mechanical subcooling systems. The performance of the compressors and the heat-exchangers has also been studied, highlighting differences between the systems and some deficiencies regarding the availability of equipment, specifically compressors, for allowing these systems to work at optimal conditions. Differences have also been detected in the heat exchangers. Specifically, it has been found that the DMS needs smaller gas-cooler and subcooler.

The importance of this work is the experimental quantification of the improvements introduced by the mechanical subcooling cycles with respect to the cycle with parallel compression since it really demonstrates the potential of these solutions for their application.

11.5. Acknowledgements

The authors thank the Ministerio de Ciencia y Tecnología (Spain) project RTI2018-093501-B-C21, the Ministerio de Educación, Cultura y Deporte (Spain), grant FPU16/00151 and the Jaume I University (Spain), project UJI-B2019-56 and grant PREDOC/2019/19 for financing this research work.

11.6. Nomenclature

APP approach temperature of the gas-cooler, K

BP back-pressure valve

COP coefficient of performance

DMS dedicated mechanical subcooling

EXV electronic expansion valve

f	frequency, Hz
h	specific enthalpy, kJ·kg^{-1}
I	contribution to the accuracy
IMS	integrated mechanical subcooling
$\dot{m}$	mass flow, kg·s^{-1}
p	absolute pressure, bar
Pc	power consumption, kW
PC	parallel compressor
$\dot{Q}$	cooling capacity, kW
SUB	degree of subcooling produced in the subcooler, K
T	temperature, ºC
u	uncertainty, %

Greek symbols

ε	efficiency
ρ	density, kg·m^{-3}
τ	compression ratio
x	vapour quality
η	compressor efficiency

Subscripts

aux	corresponding to the auxiliary cycle
dis	compressor discharge
evap	evaporator
gc	gas-cooler
gly	glycol

glo	global
in	inlet
main	corresponding to the main cycle
MS	corresponding to the mechanical subcooling cycle
0	evaporating level
out	outlet
sub	corresponding to the subcooler
suc	compressor suction
vess	corresponding to the vessel
vol	volumetric
w	water

Superscript

p	corresponding to the measured pressure value
p+	corresponding to the measured pressure value plus the measurement uncertainty
p+	corresponding to the measured pressure value minus the measurement uncertainty
t	corresponding to the measured temperature value
t+	corresponding to the measured temperature value plus the measurement uncertainty
t-	corresponding to the measured temperature value minus the measurement uncertainty

11.7. References

[1] European Commission. Regulation (EU) No 517/2014 of the European Parliament and of the Council of 16 April 2014 on fluorinated greenhouse gases and repealing Regulation (EC) No 842/2006. 2014.

[2] Karampour M, Sawalha S. State-of-the-art integrated CO2 refrigeration system for supermarkets: A comparative analysis. International Journal of Refrigeration. 2018;86:239-57.

[3] Bell I. Performance increase of carbon dioxide refrigeration cycle with the addition of parallel compression economization. Conference Performance increase of carbon dioxide refrigeration cycle with the addition of parallel compression economization.

[4] Minetto S, Cecchinato L, Corradi M, Fornasieri E, Zilio C, Schiavon A. Theoretical and experimental analysis of a CO2 refrigerating cycle with two-stage throttling and suction of the flash vapour by an auxiliary compressor. IIR International conference on thermophysical properties and transfer processes of refrigerants. Vicenza (Italy)2005.
[5] Sarkar J, Agrawal N. Performance optimization of transcritical CO2 cycle with parallel compression economization. International Journal of Thermal Sciences. 2010;49(5):838-43.
[6] Chesi A, Esposito F, Ferrara G, Ferrari L. Experimental analysis of R744 parallel compression cycle. Applied Energy. 2014;135:274-85.
[7] Gullo P, Elmegaard B, Cortella G. Advanced exergy analysis of a R744 booster refrigeration system with parallel compression. Energy. 2016;107:562-71.
[8] Andreasen G, Stoustrup J, Pardiñas ÁÁ, Hafner A, Izadi-Zamanabadi R. Data-driven modelling of a R744 refrigeration system with parallel compression configuration. Conference Data-driven modelling of a R744 refrigeration system with parallel compression configuration, vol. 2019-August. p. 2399-406.
[9] Wang Z, Zhao H, Wang X, Han J, Lai Y. Thermodynamic performance evaluation of the CO2 parallel compression supermarket refrigeration system with a subcooler. Int J Energy Res. 2020;44(8):6709-24.
[10] Nebot-Andrés L, Sánchez D, Calleja-Anta D, Cabello R, Llopis R. Experimental determination of the optimum intermediate and gas-cooler pressures of a commercial transcritical CO2 refrigeration plant with parallel compression. Applied Thermal Engineering. 2021;189.
[11] Hafner A, Hemmingsen AK. R744 refrigeration technologies for supermarkets in warm climates. Conference R744 refrigeration technologies for supermarkets in warm climates. p. 2313-20.
[12] Gullo P, Hafner A, Banasiak K, Minetto S, Kriezi EE. Multi-ejector concept: A comprehensive review on its latest technological developments. Energies. 2019;12(3).
[13] Lawrence N, Elbel S. Experimental investigation on control methods and strategies for off-design operation of the transcritical R744 two-phase ejector cycle. International Journal of Refrigeration. 2019.
[14] Yang JL, Ma YT, Liu SC. Performance investigation of transcritical carbon dioxide two-stage compression cycle with expander. Energy. 2007;32(3):237-45.
[15] Aprea C, Greco A, Maiorino A. The application of a desiccant wheel to increase the energetic performances of a transcritical cycle. Energy Conversion and Management. 2015;89(0):222-30.
[16] Sawalha S, Karampour M, Rogstam J. Field measurements of supermarket refrigeration systems. Part I: Analysis of CO2 trans-critical refrigeration systems. Applied Thermal Engineering. 2015;87(0):633-47.
[17] Arora A, Singh NK, Monga S, Kumar O. Energy and exergy analysis of a combined transcritical CO2 compression refrigeration and single effect H2O-LiBr vapour absorption system. International Journal of Exergy. 2011;9(4):453-71.

[18] Llopis R, Nebot-Andrés L, Sánchez D, Catalán-Gil J, Cabello R. Subcooling methods for CO2 refrigeration cycles: A review. International Journal of Refrigeration. 2018;93:85-107.
[19] Llopis R, Cabello R, Sánchez D, Torrella E. Energy improvements of CO2 transcritical refrigeration cycles using dedicated mechanical subcooling. International Journal of Refrigeration. 2015;55(0):129-41.
[20] Llopis R, Nebot-Andrés L, Cabello R, Sánchez D, Catalán-Gil J. Experimental evaluation of a CO2 transcritical refrigeration plant with dedicated mechanical subcooling. International Journal of Refrigeration. 2016;69:361-8.
[21] Nebot-Andrés L, Llopis R, Sánchez D, Catalán-Gil J, Cabello R. CO2 with mechanical subcooling vs. CO2 cascade cycles for medium temperature commercial refrigeration applications thermodynamic analysis. Applied Sciences (Switzerland). 2017;7(9).
[22] Nebot-Andrés L, Sánchez D, Calleja-Anta D, Cabello R, Llopis R. Experimental determination of the optimum working conditions of a commercial transcritical CO2 refrigeration plant with a R-152a dedicated mechanical subcooling. International Journal of Refrigeration. 2021;121:258-68.
[23] Dai B, Liu S, Li H, Sun Z, Song M, Yang Q, et al. Energetic performance of transcritical CO2 refrigeration cycles with mechanical subcooling using zeotropic mixture as refrigerant. Energy. 2018;150:205-21.
[24] Llopis R, Toffoletti G, Nebot-Andrés L, Cortella G. Experimental evaluation of zeotropic refrigerants in a dedicated mechanical subcooling system in a CO2 cycle. International Journal of Refrigeration. 2021;128:287-98.
[25] D'Agaro P, Coppola MA, Cortella G. Effect of dedicated mechanical subcooler size and gas cooler pressure control on transcritical CO2 booster systems. Applied Thermal Engineering. 2021;182.
[26] Cortella G, Coppola MA, D'Agaro P. Sizing and control rules of dedicated mechanical subcooler in transcritical CO2 booster systems for commercial refrigeration. Applied Thermal Engineering. 2021;193.
[27] Liu S, Lu F, Dai B, Nian V, Li H, Qi H, et al. Performance analysis of two-stage compression transcritical CO2 refrigeration system with R290 mechanical subcooling unit. Energy. 2019;189.
[28] Miran AZ, Nemati A, Yari M. Performance analysis and exergoeconomic evaluation of a TRC system enhanced by a dedicated mechanical subcooling. Energy Conversion and Management. 2019;197.
[29] Fu R, Wang J, Zheng M, Yu K, Liu X, Li X. Thermodynamic analysis of transcritical CO2 ejector expansion refrigeration cycle with dedicated mechanical subcooling. Entropy. 2019;21(9).
[30] Dai B, Zhao X, Liu S, Yang Q, Zhong D, Cao Y, et al. Heating and cooling of residential annual application using DMS transcritical CO2 reversible system and traditional solutions: An environment and economic feasibility analysis. Energy Conversion and Management. 2020;210.
[31] Dai B, Zhao X, Liu S, Yang Q, Zhong D, Hao Y, et al. Energetic, exergetic and exergoeconomic assessment of transcritical CO2 reversible system combined with

dedicated mechanical subcooling (DMS) for residential heating and cooling. Energy Conversion and Management. 2020;209.
[32] Cheng JH, He YJ, Zhang CL. New scenario of CO2 heat pump for space heating: Automatic mode switch between modified transcritical and cascade cycle in one system. Applied Thermal Engineering. 2021;191.
[33] Song Y, Cui C, Li M, Cao F, Investigation on the effects of the optimal medium-temperature on the system performance in a transcritical CO2 system with a dedicated transcritical CO2 subcooler. Applied Thermal Engineering, 2020; 168.
[34] Kantchev J, Lesage G. Mechanical subcooling of transcritical r-744 refrigeration systems with heat pump heat reclaim and floating head pressure. Google Patents; 2013.
[35] Cecchinato L, Chiarello M, Corradi M, Fornasieri E, Minetto S, Stringari P, et al. Thermodynamic analysis of different two-stage transcritical carbon dioxide cycles. International Journal of Refrigeration. 2009;32(5):1058-67.
[36] Nebot-Andrés L, Calleja-Anta D, Sánchez D, Cabello R, Llopis R. Thermodynamic analysis of a CO2 refrigeration cycle with integrated mechanical subcooling. Energies. 2019;13(1).
[37] Nebot-Andrés L, Catalán-Gil J, Sánchez D, Calleja-Anta D, Cabello R, Llopis R. Experimental determination of the optimum working conditions of a transcritical CO2 refrigeration plant with integrated mechanical subcooling. International Journal of Refrigeration. 2020;113:266-75.
[38] Catalán-Gil J, Llopis R, Sánchez D, Nebot-Andrés L, Cabello R. Energy analysis of dedicated and integrated mechanical subcooled CO2 boosters for supermarket applications. International Journal of Refrigeration. 2019.
[39] Lemmon EW, Huber ML, McLinden MO. REFPROP, NIST Standard Reference Database 23, v.9.1. National Institute of Standards, Gaithersburg, MD, U.S.A. 2013.
[40] Moffat RJ. Using Uncertainty Analysis in the Planning of an Experiment. Journal of Fluids Engineering. 1985;107(2):173-8.
[41] Aprea C., De Rossi F, Mastrullo R. The uncertainties in measuring vapour compression plant performances. Measurement. 1997; 21(3): 65-70.

Table 11.6. Main experimental results and uncertainty measurements of the optimum conditions.

	$T_{gly,in}$ (ºC)	$T_{w,in}$ (ºC)	T_o (ºC)	$p_{gc,o}$ (bar)	$T_{gc,o}$ (ºC)	APP (ºC)	SUB (ºC)	$\dot{m}_o$ (kg/s)	$\dot{m}_{aux}$ (kg/s)	$P_{c,CO2}$ (kW)	$P_{c,aux}$ (kW)	$\dot{Q}_o$ (kW)	$u_{\dot{Q}_o}$ (%)	COP (-)	u_{COP} (%)
IMS	3.7	25.0	-11.2	74.7	28.1	3.1	16.1	0.040	0.016	3.47	0.72	8.91	0.73	2.13	0.84
	3.8	30.4	-10.2	81.9	33.2	2.8	15.1	0.039	0.022	3.73	0.75	8.15	0.82	1.82	0.92
	3.8	35.2	-10.1	87.9	37.4	2.2	14.4	0.037	0.031	3.89	0.80	7.39	0.90	1.58	0.99
DMS	3.7	25.0	-12.0	74.9	26.4	1.3	12.3	0.039	0.006	3.43	0.38	8.40	0.76	2.21	0.88
	3.6	30.3	-11.5	79.9	31.6	1.3	12.64	0.038	0.008	3.58	0.49	7.85	0.84	1.93	0.95
	3.7	35.0	-10.4	89.9	35.6	0.6	13.70	0.038	0.008	3.95	0.53	7.58	0.87	1.69	0.98
							p_i (bar)								
PC	3.8	24.9	-10.9	77.6	29.1	4.2	46.8	0.041	0.018	3.60	0.77	8.94	1.16	2.05	1.24
	3.6	30.3	-10.2	88.1	32.2	1.9	49.8	0.039	0.019	3.94	0.90	8.21	1.19	1.70	1.26
	3.7	35.2	-9.5	99.1	36.9	1.8	51.6	0.037	0.024	4.25	1.12	7.73	1.23	1.44	1.29

Chapter 12 Conclusions and future research

12. Conclusions and future research

12.1. Conclusions

The thesis deals with different solutions for improving the behavior of CO_2 systems. In particular, the focus has been in improving CO_2 performance through the use of subcooling systems such as the dedicated mechanical subcooling and the integrated mechanical subcooling. The benefits provided by subcooling are both the reduction of the optimal working pressure, and with it the specific compression work as well as the increase of the specific cooling capacity. The thesis therefore focuses on the study of this subcooling carried out thanks to the use of an auxiliary vapor compression cycle. The most important stages carried out respond to the final objective of identifying the most beneficial system and its possibilities of application. For this, in-depth studies have been carried out, theoretical and experimental methodologies heve been followed.

A review has been carried out of the existing subcooling methods up to now and of all the studies, theoretical and experimental, that existed in the literature. In turn, the methods that were more promising and less developed have been identified, to study them in greater detail.

From the theoretical point of view:

- The energy evaluation of the different subcooling cycles proposed in this thesis and of the cycle with parallel compressor as the reference cycle has been carried out.
- The performances have been analyzed over a wide range of application and the improvements offered by mechanical subcooling systems have been compared.
- A detailed comparative energy analysis has been performed on upgrade solutions such as the dedicated mechanical subcooling and the integrated mechanical subcooling.

Based on the theoretical results, a laboratory plant has been designed and built, where all the cycles to be studied can be performed and in which the experimental tests of the systems have been carried out.

Regarding the experimental development of the thesis:

- The dedicated mechanical subcooling cycle has been experimentally tested and optimized also using different refrigerants in the auxiliary cycle: R-152a and compositions of this as base fluid with R-600, R-32 and CO_2.

- The experimental test and optimization of the integrated mechanical subcooling cycle is performed. Two other configurations of this cycle are proposed and analyzed.
- The cycle with parallel compressor has been experimentally tested and optimized.
- The main energetic results are compared to each other.

The main conclusions that have been drawn from the development of this work are:

- The use of dedicated mechanical subcooling (DMS) is advisable compared to the use of cascade systems for all those applications where the evaporation level is higher than -15ºC since it presents a better COP throughout the overall year.
- The integrated mechanical subcooling (IMS) is a system with a high potential for improvement that can over perform the basic CO_2 cycle with the advantage of only using CO_2 as refrigerant, which is an advantage when comparing to dedicated mechanical subcooling cycles.
- The behavior of the subcooling systems and the parallel compressor is investigated and the observed trends corroborate the initial theoretical results covering environment temperatures from 25ºC to 35ºC in transcritical conditions.

- The integrated mechanical subcooling system, extracting CO_2 from the exit of the subcooler, presents optimum experimental COP that goes from 1.40 to 1.87 for $t_{g,in}$ = -1.3ºC for water inlet temperatures ranging from 25ºC to 35ºC, from 1.56 to 2.13 for $t_{g,in}$ = 3.8ºC and from 1.81 to 2.48 for $t_{g,in}$ = 10.0ºC and is able to supply a cooling capacity from 6.5 kW to 7.7 kW for tg,in = -1.3ºC, from 7.3 kW to 8.9 kW for $t_{g,in}$ = 3.8ºC and from 8.6 kW to 10.3 kW for $t_{g,in}$ = 10.0ºC at maximum COP conditions.
- Optimum pressure of the transcritical CO_2 plant with IMS is strongly dependent on the gas-cooler outlet temperature, following a linear trend but it practically does not vary depending on the level of evaporation. On the other hand, the optimum subcooling degree is a function of the gas-cooler outlet temperature and the evaporation temperature, being always different for each of the working levels, being higher when lower is the evaporation level.
- The optimum COP with the DMS working with the R-152a goes from 1.51 to 1.95 for $t_{g,in}$= -1.3ºC, from 1.69 to 2.21 for $t_{g,in}$ = 3.8ºC and from 1.86 to 2.52 for tg,in = 10.0ºC. Cooling capacity obtained for these conditions goes from 6.5 kW to 7.3 kW for $t_{g,in}$ = -1.3ºC, from 7.6 kW to 8.4 kW for $t_{g,in}$ = 3.8ºC and from 8.8 kW to 9.8 kW for $t_{g,in}$ = 10.0ºC.

- As well as for the IMS cycle, optimum pressure when working with a DMS cycle has a higher dependence on the heat rejection temperature, being higher when higher the heat rejection level is, but it slightly depends on the evaporation temperature. The optimum subcooling degree is both dependent on the water inlet temperature and on the propylene glycol mixture inlet temperature.
- Experimental tests have been carried out in the CO_2 transcritical plant with parallel compression and the measured optimum COP range from 1.71 to 2.63 for the evaporating temperature of -5.0ºC, from 1.50 to 2.22 for -10.0ºC and from 1.25 to 1.84 for -15.0ºC. The cooling capacity from 8.94 kW to 11.34 kW for the evaporating temperature of -5.0ºC, from 7.71 kW to 9.47 kW for -10.0ºC and from 6.22 kW to 7.76 kW for -15.0ºC.
- Physical limitations have been observed for the PC lower pressures and they limit the optimum operation parameters. Gas-cooler pressure and intermediate pressure have been optimized to obtain the highest COP. The optimum pressure is strongly dependent on the gas-cooler outlet temperature, being higher when higher the temperature is, whereas it practically does not depend on the level of evaporation for the evaluated evaporation temperatures. On the other hand, the optimum intermediate pressure depends on both, the gas-cooler outlet temperature and the evaporation temperature, being higher when higher both the evaporation level and the gas-cooler outlet temperature are.
- Zeotropic mixtures can be used in the DMS as alternative refrigerants as long as the temperature glide of the mixture fits well with the temperature profile of the CO_2 in the subcooler. Additional increments in COP of 1.4% have been measured with the mixture R-600/R-152a compared to the DMS working with R-152a at 35.1ºC.
- Three different extraction points can be considered in the integrated mechanical subcooling systems, from the gas-cooler outlet, from the subcooler outlet and from the liquid tank, since these configurations present almost the same COP values. This shows that there are different ways to adapt an existing plant with an IMS system, depending on the disposal of the initial facility.
- Of the three IMS configurations, the one with extraction from gas-cooler exchanges less cooling power in the subcooler, therefore it can be designed with a heat exchanger smaller than the other two.

The main conclusion of this thesis is extracted from the experimental comparison among the three cycles. It has been demonstrated that mechanical subcooling cycles have a better energetic behavior than the cycle considered as a reference until the moment: the parallel compressor. The measured increments in COP are 4.1% at 25.0ºC,

7.2% at 30.4ºC and 9.5% at 35.1ºC thanks to the use of the IMS and of 7.8%, 13.7% and 17.5% respectively when using the DMS for an evaporating level near -10ºC. From these results it can be concluded that the best system, from an energy point of view, is the DMS since it achieves more significant increases. Despite this, it is worth noting the importance of the results obtained with the IMS, since it presents significant increases in COP with the advantage of only using CO_2 as a refrigerant.

The following figure summarizes the career of the PhD candidate in the research group and the main results of this thesis. The PhD candidate became part of the research group in 2015 when she designed the dedicated mechanical subcooling system for the laboratory plant, thus obtaining results in 2016 (point C) that represented an increase in COP of 15.3% compared to the previous state of the installation. During the development of the thesis, starting in 2018, the DMS was optimized and the IMS was implemented, obtaining increments of 28.7% (point E) and 21.3% (point D) respectively.

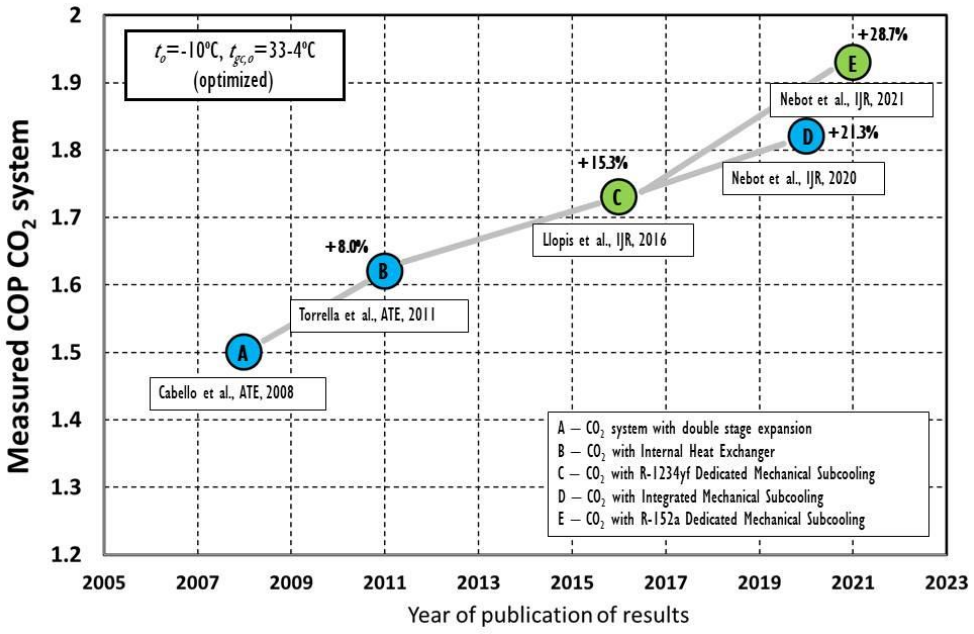

Figure 12.1. Summary of the main results obtained in the transcritical CO_2 plant.

It can be concluded that this thesis follows a very clear line of research and that the results provided are very important for the scientific field and also for the industry, since these systems are already being manufactured by some companies.

12.2. Future research

Also derived from this thesis and already in the development phase, it is intended to study, theoretically and experimentally, the use of solid-state technologies as subcooling methods for smaller CO_2 systems. Solid-state refrigeration presents high COP when the temperature difference between hot and cold sink is small, so it meets the requirements to be applied as a CO_2 subcooling method. Solid state refrigeration is an emerging technology that uses a solid as refrigerant, taking advantage of the magneto-caloric or the elasto-caloric effect, for example. Solid state refrigeration can reach efficiencies much higher than those of vapor compression systems, as long as it works with a relatively low temperature difference between the two heat sources. However, it does not have a clear field of application since the temperature differences that it allows to generate are too small. As it has been presented in this thesis, CO_2 systems will improve their COP as long as the auxiliary cycle's COP is higher than the COP of cycle without subcooling. The subcooling cycle performs heat rejection to the same hot sink as the CO_2 cycle and the cold sink is defined by the temperature at the exit of the gas-cooler and the subcooling degree. That means that the hot and the cold sinks of the auxiliary cycle are very close. Regarding solid state refrigeration, their COP decreases when the temperature span increases which can be beneficial for using this system as cooling device for the CO_2, because its hot and cold sink are very close, with leads to a high COP of the solid state refrigeration system.

The possibility of merging these two technologies, CO_2 and solid state, is a line of research that has yet to be explored and that presents real challenges since, after studying this fusion, it will be necessary to develop prototypes that allow both systems to be joined in the best possible way. This line of research deserves special attention since the results are very promising.

From 2015, mechanical subcooling systems have been widely studied and optimized for refrigeration purposes, however, future research should also focus on the analysis of these subcooling systems applied to heating applications, which can be a very interesting field of application and where some research has already begun, carried out with interesting results. Some of the researchers propose dedicated mechanical subcooling cycles, whose cycle differs from the one presented in this thesis, obtaining increments in COP of 15.3% when comparing to the standard transcritical CO_2 heat pump systems. For this configuration, the optimization of the intermediate temperature and pressure has been done.

These recent investigations show the great interest of the research line of subcooling systems for heat pumps. It would therefore be interesting to study, both theoretical and

experimental, the two systems proposed in this thesis, DMS and IMS, for their application in heating systems.

Chapter 13 Appendices

13. Appendices

13.1. Scientific production

13.1.1. Journal contributions

29 **Laura Nebot-Andrés, Daniel Calleja-Anta, Carlos Fossi, Daniel Sánchez, Ramón Cabello, Rodrigo Llopis**
Experimental assessment of different extraction points for the integrated mechanical subcooling system of a CO_2 transcritical plant
International Journal of Refrigeration – Revue Internationale de Froid. 2022
D.O.I. doi.org/10.1016/j.ijrefrig.2022.01.006 Ed.: Pergamon-Elsevier Science LTD
In press Available online : 06/01/22 ISSN: 0140-7007

28 **Laura Nebot-Andrés, Daniel Calleja-Anta, Daniel Sánchez, Ramón Cabello, Rodrigo Llopis**
Experimental assessment of dedicated and integrated mechanical subcooling systems vs parallel compression in transcritical CO_2 refrigeration plants
Energy Conversion and Management 2022
D.O.I. doi.org/10.1016/j.enconman.2021.115051 Ed.: Pergamon-Elsevier Science LTD
In press Available online : 02/12/21 ISSN: 0196-8904

27 **Daniel Calleja-Anta, Laura Nebot-Andrés, Ramón Cabello, Daniel Sánchez, Rodrigo Llopis**
A3 and A2 refrigerants: Border determination and hunt for A2 low-GWP blends
International Journal of Refrigeration – Revue Internationale de Froid. 2022
D.O.I. doi.org/10.1016/j.ijrefrig.2021.11.012 Ed.: Pergamon-Elsevier Science LTD
In press Available online : 29/11/21 ISSN: 0140-7007

26 **Rodrigo Llopis, Gabriele Toffoletti, Laura Nebot-Andrés, Giovanni Cortella**
Experimental evaluation of zeotropic refrigerants in a dedicated mechanical subcooling system in a CO2 cycle.
International Journal of Refrigeration – Revue Internationale de Froid. 2021
D.O.I. doi.org/10.1016/j.ijrefrig.2021.05.028 Ed.: Pergamon-Elsevier Science LTD
Vol. 128 Pages 287-298 ISSN: 0140-7007

25 **Ramón Cabello, Daniel Sánchez, Rodrigo Llopis, Laura Nebot-Andrés, Daniel Calleja-Anta**
Energy evaluation of a low temperature commercial refrigeration plant working with the new low-GWP blend R468A as drop-in of R404A
International Journal of Refrigeration – Revue Internationale de Froid. 2021
D.O.I. doi.org/10.1016/j.ijrefrig.2021.01.012 Ed: Pergamon-Elsevier Science LTD
Vol. 127 Pages 1-11 ISSN: 0140-7007

24 **Laura Nebot-Andrés, Daniel Sánchez, Daniel Calleja-Anta, Ramón Cabello, Rodrigo Llopis**
Experimental determination of the optimum intermediate and gas-cooler pressures of a commercial transcritical CO_2 refrigeration plant with parallel compression.
Applied Thermal Engineering 2021
D.O.I. doi.org/10.1016/j.applthermaleng.2021.116671 Ed: Pergamon-Elsevier Science LTD
Vol. 189 Art. 116671 ISSN: 1359-4311

23 **Ramón Cabello, Daniel Sánchez, Rodrigo Llopis, Laura Nebot-Andrés, Daniel Calleja-Anta**
Energy evaluation of a Low Temperature commercial refrigeration plant working with the new low-GWP blend R468A as drop-in of R404A
International Journal of Refrigeration – Revue Internationale de Froid. 2021
D.O.I. doi.org/10.1016/j.ijrefrig.2021.01.012 Ed: Pergamon-Elsevier Science LTD
Vol. Pages ISSN: 0140-7007

22 **Laura Nebot-Andrés, Daniel Sánchez, Daniel Calleja-Anta, Ramón Cabello, Rodrigo Llopis**
Experimental determination of the optimum working conditions of a commercial transcritical CO2 refrigeration plant with a R-152a dedicated mechanical subcooling.
International Journal of Refrigeration – Revue Internationale de Froid. 2021
D.O.I. doi.org/10.1016/j.ijrefrig.2020.10.002 Ed: Pergamon-Elsevier Science LTD
Vol. 121 Pages 258-268 ISSN: 0140-7007

21 **Daniel Sánchez, Jesús Catalán-Gil, Ramón Cabello, Daniel Calleja-Anta, Rodrigo Llopis , Laura Nebot-Andrés**
Experimental analysis and optimization of an R744 transcritical cycle working with a mechanical subcooling system.
Energies 2020
D.O.I. doi.org/10.3390/en13123204 Ed: MDPI AG
Vol. 13 Art. 3204 ISSN: 1996-1073

20 **Rodrigo Llopis, Daniel Calleja-Anta, Angelo Maiorino, Laura Nebot-Andrés, Daniel Sánchez, Ramón Cabello**
TEWI analysis of a stand-alone refrigeration system using low-GWP fluids with leakage ratio consideration
International Journal of Refrigeration – Revue Internationale de Froid. 2020
D.O.I. doi.org/10.1016/j.ijrefrig.2020.05.028 Ed: Pergamon-Elsevier Science LTD
Vol. 118 Pages 279-289 ISSN: 0140-7007

19 **Laura Nebot-Andrés, Jesús Catalán-Gil, Daniel Sánchez, Daniel Calleja-Anta, Ramón Cabello, Rodrigo Llopis**
Experimental determination of the optimum working conditions of a transcritical CO2 refrigeration plant with integrated mechanical subcooling.
International Journal of Refrigeration – Revue Internationale de Froid. 2020
D.O.I. doi.org/10.1016/j.ijrefrig.2020.02.012 Ed: Pergamon-Elsevier Science LTD
Vol. 113 Pages 266-275 ISSN: 0140-7007

18 **Jesús Catalán-Gil, Daniel Sánchez, Ramón Cabello, Rodrigo Llopis, Laura Nebot-Andrés, Daniel Calleja-Anta**
Experimental evaluation of the desuperheater influence in a CO2 booster refrigeration facility
Applied Thermal Engineering 2020
D.O.I. doi.org/10.1016/j.applthermaleng.2019.114785 Ed: Pergamon-Elsevier Science LTD
Vol. 168 Art. 114785 ISSN: 1359-4311

17 **Jesús Catalán-Gil, Laura Nebot-Andrés, Daniel Sánchez, Rodrigo Llopis, Ramón Cabello Daniel Calleja-Anta**
Improvements in CO2 booster architectures with different economizer arrangements
Energies 2020
D.O.I. doi.org/ 10.3390/en13051271 Ed: MDPI AG
Vol. 13 Art. 1271 ISSN: 1996-1073

16 **Daniel Calleja-Anta, Laura Nebot-Andrés, Jesús Catalán-Gil, Daniel Sánchez, Ramón Cabello, Rodrigo Llopis**
Thermodynamic screening of alternative refrigerants for R290 and R600a
Results in Engineering 2020
D.O.I. doi.org/10.1016/j.rineng.2019.100081 Ed: Elsevier B.V.
Vol. 5 Art. 100081 ISSN: 2590-1230

15 **Laura Nebot-Andrés, Daniel Calleja-Anta, Daniel Sánchez, Ramón Cabello, Rodrigo Llopis**
Thermodynamic analysis of a CO2 refrigeration cycle with integrated mechanical subcooling
Energies 2019
D.O.I. doi.org/10.3390/en13010012 Ed: MDPI AG

Vol. 13 Art. 4 ISSN: 1996-1073

14 **Rodrigo Llopis, Daniel Calleja-Anta, Daniel Sánchez, Laura Nebot-Andrés, Jesús Catalán, Ramón Cabello**
R-454C, R-459B, R-457A and R-455A as low-GWP replacements of R-404A: Experimental evaluation and optimization.
International Journal of Refrigeration – Revue Internationale de Froid. 2019
D.O.I. doi.org/10.1016/j.ijrefrig.2019.06.013 Ed: Pergamon-Elsevier Science LTD
Vol. 106 Pages 133 – 143 ISSN: 0140-7007

13 **Daniel Sánchez, Ramón Cabello, Rodrigo Llopis, Jesús Catalán-Gil, Laura Nebot-Andrés**
Energy assessment and environmental impact analysis of an R134a/R744 cascade refrigeration plant upgraded with the low-GWP refrigerants R152a, R1234ze(E), propane (R290) and propylene (R1270)
International Journal of Refrigeration – Revue Internationale de Froid. 2019
D.O.I. doi.org/10.1016/j.ijrefrig.2019.05.028 Ed: Pergamon-Elsevier Science LTD
Vol. 104 Pages 321 – 334 ISSN: 0140-7007

12 **Jesús Catalán-Gil, Rodrigo Llopis, Daniel Sánchez, Laura Nebot-Andrés, Ramón Cabello**
Energy analysis of dedicated and integrated mechanical subcooled CO_2 boosters for supermarket applications.
International Journal of Refrigeration – Revue Internationale de Froid. 2019
D.O.I. doi.org/10.1016/j.ijrefrig.2019.01.034 Ed: Pergamon-Elsevier Science LTD
Vol. 101 Pages 11 – 23 ISSN: 0140-7007

11 **Jesús Catalán-Gil, Daniel Sánchez, Rodrigo Llopis, Laura Nebot-Andrés, Ramón Cabello**
Energy evaluation of multiple stage commercial refrigeration architectures adapted to F-Gas regulation
Energies 2018
Special issue: Refrigeration, Air Conditioning and Heat Pumps: Energy and Environmental Issues
D.O.I. doi.org/10.3390/en11071915 Ed: MDPI Open Access Journal
Vol. 11 Art. 1915 ISSN: 1996-1073

10 **Rodrigo Llopis, Laura Nebot-Andrés, Daniel Sánchez, Jesús Catalán-Gil, Ramón Cabello**
Subcooling methods for CO_2 refrigeration cycles. A review.
Best article IJR 2018.
International Journal of Refrigeration – Revue Internationale de Froid. 2018
D.O.I. doi.org/10.1016/j.ijrefrig.2018.06.010 Ed: Pergamon-Elsevier Science LTD
Vol. 93 Pages 85 – 107 ISSN: 0140-7007

9 **Daniel Sánchez, Ramón Cabello, Rodrigo Llopis, Jesús Catalán-Gil, Laura Nebot-Andrés**
Energy assessment of an R134a refrigeration plant upgraded to an indirect system using R152a and R1234ze(E) as refrigerants
Applied Thermal Engineering 2018
D.O.I. doi.org/10.1016/j.applthermaleng.2018.04.114 Ed: Pergamon-Elsevier Science LTD
Vol. 139 Pages 121 – 134 ISSN: 1359-4311

8 **Rodrigo Llopis, Daniel Sánchez, Ramón Cabello, Jesús Catalán-Gil, Laura Nebot-Andrés**
Conversion of a direct to an indirect refrigeration system at medium temperature using R-134a and R-507A: An energy impact analysis.
Applied Sciences 2018
Special issue: Sciences in Heat Pump and Refrigeration
D.O.I. 10.3390/app8020247 Ed: MDPI AG
Vol. 8(2) Art. 247 ISSN 2076-3417

7 **Laura Nebot-Andrés, Rodrigo Llopis, Daniel Sánchez, Jesús Catalán-Gil, Ramón Cabello**
CO_2 with mechanical subcooling vs. CO_2 cascade cycles for medium temperature commercial refrigeration applications. Thermodynamic analysis.

Applied Sciences 2017
D.O.I. 10.3390/app7090955 Ed: MDPI AG
Vol. 7 Art. 955 ISSN 2076-3417

6 **Rodrigo Llopis, Daniel Sánchez, Ramón Cabello, Jesús Catalán-Gil, Laura Nebot-Andrés**
Experimental analysis of R-450A and R-513A as replacements of R-134a and R-507A in a medium temperature commercial refrigeration system
International Journal of Refrigeration – Revue Internationale de Froid. 2017
D.O.I. 10.1016/j.ijrefrig.2017.08.022 Ed: Pergamon-Elsevier Science LTD
Vol. 84 Pages 52-66 ISSN 0140-7007

5 **Rodrigo Llopis, Daniel Sánchez, Ramón Cabello, Laura Nebot-Andrés, Jesús Catalán-Gil**
R-407H as drop-in of R-404A. Experimental analysis in a low temperature direct expansion commercial refrigeration system
International Journal of Refrigeration – Revue Internationale de Froid. 2017
D.O.I. 10.1016/j.ijrefrig.2016.09.020 Ed: Pergamon-Elsevier Science LTD
Vol. 80 Pages 11-23 ISSN 0140-7007

4 **Daniel Sánchez, Rodrigo Llopis, Ramón Cabello, Jesús Catalán-Gil, Laura Nebot-Andrés**
Conversion of a direct to an indirect commercial (HFC134a/CO_2) cascade refrigeration system. Energy impact analysis
International Journal of Refrigeration – Revue Internationale de Froid. 2017
D.O.I. 10.1016/j.ijrefrig.2016.09.012 Ed: Pergamon-Elsevier Science LTD
Vol. 73 Pages 183 – 199 ISSN 0140-7007

3 **Ramón Cabello, Daniel Sánchez, Rodrigo Llopis, Jesús Catalán-Gil, Laura Nebot-Andrés, Enrique Torrella**
Energy evaluation of R152a as drop in replacement for R134a in cascade refrigeration plants
Applied Thermal Engineering 2017
D.O.I. 10.1016/j.applthermaleng.2016.09.010 Ed: Pergamon-Elsevier Science LTD
Vol. 110 Pages 972 – 984 ISSN 1359-4311

2 **Rodrigo Llopis, Laura Nebot-Andrés, Ramón Cabello, Daniel Sánchez, Jesús Catalán-Gil**
Experimental evaluation of a CO_2 transcritical refrigeration plant with dedicated mechanical subcooling
International Journal of Refrigeration – Revue Internationale de Froid. 2016
D.O.I. 10.1016/j.ijrefrig.2016.06.009 Ed: Pergamon-Elsevier Science LTD
Vol. 69 Pages 361 – 368 ISSN 0140-7007

1 **Rodrigo Llopis, Carlos Sanz-Kock, Ramón Cabello, Daniel Sánchez, Laura Nebot-Andrés, Jesús Catalán-Gil**
Effects caused by the internal heat exchanger at the low temperature cycle in a cascade refrigeration plant
Applied Thermal Engineering 2016
D.O.I. 10.1016/j.applthermaleng.2016.04.075 Ed: Pergamon-Elsevier Science LTD
Vol. 103 Pages 1077 – 1086 ISSN 1359-4311

13.1.2. Contribution to international conferences

36 **Laura Nebot, Daniel Sánchez, Ramón Cabello, Daniel Calleja, Carlos Fossi, Rodrigo Llopis**
Current limits of CO2 compressors working in integrated mechanical subcooling cycles
12th International Conference on Compressors and their Systems
6/09/2021 London UK 2021

35 **Daniel Calleja, Laura Nebot, Carlos Fossi, Daniel Sánchez, Ramón Cabello, Rodrigo Llopis**
Blends with HFOs as alternative to R-600a. Theoretical and experimental evaluation for domestic appliances.
2nd IIR Conference on HFO Refrigerants and Low GWP Blends
16/06/2021 Osaka Japan 2021

34 **Rodrigo Llopis, Jesus Catalan, Daniel Sanchez, Laura Nebot, Daniel Calleja, Ramon Cabello**
Worldwide performance of CO2 booster systems with auxiliary compressor
14th IIR-Gustav Lorentzen Conference on Natural Refrigerants . GL2020
07/12/2020 Kioto Japan 2020

33 **Daniel Sanchez, Patricia Aranguren, Alvaro Casi), Ramón Cabello, David Astrain, Miguel Araiz, Rodrigo Llopis, Daniel Calleja-Anta, Laura Nebot-Andrés**
Energy performance of a CO2 transcritical refrigerating plant with a thermoelectric subcooler system
14th IIR-Gustav Lorentzen Conference on Natural Refrigerants . GL2020
07/12/2020 Kioto Japan 2020

32 **Daniel Sanchez, Daniel Calleja, Laura Nebot, Ramon Cabello, Rodrigo Llopis**
Experimental analysis of CO2 blends for transcritical refrigeration systems
14th IIR-Gustav Lorentzen Conference on Natural Refrigerants . GL2020
07/12/2020 Kioto Japan 2020

31 **Laura Nebot, Daniel Sanchez, Ramon Cabello, Daniel Calleja, Rodrigo Llopis**
Experimental evaluation of CO2 refrigeration plant with integrated mechanical subcooling system at optimal working conditions
14th IIR-Gustav Lorentzen Conference on Natural Refrigerants . GL2020
07/12/2020 Kioto Japan 2020

30 **Daniel Calleja, Daniel Sanchez, Ramon Cabello, Laura Nebot, Rodrigo Llopis**
Experimental evaluation of natural refrigerant blends as substitutes for R-600a in a domestic fridge and freezer
14th IIR-Gustav Lorentzen Conference on Natural Refrigerants . GL2020
07/12/2020 Kioto Japan 2020

29 **Ramón Cabello, Daniel Sánchez, Laura Nebot, Daniel Calleja, Rodrigo Llopis**
Evaluación energética del refrigerante R468A como alternativa al R404A en aplicaciones comerciales de baja temperatura
X Congreso Ibérico y VIII Congreso Iberoamericano de Ciencias y Técnicas del Frío. CYTEF 2020
11/11/2020 Pamplona Spain 2020

28 **Laura Nebot, Jesús Catalán, Daniel Sánchez, Ramón Cabello, Daniel Calleja, Rodrigo Llopis**
Evaluación experimental de un ciclo de subenfriamiento mecánico integrado en una planta de refrigeración con CO_2
X Congreso Ibérico y VIII Congreso Iberoamericano de Ciencias y Técnicas del Frío. CYTEF 2020
11/11/2020 Pamplona Spain 2020

27 **Daniel Calleja, Laura Nebot, Andrea Ariano, Daniel Sánchez, Ramón Cabello, Rodrigo Llopis**
Evaluación experimental de mezclas alternativas al R-600a en un frigorífico y un congelador doméstico
X Congreso Ibérico y VIII Congreso Iberoamericano de Ciencias y Técnicas del Frío. CYTEF 2020
11/11/2020 Pamplona Spain 2020

26 **Rodrigo Llopis, Laura Nebot, Daniel Sánchez, Jesús Catalán, Daniel Calleja, Ramón Cabello**

Subcooled CO_2 refrigeration cycles: current status and lines of research
X Congreso Ibérico y VIII Congreso Iberoamericano de Ciencias y Técnicas del Frío. CYTEF 2020
11/11/2020 Pamplona Spain 2020

25 Daniel Sánchez, Daniel Calleja, Laura Nebot, Jesús Catalán, Rodrigo Llopis, Ramón Cabello
Experimental analysis of alternative blends of refrigerants for CO2 transcritical refrigeration systems
X Congreso Ibérico y VIII Congreso Iberoamericano de Ciencias y Técnicas del Frío. CYTEF 2020
11/11/2020 Pamplona Spain 2020

24 Daniel Sánchez, Ramón Cabello, Rodrigo Llopis, Jesús Catalán, Laura Nebot, Daniel Calleja, Eduardo Gil
Energy improvements in a stand-alone transcritical refrigeration system using a low-GWP mixture of CO_2/R1270
25th IIR International Congress of Refrigeration
24/08/2019 Montreal Canada ISBN 978-2-36215-035-7 2019

23 Daniel Calleja, Laura Nebot, Jesús Catalán, Rodrigo Llopis, Daniel Sánchez, Ramón Cabello
Experimental evaluation of low-GWP replacements of R-404A in a stand-alone commercial cabinet for fresh product
25th IIR International Congress of Refrigeration
24/08/2019 Montreal Canada ISBN 978-2-36215-035-7 2019

22 Laura Nebot, Rodrigo Llopis, Jesús Catalán, Daniel Sánchez, Daniel Calleja, Ramón Cabello
Thermodynamics analysis of CO_2 refrigeration cycles working with mechanical subcooling systems
25th IIR International Congress of Refrigeration
24/08/2019 Montreal Canada ISBN 978-2-36215-035-7 2019

21 Rodrigo Llopis, Jesús Catalán, Laura Nebot, Daniel Sánchez, Ramón Cabello
Subcooled CO_2 booster systems for supermarket application in China. An energy approach.
9th International Conference on Compressor and Refrigeration (ICCR2019)
12/07/2019 Xi'an China ISBN 978-7-5693-1224-9 2019

20 Laura Nebot, Daniel Calleja, Rodrigo Llopis, Jesús Catalán, Daniel Sánchez, Ramón Cabello
Mechanical subcooling systems for CO_2 refrigeration cycles. Thermodynamic analysis.
XI National and II International Engineering Thermodynamics Congress
14/06/2019 Albacete Spain ISBN 978-84-09-11635-5 2019

19 Daniel Calleja, Laura Nebot, Jesús Catalán, Rodrigo Llopis, Daniel Sánchez, Ramón Cabello
Thermodynamic screening for alternative refrigerants for R-290 and R-600a.
XI National and II International Engineering Thermodynamics Congress
14/06/2019 Albacete Spain ISBN 978-84-09-11635-5 2019

18 Daniel Calleja, Jesús Catalán, Laura Nebot, Rodrigo Llopis, Daniel Sánchez, Ramón Cabello
Low-GWP replacements of R-404A for commercial refrigeration. Experimental analysis.
XI National and II International Engineering Thermodynamics Congress
14/06/2019 Albacete Spain ISBN 978-84-09-11635-5 2019

17 Jesús Catalán, Laura Nebot, Daniel Calleja, Daniel Sánchez, Rodrigo Llopis, Ramón Cabello
Experimental comparison of CO_2 Booster architecture for commercial refrigeration
XI National and II International Engineering Thermodynamics Congress
14/06/2019 Albacete Spain ISBN 978-84-09-11635-5 2019

16 Daniel Sánchez, Patricia Aranguren, Jesús Catalán, Laura Nebot, Daniel Calleja, Rodrigo Llopis, Ramón Cabello

Development of a heat transfer test-bench for educational purpose based on Arduino.
XI National and II International Engineering Thermodynamics Congress
14/06/2019 Albacete Spain ISBN 978-84-09-11635-5 2019

15 Laura Nebot-Andrés, Rodrigo Llopis, Jesús Catalán-Gil, Daniel Sánchez, Ramón Cabello
Energy evaluation of the mechanical subcooling impact on a CO_2 DX-system in a commercial MT cabinet
13th IIR Gustav Lorentzen Conference on natural refrigerants
18/06/2018 Valencia Spain DOI 10.18462/iir.gl.2018.1127 2018

14 Rodrigo Llopis, Daniel Sánchez, Ramón Cabello, Laura Nebot-Andrés, Jesús Catalán-Gil
Alternative refrigerants for the primary circuit of an indirect commercial refrigeration cascade system
13th IIR Gustav Lorentzen Conference on natural refrigerants
18/06/2018 Valencia Spain DOI 10.18462/iir.gl.2018.1126 2018

13 Daniel Sánchez, Jesús Catalán-Gil, Rodrigo Llopis, Laura Nebot-Andrés, Ramón Cabello, Enrique Torrella
CO_2 vs. fluorinated refrigerants. Energy evaluation in a MT cabinet with DX-system
13th IIR Gustav Lorentzen Conference on natural refrigerants
18/06/2018 Valencia Spain DOI 10.18462/iir.gl.2018.1119 2018

12 Daniel Sánchez, Ramón Cabello, Rodrigo Llopis, Jesús Catalán-Gil, Laura Nebot-Andrés, Ángela Clemente
CO_2 as secondary fluid as alternative to DX-systems. Energy evaluation in a MT cabinet
13th IIR Gustav Lorentzen Conference on natural refrigerants
18/06/2018 Valencia Spain DOI 10.18462/iir.gl.2018.1118 2018

11 Rodrigo Llopis, Laura Nebot-Andrés, Jesús Catalán-Gil, Daniel Sánchez, Ramón Cabello
R450A and R513A as low-GWP substitutes of R-134a and R-507A in a medium temperature refrigeration system
CYTEF 2018 – IX Congreso Ibérico y VII Congreso Iberoamericano de Ciencias y Técnicas del Frío
20/06/2018 Valencia Spain ISBN 978-84-09-01619-8 2018

10 Rodrigo Llopis, Jesús Catalán-Gil, Laura Nebot-Andrés, Daniel Sánchez, Ramón Cabello
Direct vs. Indirect commercial refrigeration at medium temperature. Energy analysis.
CYTEF 2018 – IX Congreso Ibérico y VII Congreso Iberoamericano de Ciencias y Técnicas del Frío
20/06/2018 Valencia Spain ISBN 978-84-09-01619-8 2018

9 Laura Nebot-Andrés, Jesús Catalán-Gil, Rodrigo Llopis, Daniel Sánchez, Ramón Cabello
Comparativa de sistemas de subenfriamiento en ciclos de refrigeración de CO_2 en climas cálidos
CYTEF 2018 – IX Congreso Ibérico y VII Congreso Iberoamericano de Ciencias y Técnicas del Frío
20/06/2018 Valencia Spain ISBN 978-84-09-01619-8 2018

8 Laura Nebot-Andrés, Jesús Catalán-Gil, Rodrigo Llopis, Daniel Sánchez, Ramón Cabello
Evaluación energética del impacto del mechanical subcooling en un sistema de CO_2 de expansión directa en una cabinet comercial de MT
CYTEF 2018 – IX Congreso Ibérico y VII Congreso Iberoamericano de Ciencias y Técnicas del Frío
20/06/2018 Valencia Spain ISBN 978-84-09-01619-8 2018

7 Daniel Sánchez, Rodrigo Llopis, Jesús Catalán-Gil, Laura Nebot-Andrés, Ramón Cabello, Ignacio Fandós
Comportamiento energético de una instalación frigorífica de cascada trabajando con un sistema de expansión indirecta
CYTEF 2018 – IX Congreso Ibérico y VII Congreso Iberoamericano de Ciencias y Técnicas del Frío

20/06/2018 Valencia Spain ISBN 978-84-09-01619-8 2018

6 Jesús Catalán-Gil, Laura Nebot-Andrés, Daniel Sánchez, Rodrigo Llopis, Ramón Cabello

Análisis del subenfriamiento integrado en los sistemas booster con CO_2

CYTEF 2018 – IX Congreso Ibérico y VII Congreso Iberoamericano de Ciencias y Técnicas del Frío

20/06/2018 Valencia Spain ISBN 978-84-09-01619-8 2018

5 Jesús Catalán-Gil, Daniel Sánchez, Laura Nebot-Andrés, Rodrigo Llopis, Ramón Cabello

Evaluación energética de distintas arquitecturas booster con CO_2 para refrigeración comercial en climas cálidos

CYTEF 2018 – IX Congreso Ibérico y VII Congreso Iberoamericano de Ciencias y Técnicas del Frío

20/06/2018 Valencia Spain ISBN 978-84-09-01619-8 2018

4 Laura Nebot-Andrés, Rodrigo Llopis, Daniel Sánchez, Ramón Cabello

Experimental evaluation of a dedicated mechanical subcooling system in a CO_2 transcritical refrigeration cycle

12th Gustav Lorentzen Conference on Natural Refrigerants

24/08/2016 Edinburgh United Kingdom DOI 10.18462/iir.gl.2016.1162 2016

ISBN 978-236-21501-8-0

NOTE: **Award Best communication** presented by a student within the Natural Working Fluids category.

3 Daniel Sánchez, Jesús Catalán-Gil, Rodrigo Llopis, Laura Nebot-Andrés, Ramón Cabello, Enrique Torrella

Improvements in a CO_2 transcritical plant working with two different subcooling systems.

12th Gustav Lorentzen Conference on Natural Refrigerants

24/08/2016 Edinburgh United Kingdom DOI 10.18462/iir.gl.2016.1170 2016

ISBN 978-236-21501-8-0

2 Rodrigo Llopis, Daniel Sánchez, Ramón Cabello, Laura Nebot-Andrés, Enrique Torrella

Sistema de subenfriamiento mecánico para ciclos transcríticos de refrigeración con CO_2

VIII Iberian Congress and VI Ibero-American Congress of Refrigeration science and technologies. CYTEF-2016

06/05/2016 Coimbra Portugal ISBN 978-989-99080-5-5 2016

1 Rodrigo Llopis, Daniel Sánchez, Ramón Cabello, Carlos Sanz-Kock, Laura Nebot-Andrés, J. Catalán, E. Torrella

Experimental analysis of an IHX in a CO_2 subcritical cycle

VIII Iberian Congress and VI Ibero-American Congres of Refrigeration science and technologies. CYTEF-2016

06/05/2016 Coimbra Portugal ISBN 978-989-99080-5-5 2016

13.1.3. Contribution to national conferences

6 Daniel Sánchez, Ramón Cabello, Rodrigo Llopis, Jesús Catalán, Laura Nebot

Análisis energético y medioambiental de un sistema de refrigeración en cascada con expansión indirecta y refrigerantes de bajo GWP: R152a, R1234ze(E), R290 y R1270

III Congreso sobre tecnologías de refrigeración. TECNOFRIO 2018.

19/09/2018 Madrid Spain ISBN 978-84-09049028 2018

5 Jesús Catalán-Gil, Daniel Sánchez, Rodrigo Llopis, Laura Nebot-Andrés, Ramón Cabello

Evaluación energética de sistemas booster con CO_2

Congreso sobre Tecnologías de Refrigeración. TECNOFRIO'17

25-26/10/2017 Madrid Spain ISBN - 2017

4 Laura Nebot-Andrés, Rodrigo Llopis, Daniel Sánchez, Jesús Catalán-Gil, Ramón Cabello
Comparison of a CO2 transcritical refrigeration plant with dedicated mechanical subcooling or internal heat exchanger.
X Congreso Nacional de Ingeniería Termodinámica
28/06/2017 Lleida Spain 2017

3 Laura Nebot-Andrés, Rodrigo Llopis, Daniel Sánchez, Jesús Catalán-Gil, Ramón Cabello
Experimental evaluation of a CO2 transcritical refrigeration plant with dedicated mechanical subcooling.
X Congreso Nacional de Ingeniería Termodinámica
28/06/2017 Lleida Spain 2017

2 Rodrigo Llopis, Laura Nebot-Andrés, Daniel Sánchez, Jesús Catalán-Gil, Ramón Cabello
CO2 with mechanical subcooling vs. CO2 cascade cycles for medium temperature commercial refrigeration applications. Thermodynamic analysis.
X Congreso Nacional de Ingeniería Termodinámica
28/06/2017 Lleida Spain 2017

1 Rodrigo Llopis, Laura Nebot-Andrés, Daniel Sánchez, Jesús Catalán-Gil, Ramón Cabello
HFC407H a low GWP drop-in of HFC404A. Experimental analysis in a low temperature direct expansion system.
X Congreso Nacional de Ingeniería Termodinámica
28/06/2017 Lleida Spain 2017

13.2. Awards

3 Rodrigo Llopis, Laura Nebot, Daniel Sánchez, Jesús Catalán, Ramón Cabello
2018 Best Paper International Journal of Refrigeration
Institute International du Froid
Paper: Subcooling methods for CO2 refrigeration cycles: A review
Amount: 1500€ 2019

2 Rodrigo Llopis, Laura Nebot-Andrés, Daniel Sánchez, Jesús Catalán-Gil, Ramón Cabello
Best Conges Paper Award, *paper: 'CO_2 with mechanical subcooling vs. CO_2 cascade cycles for medium temperature commercial refrigeration applications. Thermodynamic analysis.'*
10º Congreso Internacional de Ingeniería Termodinámica, Lleida, 2017
Amount: 1104€ (publication fee as open access in Applied Sciences) 2017

1 Laura Nebot-Andrés, Rodrigo Llopis, Daniel Sánchez, Ramón Cabello
Best Student Paper in the Natural Working Fluids Stream, *paper: 'Experimental evaluation of a dedicated mechanical subcooling system in a CO_2 transcritical refrigeration cycle'*
International Institute of Refrigeration. 12th IIR Gustav Lorentzen Natural Working Fluids Conference 2016
Amount: 300 £ 2016